2010-07-01

Application of Reliability Analysis to Highway Design Problems: Superelevation (e) Design, Left Turn Bay Design-Safety Evaluation and Effect of Variation of Peak Hour Volumes on Intersection Signal Delay Performance

Sonny D. Abia
University of Miami, s.abia@miami.edu

UNIVERSITY OF MIAMI

APPLICATION OF RELIABILITY ANALYSIS TO HIGHWAY DESIGN PROBLEMS: SUPERELEVATION (e) DESIGN, LEFT TURN BAY DESIGN- SAFETY EVALUATION AND EFFECT OF VARIATION OF PEAK HOUR VOLUMES ON INTERSECTION SIGNAL DELAY PERFORMANCE

By

Sonny D. Abia

A DISSERTATION

Submitted to the Faculty
of the University of Miami
in partial fulfillment of the requirements for
the degree of Doctor of Philosophy

Coral Gables, Florida

June 2010

UNIVERSITY OF MIAMI

A dissertation submitted in partial fulfillment of
the requirements for the degree of
Doctor of Philosophy

APPLICATION OF RELIABILITY ANALYSIS TO HIGHWAY DESIGN PROBLEMS: SUPERELEVATION (e) DESIGN, INTERSECTION LEFT TURN BAY DESIGN- SAFETY EVALUATION AND EFFECT OF VARIATION OF PEAK HOUR VOLUMES ON INTERSECTION SIGNAL DELAY PERFORMANCE

Sonny D. Abia

Approved:

Chang-Jen Lan, Ph.D. Town Traffic Engineer Jupiter, Florida	Terri A. Scandura, Ph.D. Dean of the Graduate School
Shihab Asfour, Ph.D. Professor of Industrial Engineering	Wimal Suaris, Ph.D. Professor of Civil Engineering
Charles Nunoo, Ph.D. Senior Highway Design Engineer C3TS, Boca Raton, Florida Adjunct Professor of Civil Engineering Florida International University Miami, Florida	

ABIA, SONNY D. (Ph.D., Civil Engineering)

Application of Reliability Analysis to Highway Design Problems: Superelevation (e) Design, Left Turn Bay Design-Safety Evaluation and Effect of Variation of Peak Hour Volumes on Intersection Signal Delay Performance (June 2010)

Abstract of a dissertation at the University of Miami.

Dissertation supervised by Dr. Chang-Jen Lan.
No. of pages in text (203)

This research has three parts.

Part 1: The *Policy on Geometric Design of Highways and Street* provides 5 methods of superelevation (***e***) distribution. Many states use methods 2 and 5 for low speed, urban and rural high-speed facilities. Method 5 aims to address speed variations; but is complicated, computationally intractable and may violate design consistency. Design recommendation by *NCHRP439* accounts for speed variation, tractable; but is cumbersome along with irregular/step-wise design curves. New reliability based ***e*** distribution method is developed that addresses the speed variation; which is simple in determining and evaluating acceptable required ***e*** rates. At 95% level of reliability, the ***e*** rate obtained is lower than that from current practice resulting in cost savings.

Part 2: Current practice/research does not address safety issue of the left-turn-bay at high degree of saturation (x). Left-Turn-Bay distance has three components: clearance, breaking to a stop and queue. The variation in the queue length reduces clearance and breaking distance resulting in unsafe breaking. Failure = clearance plus breaking distance

< demand. The reliability of the left-turn-bay defined as the availability of the three components for left-turning vehicles to complete clearance and breaking maneuver safely; measured as increase in the deceleration rate over limit of 11.2ft/s^2, safety index and probability of failure. Results show that at 95% reliability, current design practice fails when x exceeds 50%.

Part 3: Current practice uses mean traffic volumes (V_d) as input for traffic signal control at roadway intersections. Variations in traffic flows affect the performance of intersection measured by the delay per vehicle traversing the intersection in seconds. Peak hour factor (PHF), the hourly volume divided by the peak 15-min flow rate within the peak hour is adopted by Highway Capacity Manual (HCM) to control surge. HCM suggests PHF design value of 0.92 for urban and 0.88 for rural areas. Fixed PHF may lead to increase in delay. Effects of variation of peak hour volumes on intersection signal delays are examined with large data. A new model is developed for PHF and V_d and used in signal timing to minimize intersection delay. The results show that the assumption of Poisson distribution for V_d is not reliable; delay reduction of 6.2 seconds per vehicle is achieved. Annual savings in travel time, fuel consumption and emissions cost is estimated in billions of dollars.

Dedication

This dissertation is dedicated to the memory of my father, the late Dan Abia Bassey, a seaman, navigator, philosopher, seer, physician, kind, and intelligent gentleman and to my mother, late Mrs. Arit D. A. Bassey (Nee Arit Okon Esin), A.K.A. Mmamma, the mother of mothers. Her motherhood stretches over many nations and continents. Father, Mother, rest in perfect peace.

Acknowledgement

I wish to express my profound appreciation to Dr. Nanni, the chairperson of the Department of Civil Engineering, for his patience and faith in me over all these years. It gives me great joy to have worked with Dr. Chang-Jen Lan, the chairman of my dissertation committee: I am deeply indebted to Dr. Lan for his guidance, sincerity of purpose, attention to detail, and the wealth of knowledge that he shared freely with me in various discussions throughout the course of this study. To Dr. Asfour, who was willing at a moment's notice to take me under his wing in my sub-specialty of Design and Analysis of Experiments: I say "Thank you". I thank Dr. Suaris and Dr. Nunoo for taking the time to evaluate my work from the qualification exams to the corrections of this dissertation.

To my brother Esin D. Abia, President of Dan Abia's Group of Engineers and Contractors, Miami, Florida, and the Director of Public Works, City of Opalocka: Thank you immensely for your kindness. A brother in need is a brother indeed. I hereby acknowledge with great gratitude and deep devotion, the contribution of my eldest brother, Sir O. D. Abia, KJW, to my education as a child and for his pioneer spirit as well as his able management of the estate of late Dan Abia Bassey, my father; a catalyst for this work.

Although I cannot mention all of the Abia's clan on this page, I would like to thank Hon. Barrister Bassey Dan-Abia, LLM, B.L., the honorable commissioner of NDDC and former Attorney General and Commissioner of Justice, Akwa Ibom State, Nigeria, Dr.

Eyo Dan-Abia, President and CEO of Dan Abia's Specialist Clinic, Uyo, Nigeria, Engineer Dan Dan Abia, ExxonMobile, Eket, Nigeria, Engineer Godwin Dan-Abia, Shell P.D,C. Dem Haag, Netherlands, Chief Mrs. Mary O. D. Attah (Nee Mary Dan Abia), the Obong Anwan of Eket and all members of the Dan Abia and the larger Abia clan: Your prayers and encouragement carried me through this monumental task.

I want to thank my wife, Dr. Inemesit Abia, my sons Abia Abia and Daniel Abia, and last but not least, my daughter, Edikan Abia, for being the best family a man could ever ask for. To Henry Oaikhena, PE, MPA, thank you for taking the time to review this work. A word of thanks also goes to all my friends and colleagues at the University of Miami for their encouragement, and sometimes; bewilderment, at my persistence in completing this doctoral program.

To all the professors, past and present faculty members, and the administrative staff, I say “Thank you” immensely for your kind assistance over all these years. I could not have done this without you.

TABLE OF CONTENTS

Chapter 1: Introduction

The *Policy on Geometric Design of Highways and Street* published by AASHTO prior to 2005, commonly known as the "*Green Book*", provides 5 methods of super elevation distributions. The *Green Book* and the majority of States' Department of Transportation use methods 2 and 5 for distributing superelevation rates for low speed, urban and rural high speed facilities, respectively. Method 5 combines technical merits of Methods 1 and 4 and distributes average superelevation rates between methods 1 and 4 based on a complicated asymmetric parabolic curve. It aims to (1) increase superelevation rates and safety margin for accommodating speed variation that is not assumed in Method 1; and (2) attenuate friction factor at sharper curves to avoid erratic driving which is inherent in Method 4. Although the rationale behind Method 5 is deemed reasonable, its complicated formulation makes it intractable for manual computation. In addition, as mentioned in *NCHRP439*, Bonneson (2000), the use of Method 5 could lead to a violation in design consistency, which stems from significantly different superelevation rates for curves of similar radius due to the use of multiple maximum superelevation rates on nearby facilities. As a consequence, As a consequence, the *NCHRP439* recommended *the incorporation* the superelevation distribution method provided by *NCHRP439 into the Green Book*. Compared to Method 5, *NCHRP439* method explicitly takes into account speed variation and is much more tractable in computation due to the use of simple exponential curve. However, the procedure is cumbersome and results in irregular or step-wise design curves. Also, there is no significant difference between the use of 95th percentile speed with speed reduction margins and the current design approach using 85th percentile speed for the design speed. It can also be argued that the *NCHRP439* imposition of maximum super elevation rate when the model fails is arbitrarily and unscientific. This research develops an alternative distribution method by addressing the speed variation issue based on reliability analysis. The proposed distribution method is simple, and can be used to (a) determine the required superelevation rates at a specific level of reliability that is acceptable for a particular design and region; and (b) evaluate existing curve to determine its reliability to speed variation. The result shows that at 95% level of reliability, the superelevation rate obtained using reliability analysis is lower than that from method 5 and *NCHRP439*. This is expected to represent cost saving when the excess embankment required using method 5 is minimized or eliminated.

It can also be argued that, this approach ensures a reliable level of ***e*** and ***f*** that will account for a wide range of drivers' speed on any given curve. It will also ensure that the potential risk of design uncertainties in ***e***-distribution design will be limited to those outside the reliability limits used in the design. Thus, justification and higher confidence or reliability is achieved in the design and such design is defensible in a litigated society. With this approach, the Engineer of Record (EOR) can confidently defend his design knowing that the risk of failure have been analyzed and accounted for in the design. And when failure occurs in the form of an accident, the reliability analysis can be performed to determine that the speed that led to failure in the system lies outside the acceptable design range. The current definition of the design speed by *AASHTO 2001* as "a selected speed used to determine the various geometric design features of the highway" supports this notion. The design speeds is now applied as an input for geometric features of the highway based on other factors, such as topography, functional classification, expected operating speed and the adjacent land use (AASHTO 2004). It is no longer considered as the maximum safe speed for which a vehicle can operate in a particular highway which led to difficulties in defending failure at speed below that of the design speed (AASHTO 1994).

This risk therefore, can be considered as an outlier, small and insignificant depending on the level of reliability adopted for the design. The result is that the higher the level of reliability, the lower the risk and vice versa. A better argument can be put forth that crashes outside the reliability limits, are beyond design controls and cannot be accounted for in the design within any reasonable or practical design values. This is also true when considering the limitations of other factors such as vehicle performance, pavement condition, roadway geometry, driver, environmental conditions, tire condition and others.

The Green Book also provides design guidance for left turn bay design at an intersection of crossing roadways at grade. The guidance relates to length of the left turn bay, traffic volumes and intersection control mechanism such as stop signs and signals and other intersection controls provided by Manual of Uniform Traffic Devices (MUTCD) Evaluation of the effectiveness of the left turn bay for safety or the reliability of the left turn bay is largely not covered by the green book but is deferred to traffic engineering operations as presented in Highway Capacity Manual (HCM 2000) in terms of intersection delay, its ability to handle a given volume. HCM and other traffic engineering publications and practice do not address the inherent safety issue of the turn bay in which a saturation condition of the turn bay is exceeded. This research presents a methodology to evaluate the reliability of a left turn bay based on its geometry and the traffic demands. There are three components in the length of left turn bay design: (1) Clearance distance, 2) breaking to a stop distance and 3) the length of storage or queue length after breaking to a stop is complete (FDOT Standard Index 2008). AASHTO and FDOT criterion is to design the intersection with a minimum of two cars length on the queue storage while the clearance and breaking distances are based on design speed, reaction time and average deceleration rate. The variation in the queue length reduces the availability of the other two components (clearance and breaking distances) and thereby decreasing the ability of the driver to clear the thru lane and come to a stop safely. Failure occurs when the available length of clearance distance plus the breaking distance is less than the demand. The reliability of the turn bay can be evaluated based on the geometry as the length of the turn bay is reduced by a successive number of cars exceeding the queue length or storage distance. The reliability of the left turn bay with respect to safety therefore, is the availability of the clearance, breaking and storage distance for left turning vehicles in any given period to complete clearance and breaking maneuver without shock to the traffic downstream. This research will develop the methodology for determining this shock in terms of increase in the deceleration rate over the AASHTO specified limit of 11.2ft/s^2 as well as the probability of failure of the lane to perform as intended.

Current practice uses mean traffic volumes as input for traffic signal control at roadway intersections. Variations in traffic flows affect the performance of intersection performance measured by the delay experience per vehicle traversing the intersection in seconds. In order to account for surge in the traffic stream, Peak hour factor (PHF), which is the ratio of the hourly volume divided by the peak 15-min flow rate within the peak hour is adopted by the Highway Capacity Manual (HCM). The use of PHF allows queue discharge at an intersection which may have built up during a short period surge. HCM suggests a design value for PHF of 0.92 for congested urban areas and 0.88 for rural areas if there is no field measurement available. Variation in traffic volumes does not lend itself to fixed PHF values as the PHF also vary with respect to time within the peak periods. Using these fixed values may not allow optimal signal operation and may allow a level of delay not proportionate to the prevailing traffic conditions. In view of this concern, a study to explore the effect of variability of the peak hour volumes on the design hourly volume and intersection delays performance was conducted. This study is divided into three sections. First, a model of PHF as a function of the degree of saturation (x- volume-to-capacity ratio) on surface streets is developed. A total of 1669 data points were obtained from the West Palm Beach County and Broward County area. The results show that, among several functional forms, the simple power function established with functional classification of roadways could be used to explain 47% (R^2) of data variation, which is considered well acceptable given the significant variability presented by the data (standard deviation of the prediction error is about 7.7% of the observed values). The 95th percentile confidence intervals on the mean estimates are also provided. The average standard deviation of the mean estimate error is around 0.26% (30 times smaller compared to the data variability), suggesting the proposed mean estimates are fairly reliable. The model is found to be transferable with view to universal application. In section two, a new model is developed that relates the standard deviation of the flow rate to the mean flow with high coefficient of determination (R^2) of 76%. It is also established that modeling the variation of the design hourly volumes with respect to the coefficient of variation (*CV*) is not reliable as it returns very low coefficient of determination *(R^2 = 0.15)- Hellinga and Abdy (2008)*. The two models are combined in section three to examine the effect of the variation of the design hourly volumes on intersection signal delay using simulation. The results show that the assumption of Poisson distribution for quantification of design hourly volume is not reliable as actual data analysis did not fit the Poisson model. It is also established that traffic signal delays varies with respect to variation of the design hourly volume and thus adaptive signal system would be advantageous. The savings in time of travel, fuel consumption and automotive exhaust emissions cost can be estimated in billions of dollars annually.

1.2 Objectives of the Research

The objectives of this study include:

(1) In the first segment, the objective is to demonstrate the application of reliability analysis to highway design problems with regards to superelevation design. The current method of determining superelevation distribution for highway curve design is cumbersome and intractable. It does not account for variations in operating speeds of various drivers traversing the highway horizontal curve. This research will present a simple and tractable method of determining superelevation rates for the design of highway curves that account for the variability in the design speed and the friction factor; and can be used easily both for design and the evaluation of the existing highway curves. A methodology for computing the reliability index of the superelevation rate used in the design of the highway curve will be provided.

(2) Provide a comparison between the current methods and the proposed reliability analysis method. This is accomplished through the use of computations, tables and charts.

(3) Present worked example and show the advantage of adopting the reliability analysis approach.

In the second segment, the objective will be:

(1) To demonstrate a methodology to evaluate the reliability of a left turn bay based on its geometry and the traffic demands with respect to safety. As a consequence of this effort, present the design of the adequate length of a left turn bay.

(2) Present worked examples and demonstrate the safety effect of inadequate length of left turn bay with respect to safety. This is measured through Safety Index, Safety Margin and Deceleration rates.

(4) Develop new theory and formulate new equation for time gap (T_g) as used in intersection Gap Acceptance Theory for Unsignalized Intersection.

In the third segment the objective will be:

(1) To develop a study of the effects of the variation of the traffic peak hour volumes on the intersection delays performance using large traffic count data. Current practice uses mean values of volumes and peak hour factors (PHF) for intersection signal delays analysis. Available prediction models for peak hour factor is limited and based on small data and equation that is not transferable from one region to another. Ignoring variation in the design hourly volume (V_d) and the PHF may result in inefficient intersection signal delays. This research will develop new models for PHF and V_d and use these models as input to determine the effects of

the variation of the design hourly volumes on the intersection signal delays. This effect will be measured in terms of intersection delay reduction in seconds per vehicle, cost of delays and reduction in exhaust gas emissions. These will be accomplished through the use of statistical analysis, optimization technique using computer program-MATLAB6p5, 2002. The results will be presented in charts and tables.

1.3 Organization of the Research

This research is organized into 7 chapters. Chapter 1 contains the overview and general motivation for this research. In chapter 2, the author conducts an extensive literature review on superelevation distribution methods used in highway design and application of reliability to highway design problems as related to intersection of left turn bay design and safety evaluation and the effect of variation of design hourly volumes on intersection delays performance. Chapter 3 presents the methodology adopted for this research. A brief description of deterministic and probabilistic approach to engineering design is presented. First Order Second Moment Method (FOSM) of reliability analysis using Taylor's approximation is presented and brief descriptions of other methods of analysis are included. In Chapter 4, the author present new design approach to superelevation design using reliability analysis. This chapter also includes application of the methods developed in chapter 3 and worked examples are presented. A comparison of Reliability Design Method is made with AASHTO's and NCHRP439 Methods of superelevation design. Chapter 5 is the application of reliability analysis to left-turn bay design and safety evaluation. The design equation is formulated based on the geometry of the intersection. Worked examples are provided and adequate left-turn bay is computed. A new time gap formulation is presented with suggested new values for time gap required for multiple lane analysis. The result is compared with AASHTO's and FDOT methods. Chapter 6 explores the effects of variation of the design hourly volumes on the intersection signal delays performance using large data from the state of Florida. New models for PHF and V_d are developed and the equations for the models are also presented. The data analyses are presented in charts and tables. Results and conclusions are summarized in each section; a general summary for the chapters is presented in chapter 7 along with the future work. One Appendix is provided; appendix A. Appendix A contains data used in the effects of design hourly volumes on the intersection signal delays performance presented in chapter 6.

Chapter 2: Literature Review

Review of Superelevation Distribution Methods

2.1 Background:

Superelevation is the tilting or rotation of a highway on a horizontal curve to resist or act against some of the lateral forces arising from the motion, weight, speed and directional change of the vehicle. The relationship of the speed, friction forces between the tires and the pavement, curve radius and the superelevation rate have been developed empirically and used in the design equation of horizontal curve since in the 1940s. It is the basis for the derivation that will be developed in chapter three of this study. When one side of the highway is raised in this way, the highway is said to be superelevated. The rotation or banking of the highway is used on speedways in motor sports racing as well as in urban and rural highways (1). A highway may be revolved about the centerline or inside edge or outside edge of the profile or straight cross slope of the highway may be revolved about the outside edge (ASHTTO 2001). The question then arises as to how much should the highway be rotated to keep the vehicles save while traversing a horizontal curve on a highway at or near the design speed or without slower the slower vehicle sliding down the slope of the superelevated roadway.

2.2 Maximum Superelevation Rates:

According to AASHTO, the maximum rates of superelevation adopted for highways are controlled by four factors:

1) Climate conditions- this pertains to the frequency and the quantity of snow and ice.

2) Terrain Condition- this pertains to whether the terrain is flat, rolling or mountainous.
3) Type of area-whether urban or rural.
4) Frequency of very slow moving vehicles- vehicles whose operations might be affected by higher superelevation rates. A very slow moving vehicle in an icy road might slide down the slope of a high superelevated road and on the other hand a fast moving vehicle in a rural road might turn over in a low superelevated roadway.

Based on these realities, AASHTO concludes that there is "no single maximum superelevation rate that is universally applicable and that a range of values should be used". The following recommendation for maximum superelevation rates is provided:

1) 4% to 6% for design of urban highways in areas where there are no constraints.
2) 8% for areas with snow and ice.
3) 10% to 12% for areas where there are no snow or ice.

These different maximum superlevation rates, according to *NCHRP439*, pose another dilemma, a violation of driver's expectancy. Because of these different maximum superelevation rates, a review of the *Green Book* shows that there are different super elevation rates for each of the maximum superelevation rate for the same design speed. Thus, the necessity to provide a method of distributing the superelevation rate that solves this dilemma becomes imperative.

In 1965, Association of State Highway and Transportation Officials (ASHTO) published the Book, Geometric Design of Rural Highway. This guideline contained 5 methods of superelevation distributions, which have been used, for curve design for the last 40 years.

To allow for the continuity of the reader of this study, these 5 methods as contained in AASHTO2001, are described here in this section as follows:

2.3 Method 1: Superelevation and side friction are directly proportional to the inverse of the radius (i.e., straight line relationship exists between $1/R = 1/R_{min.}$ as shown by curve 1 in figure 1. (Exhibit 3-12A *Green Book*).

The *Green Book* also provides the following discussion with respect to method1:

> The straight-line relationship between superelevation and the inverse of the radius of the curve in method 1 results in a similar relationship between side friction and the radius for vehicles traveling at either the design or average running speed. This method has considerable merit and logic in addition to its simplicity. On any particular highway, the horizontal alignment consists of tangents and curves of varying radius greater than or equal to the minimum radius appropriate for the design speed (R_{min}). Application of superelevation in amounts directly proportional to the inverse of the radius would, for vehicles traveling at uniform speed, result in side friction factors with a straight-line variation from zero on tangents (ignoring cross slope) to the maximum side friction at the minimum radius. This method might appear to be an ideal means of distributing the side friction factor, but its appropriateness depends on travel at a constant speed by each vehicle in the traffic stream, regardless of whether travel is on a tangent, a curve of intermediate degree, or a curve with the minimum radius for that design speed. While uniform speed is the aim of most drivers, and can be obtained on well-designed highways when volumes are not heavy, there is a tendency for some drivers to travel faster on tangents and the flatter curves than on the sharper curves, particularly after being delayed by inability to pass slower moving vehicles. This tendency points to the desirability of providing superelevation rates for intermediate curves in excess of those that result from use of method 1.

From the foregoing, method 1 accounts for the variation in friction factor in relation to change in speed, however, all vehicles must drive at constant speed. This is not always possible as speed variations occur all the time since drivers do not drive at constant speed. On the other hand, method 1 represents the physical condition of vehicle traversing a superelevated curve. This research will explore this method and account for the variation in speed and take advantage of the variation in friction factor too.

Nicholson (1998) has shown that Method 1 can be expressed mathematically as follows:

$$e = \frac{R_{\min}}{R} e_{\max} ; f = \frac{v^2}{gR} - \frac{R_{\min}}{R} e_{\max} ; R_{\min} \le R \le \infty \qquad 2.1$$

This can be further expressed as:

$$e = \frac{e_{\max}}{e_{\max} + f_{\max}} \frac{v^2}{gR} \qquad f = \frac{f_{\max}}{e_{\max} + f_{\max}} \frac{v^2}{gR} ;\ R_{\min} \le R \le \infty \qquad 2.2$$

It can be seen that method 1 has the connotation that the centrifugal force due to superelevation and side friction when R is greater than $R_{\min}$ are the same as when $R = R_{\min}$. (Nicholson, 1998).

2.4 Method 2:

In method 2, side friction is such that a vehicle traveling at design speed has all lateral acceleration sustained by side friction on curves up to requiring f_{max} superelevation is then used until e reaches $e_{max.}$ In this method, first f and then e are increased in inverse proportion to the radius of curvature, as shown by curve 3 in figure 1. (Exhibit 3-12B *Green Book*).

Discussion on Method 2:

The *Green Book* offers the following discussion on method 2:

> Method 2 uses side friction to sustain all lateral acceleration up to the curvature corresponding to the maximum side friction factor, and this maximum side friction factor is available on all sharper curves. In this method, superelevation is introduced only after the maximum side friction has been used. Therefore, no superelevation is needed on flatter curves that need less than maximum side friction for vehicles traveling at the design speed (see curve 2 in Exhibit 3-12A). When superelevation is needed, it increases rapidly as curves with maximum side friction grow sharper. Because this method is completely dependent on available side friction, its use is generally limited to locations where travel speed is not uniform, such as on urban streets. This method is particularly advantageous on low-speed urban streets where, because of various constraints, superelevation frequently cannot be provided.

This is the method adopted by most state agencies in the design of low speed urban streets, Florida Department of Transportation (FDOT) for example, (FDOT-Plans Preparation Manual (PPM), Volume 1, chapter 2). This method cannot be used for higher speed for sharper curves because of its dependent on available friction. At high speed, many drivers can exceed this maximum friction easily; the risk of skidding and loss of control becomes higher as the curve gets sharper.

Nicholson (1998) has shown that Method 2 can be expressed mathematically as follows:

$$e = \frac{v^2}{gR} - f_{\max}; f = f_{\max}; R_{\min} \le R_{jo} \qquad 2.3$$

$$e = 0;\ R_{jo} \le R \le \infty \qquad 2.4$$

Where the smallest radius when relying on side friction only is:

$$e = \frac{v^2}{gf_{\max}} \qquad 2.5$$

2.5 Method 3: superelevation is such that a vehicle traveling at the design speed has all the lateral forces sustained by superelevation on curves up to that requiring $e_{max.}$ For sharper curves, e remains at e_{max} and side friction is then used to sustain lateral acceleration until f reaches $f_{max.}$ In this method, first e then f is increased in inverse proportion to the radius of curvature.

Nicholson (1998) has shown that Method 3 can be expressed mathematically as follows:

$$e = e_{\max}; f = \frac{v^2}{gR} - e_{\max}; (R_{\min} \le R \le R_{eo}) \qquad 2.6$$

And

$$e = \frac{v^2}{gR} ; f = 0 ; R_{eo} \leq R \leq \infty \qquad 2.7$$

Where the smallest radius when relying on superelevation only is:

$$e = \frac{v^2}{ge_{\max}} ; (R_{eo} \leq R \leq \infty) \qquad 2.8$$

Discussion on Method 3:

The *Green Book* provides the following discussion on method 4:

> In method 3, which was practiced many years ago, superelevation to sustain all lateral acceleration for a vehicle traveling at the design speed is provided on all curves up to that needing maximum practical superelevation, and this maximum superelevation is provided on all sharper curves. Under this method, no side friction is provided on flat curves with less than maximum superelevation for vehicles traveling at the design speed, as shown by curve 3 in Exhibit 3-12B, and the appropriate side friction increases rapidly as curves with maximum superelevation grow sharper. Further, as shown by curve 3 in Exhibit 3-12C, for vehicles traveling at average running speed, this superelevation method results in negative friction for curves from very flat radii to about the middle of the range of curve radii; beyond this point, as curves become sharper, the side friction increases rapidly up to a maximum corresponding to the minimum radius of curvature. This marked difference in side friction for different curves is not logical and may result in erratic driving, either at the design or average running speed.

The inherent problem with this method is that different curves have different side friction depending on the sharpness of the curves. It is not also physically true that there is no side friction between the tires and the pavement. Side friction is always present in the tires since it is a function of the weight of the car normal to the pavement surface. Friction allows cornering, braking, and acceleration forces to be transmitted from the tires to the pavement. Rather than using the “coefficient of friction” from dynamics, highway engineers use a ratio of the lateral forces that the pavement can resist. This lateral ratio is most commonly referred to as the “friction factor.” (AASHTO 1984).

The friction factor to counter centrifugal forces is reduced by vehicle braking (decelerating) and accelerating. For example, when most of the friction is used for a sudden stop, there is little friction available for cornering. Antilock Braking Systems

(ABS) has greatly improved this aspect. The friction factor also depends on numerous variables, including the vehicle speed, weight, suspension, tire condition (wear, tire pressure, tire temperature), tire design (tread, contact patch, rubber compound, sidewall stiffness); pavement, and any substance between the tire and pavement. Since the friction factor decreases as speed increases, numerous studies have been performed to develop friction factors for various speeds (AASHTO 2001). Note that the friction factor diminishes substantially when the tires are spinning faster or slower than the vehicle speed (e.g., in a skid, spinning tires when attempting to accelerate or stop on ice, and during a "burn out" or "peel-out"). Thus, a better approach to the distribution method would have to take into the account the simultaneous effect of the superelevation and the side friction on the vehicle traversing a curve. The application of method 3 results in erratic driving at both the design speed and average running speed. This simultaneity of the friction and the superelevation effects in addition to the variation in speed is demonstrated in chapter 4 of this study.

2.6 Method 4:

This method is the same as method 3, except that it is based on average running speed instead of design speed.

Based on figure 3-6A (*Green Book 1990),* it follows then that, e which is related to the degree of curvature (D) of the curve and side friction, must satisfy 3 conditions:

(1) $e = 0$ when $D = 0$ (or $R = \infty$);

(2) $e = e_{\max}$ when $D = D_{\max}$ (or $R = R_{\min}$); and

(3) $\frac{\partial e}{\partial D} = 0$ when $D = D_{\max}$ (or $R = R_{\min}$);

Nicholson (1998) has shown that Method 4 can be expressed mathematically as follows:

$$e = e_{\max}\frac{R_{\min}}{R}(2-\frac{R_{\min}}{R});\ f = \frac{v^2}{gR} - e_{\max}\frac{R_{\min}}{R}(2-\frac{R_{\min}}{R});$$

2.10

$$(R_{\min} \le R \le \infty)$$

Discussion on Method 4:

The *Green Book* provides the following discussion on method 4:

> Method 4 is intended to overcome the deficiencies of method 3 by using superelevation at speeds lower than the design speed. This method has been widely used with an average running speed for which all lateral acceleration is sustained by superelevation of curves flatter than that needing the maximum rate of superelevation. This average running speed was an approximation that, as presented in Exhibit 3-26, varies from 78 to 100 [80 to 100] percent of design speed. Curve 4 in Exhibit 3-12A shows that in using this method the maximum superelevation is reached near the middle of the curvature range. Exhibit 3-12C shows that at average running speed no side friction is needed up to this curvature, and side friction increases rapidly and in direct proportion for sharper curves. This method has the same disadvantages as method 3, but they apply to a smaller degree.

The same comment as in method 3 can be offered for method 4 despite the use of speed lower than the design speed; in this case, the average running speed. In both cases, the physical effects of the friction, speed variation and superelevation are not taken together. The result is the same as that of method 3, erratic driving may occur both at the average running speed and the design speed.

2.7 Method 5: Superelevation and side friction are in a curvilinear relationship with the inverse of the radius of curve, with values between those of methods 1 and 3. Method 5 employs a curvilinear distribution method based on an unsymmetrical parabolic curve for the distribution of ***f*** that is tangent to the two legs defining method 4. Subtracting the ***f*** values from the design values of ***(e + f)*** from the simplified curve equation for ***e***, the final distribution of ***e*** is then obtained. The mathematical formulation of method 5 is explicitly written in the *Green Book*; hence, it is omitted here. However, the comparison of the method 5 results is included in chapter 4.

Discussion on method 5:

The *Green Book* offers the following discussion on method 5:

> To accommodate overdriving that is likely to occur on flat to intermediate curves, it is desirable that the superelevation approximate that obtained by method 4. Overdriving on such curves involves very little risk that a driver will lose control of the vehicle because superelevation sustains nearly all lateral acceleration at the average running speed, and considerable side friction is available for greater speeds. On the other hand, method 1, which avoids use of maximum superelevation for a substantial part of the range of curve radii, is also desirable. In method 5, a curved line (curve 5, as shown within the triangular working range between curves 1 and 4 in Exhibit 3-12A) represents a superelevation and side friction distribution reasonably retaining the advantages of both methods 1 and 4. Curve 5 has an unsymmetrical parabolic form and represents a practical distribution for superelevation over the range of curvature.

Method 5 incorporates the advantages of method 4 and 1 to produce a practical distribution for superelevation over a range of curvature by simply drawing a best-fit curve over a region of space considered to be reasonable and practical. Although this produces the desired result, its computation is cumbersome, intractable and cannot be easily used in practice. It requires solving 14 different equations in order to produce a distribution curve for design. Hence, 10 charts and table are provided in the *Green Book* for use in the design.

2.8 Fundamental Issues in Superelevation Design

From the foregoing, two fundamental approaches to superelevation distribution emerge:

(a) superelevation is used in a limited way and reliance on friction factor for cornering as in method 2 and (b) heavy dependent on superelevation along with minimum friction factor needed for faster drivers while the slower drivers make use of superelevation for added safety. This approach guards against negative friction, which may force drivers to steer against the direction of the curve, which is unsafe and may result in erratic driving (*NCHRP 439*). This research provides a simple and tractable approach to superelevation distribution through the use of reliability analysis. It combines the advantages of method 1 and the intent of method 5 and account for the variation in speed, friction factor and the simultaneous effect of all these three factors on a vehicle traversing a horizontal curve at the design or speeds lower than the design speed.

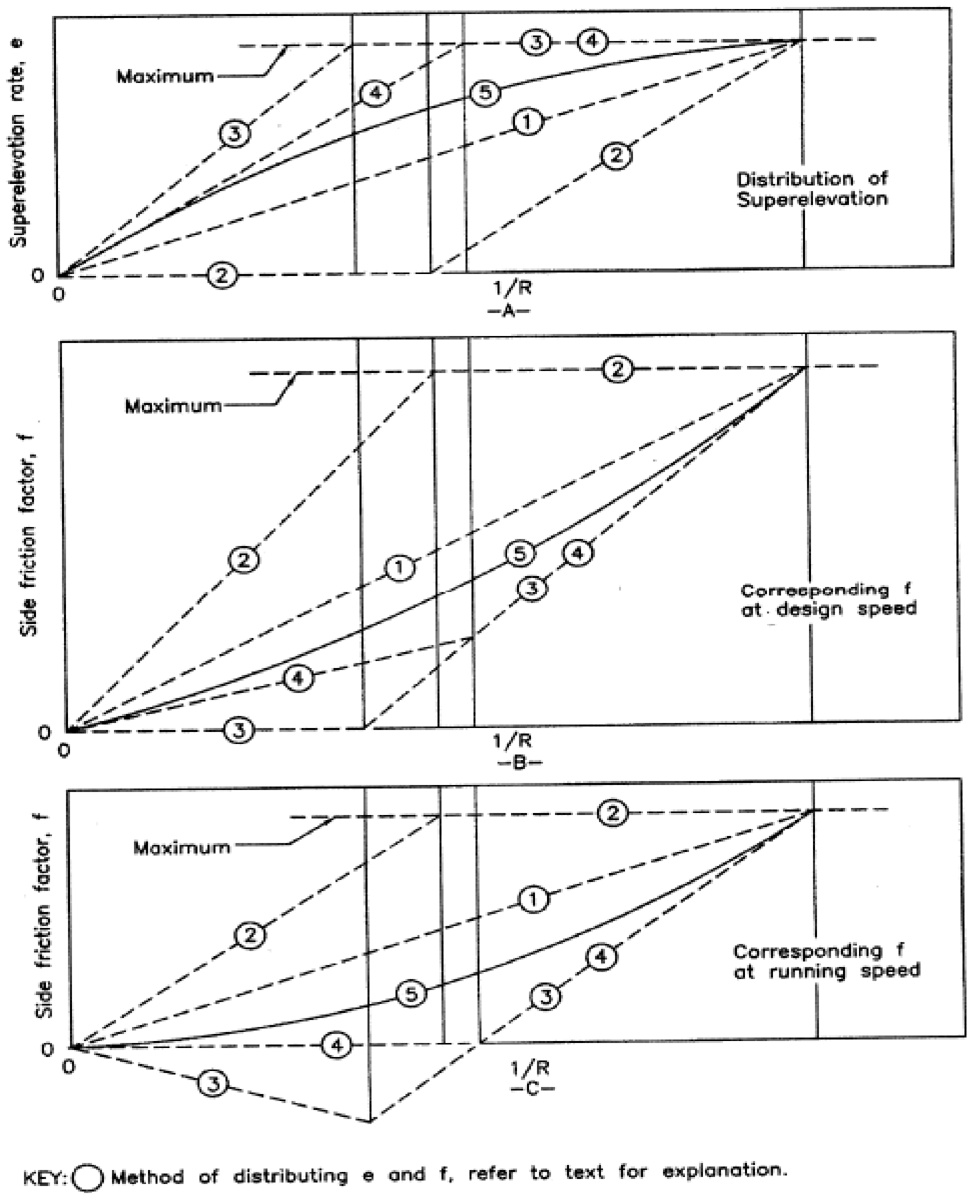

Exhibit 3-12. Methods of Distributing Superelevation and Side Friction

139

Exhibit 3-12 from the *Green Book* 2004 Edition.

2.9 Review of NCHRP 439: This publication provides a simplified distribution method that is similar to that provided by the *Green Book*. It recommends two methods of developing superelevation as illustrated in Exhibits 4 & 5. Method 1 is for low speed urban streets and method 2 is for rural highways and high-speed urban streets. Method 2 is also recommended for turning roadways. The values provided in the *NCHRP439* distribute superelevation similar to *Green Book*'s Method 2 and 5. For rural high speed facilities, superelevation is increased at a higher rate than the need for side friction as the curves radii are decreased. For low speed and turning roadways, side friction is used first as the radii decrease. Superelevation is added when the radii are decreased beyond what side friction can sustain. In order to eliminate the availability of different superelevation rates for the same design speed, and curve radius, *NCHRP439* proposes minimum and maximum superelevation rates as boundary values. These boundary values are used to evaluate the superelevation rates recommended by the *Green Book*. In order to correct the observed limitations of the *Green Book*, two equations are proposed: (1) equation to predict minimum superelevation rate that can be used without causing an excessive side friction demand (based on 95th percentile speeds for passenger cars) and (2) equation to predict the maximum superelevation rates without causing excessive counter steer (based on 5th percentile truck speed). These are the two extreme undesirable driving conditions that can limit safety for drivers traversing a superelevated curve. Thus *NCHRP439* developed seven different equations for superelevation distributions for rural high-speed facility for a given speed and radius that is between these two extremes. The lower limit is controlled by the minimum radius (maximum side friction factor) while the upper limit is controlled by maximum superelevation rate (minimum friction factor). The equations are described as follows:

$$e_d = e^*_{\max}\left(\frac{R^*_{\min}}{R}\right)^n \qquad 2.11$$

With

$$n_e = \frac{\ln(-0.01e_{NC}) - \ln(.01e^*_{\max})}{\ln(R^*_{\min}) - \ln(R_{NC})} \quad 2.12$$

Where:

e_d = design superelevation rate, percent;

$e^*_{\max}$ = defining maximum superelevation rate, percent;

$R^*_{\min}$ = defining minimum radius, (meters);

n = shape factor;

R = radius of curve;

R_{NC} = minimum radius with normal cross slope;

ln(x) = natural log of x; and

e_{NC} = normal cross slope rate (-2.0 percent assumed) percent.

and the defining $e_{\max}$ and the defining $R_{\min}$ are given as follows:

$$e^*_{\max} = 100\frac{r_v f_{\max} + 0.015}{1 - r_v} \quad 2.13$$

and

$$R^*_{\min} = \frac{V_c^2}{127(0.01e^*_{\min} + f_{\max})} \quad 2.14$$

with

$$r_v = \frac{(V_{5,tk} - d_{v,tk})^2}{V_c} \quad 2.15$$

Where:

$$V_{5,tk} = 0.3256V^{1.167} \quad 2.16$$

$$d_{v,tk} = 0.763 d_v \qquad 2.17$$

Where:

$f_{\max}$ = maximum design side friction factor (from table III-6, *NCHRP439*)

V_c = Curve design speed (V- d_v), Km/h;

V design speed Km/h;

d_v = assumed speed reduction, Km/h from Table III-7 *NCHRP439*.

$V_{5,tk}$ = 5th percentile truck approach speed, km/h;

$d_{v,tk}$ = 5th truck speed percentile reduction, km/h and

r_v = ratio of truck to passenger car curve speed.

These equations produce maximum superelevation rates larger than currently used in practice and the authors of NCHRP439 recommends the imposition of the agency's maximum superelevation rate should the calculated maximum superelevation rate be greater than the agency's use. The result of the application of these equations is the resulting "stair stepped" curve shown in exhibit III-6.

Exhibit 4 - NCHRP 439 Distribution Method for Low Speed Urban Streets

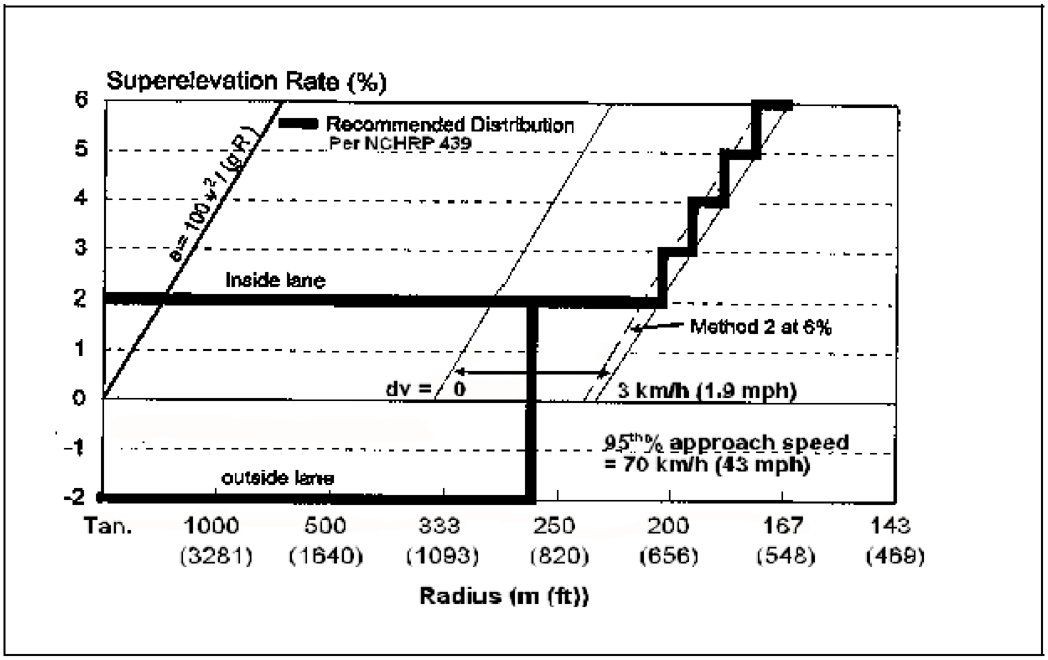

Exhibit 5 - NCHRP 439 Distribution Method for Rural Highways ad High Speed Urban Streets

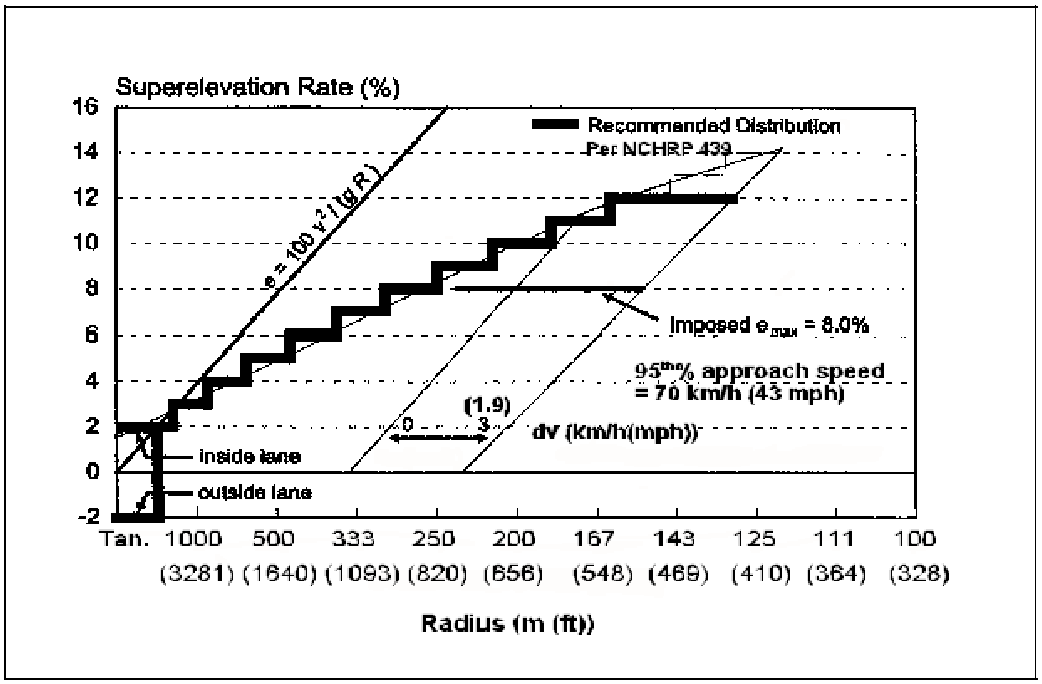

For the low speed facility, the NCHRP439 provides the following equation:

$$e_d = 100\left(\frac{v_c^2}{127R}\right) - f_{\max} \tag{2.17}$$

Where:

e_d = design superelevation rate, percent;

R = radius of curve, m;

v^2 = curve

Recommendations for AASHTO Superelevation Design September, 2003 Page 8 of 14

NCHRP uses the 95th percentile approach speed for curve design. The basis for the 95th percentile speed rather than 85th percentile speed is due to the higher probability of failure for inadequately designed horizontal curves. Speed is the only variable that determines if the vehicle can negotiate a curve under prevailing conditions. Unlike stopping sight distance, events such as a fallen object, animal, or a second vehicle are not required to cause an accident if the vehicle is traveling too fast around the curve. As shown in Exhibit 6, a small speed reduction is used for the minimum radii for a given maximum superelevation rate. This is based on observations of motorists slowing before entering sharp radius curves, as illustrated in Exhibit 7.

Exhibit 6 - *NCHRP439* Speed Reduction Values

Design Speed	Speed Reduction
30 km/h to 100 km/h (20 - 60 mph) 110 km/h (70 mph) 120 km/h (75 mph)	3 km/h (1.9 mph) 4 km/h (2.5 mph) 5 km/h (3.1 mph)

Exhibit 7 provides a comparison of speeds on the tangent and curve portions of a highway. The

Comparison illustrates that the 85th percentile tangent speed is comparable to the 95th percentile

Curve speed used in *NCHRP439*.

Exhibit 7 - Comparison of Tangent and Curve Speeds

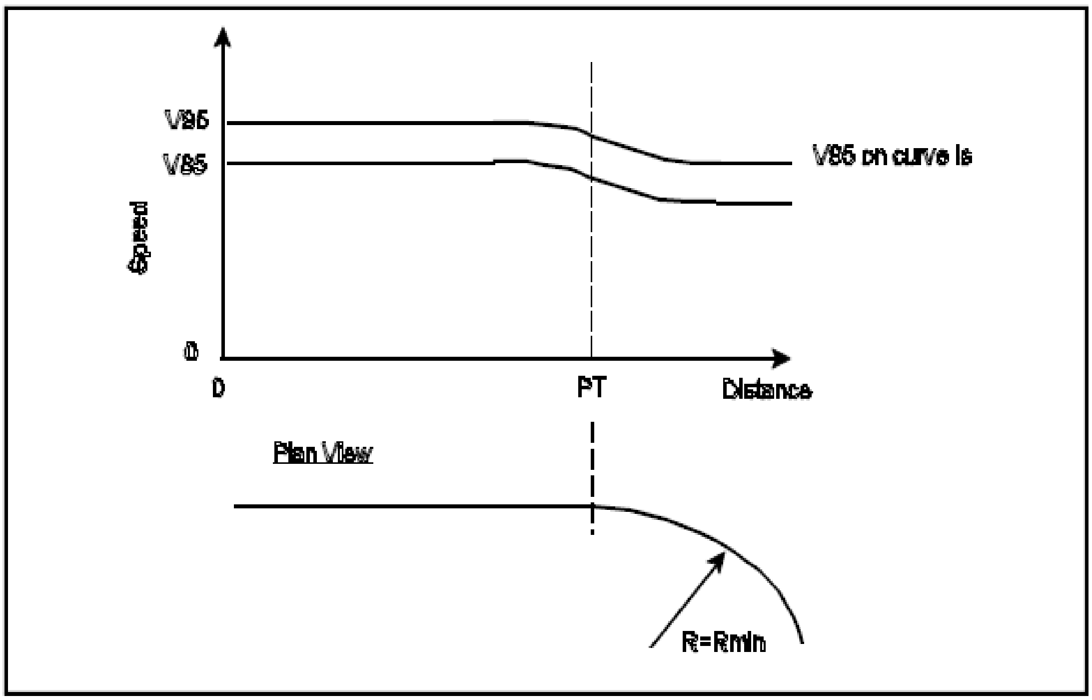

(Courtesy: J. A. Bonneson, May, 2002)

Exhibit 8 provides a comparison of speeds based on speed studies at 13 locations in New York

State. The locations included various functional classes and legal speed limits. Sample sizes

ranged from 104 to 39,236 vehicles. The comparison illustrates that the *NCHRP439* design speed Method is ± 4 km/h (3 mph) of the 85th percentile speed.

Exhibit 8 - Comparison of Design Speeds

95th Percentile Speed Km/h (mph)	95th Percentile Speed with Speed Reduction Km/h (mph)	85th Percentile Speed	Difference between 95th Percentile Speed Km/h (mph)
64 (40)	61 (38)	63 (39)	- 2 (-1)
77 (48)	74 (46)	76 (47)	- 2 (-1)
97 (60)	94 (58)	95 (59)	- 1 (-1)
97 (60)	94 (58)	95 (59)	- 1 (-1)
81 (50)	78 (48)	76 (47)	+ 2 (+1)
77 (48)	74 (46)	76 (47)	- 2 (-1)
74 (46)	71 (44)	72 (45)	- 1 (-1)
97 (60)	94 (58)	95 (59)	- 1 (-1)
105 (65)	101 (63)	98 (61)	+ 3 (+2)
101 (63)	98 (61)	97 (60)	+ 1 (+1)
118 (73)	113 (70)	111 (69)	+ 2 (+1)
116 (72)	112 (70)	108 (67)	+ 4 (+3)
87 (54)	84 (52)	81 (50)	+ 3 (+2)

Ottesen and Krames (1999***)*** also evaluated speed reduction from tangent to curve and found that the 85th percentile speeds on curves with degrees of curvature less than 4 degrees do not differ significantly from the 85th percentile speeds on long tangent. The implication here is that, the use of speed reduction prior to curve for curve design and the current use of 85th percentile speeds on tangents for curve design produces the same result. As a result, some States Department of transportation, such as Florida and New York prefer to use the current approach as proposed by ASHTTO.

Although these equations are tractable compared to method 5, there are still too many factors that may not be universally applicable such as: assumed speed reduction, 5th percentile truck approach speed, 5th truck percentile reduction and ratio of truck to passenger car curve speed. It appears that these assumptions have not taken cognizant of the new technology in automobile production and the associated performance whereby the stability and traction of light and heavy trucks have been greatly improved. Also, a stair-step function is more of a discrete function, which is contrary to the dynamics of vehicle in motion along a horizontal curve. Speed selection by various drivers along a horizontal curve is not fixed. The idea of a discrete function to describe this event will tend to require a constant speed which is not possible as various drivers with different cars with different levels of performance select different speed based on their level of comfort to avoid erratic driving or steering. Variation in speed must therefore be accounted for in the design of the curve. The reliability analysis approach accounts for the variation in speed and provide a distribution method that will accommodate a wide range of these variation depending on the level of reliability selected.

2.10 Other International Agencies Approach to Superelevation Distribution

NCHRP439 include a review of 6 international agencies and reported that four of the six agencies in question have distribution methods that provide a continuous mathematical relationship among superelevation, radius, and design speed or an equivalent table. These international agencies include Germany, France, United Kingdom and Canada. The figure below (taken from *NCHRP439*) shows a comparison of these mathematical relationships among these agencies as well as the United States and Canada.

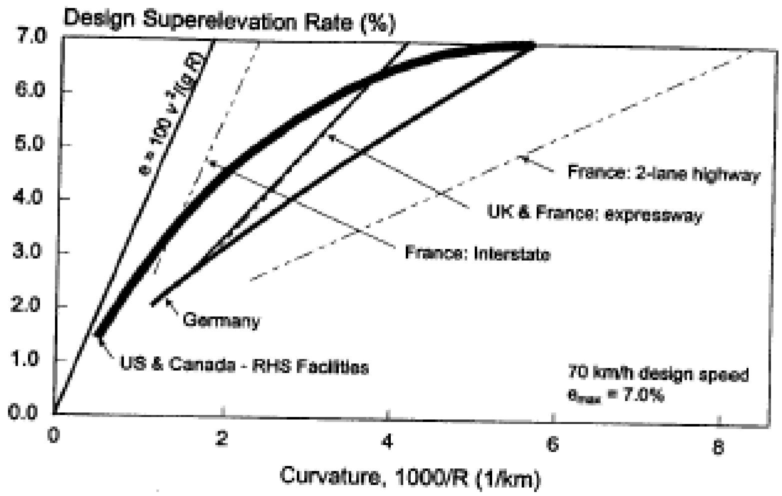

Figure 5. Superelevation distribution methods recommended by several international agencies for high-speed facilities.

The first line on the left hand side represents the amount of superelevation required to match the centripetal acceleration associated with travel on a curved path thereby acting as the upper limit control. Except the United States and Canada that use asymmetric parabolic curve, all others use a linear relationship between the curvature and the superelevation rate.

2.11 Distribution of Superelevation to Maximize Highway Design Consistency

Since AASHTO method is largely based on a subjective analysis, Easa (Easa, S.M., 2003) presented an objective method that distributes superelevation using mathematical optimization to maximize design consistency. A safety margin is defined as the difference between the maximum limiting speed corresponding to f_{max} and the design speed. Two types of analysis are employed:

1. Aggregate analysis

2. Disaggregate analysis.

In aggregate analysis, the objective function of the model minimizes the overall variation of the safety margin along the highway. In disaggregate analysis; the objective function of the model minimizes the individual variations of the safety margins between adjacent curves. The safety margin definition is based on Nicholson (1998) in which he defined the safety margin as "the difference between the speed at which maximum permissible design side friction is being called upon by the driver (sometimes called safe speed) and the design speed". The optimization model presented by Easa eliminates the need from trial and error in determining the required e by scanning the whole e-distribution space between AASHTO methods 2 and 3 to determine the best e. Although the model produces results that are comparable to method 5, the preferred AASHTO distribution method, its use is impractical for professional practice. It requires the use of a powerful optimization computer, optimization techniques and the evaluations of various constraints. However, it can be used as a planning tool for a regional system evaluation and policy formulations where a more sophisticated computer program is usually employed in the analysis.

2.12 Side Friction Factor

Many researchers have shown that there is a centripetal acceleration a_r acting on a vehicle when its traverses a horizontal curve. This acceleration is counterbalanced by friction force between the tires and the pavement and by a component of the gravity, if the curve is superelevated. The lateral acceleration (a_f) that acts on a vehicle in a curve is called the side friction factor. According to AASHTO's Policy on Geometric Design of Highways and Streets, side friction factor is the product of side friction demand factor and the gravitational constant g. Thus: $a_f = fg$. If the curve is superelevated, a portion of the frictional force is counterbalanced by gravity. Thus a third component of the lateral acceleration a_e is introduced into the equation. As depicted in exhibit 3-9 below, since there are variations in speeds of various vehicles traversing any given horizontal highway curve, there is an unbalanced force on a vehicle on any curve. This force which is counterbalanced by the friction between the tire and the pavement is as a result of the tire side thrust due to the deformation of the contact area of the tire by the pavement surface.

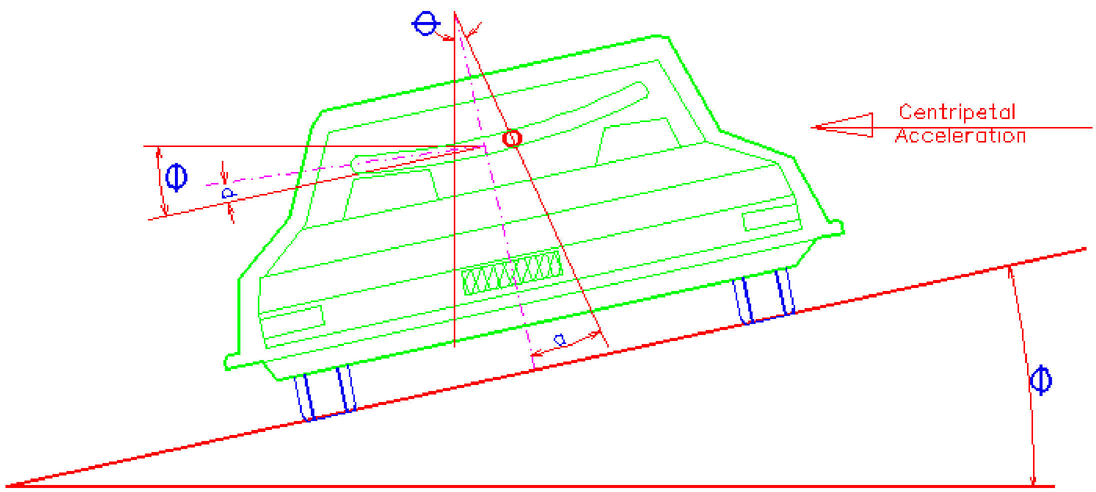

Exhibit 3-9 (AASHTO 2004) Geometry for Ball-Bank Indicator.

The coefficient of friction is the friction force divided by the component of the weight perpendicular to the pavement surface as will be illustrated in chapter 4, figure 4.1. The interaction of these forces at the center of gravity of the vehicle in motion in relation to the curve radius, the speed and the superelevation (***e***) is used in the design of horizontal curves in highway.

This relationship is given as:

$$a_f = a_r - a_e \qquad (2.18)$$

Where:

a_f = acceleration counterbalanced by friction (= gf in ft/s^2)

a_r = centripetal acceleration (= v^2/gR)

a_e = acceleration counterbalanced by gravity due to superelevation (= ge/100), ft/s^2;

e = superelevation rate in percent;

f = side friction factor or side friction demand;

v = vehicle speed, ft/s;

g = gravitational acceleration (= 32.2 ft/s2);

R = radius of curve in feet.

By substituting the values of the definitions above into equation 2.1, we can derive the simplified curve equation used in the design of highway curve with superelevation.

Knowing that these are all components of the weight, the weight quantity drops out of the equation and we have the following expression:

However, based on the laws of mechanics (proof of this formula is provided in chapter 4),

$$R = \frac{\mathrm{v}^2}{g\left(\frac{f_s + e}{1 - ef_s}\right)} \qquad (2.19)$$

The quantity $(1 - ef_s)$ is approximately equal to1.0; hence, it is often dropped in the equation, thus producing a more conservative value of ***R***. The simplified form of the formula is given as

$$R = \frac{\mathrm{v}^2}{g(e + f_s)} \qquad (2.20)$$

Where:

- ***v*** = speed MPH (Km/h)
- ***g*** = force of gravity 32.2 ft/s^2 (9.806m/s^2)
- ***e*** = superelevation rate %
- f_s = friction factor (no unit)

The above equation can be solved for ***e*** by mathematical transposition so that

$$e = \frac{v^2}{gR} - f \tag{2.21}$$

2.13 Review of Application of Reliability Analysis to Intersection Left Turn Bay Design-Safety Evaluation

American Association of States Highways and Transportations Officials (AASHTO)'s Policy on Geometric Design of Highways and Streets, provides design guidance for left turn bay design at an intersection. The guidance relates to length of the left turn bay, traffic volumes and intersection control mechanism such as stop signs and signals and other intersection controls provided by Manual of Uniform Traffic Devices (MUTCD) Evaluation of the effectiveness of the left turn bay for safety or the reliability of the left turn bay is largely not covered by the green book but is left to traffic engineering operations as presented in Highway Capacity Manual (HCM) in terms of intersection delay (D), its ability to handle a given volume. HCM and other traffic engineering publications and practice do not address the inherent safety issue of the turn bay in which the turn bay approach saturation or saturation condition is exceeded. This research will present a methodology to evaluate the reliability of a left turn bay based on its geometry and the traffic demands. There are three components in the length of left turn bay design: 1) Clearance distance, 2) breaking to a stop distance and 3) the length of storage or queue length after breaking to a stop is complete (FDOT Standard Index 2008). AASHTO and FDOT criterion is to design the intersection with a minimum of two cars length on the queue storage while the clearance and breaking distances are based on design speed, reaction time and average deceleration rate (1, 2). The variation in the queue length reduces the availability of the other two components (clearance and breaking distances) and thereby decreasing the ability of the driver to clear the thru lane and come to a stop safely. Failure occurs when the available length of clearance distance plus the breaking distance is less than the demand. The reliability of the turn bay can be evaluated based on the geometry as the length of the turn bay is reduced by a successive number of cars exceeding the queue length or storage distance. The reliability of the left turn bay with respect to safety therefore, is the availability of the turn bay length at any given period for the left turning vehicle to complete clearance and breaking maneuver without shock to the traffic downstream due to hard breaking. This research will develop the methodology for determining this shock in terms of increase in the acceleration rate over the AASHTO specified limit of $11.2 ft/s^2$

It is intended this approach will find the following uses:

1. The process can be used to assess safety need of the intersection by determining the level of it reliability, a decision for improvement can be made or the no-build alternative can be chosen.
2. It can be used to segregate contributive elements of traffic incidents such as rear end collision and sideswipes at an intersection.
3. It can be used by the maintaining agency to defend or accept negligent in a court of law for traffic incident at an intersection.

4. It may be possible to combine with the delay evaluation models to incorporate safety components in the delay equation (future).

2.14 Left Turn Bay Configuration

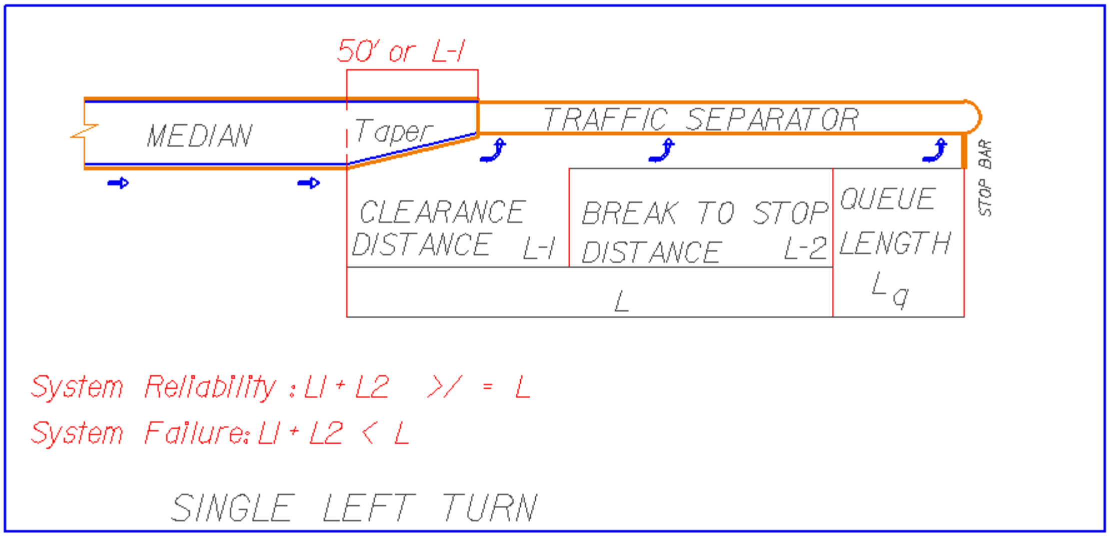

Figure 2.1: Configuration/Components of a single Left turn Lane.

Terms Definitions:

Figure 2.1 above shows an illustration of a left turn bay describing the various components associated with the left turning maneuvers. The distance L-1 is the distance required for the left turning vehicle to clear the through lane based on the perception reaction time; L-2 is the distance required for the turning vehicle to begin breaking and bring the vehicle to a stop behind the queue when the queue is full or slow down enough to move to the stop bar when the queue is empty; based on the deceleration rate, entry speed, pavement condition and drivers behavior. The distance L_q is the distance required for the vehicles in the queue to wait for opportunity to make a left turn; this may be based on the critical gap, opposing volume of traffic on the road, signal phasing, arrival and discharge rates of the left turning vehicles and other factors. This is also called storage length. The distance L is the sum of L-1 and L-2, it is the distance required for clearance and stopping maneuver of the left turning vehicle in the left turn bay. The required length of the left turn bay therefore, is the sum of the three lengths components: L-1, L-2, and L_q. In low volume roadway system where there is less demand for left turning vehicle and low volume on the through lane, L-1 length may be the same as the taper length (FDOT Standard Index, 2008).

2.15 AASHTO and FDOT Design Guidelines

The green book recommends that the storage lengths of left turn lane should be sufficient to avoid the possibility of left-turning vehicles stopping in the through lanes waiting for a signal change or for a gap in the opposing traffic; in the case of unsignalized intersection. To achieve this end, AASHTO sets the criteria that the storage length be based on "number of turning vehicles likely to arrive in a two-minute period within the peak hour" and to "provide a space for at least two passenger cars" (1). AASHTO further add the following: "Space for at least two passenger cars should be provided with over 10% truck traffic, provision should be made for at least one car and one truck. The two-minute rule may be changed to some other interval that depends on largely on the opportunities for completing the left turning maneuver". This is somewhat arbitrary and AASHTO does not provide any procedure for computation of the left turn lengths. The inherent safety issues arising from the number of vehicles present in the storage length that exceeds the two-car rule and its effect on the clearance and breaking distance is not considered in the guideline. Again, AASHTO provides the following guidelines for signalized intersection:

"At signalized intersection, the storage length needed depends on signal cycle length, the signal phasing arrangement and the rates of, arrival and departure of the left turning vehicles. The storage length is a function of the probability of occurrence of events and should usually be based on one and one half to two times the average number of vehicles that would store per cycle, which is predicated on the design volume. This length will be sufficient to store heavy surges that occur from time to time". In this case, although AASHTO recognizes that the length of left turn design should be based on the left turning volume and the opposing vehicles, no specific design procedures are provided for both cases (Chakroborty, Kukuchi, Lusczcz, 1995). It can be concluded that AASHTO guidelines is not sufficient in determining the safety level of left turn bay or its adequacy in operations. Many other studies have been conducted with this regard; however, most of the research about left turn performance is centered on measurement of the intersection delay, whether the delay is for left turn lane or the intersection as a whole. The search did not reveal any special interest in evaluating the dynamic decrease in the intersection reliability as the queue length increases. Chakroborty, Kikuchi and Luszcz (1995) presented a methodology for determining lengths of left turn lanes at unsignalized intersections based on the concept that the probability of lane overflow is less than a given threshold value of 0.015. The methodology first calculates the probability that a given lane length will result in overflow before lane lengths are suggested that will not exceed the given threshold value. Parameters used in the model are volume of turning vehicles, volume of opposing vehicles, critical gap, threshold probability, and vehicle mix. Computer simulation is used to check the validity of the model. The results of the turn lane lengths are compared with AASHTO values. The effect of considering opposing volumes and changing the threshold probability is also discussed in the paper. However, this paper appears to be computing the length of the queue on the turn lanes with no regard to the overall length of the left turn lane. AASHTO specifies two vehicles as the minimum queue length of left turn design that can be exceeded as the volume on the left turn and opposing traffic increases. The likelihood of the overflow occurring has been established; hence, the potential for reduced reliability of the clearance distance plus breaking distance is also established. This finding will be applied in this methodology to establish the reliability of turn lane with respect to safety.

As mentioned earlier, major investigation of left turn design operations has been devoted to the intersection delay. The performance of an intersection, whether the intersection is signalized or not, is measured by it delay. Traffic Engineers use this information in planning, design and analysis. One other component of importance is the queue at the intersection. That is why a lot of research has been devoted to queue and delays at intersection. The inputs required for determination of queue and delays are arrival rates and discharge rates, which is directly a function of the intersection signal operations and the traffic volumes. Sometimes the physical characteristics of the intersection may be included in the analysis (HCM2000). Beckman (1956) developed expected delay formulation for a fixed time signal using binomial arrival and deterministic service. The adoption of binomial function for the model reduced it practical usefulness because of the restrictive nature of the binomial distribution on the expected overflow queue. A study of a single stream of vehicles arriving at fixed-time signal was conducted by Darroch (1964). He developed a model based on a generalized Poisson arrival; the resulting models are complex due to the inputs requiring further modeling of other elements such as overflow queue. McNeil and Weiss (1974) considered compound Poisson arrival. The problem with this procedure is that it requires knowing the average overflow queue, which is always not known. Webster (1958 modified in 1961) was the first to produce an approximate delay formula that received wide acceptance and use. Webster's model was based on a combination of theoretical and numerical simulations. Webster's approximation model was as a direct result of the difficulties in achieving exact delay formulations. Miller (1963 and 1968) presented approximate formula for delay and queue but this was limited to specific arrival and departure rates. Newell (1965) developed delay formulae for general arrival and departure distributions. Newell's formula for average overflow queue has only graphical solutions but Cronje (1983) proposed an analytical approximation function for the graphical approach. A time-dependent delay equation was developed by Akcelik (1988) by using coordinate transformation approach. This formula was suitable for signalized intersection. Two other countries, Australia and Canada have developed generalized delay formula. This formula is a kin to the delay model proposed in 2000 edition of the Highway Capacity Model used in the United States.

Extensive work has been done in studying delay at intersections as the reviews show. Allsop (1972), Newell (1982), and Hurdle (1984) have presented detailed discussion on the various models. Again no consideration has been given to the effect of the delay at intersection on safety of the turn lane. Thus a model for evaluating the effect of the delay or queue length, which exceeds design values at an intersection, is presented in Chapter 5 of this dissertation. The methodologies developed to formulate the model are presented.

2.16 Review of Effect of Variation of the Peak Hour Volumes on Intersection Signal Delay Performance

There is limited research with respect to the effects of the variability of peak hour volumes on the design hourly volume (defined as the Peak Hourly Volume (v_i) divided by the Peak Hour Factor (PHF)) on the design hourly volume and delay performance. Dowling (1994) conducted a study to calibrate the 1985 Highway Capacity Manual (HCM) and study the effect of using default parameters for estimating signalized intersection level of service. The approach was to successively replace the HCM default values for intersection operational module with field measured data. The result showed that large data is needed for PHF and saturation rates (defined as the ratio of the approach's hourly volume (v) to the capacity of the approach (c) to ensure accuracy of the effect of PHF on intersection level of service (field measurement for PHF was 0.87 as opposed to HCM default value of 0.90). The study also concluded that higher saturation rate in excess of 85% of the capacity had significant impact on the delay performance of the signalized intersection. And, that the use of PHF as an input parameter for intersection signals delays analysis requires accurate measurement of the degree of saturation (X). Tarko and Perez-Cartagena (2005) conducted a study to investigate the variability of PHF over time and across locations; they also developed a prediction model for PHF based on field data. This study was divided into two parts. First, day-to-day variability of PHF was investigated using simulation with assumed low traffic pattern and then compared with 13 consecutive week-days counts on two locations in Indiana. Variances of the PHF were computed using Taylor linear expansion with assumption of Poisson arrivals. The derived equation for the variance of PHF is given as:

$var\ PHF = (V_h - V_{15max}).(PHF)/4.V^2_{15max}.$

where:

V_h is the hourly volume,

V_{15max} is the highest 15 minutes count and

PHF is the calculated value of the PHF based on the count. PHF values were calculated as $V_h/4.V_{15max.}$

PHF variance of 0.20 was reported for the same flow direction with PHF ranging from 0.69 to 0.91 from the counts. And PHF values ranging from 0.63 to 0.99 were obtained from the traffic simulation. They concluded that the day-to-day variability of PHF may be considerable at the same location and direction; also, that average PHF values differ between traffic directions and between different times of day. They further concluded that the day-to-day variability of PHF means that a single day count is insufficient for use in traffic analyses. Thus, a compelling reason for a predictive model for PHF that can be used either in combination of a count or when a count is not available. The second part of this study developed a regression model based on traffic counts at or near signalized intersection. The prediction equation presented by Tarko and Perez-Cartagena (2005) is as given below:

$$PHF = 1 - \exp(-2.23 + 0.435\ AM + 0.209\ POP - 0.258\ v)$$

where:

PHF = estimated peak hour factor;

AM = 1 for AM period (= 0 otherwise);

POP = 1 for the area with population larger than 20,000 (= 0 otherwise); and

v = peak hour volume (in 1,000 vph).

A total of 180 observed *PHF*s were sampled from 45 intersections located in various cities in the state of Indiana. The coefficient of determination is 0.268. No *t*-statistics were reported but it is indicated that all parameters in the prediction model were statistically significant. Note that the coefficient of population is positive, indicating that peak hour factors will be predicted lower in areas with larger population. This is confirmed by figure five where afternoon peak PHF for population less than 20,000 is higher than PHF values for population greater than 20,000. It is also in direct contradiction to the statement of the authors on page 128 column two paragraph three: *"…The model obtained indicates that rural and semi-rural areas tend to have PHF that is slightly lower than that for developed areas…"* If developed areas represent higher population class, then the PHF for that class cannot be lower than the lower population class. However, the model proposed by the authors returned a lower PHF values for higher population class than the lower population class. Thus, the population parameter included in the model may not be a reliable component of the PHF predictor, at least, not in its present form. This also, seems to contradict with the postulated values suggested by HCM (2000). The study further indicated that there is a strong variability in PHF from site to site and a prediction model is needed based on empirical data. In addition, a single day count is an insufficient data for use in traffic signal design analyses. However, the data used in this model provided 180 data points which may not be adequate to provide a sound model for PHF prediction which could have been responsible for the population parameter failing the postulates of the authors. The effects of variability of PHF and the peak hour volumes on the design hourly volumes and delay performance were not explored in this study.

Sullivan et al (2006) studied the effects of urban traffic volume variation on service levels using traffic count data in the city of Milwaukee in combination with simulations. The study concluded that there exist a relationship between the day-to-day variation of traffic volume and level of service. That coefficient of variation of day-today decreases as the daily volumes increases; the magnitude of which was in the order of 16% for a weekday peak hour traffic of 600 vehicles per hour and decreases to 6.0% for a weekday peak hour volume of 1800 vehicles per hour. Also, in low saturation condition less than 0.70 of capacity, the day-today variation in traffic volume has little effect on level of service and level of service rapidly deteriorates when the degree of saturation exceeds 0.70.

Hellinga and Abdy (2008) conducted a study to quantify the impact of day-to-day variability of intersection peak-hour approach volumes on intersection delay and demonstrated that the impact is significant and therefore should not be ignored. A linear regression model was developed that related the mean peak hour approach volumes to the coefficient of variation of the peak hour approach. The linear model developed was given as:

$COV = 0.129\text{-}0.036V$

Where:

COV = coefficient of variation of the peak hour approach volume

V = mean peak hour approach volume

The regression coefficient was reported to be statistically significant at the 95% confident interval but the coefficient of determination ($R^2=0.15$) was too low. Thus, the model could not be assumed to explain the variability of the data. Their study also suggests that for intersections operating near capacity three (3) days of peak-hour volume observations are required to estimate the average intersection delay with an estimation error of 50% of the true mean, and seven (7) days of traffic counts are required to estimate intersection delay with an error of 30% of the true mean. The number of observation needed to achieve a given level of accuracy in the estimate of the mean delay was given by the formula:

$n_2 = [(t_{n2-1,\,\alpha} s)/d]^{2;}$

where:

n_2 = required number of days of observations of peak hour volume

$t_{n2-1,\,\alpha}$ = student t distribution value for n_{2-1} degree of freedom and a probability of α

s = sample standard deviation of intersection delay computed from initial sample

d = maximum desired error in the estimation of the true mean intersection delay

Their study reached seven conclusions relating to the variability of peak hour volumes, saturation flow rate, PHF and their effects on intersection performance and they are stated as follows:

1. The day-to-day variation of weekday peak hour volumes can be represented by Normal distribution with coefficient of variation of 0.87. These findings are consistent with Sullivan et al (2006).
2. The coefficient of variation of peak hour volumes is linearly related to the mean peak hour volume, however, this relation is very weak ($R^2 = 0.15$)
3. The variation of peak hour approach volumes are not statistically independent but appear to exhibit a moderate correlation (mean $\rho = 0.3$).

4. Correlation between the peak hour volumes on each intersection approach impacts the variability of the variability of intersection delay. The higher the degree of correlation, the greater the variability in intersection delays.
5. The day-to-day variation in the week day PHF can be represented by a Normal distribution with mean coefficient of variation of *0.039*. The impact of variability of PHF on intersection delay was not examined.
6. The values of PHF were compared to those estimated via the regression model proposed by Targo (2005). Targo's model was found to overestimate the PHF.
7. The estimation of average intersection delay on the basis of average peak hour volumes underestimated the true delay by as much as 15 %. Furthermore, the greatest underestimation error occurs for intersections operating in range of $X \approx 1$. Depending on the g/C ratio, this can be associated with an intersection LOS D or even C.

From the foregoing, two issues are engendered:

1. A new model is needed for predicting PHF. It is apparent that the data presented in previous research may not be adequate to support the conclusions that should be universally accepted for practice.

2. Exploration of the effects of variability of PHF on design hourly volume and its effect on intersection signal delay performance. Determination of this variation therefore, requires further study with large data which is explored in three parts in the following sections of this study.

Chapter 3: Methodology

3.1 Background:

Reliability analysis is common in other fields of engineering than is used in transportation engineering. It has been used in electrical engineering and computer science as well as civil engineering design. Most of the reliability application in civil engineering is in the field of structural design. It has also been applied to intersection sight distance (Said M. Easa, 2000) and pavement design- AASHTO Design of Pavement Structures Manual. AASHTTO Guide for Design of Pavement Structures, 1993 incorporates reliability factor (F_R) into the pavement design equation to account for the total chance variation in (1) the traffic predictions and (2) pavement performance. The reliability component is used as a fixed factor to ensure that a designed pavement section will survive the predicted traffic loads which is represented by total (18 Kips) equivalent single axle loads called $ESAL_{18}$ on the particular designed section. The reliability factor for the traffic load ensures that the design traffic load is always greater than the predicted traffic. Pavement performance on the other hand, is measured quantitatively by pavement serviceability index (PSI). Since F_R is greater than 1, it is used as a multiplier to both load on the road due to traffic prediction and the performance index to ensure that the designed section will provide the required service from the opening year to the terminal serviceability level. Thus, the reliability is defined by ASHTTO as: "The reliability of pavement designed-performance process is the probability that a pavement section using the process will perform satisfactorily over the traffic and environmental conditions for the period". This research is analogous to this concept in that it ensures that the predicted superelevation will be sufficient for the expected variation in speeds for vehicles traversing a horizontal curve that is superelevated. The computational method is different but the concept remains the same.

3. 2 Deterministic and Probabilistic Approaches in Engineering Design

As an illustration of the concept, in structural engineering, the reliability of a structure is to ensure that its resistance or strength (P) is greater than the applied load (L) within certain acceptable level of risk. However, there are uncertainties or variation in the resistance or strength of the structures which if not accounted for leads on to failure. There is also variation in the loads on a structure. Thus, P and L are random variables having the means, μ_p and μ_L, standard deviation σ_p and σ_L; and probability density functions f_p(p) and f_L(l). In deterministic design, the uncertainties of the nominal Resistance (P_N) and Load (L_N) are accounted for by a safety factor, which results sometimes, in over design or excessive use of materials. The factor of safety can be 1, 2, or 3 standard deviations below the mean for the resistance of the structure and many standard deviations above the mean load.

It is usually of the form: Nominal Factor of Safety = P_N / L_N (3.1)

From the foregoing it is clear that the factor of safety introduced in the nominal P and L depends on many factors:

(1) the uncertainties in the resistance of the structure,

(2) the load of the structure and

(3) How conservative the designer wants to be.

The deterministic approach thus, does not convey clearly the level of uncertainties in the resistance and the load. For instance, in allowable stress design, a factor of safety is applied to the ultimate stress to ensure that the stress caused by the load do not exceed the allowable stress; on the other hand, the reliability approach seek to compute the risk by accounting for all the uncertainties and selecting the variables or design inputs such that an acceptable risk of failure is achieved. To achieve this, the information on the probability functions for the load f_p(p) and resistance f_L(l) must be known. This is usually difficult to obtain and the engineers must formulate an acceptable design methodology by using only the information from the means and standard deviations. Nevertheless, probabilistic design addresses the underlying design conservatism more explicitly, more comprehensively through the treatment of the uncertainties in the random variables, the level of conservatism used in selecting the variables, and the desired level of reliability. (Haldar and Mahadevan, 2000).

3.3 Reliability Analysis

The first step in reliability analysis is to formulate a performance function that is the difference between the demand and the supply (Easa, 2000; Haldar and Mahadevan, 2000). The probability of failure of the supply and the demand function corresponds to the area where its probability distribution function is negative. The reliability therefore, is one minus the probability of failure. There are three methods of reliability analysis in current use: (1) exact method or first order reliability method (FORM), (2) first-order second-moment method (FOSM) or mean value first-order method, and (3) point estimate method (MVFOSM) (Haldar and Mahadevan, 2000). In First order reliability method the full probability distributions information of the component variables is used. Analytical, numerical or simulation technique may be used. This method is usually used when the reliability level is of critical importance. This method is very difficult to apply because the performance function for most engineering problems can be very difficult and highly non-linear. The FOSM method is based on a first order Taylor series approximation of the performance function linearized at the mean values of the random variables, and it uses only second moment statistics (means and variances) of the random variables. If we return to our earlier load and resistance illustration, the performance function in this case is given as:

$$Z = P - L \tag{3.2}$$

And the probability of failure for Z is: $P_f = P\,(Z<0)$ (3.3)

The point estimate methods are usually employed when the performance function is given in form of charts or as finite elements solution (Haldar & Mahadevan, 2000).

The FOSM methods can be simple as stated above or more complex using the advanced FOSM that expands the random variables at the failure boundaries iteratively until convergence is attained. In this research, the mean value FOSM method is adopted for the superelevation design, and left turn bay safety evaluation.

3.4 First Order Probabilistic Analysis

To perform a reliability analysis, at the least, the first two moments of the underlying system function are required. The most common way to do so, in a tractable form with accuracy is through the following **Taylor's** expansion up to the second order.

$$F(X) = F(\overline{X}) + \sum \frac{\partial F(\overline{X})}{\partial x_i}\bigg|_{x_i=\overline{x}_i} (x_i - \overline{x}_i) + \sum_{i=1}^{n} \sum_{i \neq j\ j=1}^{n} \frac{\partial^2 F(\overline{X})}{\partial x_i \partial x_j}\bigg|_{X=\overline{X}} \frac{(x_i - \overline{x_i})(x_j - \overline{x_j})}{2!} + \ldots \quad (3.7)$$

The expected value of the function can be obtained by placing expectation operator (**E**) on both sides. The 2nd order operation is usually sufficient, although higher order can be obtained for higher accuracy. This is shown in the equation below.

$$E[F(X)] = F(\overline{X}) + \sum \frac{\partial F(\overline{X})}{\partial x_i}\bigg|_{x_i=\overline{x}_i} E(x_i - \overline{x}_i) + \sum_{i=1}^{n} \sum_{x \neq j\ j=1}^{n} \frac{\partial^2 F(\overline{X})}{\partial x_i \partial x_j}\bigg|_{X=\overline{X}} E\left[\frac{(x_i - \overline{x_i})(x_j - \overline{x_j})}{2!}\right] + \ldots$$

$$= F(\overline{X}) + \sum_{i=1}^{n} \frac{\partial^2 F(\overline{X})}{\partial x_i^2}\bigg|_{x_i=\overline{x}_i} \mathrm{var}(x_i) + \sum_{i=1}^{n} \sum_{i \neq j\ j=1}^{n} \frac{\partial^2 F(\overline{X})}{\partial x_i \partial x_j}\bigg|_{X=\overline{X}} \frac{\mathrm{cov}(x_i, x_j)}{2!} + \ldots \quad (3.8)$$

The variance of the e-function can also be easily derived by definition, utilizing only the 1st order approximation as follows:

$$Var[F(X)] = E[F(X)\text{-}F(\overline{X})]^2 = E\left[\sum_{i=1}^{n} \frac{\partial F(\overline{X})}{\partial x_i}\bigg|_{x_i=\overline{x}_i} (x_i - \overline{x}_i)\right]^2 \ldots$$

$$= \sum_{i=1}^{n} \frac{\partial F(\overline{X})}{\partial x_i}\bigg|_{x_i=\overline{x}_i} \mathrm{var}(x_i) + \sum_{i=1}^{n} \sum_{i \neq j\ j=1}^{n} \frac{\partial F(\overline{X})}{\partial x_i}\bigg|_{x_i=\overline{x}_i} \frac{\partial F(\overline{X})}{\partial x_j}\bigg|_{x_j=\overline{x}_j} \mathrm{cov}(x_i, x_j) + \ldots \quad (3.9)$$

Where the Cov(xi, xj) is the covariance of Xi and Xj. If the variables are uncorrelated, then the variance is simply

$$\sigma_F^2 \approx \sum_{i=1}^{n} \left\langle \frac{\partial F(\overline{X})}{\partial x_i} \right\rangle^2 Var(X_i). \quad 3.10$$

The safety index can be calculated by taking the ratio of the mean and standard deviation of ***F***. This ratio is also known as the reliability index and is denoted as β: Thus:

$$\beta = \frac{\mu_F}{\sigma_F} \quad 3.11$$

Probability of failure $P_f = P(F<0)$ 3.12

Or

$$P_f = 1 - \Phi\left[\frac{\mu_F}{\sigma_F}\right] = 1 - \Phi(\beta). \quad 3.13$$

Where

Φ is the CDF of the standard normal variate and $\Phi^{-1}(1-P_f)$ is the value of the standard normal variate at the probability level $(1-P_f)$.

This concept will be applied to each of the remaining two sections to demonstrate the use of reliability analysis to highway design problems. However, in section 5 additional concept of reliability based on time dependent event is adopted for the analysis of left turn bay design. The analysis uses Poisson Probability distribution to model the arrival and departure of vehicles in the left turn bay based on Pollaczek-Kintchine equation.

Chapter 4: Application of Reliability Analysis to Superelevation Design

4.1 Derivation of Design Equation

Dynamics of vehicle motion on a curve has been established through various researches. When a vehicle travels through a curve, there is a centripetal acceleration that forces the vehicle towards center of the curve. Two forces in a superelevated curve sustain this centripetal acceleration:

1) The frictional acceleration between the tires and the pavement and
2) The acceleration due to the component of the vehicle weight due to the embankment called super elevation (See figure 4.1).

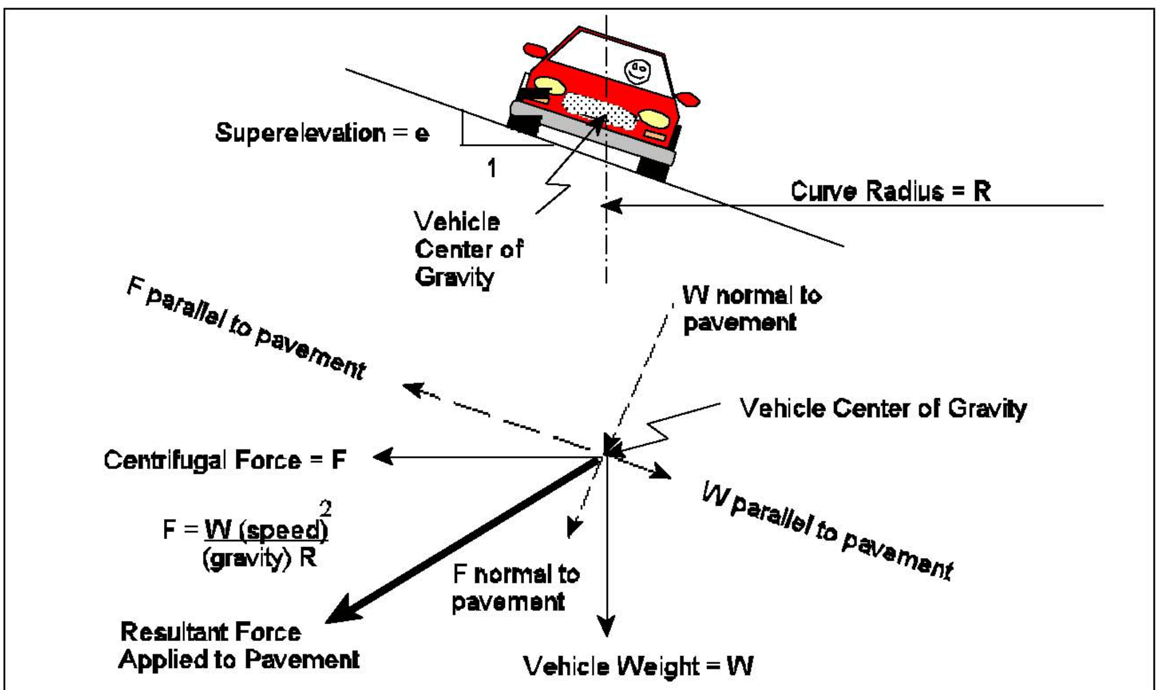

Figure 4.1: Dynamics of Vehicle Motion on Superelevated Curve (NYDOT Report 2004)

The interaction of these forces at the center of gravity of the vehicle in motion in relation to the curve radius, the speed and ***e*** *i*s used in the design of horizontal curves in highway. The centrifugal force F is a lateral force that pushes the vehicle and occupants outward. This is as a result of the lateral change of direction of the vehicle as it traverses the curve. The effect of the centrifugal force produces a lateral acceleration which pushes the vehicle toward the center of the curve as a consequence of rapidly changing velocity vector of the vehicle. The superlevation causes a portion of the centrifugal force to act perpendicularly to the slope of the superlevated curve; this is designated as F normal to the pavement in Figure 4.1. This force along with component of the weight of the vehicle (W normal to the pavement) adds up to the total normal reaction between the vehicles tires. The remaining portion of the force F can be resolved along the slope of the superlevation and is depicted as F parallel to the slope. The weight of the vehicle also can be resolved to two components; weight parallel to the slope designated as W parallel and weight normal to the slope, designated as W normal to the slope. In figure 4.2 below, these forces with relation to the superelevation, friction factor and the radius (R) of the curve can be derived.

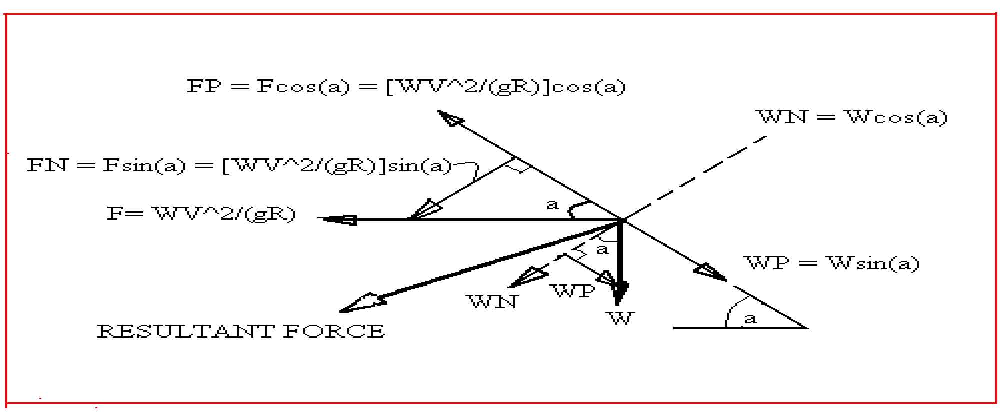

Figure 4.2: Free body diagram of the forces at the center of gravity of the vehicle in motion on a superelevated curve.

From figure 4.2 and based on the laws of mechanics, it can be shown that

$$WN = W\cos(a) \quad 4.1$$

$$WP = W\sin(a) \quad 4.2$$

$$FN = F\sin(a) = \frac{WV^2}{gR}\sin(a) \quad 4.3$$

$$FP = F\cos(a) = \frac{WV^2}{gR}\cos(a) \quad 4.4$$

The frictional force on the tires can be written as the normal force times the friction factor.That is: (WN+FN)*f_s $= W\cos(a) * f_s + \frac{WV^2}{gR}\sin(a) * f_s$ 4.5

From figure 4.1,

$$e = \tan(a) = \frac{\sin(a)}{\cos(a)} \quad 4.6$$

In order to avoid sliding or running off the road for vehicles operating within the designed speed, the lateral forces must be counter balanced by the effect of the superelevation and the frictional forces on the tires. Thus:

Summing forces along the slope, we have the following:

$$W\cos(a) * f_s + \frac{WV^2}{gR}\sin(a) * f_s = \frac{WV^2}{gR}\cos(a) - W\sin(a) \quad 4.7$$

This can be simplified as:

$$\frac{W\sin(a)}{W\cos(a)}\left(\frac{V^2}{gR}f_s + 1\right) = \frac{V^2}{gR} - f_s \quad 4.8$$

$$= \tan(a)\left(\frac{V^2}{gR} f_s + 1\right) = \frac{V^2}{gR} - f_s \quad 4.9$$

Replacing tan(a) in equation 4.9 with e as in 4.6, we obtain the following:

$$ef_s \frac{V^2}{gR} + e = \frac{V^2}{gR} - f_s \quad 4.10$$

By solving equation 4.10 for R, the Radius of the curve with respect to the superelevation, the operating speed and the friction factor, we obtained the expression for R as:

$$R = \frac{\mathrm{v}^2}{g\left(\frac{f_s + e}{1 - ef_s}\right)} \quad 4.11$$

The quantity $(1 - ef_s)$ is approximately equal to1.0; hence, it is often dropped in the equation, thus producing a more conservative value of ***R***. The simplified form of the formula is given as

$$R = \frac{\mathrm{v}^2}{g(e + f_s)} \quad 4.12$$

Where:

- ***v*** = speed MPH (Km/h)
- ***g*** = force of gravity 32.2 ft/s^2 (9.806m/s^2)
- ***e*** = superelevation rate %
- $\boldsymbol{f_s}$ = friction factor (no unit)

The above equation can be solved for ***e*** by mathematical transposition so that

$$e = \frac{v^2}{gR} - f \quad 4.13$$

Based on the method 1,

$$f = \frac{R_{\min}}{R} f_{\max} \quad \text{and} \quad R_{\min} = \frac{v^2}{g(e_{\max} + f_{\max})} \qquad 4.14$$

$$e = \frac{v^2}{gR} - \frac{v^2}{gR}\left(\frac{f_{\max}}{e_{\max} + f_{\max}}\right)$$

$$\qquad 4.15$$

$$= \frac{v^2}{gR}\left(\frac{e_{\max}}{e_{\max} + f_{\max}}\right)$$

The side friction demand by driver is directly proportional to the lateral acceleration for a particular speed ***v***, ***e***, and ***R***. Therefore; it is a random quantity that is normally distributed with mean $\overline{f}$ and variance $\sigma_{f_s}^2$. The speed also is a random quantity and is normally distributed with mean $\overline{v}$ and variance σ_v^2. Since these two quantities are random variables, their probability density functions can be generated and those functions then used in Reliability analysis of ***e.***

Returning to the simplified curve equation and transposed for e, the *1^st^* and *2^nd^* partial derivatives of the e-function are as follows:

<u>e-function</u>:

$$e = \frac{v^2}{gR} - \frac{v^2}{gR}\left(\frac{f_{\max}}{e_{\max} + f_{\max}}\right)$$

$$\qquad 4.16$$

$$= \frac{v^2}{gR}\left(\frac{e_{\max}}{e_{\max} + f_{\max}}\right)$$

Partial derivatives:

- $$\frac{\partial e}{\partial v} = \frac{2v}{gR}\left(\frac{e_{\max}}{e_{\max} + f_{\max}}\right)$$

  (4.17)

- $$\frac{\partial^2 e}{\partial v^2} = \frac{2}{gR}\left(\frac{e_{\max}}{e_{\max} + f_{\max}}\right)$$

  (4.18)

- $$\frac{\partial^2 e}{\partial v \partial f} = 0$$

  (4.19)

- $$\frac{\partial e}{\partial f} = 0 \qquad 4.20$$

- $$\frac{\partial^2 e}{\partial f^2} = 0 \qquad 4.21$$

The next task is to apply the above formulation to the superelevation equation. This is accomplished as follows: From equation (4.16), and by assuming v and f as appropriate probability distribution function, the expected value and the variance of the required superelevation rate, e can be obtained. Firstly, we apply Taylor's theorem to the e expression using *2nd* order approximation, and the above formula can be expressed as:

$$e \approx \frac{\bar{v}^2}{gR}\left(\frac{e_{\max}}{e_{\max} + f_{\max}}\right) +$$

$$\frac{2\bar{v}}{Rg}\left(\frac{e_{\max}}{e_{\max} + f_{\max}}\right)\left(v - \bar{v}\right) + \frac{\partial e}{\partial f}\left(f - \bar{f}\right) + \frac{\partial^2 e}{\partial v^2}\frac{\left(v - \bar{v}\right)^2}{2!} - \frac{\partial^2 e}{\partial v \partial f}\operatorname{cov}(v, f) + \frac{\partial^2 e}{\partial f^2}\frac{\left(f - \bar{f}\right)^2}{2!} =$$

$$\frac{\bar{v}^2}{gR}\left(\frac{e_{\max}}{e_{\max} + f_{\max}}\right) + \frac{2\bar{v}}{Rg}\left(\frac{e_{\max}}{e_{\max} + f_{\max}}\right)\left(v - \bar{v}\right) + \left(\frac{2}{Rg}\right)\left(\frac{e_{\max}}{e_{\max} + f_{\max}}\right)\frac{\partial^2 e}{\partial v^2}\frac{\left(v - \bar{v}\right)^2}{2!}$$

After simplification,

$$e \approx \frac{\bar{v}^2 + 2\bar{v}(v-\bar{v})}{gR}\left(\frac{e_{\max}}{e_{\max}+f_{\max}}\right) \qquad 4.22$$

The expected value, *E(e)* can be obtained by placing the expected value operator (E) on the right side of the expression to the *2nd* order approximation, which yields:

$$E(e) \approx \frac{\bar{\mathrm{v}}^2}{gR}\left(\frac{e_{\max}}{e_{\max}+f_{\max}}\right)+\left(\frac{2}{Rg}\right)\left(\frac{e_{\max}}{e_{\max}+f_{\max}}\right)E\frac{\left(v-\bar{v}\right)^2}{2!} \qquad 4.23$$

We can replace the variance of the speed, $\left(v-\bar{v}\right)^2$ with the symbol $\sigma_v{}^2$ and rewrite the expected value as

$$E(e) = \frac{\bar{v}^2 + 2\sigma_v^2}{gR}\left(\frac{e_{\max}}{e_{\max}+f_{\max}}\right) \qquad 4.24$$

The variance of e can be obtained as follows using only the *1st* order approximation if information involving the third and forth moment of the underlying variables are not available.

$$\sigma_e^2 \approx \frac{4\bar{v}^2\sigma_v^2}{\left(gR\right)^2}\left(\frac{e_{\max}}{e_{\max}+f_{\max}}\right)^2 \qquad 4.25$$

The Safety or Reliability Index from equation 3.11 can be written as the ratio of the expected value of ***e*** to the standard deviation of ***e***.

Thus:

$$\beta_e = \frac{\mu_e}{\sigma_e} = \frac{\bar{v}^2 + \sigma_v^2}{gR}\left(\frac{e_{\max}}{e_{\max}+f_{\max}}\right) \div \frac{2\bar{v}\sigma_v}{\left(gR\right)}\left(\frac{e_{\max}}{e_{\max}+f_{\max}}\right) \qquad 4.25a$$

And the Probability of failure $P_{f\,=}\,P(e<e_{req})$ 4.25b

or

$$P_f = 1 - \Phi\left[\frac{\mu_e}{\sigma_e}\right] = 1 - \Phi(\beta_e) \qquad 4.25c$$

Where:

Φ is the CDF of the standard normal variate and $\Phi^{-1}(1-P_f)$ is the value of the standard normal variate at the probability level (*1-P_f*).

The application of these equations to superelevation design is demonstrated in the next section.

4.2 Design Application

In designing proper horizontal alignment for highways, distributions of superelevation rates (or the corresponding turning radii/curvatures) and side friction factors are critical. Based on the law of mechanics, the superelevation rate, *e*, required by drivers to negotiate turning on a horizontal curve can be derived as:

$$e = \frac{v^2}{gR} - f \qquad (4.26)$$

Where v = vehicle running speeds, R = turning radius, f = side friction factor, and g = gravity constant (= 32.2 ft/s^2). There exist practical design values for upper limits of e and f, i.e., e_{max} and f_{max}, considering various conditions related to weather, traffic, pavement, safety, and driving comfort. See discussions in AASHTO for details. According to AASHTO, at a specific design speed, minimum turning radius, i.e., R_{min}, can be determined as follows if both e_{max} and f_{max} are selected.

$$R_{min} = \frac{v_d^2}{g(e_{max} + f_{max})} = \frac{v_d^2}{15(e_{max} + f_{max})} \qquad (4.27)$$

Where v_d = curve design speeds (in mph). This limiting value serves as a threshold value for confining superelevation rates or side friction factors beyond the limits considered practical for operation or comfortable by drivers. On the other hand, the use of radius larger than R_{min} allows both e and f to have design values below their upper limits. In particular, while sustaining the centripetal acceleration for safety, the relaxation from f_{max} enables drivers experience less lateral acceleration force, f_g, and provides drivers comfortableness. This relaxation is also considered critical especially under the situation where an increasing portion of vehicles tends to drive at various speeds higher than the design speed.

Let v be the vehicle running speed and v_d be the design speed. Based on Method 1 for distributing side friction factors,

$$f = \frac{R_{min}}{R} f_{max} \tag{4.28}$$

It follows that:

$$\begin{aligned} e &= \frac{v^2}{gR} - \frac{v^2}{gR}\left(\frac{f_{max}}{e_{max} + f_{max}}\right) \\ &= 1 - \frac{v^2}{gR}\left(\frac{e_{max}}{e_{max} + f_{max}}\right) \end{aligned} \tag{4.29}$$

Based on AASHTO, the maximum side friction factor can be established as a two-piece linear function of the design speed as follows:

$$\begin{aligned} f_{max} &= 0.19 - 0.001 v_d \,, v_d \leq 50 \text{ mph} \\ &= 0.24 - 0.002 v_d \,, v_d \geq 50 \text{ mph} \end{aligned} \tag{4.30}$$

These equations are presented in the table 4-1 below.

Table 4-1: Maximum Friction Factor for Superelevation Design.

Speed < 50 MPH	Max Friction Factor (f_{max})	Speed > 50 MPH	Max Friction Factor (f_{max})
15.00	0.18	50.00	0.14
20.00	0.17	55.00	0.13
25.00	0.17	60.00	0.12
30.00	0.16	65.00	0.11
35.00	0.16	70.00	0.10
40.00	0.15	75.00	0.09
45.00	0.15	80.00	0.08

Or the f_{max} can be read directly from the following charts (4-1 and 4-2). The first chart is a graphical depiction of the maximum friction factor for design speed less than 50 miles per hour (MPH) and the second chart is for design speed greater than 50 MPH. Intermediate values can be easily obtained through a simple mathematical interpolation.

Figure 4-1: Max Friction Factor for Speed < 50 MPH

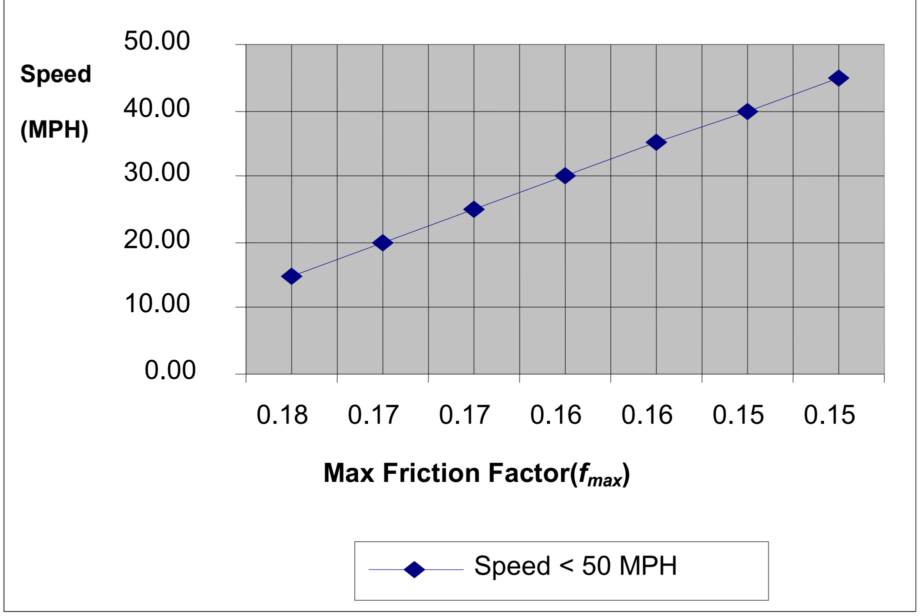

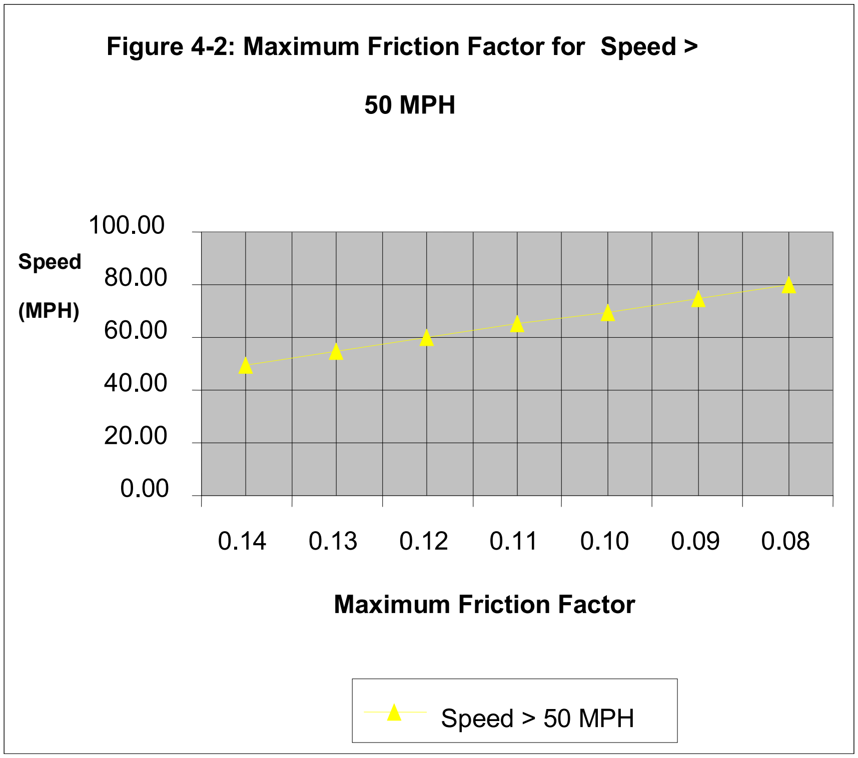

Figure 4-2: Graphical representation of Maximum Friction Factors for speed greater than 50 MPH.

Application of expectation operator on both sides of Equation (4.29) yields the expected superelevation:

$$\begin{aligned} E(e) &= E(1-\frac{(v^2)}{gR}\left(\frac{e_{\max}}{e_{\max}+f_{\max}}\right)) \\ &= \frac{\bar{v}^2+\sigma_v^2}{gR}\left(\frac{e_{\max}}{e_{\max}+f_{\max}}\right) \end{aligned} \tag{4.31}$$

Also, approximation of Equation (4.31) using the Taylor expansion to the first order yields:

$$e \approx \frac{\bar{v}^2+2\bar{v}(v-\bar{v})}{gR}\left(\frac{e_{\max}}{e_{\max}+f_{\max}}\right) \tag{4.32}$$

The variance of e can then be derived as:

$$\sigma_e^2 \approx \frac{4\bar{v}^2\sigma_v^2}{(gR)^2}\left(\frac{e_{\max}}{e_{\max}+f_{\max}}\right)^2 \tag{4.33}$$

Based on the reliability analysis, at (1-α) level of confidence, the required superelevation can be determined as:

$$\begin{aligned} e_{req} &= E(e)+z_\alpha\sigma_e \\ &= \frac{\bar{v}^2+\sigma_v^2+2z_\alpha\bar{v}\sigma_v}{gR}\left(\frac{e_{\max}}{e_{\max}+f_{\max}}\right) \\ &= \frac{\bar{v}^2+\sigma_v^2+2z_\alpha\bar{v}\sigma_v}{15R}\left(\frac{e_{\max}}{e_{\max}+f_{\max}}\right) \end{aligned} \tag{4.34}$$

Where R is expressed in ft and both $\bar{v}$ and σ_v is expressed in mph. Substitution of $R_{\min}$ into Equation (4.34) yields:

$$e_{req} = \frac{e_{\max}R_{\min}}{R}\left(\frac{\bar{v}^2+\sigma_v^2+2z_\alpha\bar{v}\sigma_v}{v_d^2}\right) \tag{4.35}$$

Since $e_{req} \le e_{\max}$, the minimum required curve radius, R_{req}, can be written as:

$$R_{req} \ge R_{\min}\frac{\bar{v}^2+\sigma_v^2+2z_\alpha\bar{v}\sigma_v}{v_d^2} \tag{4.36}$$

When R = min R_{req}, $e_{\mathrm{req}} = e_{\max}$, which ensures Equation (4.34) predict a design superelevation rate equal to $e_{\max}$ when the curve radius equals minimum required curve radius subjected to reliability constraint.

4.3 Average Running Speed Standard Deviation:

The average running speeds and standard deviations of vehicle speeds in relation to the design speeds are established based on the data retrieved from Fitzpatrick et al, in NCHRP 504. Based on the mean speed and 85-percentile speed measurements reported in NCHRP 504 and the common practice that the 85-percentile speed is often selected as the design speed, the following relationships is established:

$$\bar{v} = \underset{(100.9)}{0.9749} v_{85} - \underset{(7.8)}{3.6758}, \qquad R^2 = 0.993 \tag{4.37}$$

$$\sigma_v = \underset{(5.2)}{1.3821} + \underset{(13.7)}{0.7333}\left(v_{85} - \bar{v}\right), \quad R^2 = 0.712 \tag{4.38}$$

The values in parenthesis are t values that indicate that all coefficients are statistically significant. The R^2 (square of the multiple correlation coefficients R) also suggests that the fitting quality is well acceptable. For convenience, these values are also tabulated in Table 4.2 for design purposes. One could observe that, compared to average running speeds reported by AASHTO, the average running speeds proposed here are slightly lower when the design speed is 40 mph and below but are significantly higher when the design speed increases. The speed variation also increases as the design speed increases. In this way the variability in the drivers selected speed while traversing the curve is incorporated in the design of the superelevation. This approach ensures that the design risk is minimized.

Table 4.2: Specifications of design speeds and average running speeds

Design Speed V_d mph	Average Running Speed $\bar{v}$ mph	Standard Deviation σ_v mph	Average Running Speed by AASHTO mph
30	25.6	4.6	28
40	35.3	4.8	36
45	40.2	4.9	40
50	45.1	5	44
55	49.9	5.1	48
60	54.8	5.2	52
65	59.7	5.3	55
70	64.6	5.4	58

When intermediate values of these data in table 4.2 are required, a linear interpolation of these values can be computed or read directly from figure 4.3 below.

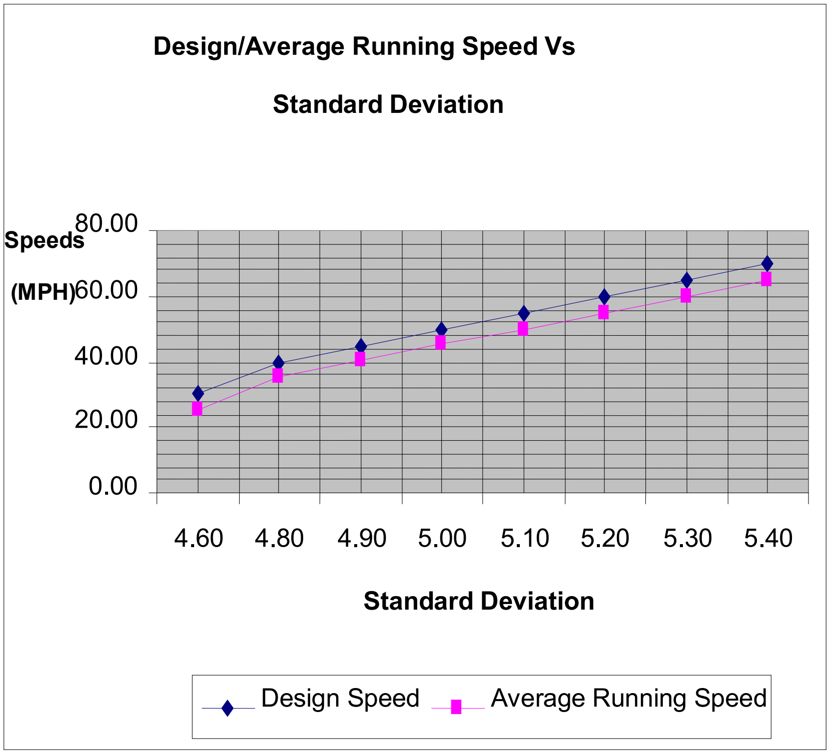

Figure 4.3: Standard Deviation Values Corresponding to Design Speeds and Operating Speeds based on NCHRP504.

4.4 Summary of the Design Procedure

The design procedure for the reliability approach to superelevation design is as follows:

1. Determine the facility type and design speed based on speed profile: - speed greater or lower than 50 mph

2. Select maximum superelevation based on the speed profile per AASHTO (4%, 6%, 8%, 10% and 12%).

3. Compute maximum friction factor based on equation 4-30.

4. Compute average speed based on equation 4-37 or table 4.1 or regional speed studies if available.

5. Compute standard deviation of the speed based on equation 4-38, table 4.2 or regional speed studies if available.

6. Select Reliability level desired (95% or 99%) and Radius of the proposed or existing curve and determine the Z value using Standard Normal Probability Table (Appendix C).

7. Compute required superelevation for the curve per equation 4.35.

8. Compute minimum required radius per AASHTO.

9. Compute minimum required Radius for the curve based on reliability design approach per equation 4.36.

10. Compare the minimum radius required per AASHTO with minimum required Radius based on reliability analysis. If the reliability design radius is equal to or greater than that produced by AASHTO, then the design radius is adequate.

This design procedure is illustrated in a simple flow chart in figure 4.3 below.

RELIABILITY APPROACH TO SUPERELEVATION DESIGN PROCEDURE FLOWHART

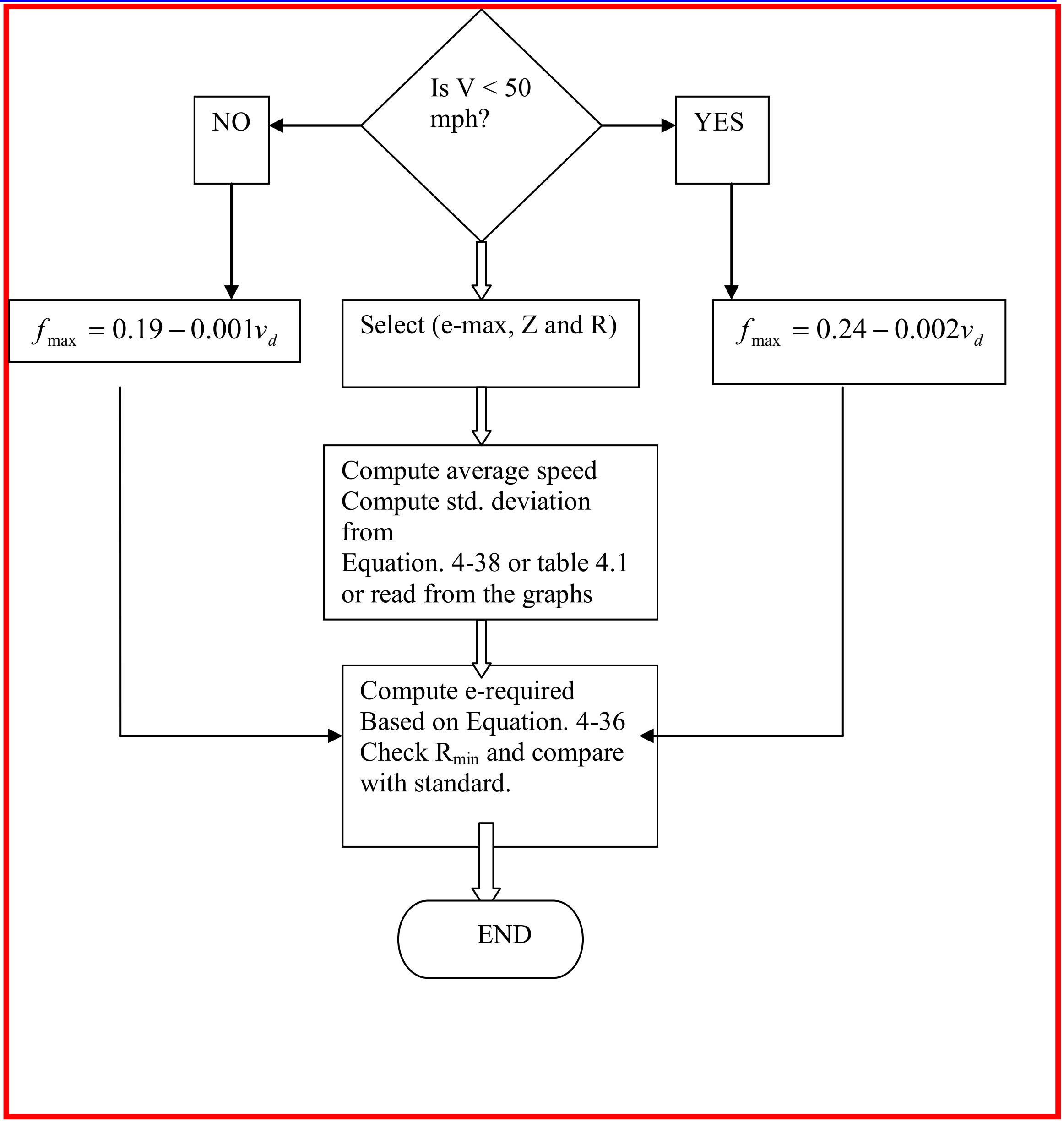

Figure 4.4: Flow Chart illustrating the design procedure: Reliability Design for Superelevation Distribution. Again, this flow chart illustrates the simplicity of the design methodology.

4.5 Results and Numerical Examples

The "defining" maximum superelevation rates, e_{max}, in NCHRP 439 are in general larger than 12% (see Table 5). To make a fair comparison with NCHRP 439, the e_{max} is defaulted as 12% in the proposed method and Method 5. The resulted superelevation rates are presented in Tables 4.4, 4.5 and 4.6. Note that if the "defining" e_{max} from NCHRP 439 were used in the proposed method and Method 5 instead of 12%, the resulted superelevation rates will be slightly larger than the values listed in Tables 3 and 4. As a comparison, the reliability-based superelevation rates are in general comparable with NCHRP 439. At a specific design speed, the reliability-based superelevation rates are larger (more conservative with a higher safety index) than NCHRP 439 at sharper curves. In particular, users must be cautioned that the required minimum turning radius from reliability constraint (see Equation 11) is larger than the R_{min} defined in NCHRP 439 and Method 5. Ignoring these differences is likely to place drivers at risk when cornering on sharp curves. As curve radius increases, these differences diminish and the reliability-based superelevation becomes less than NCHRP 439. For a given design speed, the reliability-based superelevation is typically 1% less than NCHRP 439 at much flatter curves. This implies that the results provided by the proposed method, if adopted for design, should produce cost savings to state agency when excess embankment required for elongated curves is eliminated. Figures 4.5-4.7 shows the superelevation rates plotted against degrees of curve that are often used by state agencies.

In comparison with Method 5, almost all the reliability-based superelevations at 95% level of confidence are much (1%-2%) less at any design speed and curve radius. These differences are more pronounced at lower design speeds (60 mph and below). Similar comparisons were also found in between NCHRP 439 and Method 5, indicating that the superelevation rates as recommended by AASHTO prior to 2005 are overly conservative. A numerical example is provided in the followings to demonstrate how one computes the reliability-based superelevation.

4.5.1 Numerical Example: Assume that v_d = 70 mph, e_{max} = 12%, and R = 3000 ft. Determine the required superelevation rate at the 95% and 99% level of confidences, respectively.

Solution: Based on Equations (4.27) and (4.28), the average running speed and standard deviation of speed can be calculated as:

$\bar{v}$ = 64.6 mph, and σ_v = 5.4 mph, respectively, (it can also be read from Table 4.2). f_{max} can be determined from Equation (4.30) as:

$$f_{\max} = 0.24 - 0.002 \cdot 70 = 0.1$$

At the 95% confidence level, z_α = 1.645. Therefore, from Equation (4.35), the required superelevation rate is:

$$\begin{aligned} e_{req} &= \frac{\bar{v}^2 + \sigma_v^2 + 2z_\alpha \bar{v}\sigma_v}{15R}\left(\frac{e_{\max}}{e_{\max} + f_{\max}}\right) \\ &= \frac{(64.6)^2 + (5.4)^2 + 2 \cdot 1.645 \cdot 64.6 \cdot 5.4}{15 \cdot 3000}\left(\frac{0.12}{0.12 + 0.1}\right) \\ &= 6.5\% \end{aligned}$$

which is consistent with Table 4.4. At the 99% confidence level, z_α = 2.326. Using Equation (9), e_{req} can be computed as 7.1%. NCHRP 439 predicts a design superelevation rate equal to 6.9% with e_{max} = 12.2% (see Table 5). The corresponding z_α value is 2.15 and the level of confidence is 98.4%. The superelevation rate resulted from Method 5 is 7% (see Table 4), which is slightly higher than the NCHRP 439 but very close to the reliability-based superelevation rate at 99%.

The minimum required curve radius can be determined using Equations (14) and (27):

$$R_{\min} = \frac{v_d^2}{15(e_{\max} + f_{\max})} = \frac{70^2}{15(0.12 + 0.1)}$$
$$= 1485 \text{ ft}$$

Then the minimum required curve radius under 95% level of reliability is:

$$\text{Min. } R_{req} = R_{\min} \frac{\bar{v}^2 + \sigma_v^2 + 2z_\alpha \bar{v}\sigma_v}{v_d^2}$$
$$= 1485 \cdot \frac{64.6^2 + 5.4^2 + 2 \cdot 1.645 \cdot 64.6 \cdot 5.4}{70^2}$$
$$= 1621 \text{ ft}$$

The $R_{\min}$ determined from NCHRP 439 is equal to 1431 ft. This illustrates that, under reliability constraint, the required curve radius is more conservative than $R_{\min}$ imposed by both AASHTO and NCHRP 439.

On the other hand, it is also interesting to note that, if one ignores the speed variation (i.e., σ_v^2 = 0) and applies the design speed as the speed measure instead, the required superelevation becomes:

$$e_{req} = \frac{v_d^2}{15R}\left(\frac{e_{\max}}{e_{\max} + f_{\max}}\right)$$
$$= \frac{70^2}{15 \cdot 3000}\left(\frac{0.12}{0.12 + 0.1}\right)$$
$$= 5.9\%$$

This suggests that ignoring speed variation will lead to an underestimation of the required superelevation rates. This underestimation could become more significant as speed variation increases. The corresponding z_α is 1.0, which gives 84.1% level of confidence, indicating that ignoring speed variation will possibly leave more than 15% drivers at risk.

4.3-1 Safety or Reliability Index and probability of Failure:

In Chapter 3, it was stated that safety index or the reliability index and probability of failure can be computed using the following equations:

$\beta = \frac{\mu_F}{\sigma_F}$ **,** from equation 3.11

Probability of failure $P_f = P\ (F<0)$, from equation 3.12 or

$P_f = 1 - \Phi\left[\frac{\mu_F}{\sigma_F}\right] = 1 - \Phi(\beta)$**,** from equation 3.13, where:

Φ is the CDF of the standard normal variate and $\Phi^{-1}(1 - P_f)$ is the value of the standard normal variate at the probability level (*1-P_f*).

Reliability or Safety Index for the above example using the reliability analysis from equation 4.25b is calculated as follows:

$$\beta_e = \frac{\mu_e}{\sigma_e} = \frac{\bar{v}^2 + \sigma_v^2}{gR}\left(\frac{e_{\max}}{e_{\max} + f_{\max}}\right) \div \frac{2\bar{v}\sigma_v}{(gR)}\left(\frac{e_{\max}}{e_{\max} + f_{\max}}\right)$$

$$\beta_e = \frac{\mu_e}{\sigma_e} = \frac{64.6^2 + 5.4^2}{32.2(3000)}\left(\frac{0.12}{0.12 + 0.10}\right) \div \frac{2(64.6)(5.4)}{32.2(3000)}\left(\frac{0.12}{0.12 + 0.10}\right)$$

$\beta_e = 6.0233$

$Pf = 1 - \Phi(6.0233) = 9.9E - 10$ and the safety index is calculated to be 6.0233 with a probability of failure computed to be 9.9E-10.

This result ensures a reliable design that accommodates majority of the drivers with minimal risk. This information will be very useful for the designer and the evaluator alike, especially, when dispute with respect to the adequacy of the design is called to question. Incorporating the safety index in the design of the turning radius and the superelevation distribution ensures full analysis of the risk inherent in the design methodology. A comparison of the methodologies is provided in table 4.3 below.

Table 4.3: Comparisons of distribution methods for *e* and *f* in AASHTO, NCHRP439, Easa & Reliability Analysis.

Method	Advantages	Disadvantages
1	-Simple (*e* and *f* are proportional to 1/*R*) -Avoid uses of e_{max} and f_{max} -Ideal and logical for distributing *f* or *e*	-Risky when vehicle speeds are not uniform
2	-Suitable on low-speed urban streets where *e* is less attainable	-Heavily dependent on available *f* in which driving comfort is an issue
3	-No *f* is needed on flatter curve at design speeds	-Results in negative *f* on flatter curve at average running speeds -*f* increasing sharply to f_{max} at sharper curves might result in erratic driving
4	-No *f* is needed on flatter curve at average running speeds and *f* is reserved for overdriving	-*f* increasing sharply to f_{max} at sharper curves might result in erratic driving
5	-Retain advantages of methods 1 and 4	-Computationally complicated, arbitrarily chosen distribution path.
NCHRP439	Retain advantages of methods 1 and 4, eliminate design inconsistency of different e for the same v_d. Unique radius.	Stepped function used in design similar to discrete function. Requires speed reduction from 95th percentile speed. No difference from 85th percentile speed. Seven different equations required to determine design superelevation, e_d.
Easa	Maximizes design consistency in a single alignment-Aggregate analysis. Minimizes variation in safety margin in a single alignment with a large number of curves regardless of their sequence. In Disaggregate Analysis-sequence of horizontal curves in a single alignment is considered. Produces lower e than method 5.	Required powerful optimization computer software to provide a solution. Complicated computation method. Produces higher f than method 5. Uses discrete function, which is contrary to the dynamic equation for vehicle motion along horizontal curve.
Reliability Analysis	Simple mathematical formulation. Takes advantage of the advantages of methods 1 and 4. Lower value of e_d resulting in economic savings. Can be easily applied to evaluate existing and proposed alignments.	Require different e-max. But this is not a disadvantage per se, since different e-max for different design environment is the practical approach to superelevation design.

Table 4.4 Required superelevation rate (%) at the 95% level of confidence based on reliability analysis ($e_{\max}$ = 12%)

v_d(mph) / R (ft)	15	20	25	30	35	40	45	50	55	60	65	70	75	80
23000														
20000														
17000														
14000														RC
12000													RC	2.3
10000												RC	2.3	2.8
8000										RC	RC	2.4	2.9	3.5
6000									RC	2.2	2.7	3.2	3.9	4.6
5000								RC	2.2	2.7	3.2	3.9	4.7	5.5
4000								2.2	2.7	3.3	4.0	4.9	5.8	6.9
3500							RC	2.5	3.1	3.8	4.6	5.6	6.7	7.9
3000						RC	2.3	2.9	3.6	4.4	5.4	**6.5**	7.8	9.2
2500					RC	2.2	2.8	3.5	4.3	5.3	6.5	7.8	9.3	11.1
2000					2.1	2.7	3.5	4.3	5.4	6.6	8.1	9.7	11.7	
1800					2.3	3.0	3.8	4.8	6.0	7.4	9.0	10.8		
1600				RC	2.6	3.4	4.3	5.4	6.7	8.3	10.1			
1400				2.2	3.0	3.9	4.9	6.2	7.7	9.5	11.5			
1200			RC	2.5	3.5	4.5	5.8	7.2	9.0	11.0				
1000			2.1	3.1	4.1	5.4	6.9	8.6	10.8					
900			2.4	3.4	4.6	6.0	7.7	9.6						
800			2.7	3.8	5.2	6.8	8.7	10.8						
700		RC	3.0	4.4	5.9	7.8	9.9							
600		2.3	3.6	5.1	6.9	9.1	11.5							
500		2.8	4.3	6.1	8.3	10.9								
450		3.1	4.7	6.8	9.2									
400	RC	3.5	5.3	7.6	10.4									
350	2.3	4.0	6.1	8.7	11.9									
300	2.7	4.6	7.1	10.2										
250	3.2	5.6	8.5											
200	4.0	6.9	10.7											
150	5.4	9.3												
100	8.0													
75	10.7													
Min. R_{req} (*ft*)	67	116	178	255	346	453	578	720	898	1105	1345	1622	1942	2310

Table 4.4. Required superelevation rate (%) based on Method 5 (e_{max} = 12%)

v_d(mph) / R (ft)	15	20	25	30	35	40	45	50	55	60	65	70	75	80
23000														
20000														
17000														
14000													RC	RC
12000												RC	2.1	2.3
10000										RC	RC	2.2	2.5	2.7
8000								RC	RC	2.2	2.5	2.7	3.1	3.4
6000							RC	2.1	2.5	2.9	3.2	3.6	4.1	4.5
5000						RC	2.1	2.5	2.9	3.4	3.9	4.3	4.8	5.4
4000						2.1	2.5	3.1	3.6	4.2	4.6	5.4	6.0	6.7
3500					RC	2.4	2.9	3.5	4.1	4.8	5.4	6.1	6.8	7.7
3000					2.2	2.7	3.3	4.0	4.7	5.5	6.2	**7.0**	7.9	8.9
2500				RC	2.6	3.2	4.0	4.7	5.6	6.5	7.4	8.3	9.4	10.6
2000				2.5	3.2	4.0	4.8	5.8	6.8	7.9	9.0	10.2	11.5	
1800			RC	2.7	3.5	4.4	5.3	6.3	7.4	8.6	9.8	11.1	12.0	
1600			2.3	3.1	3.9	4.9	5.9	7.0	8.2	9.5	10.8	11.9		
1400		RC	2.6	3.4	4.4	5.5	6.6	7.8	9.1	10.6	11.7			
1200		2.1	3.0	4.0	5.1	6.2	7.5	8.8	10.3	11.5				
1000		2.5	3.5	4.7	5.9	7.3	8.7	10.1	11.4					
900		2.8	3.9	5.1	6.5	7.9	9.4	10.8	11.8					
800		3.1	4.3	5.6	7.1	8.6	10.2	11.4						
700	RC	3.5	4.8	6.3	7.9	9.5	11.0	11.9						
600	2.4	4.0	5.5	7.1	8.8	10.5	11.7							
500	2.8	4.7	6.4	8.2	10.0	11.4								
450	3.1	5.1	6.9	8.8	10.6	11.8								
400	3.4	5.6	7.5	9.5	11.2	12.0								
350	3.8	6.2	8.3	10.2	11.7									
300	4.4	7.0	9.1	11.0	12.0									
250	5.1	7.9	10.1	11.7										
200	6.1	9.0	11.2											
150	7.5	10.5	12.0											
100	9.6	11.9												
75	11.0													
R_{min} (*ft*)	51	92	147	215	298	397	511	643	809	1003	1228	1489	1791	2140

Table 4.5. Required superelevation rate (%) based on NCHRP 439

v_d(mph) / R (ft)	15	20	25	30	35	40	45	50	55	60	65	70	75	80
23000														
20000														RC
17000												RC	RC	2.2
14000											RC	2.1	2.3	2.6
12000										RC	2.1	2.4	2.6	2.9
10000									RC	2.2	2.4	2.7	3.0	3.4
8000								RC	2.2	2.6	2.9	3.3	3.6	4.0
6000							RC	2.4	2.8	3.2	3.6	4.1	4.5	5.0
5000						RC	2.3	2.7	3.2	3.7	4.2	4.7	5.2	5.8
4000					RC	2.3	2.7	3.2	3.8	4.3	4.9	5.5	6.2	6.9
3500					2.1	2.5	3.0	3.6	4.2	4.8	5.5	6.1	6.9	7.7
3000				RC	2.3	2.8	3.4	4.0	4.7	5.4	6.1	**6.9**	7.8	8.6
2500				2.1	2.6	3.2	3.9	4.6	5.4	6.2	7.0	8.0	8.9	10.0
2000				2.4	3.0	3.8	4.5	5.4	6.3	7.3	8.4	9.5	10.6	
1800			RC	2.6	3.3	4.1	4.9	5.8	6.9	7.9	9.0	10.2	11.5	
1600			2.1	2.8	3.6	4.4	5.4	6.4	7.5	8.7	9.9	11.2		
1400			2.3	3.1	3.9	4.9	5.9	7.0	8.3	9.6	11.0			
1200		RC	2.6	3.4	4.4	5.4	6.6	7.9	9.3	10.8	12.3			
1000		2.1	2.9	3.9	5.0	6.2	7.6	9.0	10.6	12.3				
900		2.3	3.1	4.2	5.4	6.7	8.2	9.8	11.5					
800		2.4	3.4	4.5	5.8	7.3	8.9	10.7	12.6					
700		2.6	3.7	5.0	6.4	8.0	9.8	11.8						
600	RC	2.9	4.1	5.5	7.1	9.0	11.0	13.2						
500	2.2	3.3	4.7	6.3	8.1	10.2	12.6							
450	2.3	3.5	5.0	6.8	8.8	11.0	13.6							
400	2.5	3.8	5.4	7.3	9.5	12.0								
350	2.7	4.1	5.9	8.0	10.5	13.2								
300	2.9	4.6	6.6	8.9	11.7									
250	3.3	5.1	7.4	10.1	13.3									
200	3.7	5.9	8.6	11.8										
150	4.4	7.1	10.4											
100	5.7	9.2												
75	6.7	11.1												
e_{max}	11.1	12.5	13.5	14.0	14.3	14.4	14.2	13.9	13.4	12.8	12.5	12.2	11.9	11.5
R_{min} (*ft*)	33	63	103	157	225	312	422	561	739	950	1181	1431	1730	2089

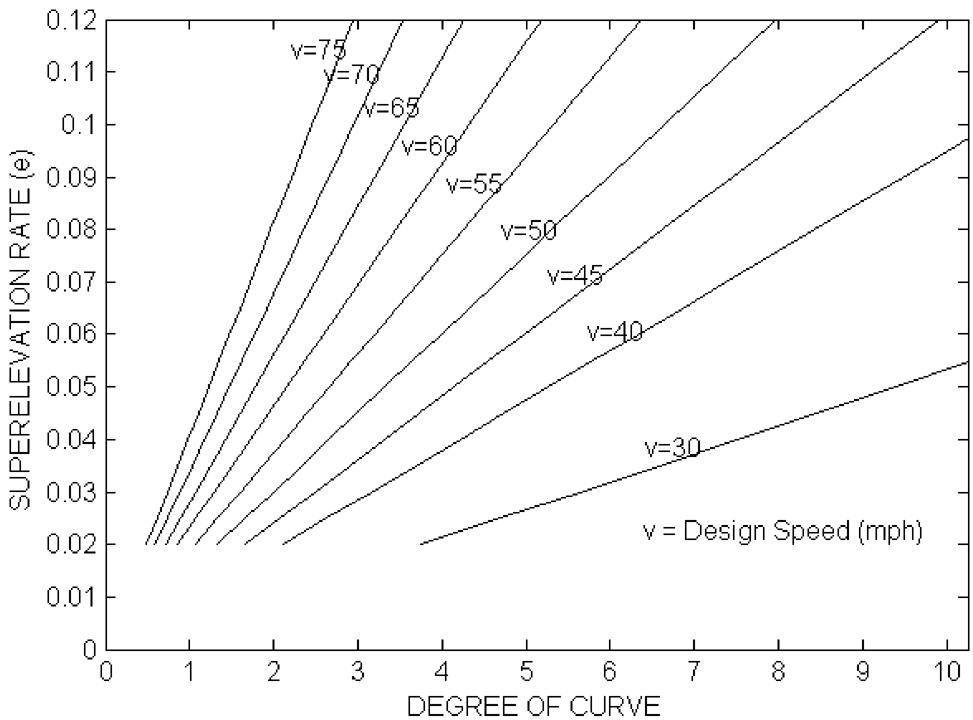

Figure 4.5. Required superelevation rates (e_{max} = 0.12) v.s. degree of curve based on reliability analysis (95% level of confidence)

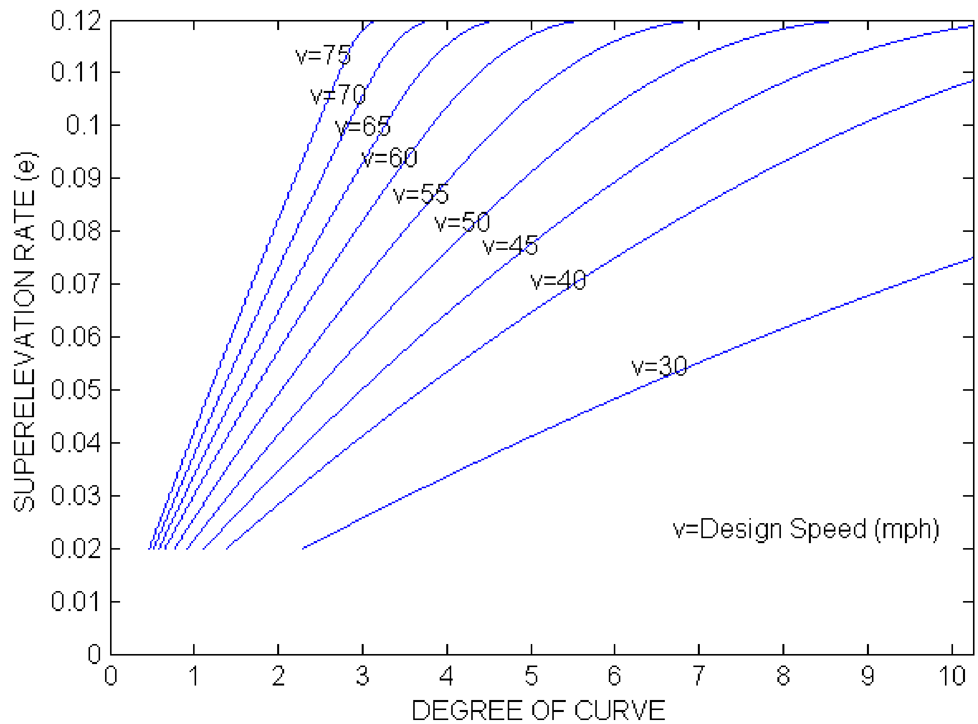

Figure 4.6: Required superelevation rates (e_{max} = 0.12) v.s. degree of curve based on Method 5

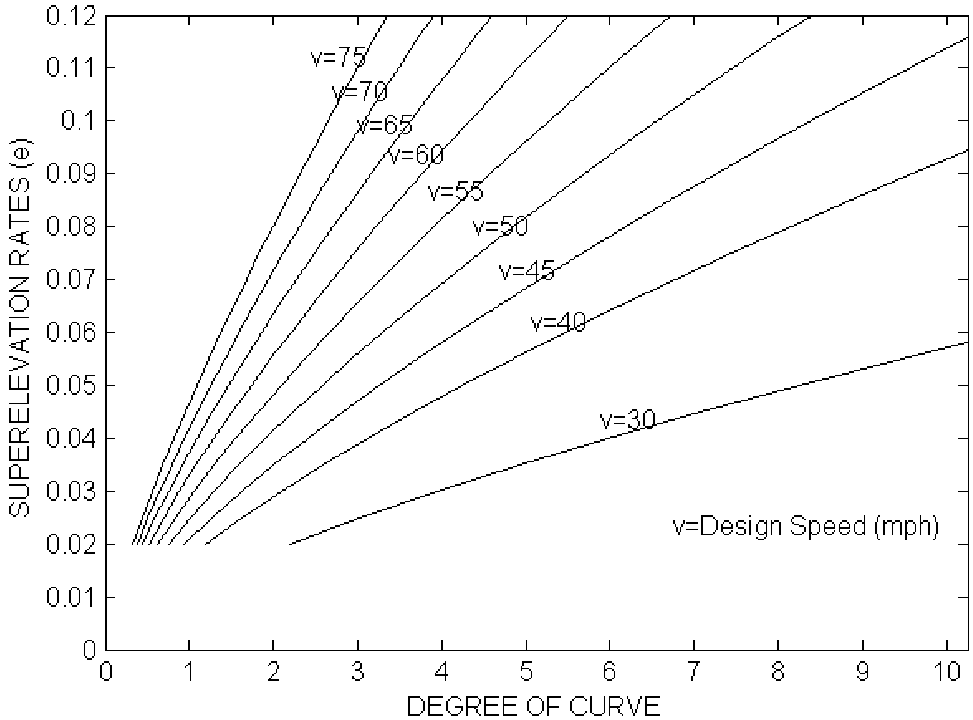

Figure 4.7: Required superelevation rates v.s. degree of curve based on NCHRP 439 distribution method

4.6: Cost Comparison between Reliability Design Approach and AASHTO Method 5.

Figure 4.8 below is an illustration of a superelevated horizontal highway curve. Section A-A, shows the required embankment resulting from the rotation of the roadway due to superelevation. From these figures, it can be seen that the higher the superelevation rate, the higher the amount of embankment required to attain full superelevation at the sharpest point of the curve.

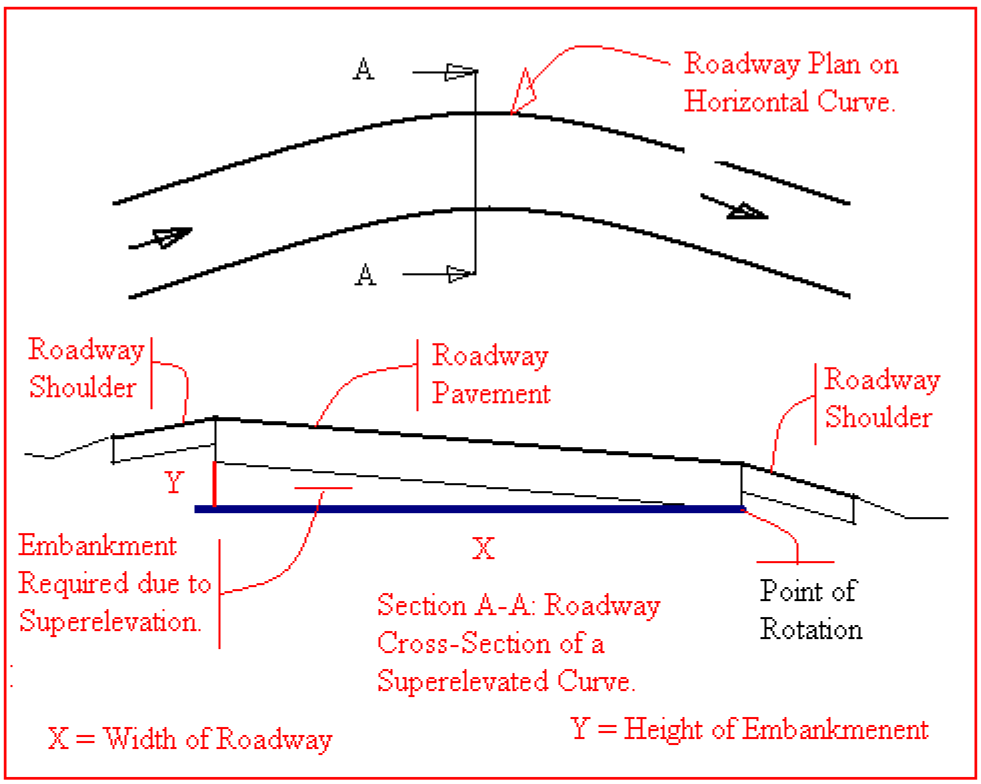

Figure 4.8: Plan and Cross-Section of a Superelevated Highway Horizontal Curve.

Figure 4.9 provides a geometric comparison between the Reliability Design Method and AASHTO Design Method 5. This figure also shows the superelevation rates arising from the two design methods. Based on the difference in the superelevation rates, the amount of embankment required for both design methods can be can be computed. A comparison of the cost can be made to allow design professional as well as planners to select the best design methods with respect to cost constraints.

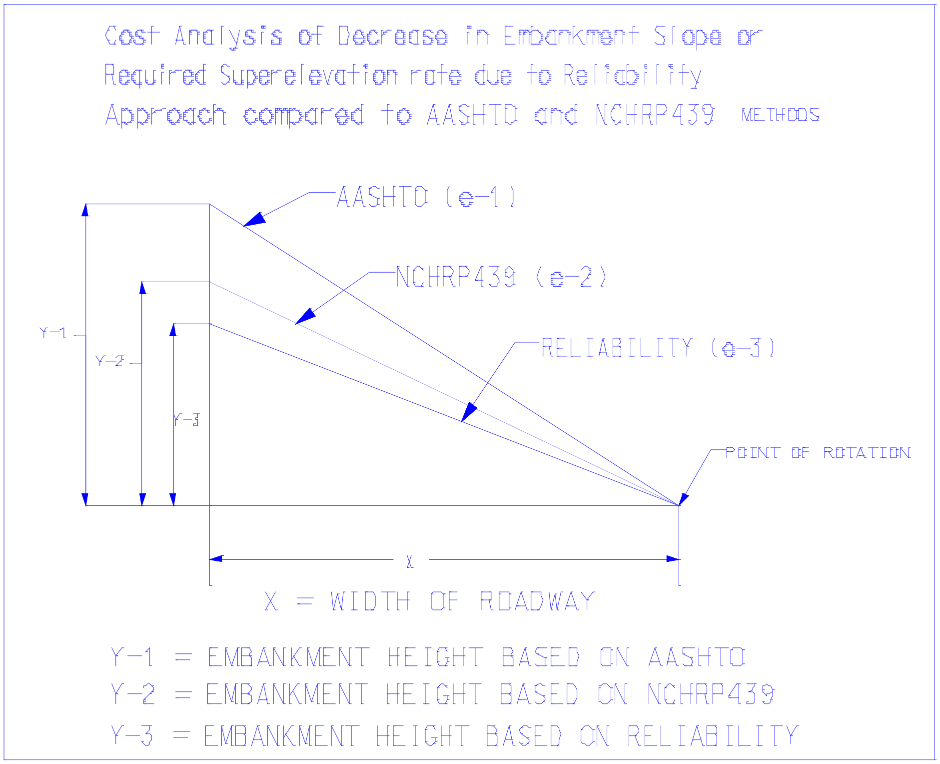

Figure 4.9: Exaggerated Superelevation Difference between Method 5, NCHRP439 and Reliability Approach Design Method.

4.7: Derivation of Basic Equation for Embankment Computation

Assume a minimum length of curve of 400 feet, the prismatic area of the cross section of the embankment based on the geometry can be derived as follows:

Let Y-1 be represented by the total height of embankment due to method 5 design and Y-2 be the height of embankment due to reliability approach design. The area of the prismatic cross-section can be written as:

Area $A_{Y-1} = ½(Y-1)*X$ 3.30

And

Area A_{Y-2} = ½(Y-2)*X 3.31

Also,

The slope of each embankment can be calculated as follows:

[(Y-1)/(X)]*100 = (e-1)% 3.32

So that, Y-1 = (e-1)*X/100 3.33

And

((Y-2)/X)*100 = (e-2)% 3.34

So that, Y-2 = (e-2)X/100 and Y-3 = (e-3)X/100 3.35

The difference in the prismatic cross-sectional area is given as:

(AY-1) – (AY-2) = ½(Y-1)*X – ½(Y-1)*X = ½(X)[(Y-1) –(Y-2)] 3.36

Substituting the values of Y-1 and Y-2 or Y-3 from Equations 3.33 and 3.35, we can write the area difference as:

½(X)[(e-1)X – (e-2)X]/100 = 1/2((e-1)-(e-2))X^2/100 3.37

The cost comparisons based on equation 4.37 are shown on table 4.6 below.

Table 4.6				
COST DIFFERENCE BETWEEN AASHTO, NCHRP439 AND RELIABILITY DESIGN				
DESIGN SPEED = 70 MPH, e (max) = 12%, Unit price = $22.67/Cubic Yard**				
Min Curve Length = 400ft, and lane width of 48 feet				
RADIUS	NCHRP439 Design	Reliability Design		
8000	-$773.80	$386.90		
6000	-$644.84	$515.87		
5000	-$515.87	$515.87		
4000	-$128.97	$644.84		
3500	$0.00	$644.84		
3000	$128.97	$644.84	Key:	
2500	$386.90	$644.84	-$773.80 = Loses	
2000	$902.77	$644.84	$386.90 = savings	
1800	$1,289.67	$515.87		
** Based on FDOT Historical Unit Cost from 06/01/2009 to 06/01/2010				

The above computation shows that the cost of embankment difference between the current AASHTO's method 5 when compared to the reliability approach with e-max of 12% can be significant. If this method is adopted throughout the industry, it will result in a tremendous savings in cost and materials required for the construction of highway embankments necessitated by superelevation of the curve. Similarly, comparison of the reliability approach to NCHRP439 method produced a cost difference which is not consistence, low for high radius and low for low radius resulting in underestimation and overestimation.

4.8 Conclusions

As it is illustrated above the reliability approach is straightforward to apply and produces superelevation rates that are reasonably comparable to Method 5 and NCHRP 439 distribution method. As stated earlier, the use of Method 5 represents a mathematical convenience without much consideration to the speed variation, as well as the inherent lengthy process required to obtain the superelevation *e* distribution. The NCHRP 439 approach in attempt to eliminate the inconsistency in using significantly different superelevation rate at the same design speed on curves of similar radius due to the use of multiple maximum superelevation rates on nearby facilities is commendable. In addition, simplification of computational procedure enables users to manually calculate superelevation rates without relying on look-up Tables and Figures.

Compared to NCHRP 439 method, the reliability analysis proposed here results in an even simpler and more straightforward distribution method for calculating required superelevation at a specific level of confidence. It can be easily applied as an alternative means to evaluate existing curves as well as used in the design of new curves. It is believed that the use of method 1 to account for the distribution of side friction factor is logical but the inherent assumption of uniform speed might place drivers at risk when cornering on curves. The use of reliability approach accounts for the variation in speed and thus eliminates the expectation of constant speed that is the major drawback for method 1. The resulted reliability-based superelevation rates are fairly comparable to NCHRP 439 in general, but are more conservative at sharper curves given the same design speed. In addition, users must be cautioned that the required minimum turning radius from reliability constraints is also more conservative than the $R_{\min}$ defined in NCHRP 439 and Method 5. As curve radius increases, these differences diminish and the reliability-based superelevation becomes less than NCHRP 439, which is typically 1% less than NCHRP 439 at much flatter curves for a given design speeds. This implies that the results provided by the proposed method, if adopted for design, should produce cost savings to state agency when excess embankment required for elongated curves is eliminated.

In comparison with Method 5, almost all the reliability-based superelevations at 95% level of confidence are much (1%-2%) less at any design speed and curve radius. These differences are more pronounced at lower design speeds (60 mph and below). Similar comparisons were also found in between NCHRP 439 and Method 5, indicating that the superelevation rates as recommended by AASHTO are overly conservative. A new concept in highway design is highlighted through the incorporation of factor of safety or reliability index in the design. Finally, it is also demonstrated here that ignoring speed variation will lead to a significant underestimation of the required superelevation rates, which will in turn place greater portion of drivers in risk when cornering curves.

Chapter 5: Application of Reliability Analysis to Intersection Left Turn Bay Design- Safety Evaluation

5.1 Background:

American Association of States Highways and Transportations Officials (AASHTO)'s Policy on Geometric Design of Highways and Streets – commonly known as Green Book (GB), provides design guidance for left turn bay design at an intersection. The guidance relates to length of the left turn bay, traffic volumes and intersection control mechanism such as stop signs and signals and other intersection controls provided by Manual of Uniform Traffic Devices (MUTCD) Evaluation of the effectiveness of the left turn bay for safety or the reliability of the left turn bay is largely not covered by the green book but is deferred to traffic engineering operations as presented in Highway Capacity Manual (HCM) in terms of intersection delay (D), its ability to handle a given volume. HCM and other traffic engineering publications and practice do not address the inherent safety issue of the turn bay in which a saturation condition of the turn bay is exceeded. This research will present a methodology to evaluate the reliability of a left turn bay based on its geometry and the traffic demands. There are three components in the length of left turn bay design: 1) Clearance distance, 2) breaking to a stop distance and 3) the length of storage or queue length after breaking to a stop is complete (FDOT Standard Index 2008). AASHTO and FDOT criterion is to design the intersection with a minimum of two cars length on the queue storage while the clearance and breaking distances are based on design speed, reaction time and average deceleration rate. The variation in the queue length reduces the availability of the other two components (clearance and breaking distances) and thereby decreasing the ability of the driver to clear the thru lane and come to a stop safely. Failure occurs when the available length of clearance distance plus the breaking distance is less than the demand. The reliability of the turn bay can be evaluated based on the geometry as the length of the turn bay is reduced by a successive number of cars exceeding the queue length or storage distance. The reliability of the left turn bay with respect to safety therefore, is the availability of the turn bay for the left turning vehicle to complete clearance and breaking maneuver without shock to the traffic downstream. This research will develop the methodology for determining this shock in terms of increase in the acceleration rate over the AASHTO specified limit of $11.2 ft/s^2$ along with reliability indices and probability of failures for the turn lanes.

5.2 Model Formulation

5.2.1 Safety Margin/Performance Function

The effect of long queues at any intersection whether signalized or not on the safety of the left turn lane depends on many factors. The primary measure of intersection performance is delay. Delay at intersection depends on probabilistic distribution of arrival and departure rates, signal timing (for signalized intersection), the flow rates on the intersection approach and the volume of the opposing traffic (un-signalized intersection). For the development of this model, the following assumptions factors are made:

1. The intersection may or not signalized
2. The intersection may be of a single through lane with a single lane left turn bay or more.

3. The left turn turning and opposing vehicles are assumed to arrive according to the Poisson distribution.
4. The probability of k vehicles arriving within a time period t is given as

   $$P(k) = ((\lambda t)^k e^{-\lambda t})/k! \tag{5.1}$$

   Where: λ is either the arrival rates of the left turning or opposing vehicle.
5. The critical gap, t_g, in seconds.

5.2.2 Definition of Terms

The basic inputs required for the development of the safety consideration of the left turn lane are as illustrated in figure 5.1. The figure shows the geometric definition of the safety margin required for evaluation of the level of safety or the reliability of the left turn bay for a single lane left turn bay. The terms and the definitions of term are as follows:

- **L-1** is the clearance distance; it is the distance required for the driver to clear the through lane, based on the reaction time of the driver from the moment the driver enters the functional area of the intersection and take foot off the acceleration pedal without breaking.

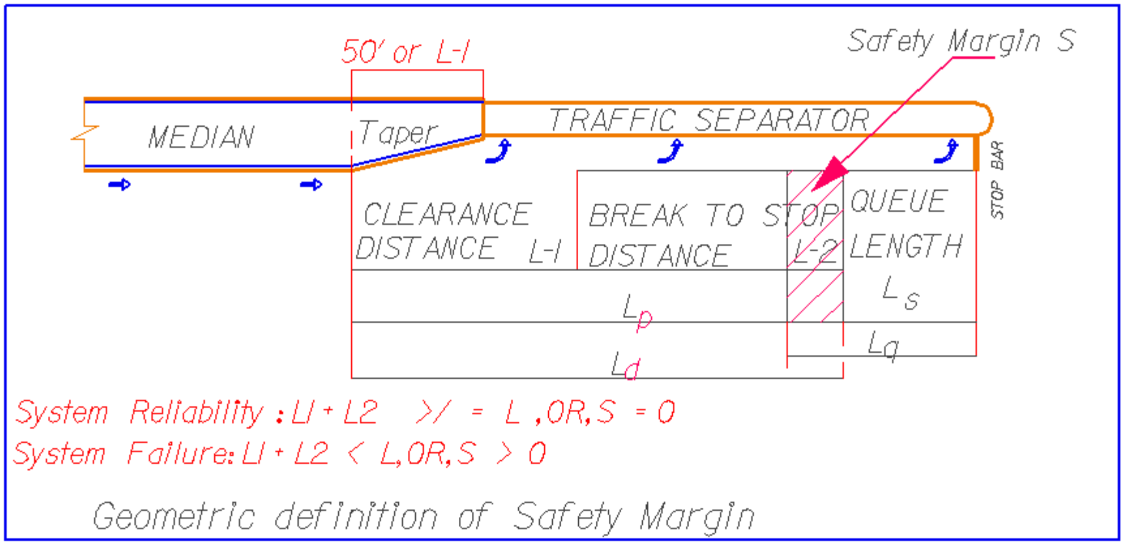

Figure 5.1: Geometric definitions of left turn factors for safety consideration.

- **L-2** is the break to stop distance; it is the distance required for the vehicle to come to a complete stop after the break is applied before joining the queue.
- $\mathbf{L_s}$ is the designed storage distance or distance for 2 vehicle to store per AASHTO criteria or numbers of cars for a 2-minute surge.
- $\boldsymbol{L_d}$ is the sum of *L-1* and *L-2* and it is the designed safe distance required for the vehicle to complete the stopping maneuver at the left turn lane.
- $\boldsymbol{L_p}$ is the actual distance provided for the left turning vehicle to complete the stopping maneuver at the left turn lane when $\boldsymbol{L_q}$ is greater than $\boldsymbol{L_s}$
- $\boldsymbol{L_q}$ is the actual queue length formed by the vehicles waiting to make a left turn at the intersection.
- ***S*** is the Safety Margin required for the left turning vehicle to complete the left turn maneuvers.

From the diagram above, we can establish the following relationships:

$$L_d = L_1 + L_2 \tag{5.2}$$

$$S = L_q - L_S \tag{5.3}$$

$$L_P = L_d - S \tag{5.4}$$

$$L_P = L_d - L_q + L_S \text{ (From 5.3 and 5.4)} \tag{5.5}$$

Where L_P is the available distance for the left turning vehicle to complete the clearance and breaking maneuvers and it defines the system reliability in that, when L_q is greater than L_S, L_d decreases and L_P reliability decreases as *S* values increases. It is to be noted that an ideal condition calls for *S* to be zero where adequate lane length has been provided. A negative *S* indicates that more than adequate lane length has been provided in the design. A positive value of *S* is an indication that the length of the turn lane is inadequate for the prevailing traffic demand.

From AASHTO Green Book, the clearance and breaking distance to a stop is based on the vehicle speed (v), break reaction time (t) and the deceleration rates and it is given by the equation:

$$d = 1.47vt + \frac{1.075v^2}{a} \tag{5.6}$$

Where d is the distance traversed during the break reaction time and the distance to break the vehicle to a stop. We will replace this distance with L_d.

t = brake reaction time, 2.5 seconds

v = design speed, mph.

a = deceleration rate, ft/s^2 (11.2 ft/s^2)

By substituting $L_d = 1.47vt + \frac{1.075v^2}{a}$, and (5. 7)

$$L_P = 1.47vt + \frac{1.075v^2}{a} - L_q + L_s \tag{5.8}$$

Per AASHTO criteria, $L_s = 50'(Min)$

Per Chakroborty et al (1995) and Wu (1994), $L_q = N^*$

Where N^* is the adequate lane length in numbers of vehicles to the nearest integer converted to distance by multiplying by equivalent vehicle length – assumed to be 25 ft; by substituting the values for L_s and L_q into Equation (5.8), we can rewrite it as follows:

$$L_P = 1.47vt + \frac{1.075v^2}{a} - N^* + 50 \tag{5.9}$$

If L_s is based on 2 cars estimate, otherwise, an analysis of L_s based on a 2-minute surge during the peak hour should be used. From a deterministic design approach, Equation (5.9) is sufficient once an estimate value of N* is obtained. However, it is known that variation in the input of N* remains and those variations need to be analyzed for the inherent risk; the reliability design approach addresses this risk.

From the probability of failure standpoint, the above deterministic derivation can be restated in the following fashion. It is apparent that the demand of the turn lane is $L_P + L_Q$ and the supply of the turn lane is $L_d + L_s$. We can redefine the safety margin as:

$$Z = \text{Supply} - \text{Demand} = L_d + L_s - (L_P + L_Q) \qquad 5.10$$

To be reliable, the probability of failure needs to be less than a specified level of significance, *α*, i.e.

$$P_f = P(Z < 0) = P(L_d + L_s < L_P + L_Q) < \alpha \qquad 5.11$$

The above statement can also be restated as the probability of success being greater than (1- α), i.e.,

$$P(Z > 0) = P(L_d + L_s > L_P + L_Q) > 1\text{-}\alpha \qquad 5.12$$

5.3: Determination of Sufficient Lane Length Based on the Demand

Let' us replace the $L_d + L_s$ with a single variable L_D and $L_P + L_Q$ with L_S for simplicity of use.

We can rewrite the margin of safety equation as:

$$Z = \text{Supply} - \text{Demand} = L_D - L_S \qquad 5.13$$

The sufficient lane length can be defined as the lane length that is sufficient for a selected reliability level for the intersection based on the traffic demand. This can be expressed as in equation 5.12. We can write this equation as shown below, using the simplified variables proposed above. Thus;

$$P(Z>0) = P(L_D > L_S) < 1\text{-}\alpha \qquad 5.14$$

Where,

L_D = the left turn length in number of vehicles, and

L_S = the left turn length demanded by the turning vehicles (number of vehicles in the queue).

1-α = the level of reliability selected for the intersection operations.

In order to compute the probability $P(L_D > L_S)$, the probability density function of number of left turning vehicles in the queue must be determined. This is a difficult process that requires actual observation for several intersections in the regions along with some calibrations before this can be used. The distribution of the service time can be very complex as stated in the literature review with respect to intersection delays. Nevertheless, we can employ Chebyshev's inequality formula which allows the computation of this probability without any specific assumptions about the PDF.

With this tool we can write the safety margin equation as follows:

$$P(L_D > E[L_D] + \alpha) <= \frac{\mathrm{var}(L_D)}{\mathrm{var}(L_D) + (\alpha)^2} \qquad 5.15$$

where:

α is any real number. This inequality is true for any probability distribution for L_D

Substituting E[L_D] + α by L_S, we can write equation 6.14 as follows:

$$P(L_D > L_S) <= \frac{\mathrm{var}(L_D)}{\mathrm{var}(L_D) + (L_S - E[L_D])^2} <= 1\text{-}\alpha \qquad 5.16$$

From the forgoing and by inspection, it is clear that the worst case condition occurs when the equation 6.15 is equality. That is, the probability that number of vehicles in the queue is greater than the lane length. When equation 5.16 is equality, L_D is L_S and the system is in a breakdown condition depending on the reliability level desired. Thus we can rewrite equation 5.16 as follows:

$$P(L_D > L_S) <= \frac{\mathrm{var}(L_D)}{\mathrm{var}(L_D) + (L_S - E[L_D])^2} = 1\text{-}\alpha \qquad 5.17$$

And after simplification,

$$(L_S)^2 - 2E[L_D]L_S + E[L_D]^2 + \mathrm{var}(L_D) - \frac{1}{(1-\alpha)\,\mathrm{var}(L_D)} = 0 \qquad 5.18$$

The resulting quadratic equation in L_S, can be solved for L_S, using the quadratic equation formula such that:

$$L_S = E[L_D] + \sigma[L_D]\sqrt{\frac{1}{1-\alpha} - 1} \qquad 5.19$$

Where:

$E[L_D]$, is the average or mean queue length and $\sigma[L_D]$ is the standard deviation of the queue length.

Equation 5.19 requires that only one root of the equation should be considered in that the sufficient lane length required should increase as α increases and not as required by the second root.

$$L_S = \frac{\text{var}(L_D)}{\text{var}(L_D) + (L_S - E[L_D])^2} <= 1\text{-}\alpha, \text{ is also true} \qquad 5.20$$

Drew (1968) and as developed by Chakroborty et all (1995), under the assumption of Poisson arrival of the opposing traffic flow, the time headways in the opposing flow are distributed exponentially with parameter λ_o, It is also assumed that the critical gap T_g is the same for all drivers and is independent of how long the driver has waited in the queue, the following equations is obtained from the moment generating function or the service time distribution.

$$E[u] = \frac{e^{\lambda_o T_g} - 1 - \lambda_o T_g}{\lambda_o} \qquad 5.21$$

Where:

E[u] is the mean service time for the left turning vehicles (or left turning vehicle waits at the top of the queue).

The variance of the service time is also given as:

$$\text{var[u]} = \frac{e^{2\lambda_o T_g} - 2\lambda_o T_g e^{\lambda_o T_g} - 1}{\lambda^2{}_o} \qquad 5.22$$

It is important to note that for signalized intersection, the service time in the turning lane will default to the red phase for the left turn.

In order to compute the length of queue, we will need to know the arrival rate of the left turning vehicles λ_t on the turn lane.

Based on Pollaczek-Kintchine equation, the relationship of the arrival rate and the mean queue length is given as:

$$E[L_D] = \lambda_t E[u] + \frac{\lambda_t^2 E[u^2]}{2(1-\lambda_t E[u])} \qquad 5.23$$

and

the variance of the queue length is given as:

$$\text{var}[[L_D] = 2(E[u]) - \lambda_t E[u])^2 + 3(E[L_D]) - 2\lambda_t (E[u]) + \frac{\lambda_t^3 E[u^3]}{3(1-\lambda_t E[u])} - E[L_D]^2 \qquad 5.24$$

The $E[u^2]$ and $E[u^3]$ has been derived by Chakroborty, et al and are presented in equation 5.25 and 5.26.

$$E[u^2] = \frac{2(\lambda_o E[u])^2 + 2\lambda_o E[u] - (\lambda_o T_g)^2}{\lambda_o} \qquad 5.25$$

and

$$E[u^3] = \frac{6}{\lambda^3{}_o}[2\lambda_o E[u]\{[\lambda_o E[u] - \frac{(\lambda_o T_g)^2}{2}\} + (\lambda_o E[u])^3 + \{\lambda_o E[u] - \frac{(\lambda_o T_g)^2}{2} - \frac{(\lambda_o T_g)^3}{6}\}]$$

5.26

Once the means and variances of the arrivals rates of the left turning vehicles (λ_t) and the opposing vehicles (λ_o) are known, the computation is easy when the value of the critical gap T_c is known. The queue length plus the breaking distance becomes the total sufficient lane length for the intersection based on the input parameters of volumes, arrival rates, critical gap and the approaching speed. The above approach computes the required length of the turn lane directly based on the desired level of reliability. A more direct approach is to compute the queue length and then solve equation 5.8 and compare with current standard. This can be accomplished with less effort than the first method shown above.

The quantity L_q can also be computed directly using sets of equations developed by Wu (1994 in Troutbeck & Brilon, 2003). There are many proposed equations for queue lengths based on Little's rule (1961), and M/G/1 queuing theory (Troutbeck and Brilon, 1997), however, they are too complicated for practical use. According to Troutbeck, it is the percentiles of the queue length that is really needed to evaluate the degree of functionality of the turn lane. Thus, Wu's sets of equations which are based on an M/M/1 queuing analysis provide a better approximation for the computation of the queue length L_q. These equations (Brilon,WU & Bondzio, 1997) are as follows:

$$p(0) = 1 - x^a \qquad 5.27$$

$$p(n) = p(0).\, x^{a(b(n-1)+1)} \qquad 5.28$$

Where:

P(0) is the probability of an empty queue on the minor street (Left turning lane).

P(n) is the probability that n vehicles are queuing on the minor street (left turning lane).

$x = q_n/q_m$, is the degree of saturation of the minor street.

q_n, is the traffic flow on the minor street in vehicles per second

q_m, is the traffic flow capacity of the minor street in vehicles per second.

And:

$$a = \frac{1}{1 + 0.45.\frac{t_c - t_f}{t_f}.q_p} \qquad 5.29$$

$$b = \frac{1}{1 + 0.68.\frac{t_c}{t_f}.q_p} \qquad 5.30$$

In the realistic case where, $t_c = 2t_f$, the expressions for a and b are further reduced to:

$$a = \frac{1}{1 + 0.45.q_p} \qquad 5.31$$

$$b = \frac{1.51}{1 + 1.36.q_p} \qquad 5.32$$

Where:

t_c, is the critical gap for the minor road (left turning) vehicles to cross the intersection.

t_f , is the follow up time between minor road (left turning) vehicles to cross the stop bar.

q_p , is the traffic flow in vehicles per seconds in the major road.

t_c is the critical gap for the minor road (left turning) vehicles to cross the intersection.

The cumulative distribution function of the queue length is derived from equation 5.28 by combining *p(0)* and *p(n)* and is given as:

$$F(n) = p(Ls \leq n) = 1 - x^{a(b.n+1)} \qquad 5.33$$

For any given percentile, such as $\boldsymbol{\alpha} = F(n) = 0.95$, equation 5.33 can be solved for n to calculate the queue length that is exceeded for $(1 - \alpha).100$ percent of the time. Thus the queue length obtained in this way will be deemed as the 95th percentile queue length. And this is a good estimate of the queue length that can be employed in practical application.

By setting alpha values to be 0.05 and 0.01, n_{95} and n_{99} are calculated as shown below:

$$n_{95} \approx \frac{q_m}{4}\left\{x - 1 + \sqrt{(1 - x)^\wedge 2 + \frac{8x}{q_m} \cdot [-\ln(0.05)]}\right\}$$

$$\approx \frac{q_m}{4}\left\{x - 1 + \sqrt{(1 - x)^2 + \frac{8x}{q_m}.(3.0)}\right\} \qquad 5.34$$

$$n_{99} \approx \frac{q_m}{4}\left\{x - 1 + \sqrt{(1 - x)^2 + \frac{8x}{q_m}.(4.6)}\right\} \qquad 5.35$$

As mentioned earlier, the quantity q_m is computed based on Fisk and Tanner equations for multiple lanes or single lane Gap Acceptance Theory.

For single lane, the Tanner equation is used and for multiple lanes the Fisk equation is used.

Thus:

The capacity q_m or a single lane based on tanner equation is given as

$$q_m = \frac{q_p e^{-(q_p/3600)*t_g}}{1-q_p e^{-(q_p/3600)*t_f}} \qquad 5.36$$

The capacity q_m for multiple lanes is provided by the Fisk equation and is given as:

$$q_m = \frac{q_p e^{-(q_p/3600)*t_g}}{1-q_p e^{-(q_p/3600)*t_f}} \qquad 5.37$$

Where:

q_p = the traffic flow on the opposing lane

t_c = tg = critical time gap in the opposing lane priority movement to allow the minor street or left turning vehicles to make the left turn.

5.3.1: Time Gap for Left Turning Vehicles.

According to AASHTO' Green Book (2004), the time gap for left turning vehicles – Case B1, Left Turn from Stop Control is as shown in the table 5.1 below.

Design Vehicle	Time Gap Tg (s) at Design Speed of Major Road	Percentage of Grade of Minor Road	Numbers of Lanes Major Road
Passenger Car	7.5	Flat	2
Passenger Car	8	Flat	4
Passenger Car	7.7	3 Percent	2
Passenger Car	8.2	3 Percent	4
Trucks	9.5	Flat	2
Trucks	10.2	Flat	4
Trucks	9.7	3 Percent	2
Trucks	10.4	3 Percent	4
Combination Trucks	11.5	Flat	2
Combination Trucks	12.2	Flat	4
Combination Trucks	11.4	3 Percent	2
Combination Trucks	11.9	3 Percent	4

Table 5.1: Critical Time Gap (tg) for 2 and 4 lanes on major road for left turning vehicles

There is an increase of .5 seconds for passenger car per lane and 0.5 seconds per truck per lane. Additional consideration is given to grade condition on the minor road; a 0.2 second is added to the time gap for upgrades in the minor road greater than 3 percent. These values according to AASHTO 2004 are based on sight triangles without consideration to the median on the major road and the approach speed. It is also said to be based on field measurement and independent of the approach speed. However, based on dynamics, the approach speed of the vehicles will largely affect the gap that the turning vehicle is willing to accept. If the approach speed is higher, a seemingly large gap will deteriorate rapidly. The numbers of drivers that are willing to accept a rapidly diminishing gap will likely increase. Thus, the design speed needs to be included in the determination of the critical gap. A new critical gap is proposed.

5.3.2: Proposed New Time Gap for Left Turning Vehicles

Fisk (1989) demonstrated the impact of considering the distribution of flows in the major road lanes and different critical gaps in each lane. She developed an extension to Tanner's (1962)(1967) formula for the capacity of a non-priority movement at an isolated intersection to accommodate bunching of the major road traffic using conditional probability developed earlier by Brennan and Fitzgerald (1979). Based on such thinking, a new time gap is hereby proposed on a combination of the conditional probability and the geometry of the intersection, design speed and number of lanes. Assume the critical gap is as developed by the Gap Acceptance Theory (T_o) for a single lane (HCM2000). If a left turning vehicle accepts a gap (T_o) for the first lane and a car enters service in the second lane, the driver will need a gap (T_o) plus clearance distance equal to the speed of the vehicle in the opposing lane divided by the width of the intersection. The intersection width (W) in this case, is defined as the distant from the far side of the curb return to the near side of the curb return with consideration to the median width. The width of the intersection can be approximated to multiples of the lanes' of a single lane width plus the width of the median see figure 5.2.

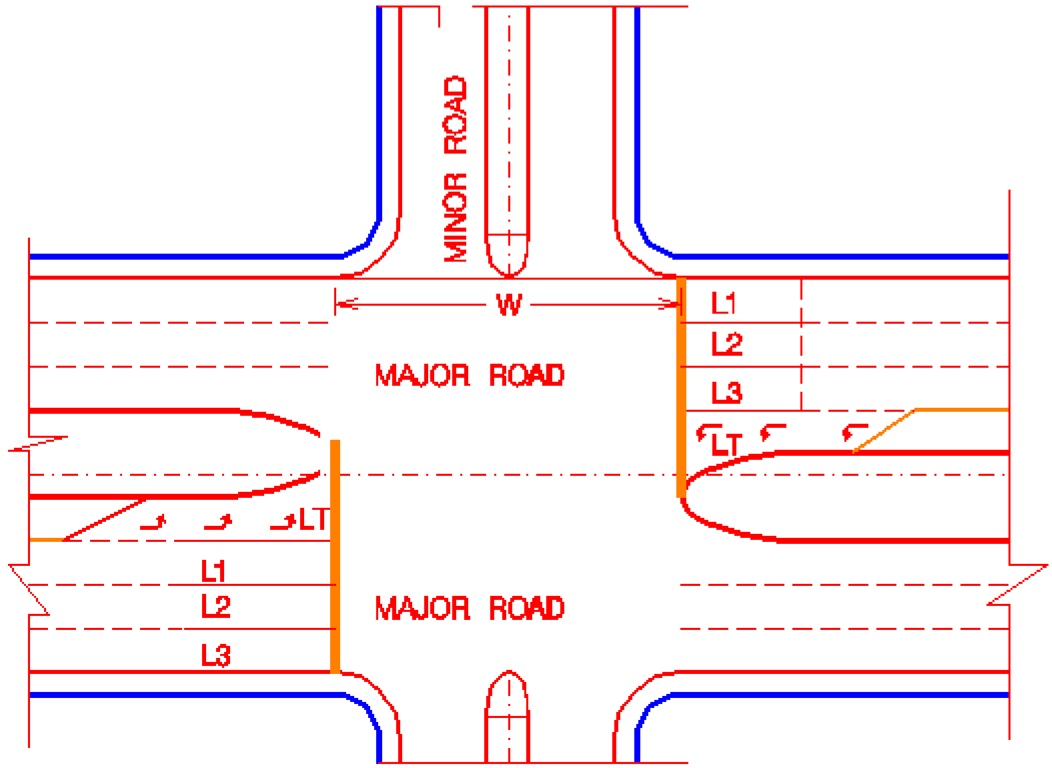

Figure 5.2: Illustration for New Time Gap

Thus:

Critical gap (T_g) for two lanes = $(T_o)+W/V_d$ 5.38

Critical gap (T_g) for three lanes = $(T_o) + W/V_{d/} + W/V_d$ 5.39

Critical gap (T_g) for n lanes = $(T_o) + W/V_{d/} + W/V_d + W/V_d$ 5.40

This can be generalized as follows:

Critical gap (T_{gn}) = (T_o) + (n-1)*(Service time for major road) = (T_o) + (n-1)*W/V_d 5.41

Where W is the width of the minor road in feet.

V_d is the design speed in mph,

T_o is the critical gap for the first lane as defined in HCM2000,

T_{gn} is the critical gap for the n number of lanes, default to To when n =1,

And

n is the number of lanes in the major road for which the left turning vehicle will have to cross. Based on equation 5.41 above, critical gaps for left turning vehicle were developed as depicted on table 5-2 below; the same data are presented in graphic form on figure 5.3.

Table 5.2 **Design Speed =30mph.**				**Lane Adjustment factor** Number of Lanes		
			1	**2**	**3**	**4**
Critical gap		**26**	0	0.59	1.18	1.77
	T_o		6	6	6	6
	T_{gn}		**6**	**6.59**	**6.18**	**7.77**
		48	0	1.09	2.18	3.27
	T_o		6	6	6	6
	T_{gn}		**6**	**7.09**	**8.18**	**9.27**

Computation. **Design Speed =40mph.**		**Width (W) of Minor Rd.**		**Lane Adj Factor**		Table 5.2 Contd.
# of Lanes	**Major Rd.**		**1**	**2**	**3**	**4**
		26	0	0.44	0.88	1.33
	T_o		6	6	6	6
	T_{gn}		**6**	**6.44**	**6.88**	**7.33**
		48	0	0.82	1.63	2.45
	T_o		6	6	6	6
	T_{gn}		**5**	**6.82**	**7.63**	**8.45**

Table 5.2 Contd 50 mph			Lane Adj Factor			
# of Lanes	Major Rd.		1	2	3	4
		Width of Minor Road				
		26	0	0.35	0.71	1.06
	T_o		6	6	6	6
	T_{gn}		**6**	**6.35**	**6.71**	**7.06**
		48	0	0.65	1.31	1.96
	T_o		6	6	6	6
	T_{gn}		**6**	**6.65**	**7.31**	**7.96**

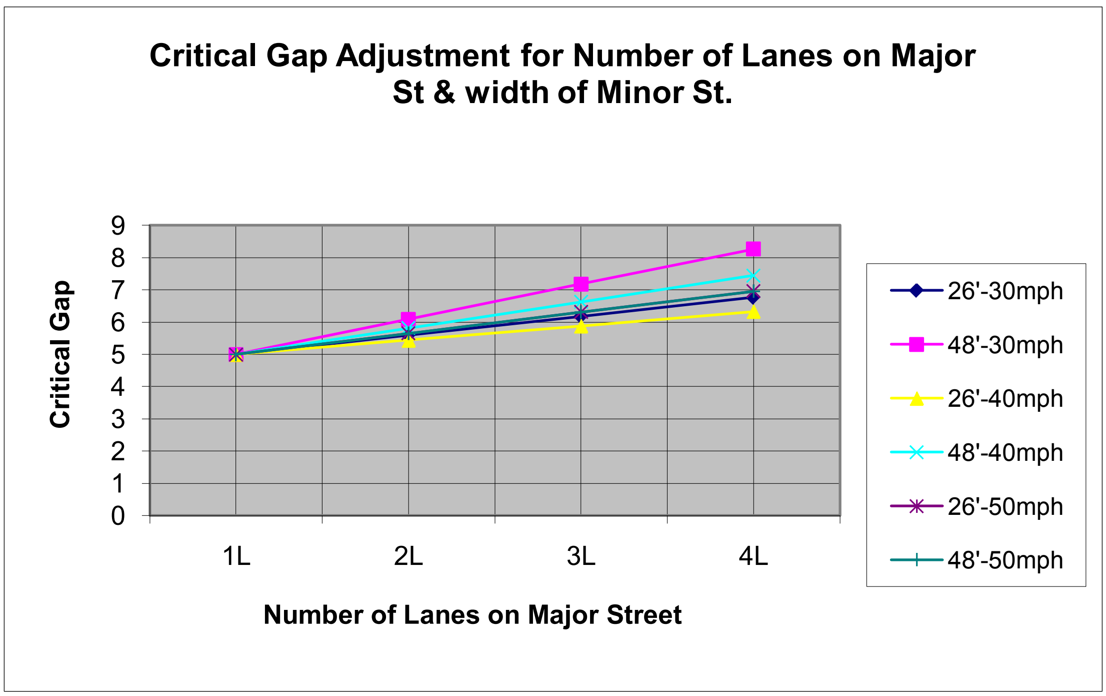

Figure 5.3: New critical gap values chart.

The proposed values of the critical gaps are close to that used in the Green Book as well as HCM. It is suggested here that the dynamic of vehicles approaching the intersection in the priority movement should be taken into consideration in determining the critical gaps as rapidly increasing approach speed may also affect the readiness for a given driver to accept a gap.

5.4 Numerical Example and Results:

Example 1:

Given:

A stop control 2-way 2-lane urban street has Design and Posted Speeds of 40 mph, with 30 mph entry speed. The left turn traffic volume is 150 vehicles per hour (vph) and the opposing through traffic volume is 600 vph. Given a passenger car with a time gap (T_g) of 7.5 seconds and a level of significance of 5%, find the left turn lane length required using the reliability approach?

Solution:

Assuming a steady state of both arrival rates and employing Method I for computing the length of the left turn lemgth:

λ_o = 600/3600 = 0.167 vehicles/second

λ_t = 150/3600 = 0.042 vehicle/second

T_g = 7.5seconds

From equation 5.21,

$$E[u] = \frac{e^{\lambda_o T_g} - 1 - \lambda_o T_g}{\lambda_o} = \frac{e^{0.167*7.5_o} - 1 - 0.167*7.5}{0.167} = 7.47$$

From equation 5.25:

$$E[u^2] = \frac{2(\lambda_o E[u])^2 + 2\lambda_o E[u] - (\lambda_o T_g)^2}{\lambda_o}$$

$$= \frac{2(0.167*7.47)^2 + 2*0.167*7.47 - (0.167*7.5)^2}{0.167} = 24.18$$

From Equation 5.26:

$$E[u^3] = \frac{6}{\lambda^3_o}[2\lambda_o E[u]\{[\lambda_o E[u] - \frac{(\lambda_o T_g)^2}{2}\} + (\lambda_o E[u])^3 + \{\lambda_o E[u] - \frac{(\lambda_o T_g)^2}{2} - \frac{(\lambda_o T_g)^3}{6}\}]$$

=

$$E[u^3] = \frac{6}{0.167^3}[2*0.167*7.47*\{[0.167*7.47 - \frac{(0.167*7.5)^2}{2}\} + (0.167*7.47)^3 +$$

$$\{0.167*7.47 - \frac{(0.167*7.5)^2}{2} - \frac{(0.167*7.5)^3}{6}\}] = 4164.25$$

From Equation 5.23:

$$E[L_D] = \lambda_t\ E[u] + \frac{\lambda_t^{\ 2} E[u^2]}{2(1-\lambda_t E[u])} = 0.042*7.47 + \frac{0.042^2*0.042*24.18}{2(1-0.042*7.47)} = 0.345$$

And the variance of the queue length is given as:

$$\text{var}[[L_D] = 2(E[L_D] - \lambda_t E[u])^2 + 3(E[L_D]) - 2\lambda_t(E[u]) + \frac{\lambda_t^{\ 3} E[u^3]}{3(1-\lambda_t E[u])} - E[L_D]^2 =$$

$$2(0.345 - 0.042*7.47)^2 + 3(0.345) - 2*0.042(7.47) + \frac{0.042^3*4164.25}{3(1-0.042*7.47)} - 0.345^2 = 0.56$$

From Equation 5.19

$$L_S = E[L_D] + \sigma[L_D]\sqrt{\frac{1}{1-\alpha} - 1} = L_S = 0.345 + \sqrt{0.56}\sqrt{\frac{1}{1-0.05} - 1} = 1.11 \text{ or } 2 \text{ cars.}$$

In this case, the minimum storage length required will be per AASHTO or FDOT standard of 2 cars. For a car length of 25' feet the storage distance will be 50 feet from the stop bar. The total lane length will be the sum of the storage distance and the reaction clearance distance (L_d), which is given as:

$$L_d = 1{,}47vt + \frac{1.075v^2}{a} = L_d = 1.47 * 30 * 2.5 + \frac{1.075 * 30^2}{11.2} = 194.38 \text{ feet.}$$

And, the designed lane's length total = 50 + 194.38 = 244 feet. Use 245 feet for design. This is more conservative than the current 205 feet used by the FDOT Standard index 301(See exhibit 5.1). The advantage of this design procedure is that it takes into account the left turn volume expected and the opposing flow expected without the actual traffic count. This can allow planning office to set budget and plan for adequate turn lane length prior to actual engineering design. The above procedure was used in producing the results shown in table 5.3.

The problem can also be solved using equation 5.34 to determine the queue length L_q directly with the same confident level as follows:

Given:

$T_g = 7.5$

$t_f = t_g/2 = 3.75$

$q_n = 150$ *vph*

$q_p = 600$ *vph*

Determine q_m as per equation 5.36.

$$q_m = \frac{q_p e^{-(q_p/3600)*t_g}}{1 - q_p e^{-(q_p/3600)*t_f}}$$

$$= \frac{600 * e^{-(600/3600)*7.5}}{1 - e^{-(600/3600)*3.75}}$$

$= 369.89$ *vph*

Determine x;

x = $q_n/q_m = 150/369.89 = 0.4055$

Determine L_q

$$Lq \approx \frac{q_m}{4}\left\{x - 1 + \sqrt{(1-x)^2 + \frac{8x}{q_m}.(3.0)}\right\}$$

$$Lq \approx \frac{369.89}{4}\left\{0.4055 - 1 + \sqrt{(1-0.4055)^2 + \frac{8*(0.4055)}{369.89}.(3.0)}\right\}$$

$Lq \approx 2.00$

As before, since, Lq is less than or equal to Ls, then, AASHTO standard is adequate. The next step normally will be to add L_d to Lq for the overall length of the left turn lane as follows:

$$L_d = 1{,}47vt + \frac{1.075v^2}{a} = L_d = 1.47*30*2.5 + \frac{1.075*30^2}{11.2} = 194.38 \text{ feet.}$$

$$L_P = 194.38 + (2*25) = 244.38 \text{ feet; use 245 feet.}$$

5.4.1 Comparison of the Two Methods

In this example both methods produce adequate result. Method I, though lengthy, produces result that estimates the overall length of the left turn lane (LS) given a level of reliability desired but is limited to single lane. However, this approach when compared with the total volume for the multiple lanes performs well for low degree of saturation and rapidly deteriorates for higher degree of saturation as shown on table 5.3. On the other hand, method II provides a robust computation method as well as good result that is practical and can readily be employed in design and evaluation of existing left turn lane for both single and multiple lanes as depicted on tables 5.5 through 5.6. A comparison of the reliability method for left turn design using the two computational approaches for queue length and the AASHTO recommendation are shown. The results show that the AASHTO approach can underestimate the left turn lane when traffic is near saturation level. This situation will reduce the safety level of the roadway as more and more drivers violate the safe breaking deceleration rate. A high degree of deceleration rate for less than normal tires and tire pressures in some cars may not stop the cars prior to impact on the vehicle in front. Additional assessment of the reliability of the intersection can be deduced from each Method by adopting equation 3-11 for computation of the reliability index. The approach is simple and is accomplished by dividing the expected value of the left turn length by its standard deviation and then using the CDF of the Standard Normal Distribution table to determine the probability of failure, based on assumption of normality in the arrival flows. This was performed with respect to Method I to produce table 5.4 which are plotted in figures 5.4 and 5.5. The same principle can be adopted for Method II but the safety index for Method II is fixed at 1.645. This is one of the advantages of Method I over Method II, although Method two is recommended for design. It can be seen on figure 5.4 and 5.5 that the Safety Index decreases as the capacity of the left lane and the opposing volumes increases. Also, that it is to be expected that the probability of failure of the LT lane increases as both the capacity of the LT turn lane and the opposing volumes increases as depicted in figures 5.4 and 5.5. Generally, Method I produces a low safety index and high probability of failure and deteriorate quickly as the LT turn lane capacity approaches 300 vph and the opposing volumes exceeds 1000 vph. From tables 5., 5.6 and figure 5.6, It is evidence that Method II allows higher LT turn lane capacity in the excess of 500 vph for opposing lane volumes up to 1200 vph with a higher safety Index (*1.645,* $P_f = 0.05$) in comparison to Method I. Based on this approach, a designer can reliably assessed the safety implication of his design based on the expected traffic loads on the intersection. Thus, the reliability approach to the design of the left turn should be given serious consideration to enable the designer to properly evaluate the safety performance as well as the risk of the left turn bay at the intersection; using Method II as the recommended method for design.

				Method I (INPUT)								LN Length Rqu'd (OUTPUT)			
Opps'g Vol. vph	arrival rate (vps)	LT Vol. vph	arrival rate (vps)	Tg	E(u)	E(u2)	E(u3)	E(# veh in queue)	Var(# veh in queue)	std(# veh in queue)	# of Cars Ls	LN (ft)	AASHTO Design	Safety Margin	RMK
								threshold probability of overflow			0.05				
1000	0.28	100	0.03	4	4	13	765	0.12	0.13	0.35	**1.67**	**42**	246.00	-204.34	OK
1000	0.28	200	0.06	4	4	13	765	0.26	0.30	0.55	**2.66**	**67**	246.00	-179.46	OK
1000	0.28	300	0.08	4	4	13	765	0.42	0.62	0.79	**3.85**	**96**	246.00	-149.68	OK
1000	0.28	400	0.11	4	4	13	765	0.62	1.24	1.11	**5.48**	**137**	246.00	-109.12	OK
1200	0.33	100	0.03	4	6	26	1579	0.17	0.18	0.42	**2.00**	**50**	246.00	-196.03	OK
1200	0.33	200	0.06	4	6	26	1579	0.37	0.49	0.70	**3.41**	**85**	246.00	-160.83	OK
1200	0.33	300	0.08	4	6	26	1579	0.63	1.19	1.09	**5.40**	**135**	246.00	-111.05	OK
1200	0.33	400	0.11	4	6	26	1579	1.04	3.06	1.75	**8.67**	**217**	246.00	-29.21	OK
1300	0.36	100	0.03	4	6	35	2234	0.19	0.21	0.46	**2.19**	**55**	246.00	-191.25	OK
1300	0.36	200	0.06	4	6	35	2234	0.44	0.63	0.79	**3.89**	**97**	246.00	-148.65	OK
1300	0.36	300	0.08	4	6	35	2234	0.80	1.75	1.32	**6.56**	**164**	246.00	-82.01	OK
1300	0.36	400	0.11	4	6	35	2234	1.46	5.49	2.34	**11.68**	**292**	246.00	46.01	NG
1400	0.39	500	0.14	4	7	48	3135	-53.02	2539.33	50.39	**166.63**	**4166**	246.00	3919.81	OK
1400	0.39	200	0.06	4	7	48	3135	0.53	0.83	0.91	**4.50**	**112**	246.00	-133.60	OK
1400	0.39	300	0.08	4	7	48	3135	1.03	2.70	1.64	**8.20**	**205**	246.00	-41.12	OK
1500	0.42	100	0.03	4	8	65	4369	0.26	0.30	0.55	**2.65**	**66**	246.00	-179.84	OK
1500	0.42	200	0.06	4	8	65	4369	0.64	1.12	1.06	**5.26**	**131**	246.00	-114.53	OK
1500	0.42	300	0.08	4	8	65	4369	1.39	4.55	2.13	**10.69**	**267**	246.00	21.23	NG
1500	0.42	400	0.11	4	8	65	4369	5.46	48.89	6.99	**35.94**	**898**	246.00	652.40	NG

Table 5.3: Computation of Left Turn Length Using Method I & HCM 200 value for tc = 4.4s

Table 5.4: Safety Index and Probability of Failure - Method I (Using HCM 2000 value for tc=4.4 s						
Opposing Volumes	E(# veh in queue)	Std(# veh in queue)	Safety Index E(V)/Sigma(V)	fi(X) Reliability	Probability of Failure Pf)	LT Turn Volume vph
1000	0.12	0.35	0.35	0.64	0.36	100
1000	0.26	0.55	0.47	0.68	0.32	200
1000	0.42	0.79	0.53	0.70	0.30	300
1000	0.62	1.11	0.56	0.71	0.29	400
1000	0.89	1.59	0.56	0.71	0.29	500
1000	1.31	2.35	0.56	0.71	0.29	600
1000	2.19	3.78	0.58	0.72	0.28	700
1200	0.17	0.42	***0.40***	0.66	0.34	100
1200	0.37	0.70	0.53	0.70	0.30	200
1200	0.63	1.09	0.58	0.72	0.28	300
1200	1.04	1.75	0.60	0.73	0.27	400
1200	1.90	3.07	0.62	0.73	0.27	500
1200	6.34	8.51	0.75	0.77337	0.23	600
1200			0	0.00	1.00	700
1300	0.19	0.46	***0.42***	0.67	0.33	100
1300	0.44	0.79	0.56	0.71	0.29	200
1300	0.80	1.32	0.60	0.73	0.27	300
1300	1.46	2.34	0.62	0.73	0.27	400
1300	3.94	5.57	0.71	0.76	0.24	500
1300	-7.41	2.27	-3.26	0.00	1.00	595
1300				0.00	1.00	700
1400	0.22	0.50	***0.45***	0.67	0.33	100
1400	0.53	0.91	0.58	0.72	0.28	200
1400	1.03	1.64	0.62	0.73	0.27	300
1400	2.34	3.57	0.66	0.68	0.32	400
1400	-53.02	50.39	-1.05	0.15	0.85	500
1400				0.00	1.00	600
1400				0.00	1.00	700
1500	0.26	0.55	***0.48***	0.73	0.27	100
1500	0.64	1.06	0.60	0.74	0.26	200
1500	1.39	2.13	0.65	0.72	0.28	300
1500	5.46	6.99	0.78	0.54	0.46	400
1500	-6.166563075	1.84139183	-3.35	0.00	1.00	472.00
1500				0.00	1.00	600.00
1500				0.00	1.00	700.00

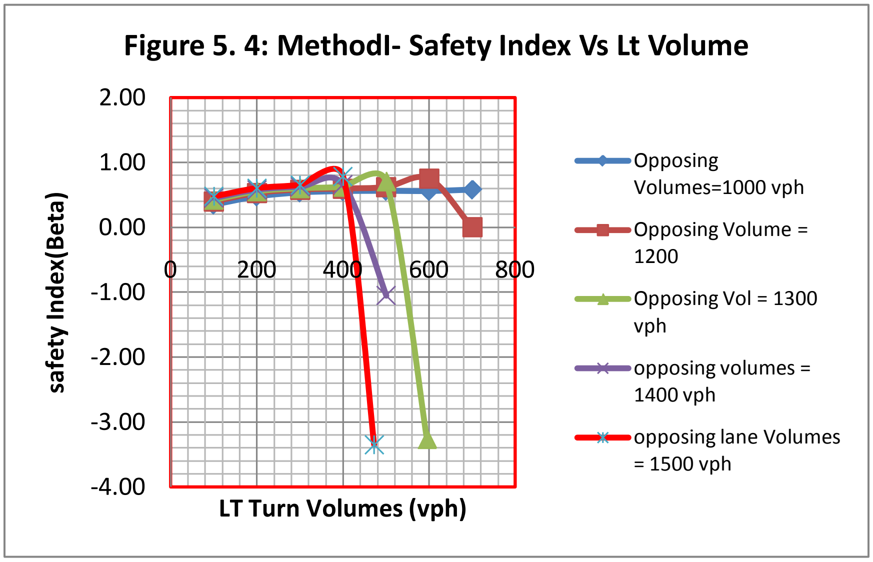
Figure 5. 4: MethodI- Safety Index Vs Lt Volume
2.00
1.00
0.00
-1.00
-2.00
-3.00
-4.00
0
200
400
600
800
safety Index(Beta)
LT Turn Volumes (vph)
Opposing Volumes=1000 vph
Opposing Volume = 1200
Opposing Vol = 1300 vph
opposing volumes = 1400 vph
opposing lane Volumes = 1500 vph

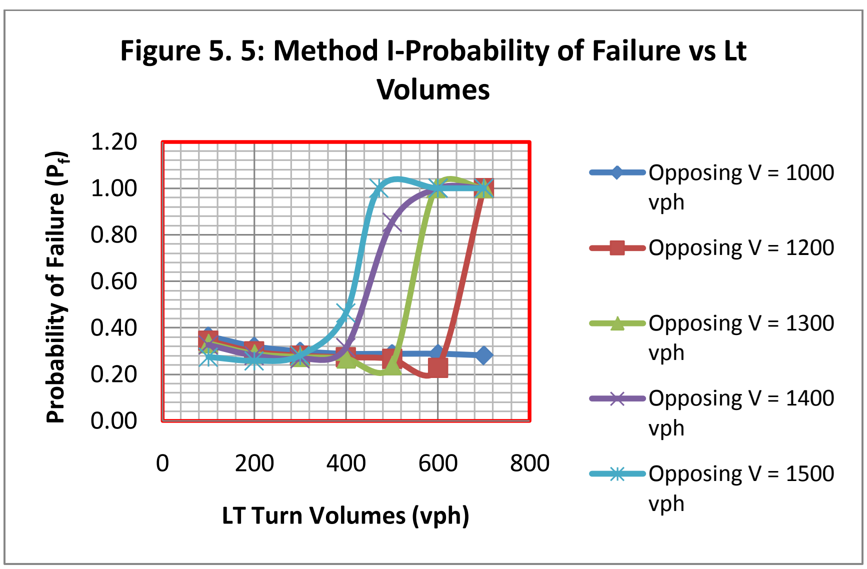
Figure 5. 5: Method I-Probability of Failure vs Lt Volumes
1.20
1.00
0.80
0.60
0.40
0.20
0.00
0
200
400
600
800
Probability of Failure (P_f)
LT Turn Volumes (vph)
Opposing V = 1000 vph
Opposing V = 1200
Opposing V = 1300 vph
Opposing V = 1400 vph
Opposing V = 1500 vph

pposing Volume vph	arrival rate (vps)	LT Vol. vph	arrival rate (vps)	Tg	Method I (INPUT) E(u)	E(u2)	E(u3)	E(# veh in queue`	Var(# veh in queue)	std(# veh in queue)	# of Car LS (threshold probability of overflow 0.05)	LN Length Rq'd LN (ft)	AASHTO Design	Safety Margin	RMK
300	0.08	200	0.06	5	1	0.7	78	0.08	0.08	0.28	**1.32**	**33**	246.00	-212.97	OK
450	0.13	200	0.06	5	2	2.3	213	0.13	0.14	0.37	**1.75**	**44**	246.00	-202.32	OK
500	0.14	200	0.06	5	3	3.2	286	0.15	0.16	0.40	**1.90**	**47**	246.00	-198.60	OK
600	0.17	200	0.06	5	3	5.6	494	0.20	0.21	0.46	**2.22**	**55**	246.00	-190.59	OK
700	0.19	200	0.06	5	4	9	820	0.25	0.29	0.54	**2.58**	**65**	246.00	-181.45	OK
800	0.22	200	0.06	5	5	15	1320	0.31	0.39	0.62	**3.02**	**75**	246.00	-170.56	OK
900	0.25	200	0.06	5	6	23	2077	0.39	0.53	0.73	**3.56**	**89**	246.00	-157.10	OK
1050	0.29	200	0.06	5	8	42	3971	0.54	0.90	0.95	**4.67**	**117**	246.00	-129.14	OK
1100	0.31	200	0.06	5	8	51	4896	0.61	1.10	1.05	**5.17**	**129**	246.00	-116.68	OK
1200	0.33	200	0.06	5	10	73	7382	0.79	1.70	1.30	**6.47**	**162**	246.00	-84.17	OK
1300	0.36	200	0.06	5	11	104	11029	1.06	2.87	1.69	**8.44**	**211**	246.00	-35.05	OK
1400	0.39	200	0.06	5	13	147	16357	1.54	5.53	2.35	**11.79**	**295**	246.00	48.80	NG
1500	0.42	200	0.06	5	15	205	24116	2.71	14.35	3.79	**19.22**	**481**	246.00	234.56	NG
1600	0.44	200	0.06	5	17	283	35386	10.22	139.00	11.79	**61.61**	**1540**	246.00	1294.26	NG
1700	0.47	200	0.06	5	20	388	51720	-5.64	6.46	2.54	**5.44**	**136**	246.00	-109.98	NG
1800	0.50	200	0.06	5	22	530	75362	-2.14	-8.4	-	-	-	246.00	-	NG
1900	0.53	200	0.06	5	25	720	109543	-1.27	-8.97	-	-	-	246.00	-	NG
2000	0.56	200	0.06	5	29	973	158928	-0.86	-9.28	-	-	-	246.00	-	NG

Table 5.4 A: Computation of Values for Fixed Lt Volume (200 vph) Analysis: Table 5.4A-B(tc=5.4s)

Figure 5.5A: Method I: Lane Length Vs Opposing Volumes (LT Turning Volume =200vph, tc = 5.3s

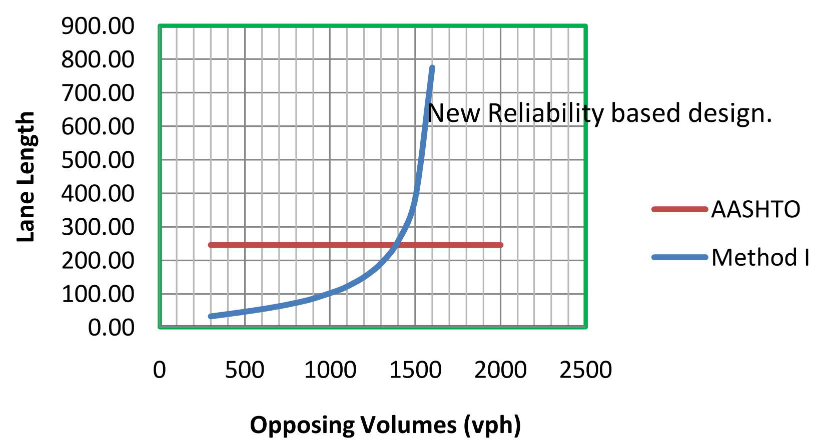

Table 5.5: Cumputation of Left Turn Lane Using Method II (Single Lane Analysis**

Tc=	5.3		Single Lane		INPUT			OUTPUT				
Tf=	2.6							Ld = 196 ft for 30 mph entry speed				
b1=	1.50		opposing traffic	Capacity of	Capacity of	LT traffic 200	95% Veh	Lq # of		Lq+Ld	Safety	
v1	v2	v3	v	Multi-lane	Single-lane	v/c	Queue	cars	AASHTO	Method II	Margin	RMK
100	100	100	300	987.53	990.18	0.20	1.8	2	246	240	-6	OK
200	100	100	400	879.89	884.71	0.23	1.9	2	246	243	-3	OK
250	100	150	500	783.23	790.13	0.25	2.0	2	246	246	0	OK
200	200	200	600	697.61	705.35	0.28	2.2	2	246	250	4	OK
300	200	200	700	619.48	629.40	0.32	2.4	2	246	255	9	OK
300	260	240	800	550.15	561.39	0.36	2.6	3	246	261	15	OK
400	300	200	900	486.76	500.51	0.40	2.9	3	246	269	23	OK
350	350	300	1000	431.95	446.05	0.45	3.3	3	246	278	32	OK
400	340	360	1100	382.04	397.34	0.50	3.7	4	246	289	43	OK
400	400	400	1200	337.57	353.80	0.57	4.3	4	246	304	58	0k
500	400	400	1300	297.58	314.90	0.64	5.1	5	246	323	77	ok
500	450	450	1400	262.39	280.17	0.71	6.0	6	246	346	100	NG
500	500	500	1500	230.96	249.16	0.80	7.1	7	246	374	128	NG
525	550	525	1600	202.96	221.49	0.90	8.4	8	246	407	161	NG
530	600	570	1700	178.08	196.81	1.02	9.9	10	246	443	197	NG
600	600	600	1800	156.13	174.81	1.14	11.4	11	246	480	234	NG
690	630	580	1900	136.51	155.21	1.29	12.9	13	246	519	273	NG
650	690	660	2000	119.39	137.76	1.45	14.4	14	246	556	310	NG

** tc = 5.3s, tf = 2.6s per Wu's best fit parameters.

Figure 6: Method II: Lane Length vs Opposing Volumes (LT Turn Vol. = 200vph)

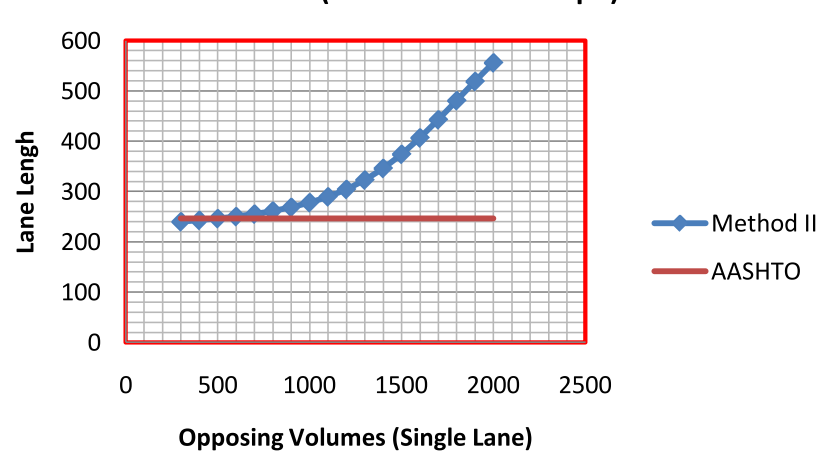

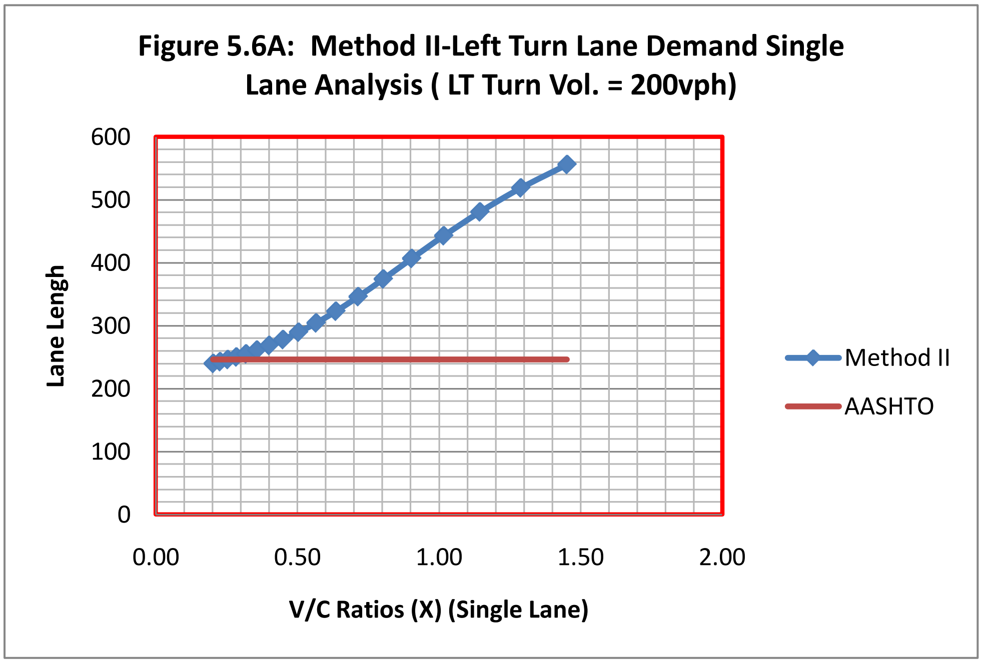

Figure 5.6 and 5.6A can be easily adopted for evaluation and design of the left turn lane for a single lane opposing lane by knowing the degree of saturation (x) or v/c ratio of the turning movement. The v/c ratio also is a function of the opposing movement which is incorporated in the computation of q_m. Once the x value is determined, the length of the lane length can be read from figure 5.6 and use in the design or evaluation of the existing left turn lane.

Table 5.6A: Computation of Left Turn Length Using Method II (Multiple Lanes)

Tc= 5.3			INPUT						OUTPUT				
Tf= 2.60									Ld = 196 ft for 30 mph entry speed				
b1= 1.50			Oppsng	Capacity	Capacity	LT traffic					95th %		
Lane volumes			traffic	of	of	200	Avg	95%	# of		LT Lngth	Safety	
v1	v2	v3	v	Multi-lane	Single-lane	v/c	QL	QL	cars	AASHTO	Method II	Margin	Rmk
50	50	50	150	1170.71	1171.48	0.17	30	**40**	40	246	236.35	-10	OK
100	100	100	300	987.53	990.18	0.20	31	**44**	44	246	239.87	-6	OK
150	150	150	450	831.03	836.13	0.24	33	**48**	48	246	244.46	-2	OK
200	200	200	600	697.61	705.35	0.29	35	**55**	55	246	250.54	5	NG
250	250	250	750	584.14	594.46	0.34	38	**63**	63	246	258.80	13	NG
300	**300**	**300**	**900**	**487.87**	**500.51**	**0.41**	42	**74**	**74**	**246**	**270.33**	**24**	**NG**
350	350	350	1050	406.38	421.01	0.49	48	**91**	91	246	286.86	41	NG
400	400	400	1200	337.57	353.80	0.59	59	**115**	115	246	311.03	65	NG
450	450	450	1350	279.63	297.04	0.72	77	**150**	150	246	346.16	100	NG
500	500	500	1500	230.96	249.16	0.87	111	**198**	198	246	394.32	148	NG
550	550	550	1650	190.19	208.80	1.05	166	**257**	257	246	453.23	207	NG
600	600	600	1800	156.13	174.81	1.28	236	**321**	321	246	516.50	271	NG
650	650	650	1950	127.76	146.23	1.57	306	**382**	382	246	577.91	332	NG
700	700	700	2100	104.19	122.21	1.92	370	**438**	438	246	633.79	388	NG

Figure 5.7: LT Lane Demand (Multiple Lanes Analysis Method II) (LT Turn Vol. = 200vph, tc = 5.3s and tf=2.6s)

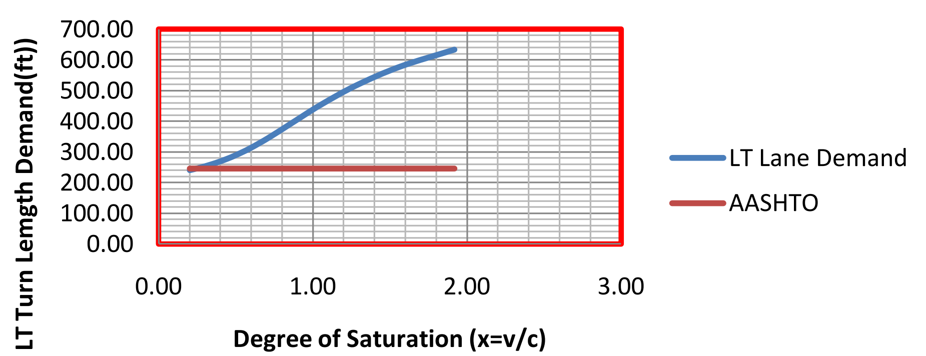

5.4.1.2 Validation of the Model:

Two Methods were adopted for the computation of queue length for the analysis, Viz:

1. Wu's (HCM) 95th percentile queue length estimates (Method II)and

2. Chakarborty's 0.05 thresh hold probability of failure estimate of the lane length (Method I).

The comparison of the two methods with numbers of vehicles making left turn fixed at 200 vph, the time gap t_c = 5.3, and following time, t_f = 2.6s, service time on the major road, β_1 = 1.5s (per Fisk); t_c is based on the best fit solution based on the M/M/1 approximation derivation per WU (1994 in Troutbeck, HCM-Germany) are presented in table 5.7 below. A common base for comparison was achieved by combining Tanner/Fisk approach in the computation of the capacity of the turn lane based on the opposing flow for multiple lanes. The degree of saturation was computed as the ratio of the volume of the LT turning vehicle to the capacity computed per Tanner/Fisk formulae.

Table 5.7**: Comparison of Method I and II (see Figure 5.8)(tc=5.3s, tf=2.6s)

Opposing Volumes (vph)	Capacity of LT Lane Per Tanner/ (HCM)	Degree of Saturation (X = V/C)	Number of Cars Making LT Turns (vph)	Lane Leng Method I Design	Lane Lengt Method II Design	Ln Length AASHTO Design
150	**1165.84**	**0.17**	**200**	**22.00**	**211.43**	**246.00**
300	**979.34**	**0.20**	200	33.00	215.07	246.00
450	820.71	0.24	200	44.00	219.84	246.00
600	686.08	0.29	200	55.00	226.21	246.00
750	572.10	0.35	200	70.00	234.95	246.00
900	475.82	0.42	200	89.00	247.26	246.00
1050	394.69	0.51	200	117.00	265.09	246.00
1200	326.50	0.61	200	162.00	291.39	246.00
1350	269.34	0.74	200	246.00	329.62	246.00
1500	221.53	0.90	200	481.00	381.31	246.00
1650	181.67	1.10	**200**	**1957.00**	**442.89**	**246.00**
1800	**148.51**	**1.35**	200		507.27	246.00
1950	121.02	1.65	200		568.48	246.00
2100	98.29	2.03	200		623.37	246.00

** 95th Percentile Queue Analysis

The values shown on table 5.7 are also depicted graphically below on figure 5.8. Column one of table 5.7 contains the opposing volumes on the major road, column two is the capacity of the left turn based on the parameters stated above, column three is the degree of saturation defined as the ratio of the left turn volumes to the capacity of the left turn;

column four is the assumed left turn volumes, the rest of the columns are self explanatory, they represent the two models and AASHTO's minimum design criteria for left turn lane length in feet. Figure 5.8 is the graph of the lane length with respect to the degree of saturation as the independent variable.

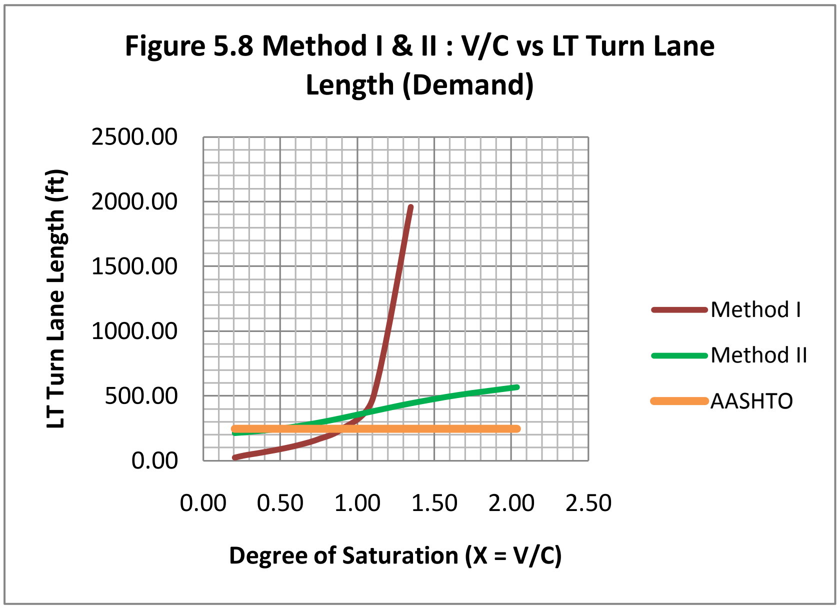

It can be seen from both the table and figure that method I grossly underestimate the lane length for lower degree of saturation when compared to AASHTO minimum criteria. The length of turn lane demand rapidly increased when the degree of saturation exceeds 74% of capacity. It predicts excessive lane length when the degree of saturation exceeds 74% of capacity and produces unreliable result thereafter. On the other hand, Method II provides steady estimates of the length of the left turn lane demand at the lower degree of saturation slightly lower than AASHTO up to 42% of capacity where it predicts about equal left turn length with AASHTO. Although the increase in the turn length demand also occurs when the degree of saturation exceeds 42% of capacity, the increase is gradual and remains within 50 feet of AASHTO design up to 55% of capacity. Method two is the recommended method as it is stable and provide adequate left turn lane for low degree of saturation that meets AASHTO standard as opposed to Method I which does not. Based on Method II, it can be concluded that AASHTO design approach is reliable only up to less than 50% of capacity of the left turn lane provided. The reliability approach have now provided a tool for evaluating the performance of the turn bay with respect to SAFETY rather than the LOS based on the delay computations. This tool is intended to be used in combination for the intersection evaluation with the standard delay and LOS practice.

It is pertinent to add that both methods can be used to evaluate the reliability of the turn lane for safety. Both methods have shown that at a specified reliability level, the adequacy of a turn lane can be evaluated, which meets the objective of this research.

In order to validate the model, 13 scenarios were selected for simulation with SYNCRO. The first scenario included seven different opposing volumes, v/c ratios, 200 vph making left turns, t_c = 5.3s, t_f =2.6s, six-lane urban roadway with 50 runs for each scenario. The second scenario included six different opposing volumes, v/c ratios, 300 vph making left turns, t_c = 5.3s, t_f =2.6s, six-lane urban roadway with 50 runs for each scenario. The purpose of the simulation was to generate queue lengths for 15 minutes with results observed every two minutes as proposed by AASHTO and compare the results so obtained with rational results based on the models. The results of the 50th and 95th percentile queue lengths from the simulation are presented on table 5.8 below.

Table 5.8: Models' Comparisons with SYNCHRO Simulations (50 Samples for each Scenario)

1st Scenario: tc=5.3, tf = 2.6, Beta-1 = 1.5, Left Turn Volume = 200 vph, Opposing Volumes 300-2100vph											
Degree of Satrtn V/C	Opsng Vol. in vph	SYNCHRO SIMULATION 50th Pcntl Queue	SYNCHRO SIMULATION 95th Pcntl Queue	Method II Queue Length 50th Pcntl	Method II Queue Length 95th Pcntl	Method II Deviation from SYNCHRO 50th Pcntl	Method II Deviation from SYNCHRO 95th Pcntl	Method I Queue Length 50th Pcntl	Method I Queue Length 95th Pcntl	Method I Deviation from SYNCHRO 50th Pcntl	Method I Deviation from SYNCHRO 95th Pcntl
0.20	300	29.00	61.00	31.33	43.87	2.33	17.13	8.89	32.30	20.11	28.70
0.29	600	40.00	72.00	34.98	54.54	5.02	17.46	15.98	53.83	24.02	18.17
0.41	900	48.00	85.00	42.05	74.33	5.95	10.67	26.59	85.08	21.41	0.08
0.59	1200	63.00	125.00	58.70	115.03	4.30	9.97	48.31	149.73	14.69	24.73
0.87	1500	87.00	177.00	110.66	198.32	23.66	21.32	128.66	384.10	41.66	207.10
0.99	**1600**							**269.00**	**775.00**		
1.28	1800	248.00	306.00	236.11	320.50	11.89	14.50	NG	NG	NG	NG
1.92	2100	408.00	472.00	369.72	437.79	38.28	34.21	NG	NG	NG	NG
Avg**		131.86	185.43	126.22	177.77	13.06	17.89	82.90	246.67	24.38	55.76
Stdev		142.91	152.11	129.47	150.64	13.27	8.22	101.05	288.68	10.24	85.31
2nd Scenario: tc=5.3, tf = 2.6, Beta-1 = 1.5, Left Turn Volume = 300 vph, Opposing Volume from 300-1800 vph											
0.30	300	39	**75**	35.85	57.20	3.15	17.80	11.70	41.25	27.30	3.15
0.43	600	54	**97**	43.58	79.15	10.42	17.85	22.59	73.90	31.41	10.42
0.61	900	71	**133**	62.52	126.91	8.48	6.09	43.20	136.34	27.80	8.48
0.89	1200	109	**214**	130.26	237.70	21.26	23.70	115.23	353.13	6.23	21.26
1.14	**1400**								**1019.00**		
1.30	1500	318	**394**	320.16	418.97	2.16	24.97	NG	NG	NG	NG
1.92	1800	575	**653**	521.78	597.29	53.22	55.71	NG	NG	NG	NG
AVG		194.3333	261.00	185.69	252.868	16.45	24.36	48.181	324.72	23.18	10.82
Stdev		212.85	224.249	195.9	214.8	19.2692	16.7507	46.57	406.7	11.45	7.6045
CAvg		160.69	220.31	153.67	212.43	14.62	20.88	69.02	208.47	23.85	35.79
TAvg			190.50		183.05		17.75		180.66		29.82
CTstdev			178.16		168.7		14.3491		263.9		45.523
t-statistics: Ho: Avg Simulation = Avg Method (I or II)						Method II			Method I		
t-Calculated for the Total Avg =						0.148			-0.039		
t(1-alpha/2=0.975, df(50)						2.0083					
t(1-alpha/2=0.975, df(46)									2.014		

Cavg = Combined Average of First and Second Scenarios for each Percentile (50th/95th)
Tavg = Total Average of First and Second Scenarios for both Percentiles(50th/95th)
CTstdev = Combined Total Standard Deviation for First and Second Scenarios for both Percentiles(50th/95th)
In All Cases: $t_{alpha/2,\, df}$ < t-calculated < $t_{1-alpha,\, df}$
Therefore, Ho is not rejected.

Results: The average or the 50th percentile queue length in feet produced by the simulations ranged from 29 feet to 575 feet for degree of saturation ranging from 20% to 192%. The queue length recorded for the 95th percentile queue range from 61 feet to 653 feet. When the models were compared with the simulation results, Model I could only produce result up to 99% of capacity; also, it underestimated the queue length in low degree of saturation and up to 59% of capacity and rapidly overestimated the queue length when the degree of saturation exceeded 59% of capacity. The overall average deviation from the simulation result was high for 50^{th} percentile queue (23.85 feet) and high (35.79 feet) for 90^{th} percentile queue length.

The simulation result was also compared with Method II, Method II estimates of the queue lengths were very closed to the to the simulated results for both low and high degree of saturations. The overall average deviation for model II was 17.75feet; a magnitude of about two times less than that recorded for Method I. The data shown on table 5.8 were also plotted to illustrate the compatibility of the Models and the simulation results. Figures 5.9, 5.9A-E, illustrate these results graphically. T-statistics was also performed on each of the scenarios' averages as well as overall averages for statistical significance. The results show that average queue lengths for all categories are about the same as the average queue length generated by the simulation, hence, the null hypothesis that the average queue lengths from the simulations are the same as those of the models is not rejected.

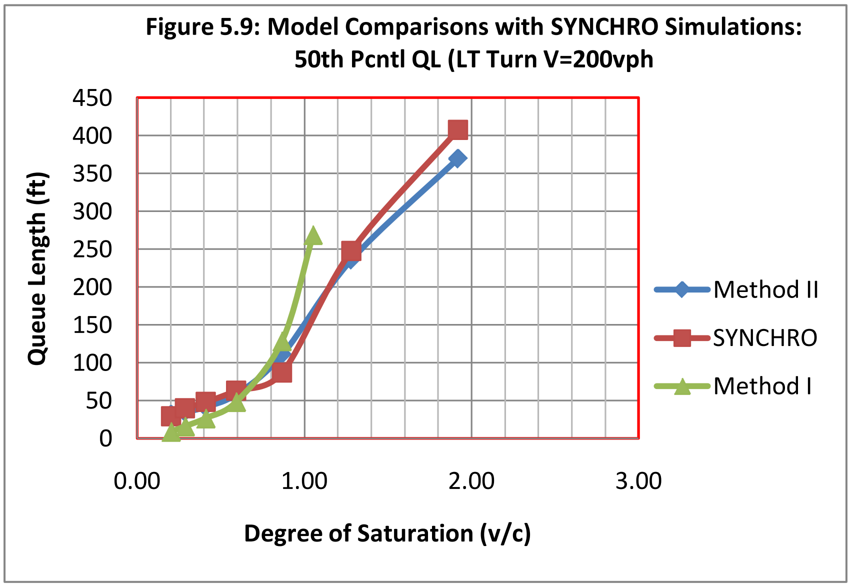

Figure 5.9 above is an illustration of the similarities or closeness of the models with respect to the simulations. The input values are from table 5.8, first scenario and data from columns 3, 5, and 9 with column 2 as the independent variable.

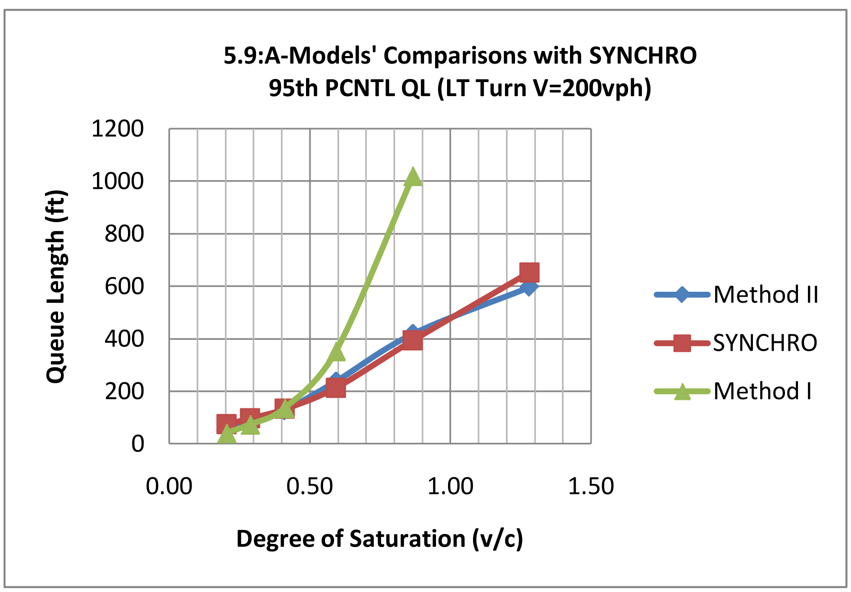

Figure 5.9A above is an illustration of the similarities or closeness of the models with respect to the simulations. The input values are from table 5.8, first scenario and data from columns 4, 6, and 10 with column 2 as the independent variable.

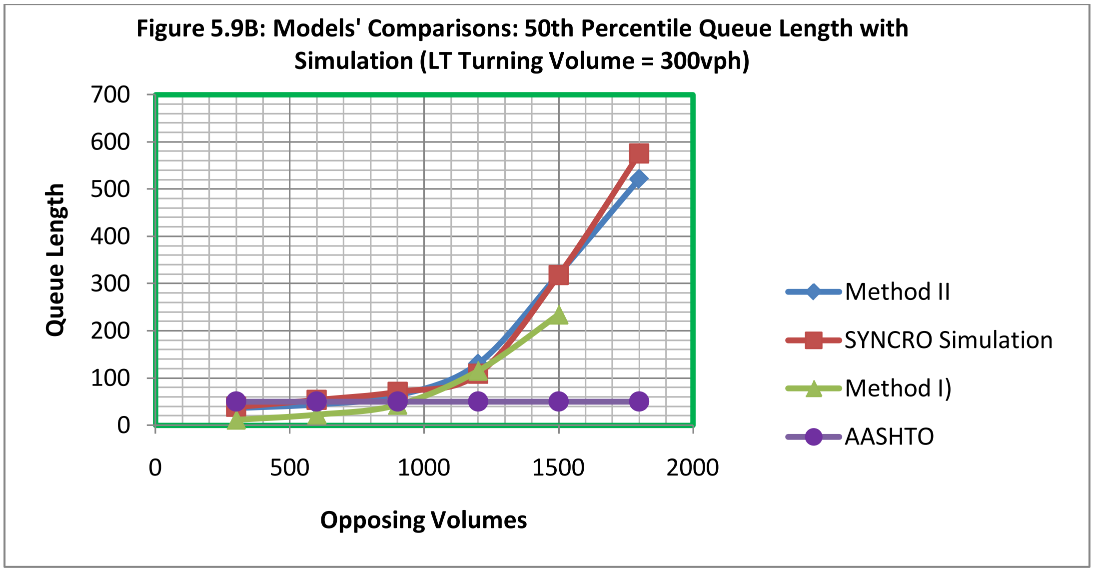

Figure 5.9B above is an illustration of the similarities or closeness of the models with respect to the simulations. The input values are from table 5.8, second scenario and data from columns 3, 5, and 9 with column 2 as the independent variable.

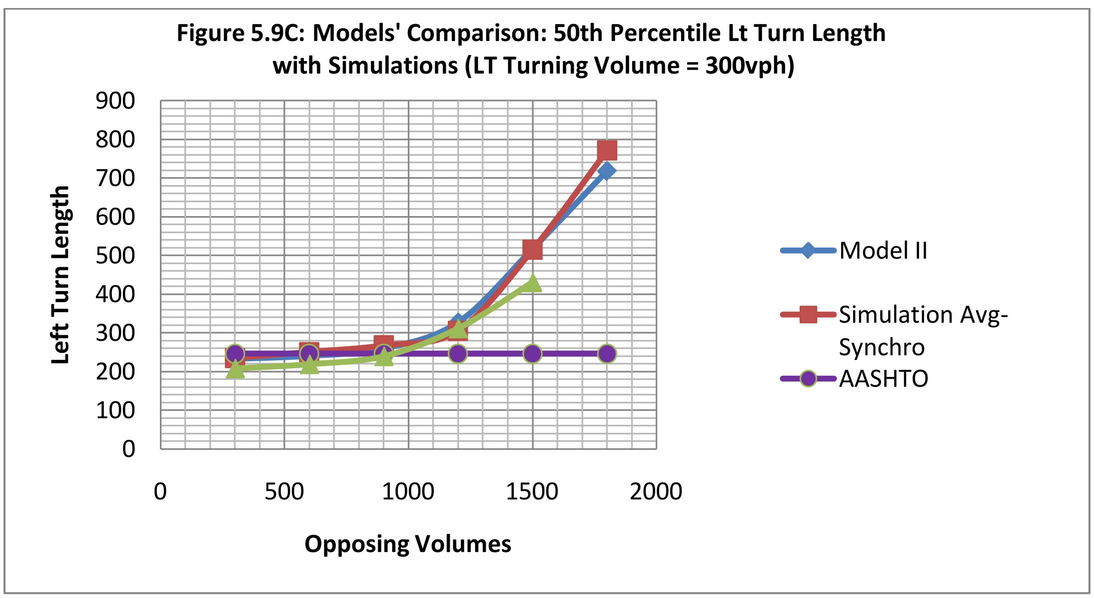

Figure 5.9C above is an illustration of the similarities or closeness of the models with respect to the simulations. The input values are from table 5.8, second scenario and data

from columns 4, 6, and 10 with column 2 as the independent variable. The left turn length is computed by adding the deceleration distance of 196 feet to the queue length.

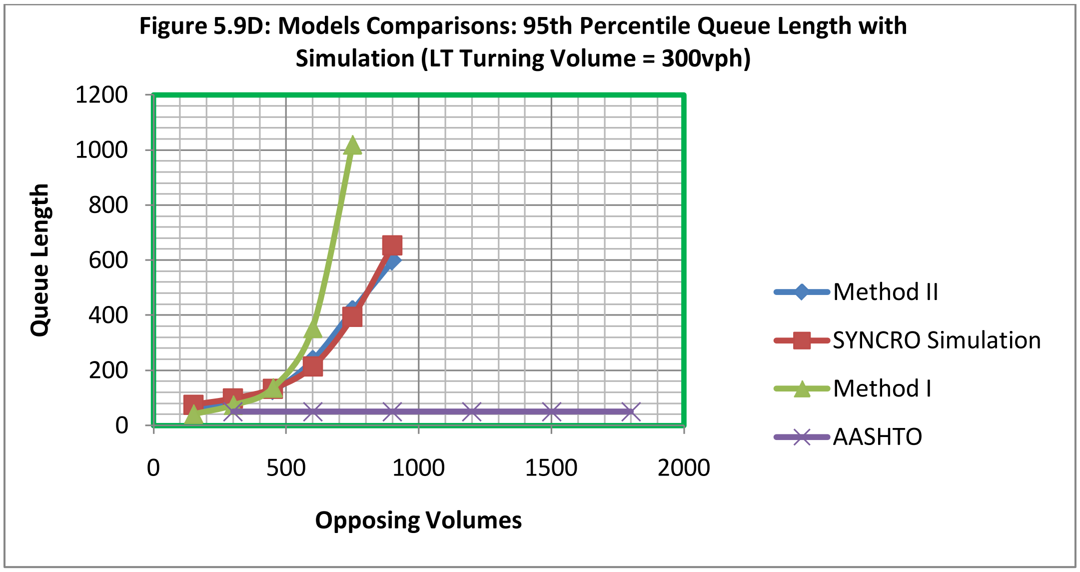

Figure 5.9D above is an illustration of the similarities or closeness of the models with respect to the simulations. The input values are from table 5.8, second scenario and data from columns 3, 5, and 9 with column 2 as the independent variable.

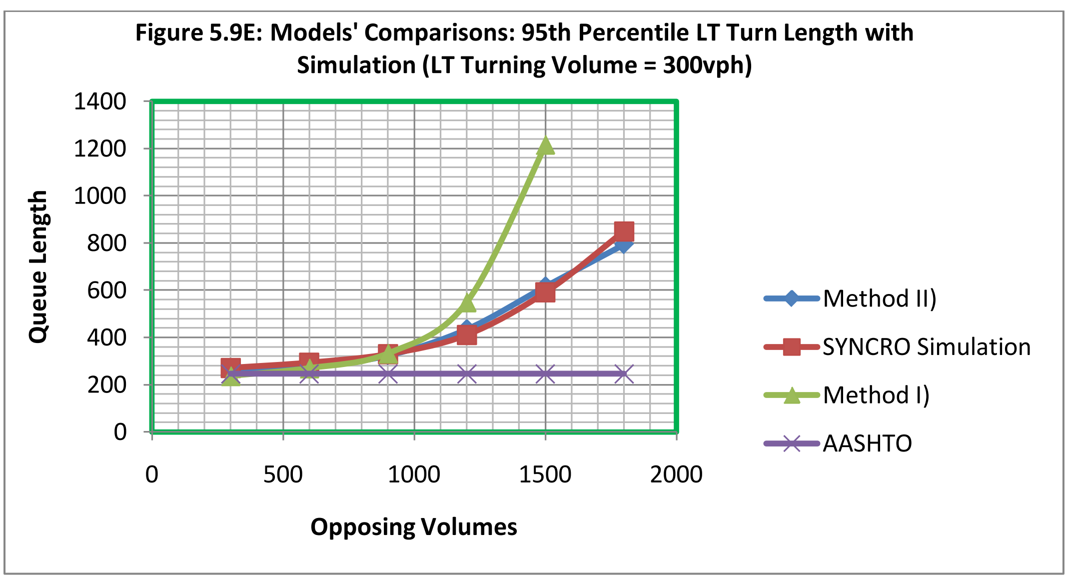

Figure 5.9E above is an illustration of the similarities or closeness of the models with respect to the simulations. The input values are from table 5.8, second scenario and data from columns 4, 6, and 10 with column 2 as the independent variable. The left turn length is computed by adding the deceleration distance of 196 feet to the queue length.

As can be seen by the comparisons shown above in tables: 5.8 and figures: 5.9, 9A-E, the proposed Model II's queue length, the design left turn lengths and the simulation results are compatible with Method II at low and high degree of saturation. Model (I) queue length, the left turn design and the simulation results are close for lower degree of saturation and cannot be used when considering near and oversaturated conditions. Based on the overall deviation of the queue lengths at both 50th and 95th percentile probability, Model II is a close fit to the simulations.

Recommendation:

The validation study has shown that Method II is the reliable method for evaluating the reliability of the left turn bay for safety. Method II is recommended for all ranges of degree of saturation for the reliability analysis technique developed in this research. Based on the simulation results, wider application (HCM 2000)(Brilon, Wu & Bondzio, 1997) and ease of computation, the author recommends the use of Method II for the computation of the queue length for reliability evaluation of left turn bay for safety.

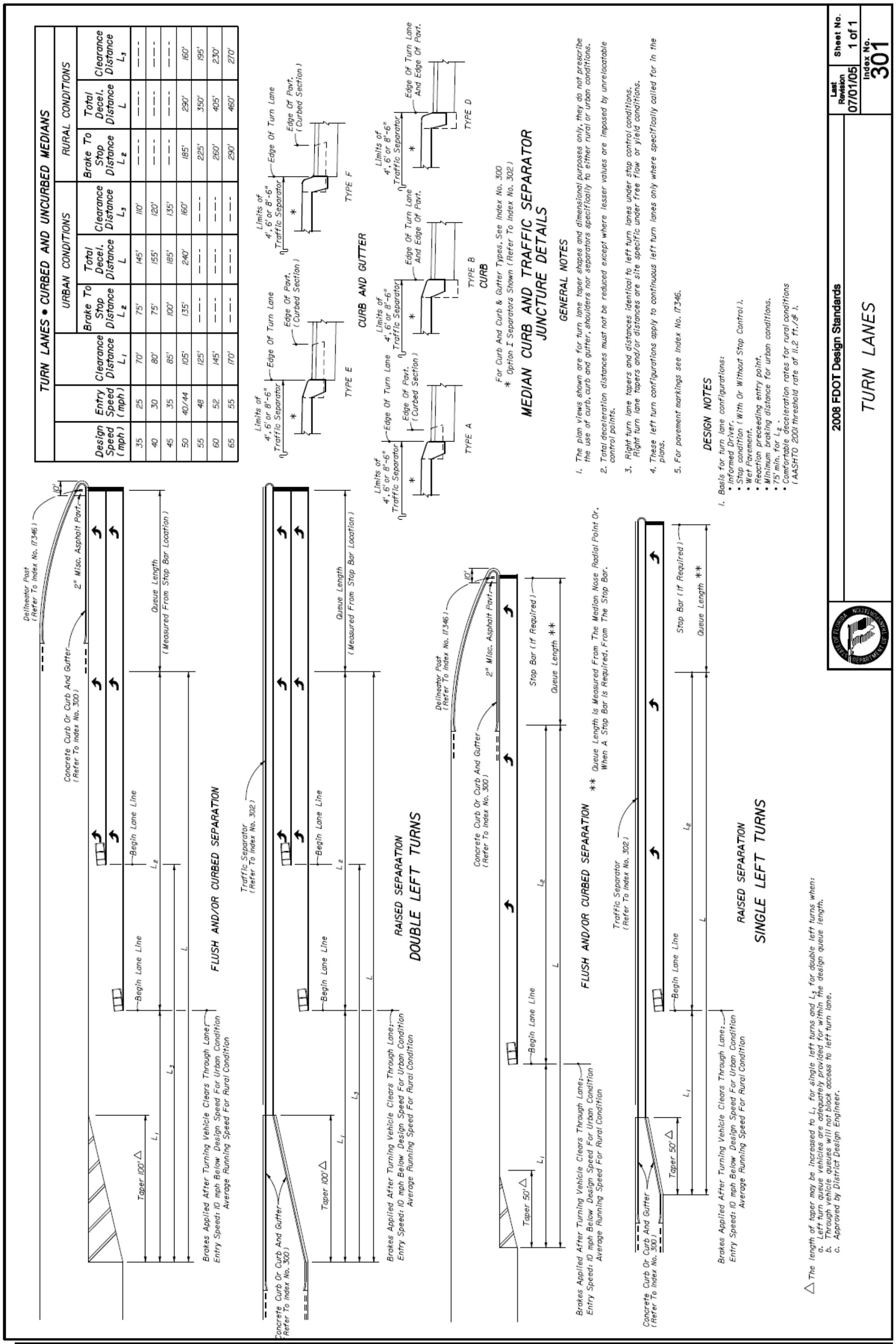

TURN LANES • CURBED AND UNCURBED MEDIANS

Design Speed (mph)	Entry Speed (mph)	Clearance Distance L_1	URBAN CONDITIONS Brake To Stop Distance L_2	URBAN Total Decel. Distance L	URBAN Clearance Distance L_3	RURAL CONDITIONS Brake To Stop Distance L_2	RURAL Total Decel. Distance L	RURAL Clearance Distance L_3
35	25	70'	75'	145'	110'	---	---	---
40	30	80'	75'	155'	120'	---	---	---
45	35	85'	100'	185'	135'	---	---	---
50	40/44	105'	135'	240'	160'	185'	290'	160'
55	48	125'	---	---	---	225'	350'	195'
60	52	145'	---	---	---	260'	405'	230'
65	55	170'	---	---	---	290'	460'	270'

GENERAL NOTES

1. The plan views shown are for turn lane taper shapes and dimensional purposes only, they do not prescribe the use of curb, curb and gutter, shoulders nor separators specifically to either rural or urban conditions.
2. Total deceleration distances must not be reduced except where lesser values are imposed by unrelocatable control points.
3. Right turn lane tapers and distances identical to left turn lanes under stop control conditions. Right turn lane tapers and/or distances are site specific under free flow or yield conditions.
4. These left turn configurations apply to continuous left turn lanes only where specifically called for in the plans.
5. For pavement markings see Index No. 17346.

DESIGN NOTES

1. Basis for turn lane configurations:
   - Informed Driver.
   - Stop condition (With Or Without Stop Control).
   - Wet Pavement.
   - Reaction preceeding entry point.
   - Minimum braking distance for urban conditions.
   - 75' min. for L_2.
   - Comfortable deceleration rates for rural conditions (AASHTO 2001 threshold rate of 11.2 ft./s²).

Exhibit 5.1: FDOT Standard Index 301- Left Turn Lane Criteria

5.5: Model Sensitivity

By inspection, the model is very sensitive to increase in left turn volume, opposing flow volume, the critical time gap and the reliability level desired. It is to be expected that an increase in the opposing volume reduces the availability of the time gap, since the time gap required for the left turning maneuver is constant and discrete event. Also, the increase in number of vehicles for the left turn or the turn lane volume will increase the number of vehicle waiting behind the queue. Hence, both the opposing volume and the left turn volumes have similar effect on the opportunity for the vehicles in the turn lane to make the turn. An examination of the model further reveals the extent of its sensitivity with respect to the reliability level desired. When the level of significance increases, the value of number of vehicles in the queue will increase. An increase in the number of vehicles in the queue signifies a low level of reliability of the turn lane or low level of reliability for the vehicles in the turn lane to complete the turning maneuver. The sensitivity of the selected models is illustrated in table 5.9 and figure 5.10 below.

Figure: 5.9: Sensitivity Analysis: LT Turn Length Demanded (Single Lane Method II)

Tc = 8	V/C	Tc = 7	V/C	Tc = 6	V/C	Tc = 5	V/C
263	0.37	253	0.30	**245**	0.24	238	0.19
275	0.44	260	0.35	249	0.28	241	0.21
293	0.52	270	0.41	254	0.31	244	0.23
317	0.62	283	0.47	261	0.36	247	0.26
351	0.73	300	0.55	270	0.41	251	0.29
396	0.87	324	0.64	280	0.46	256	0.32
449	1.04	356	0.75	294	0.53	262	0.36
506	1.24	396	0.87	313	0.60	269	0.40
561	1.48	442	1.01	336	0.68	278	0.45
612	1.77	491	1.18	366	0.78	288	0.50
658	2.11	541	1.38	402	0.89	302	0.56
697	2.53	587	1.62	442	1.01	319	0.62
732	3.03	630	1.89	485	1.16	340	0.69
761	3.64	668	2.21	527	1.32	365	0.77
786	4.37	702	2.59	568	1.52	394	0.86
807	5.25	732	3.04	607	1.73	427	0.97
825	6.31	758	3.57	642	1.98	462	1.08
839	7.59	780	4.19	674	2.27	498	1.21

** V = 200vph

Figure 5.10: Sensitivity Analyses: LT Turn Length Demanded
Single Lane Analysis (Method II) (Differnt Tc)

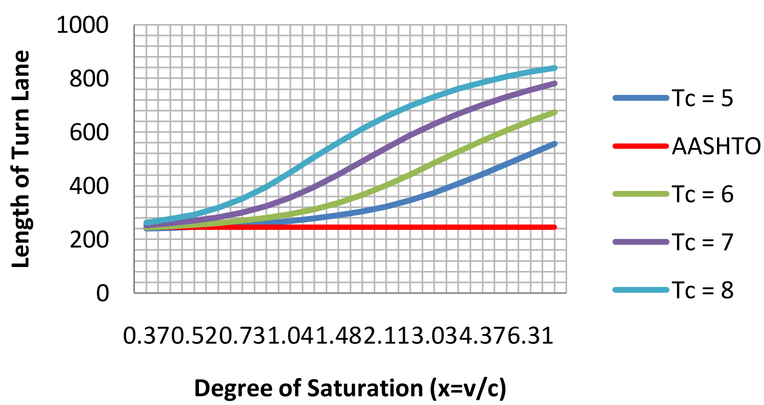

5.6: Safety Consideration

From this analysis, the safety of the turn lane is greatly diminished as the queue length increases. In the case of 12 seconds time gap, the encroachment into the reaction-breaking distance is total. There is no opportunity to clear the through lane before coming to a stop. The reaction-breaking maneuver occurs in the through lane thereby compromising safety in the through lane. In a 2-way 2-lane roadway, the through traffic will have to stop for the duration of the truck in the turn lane. In a multiple lane configuration, the vehicles in the inside lane would have to make unplanned lane change in order to avoid the overflow. This also is an undesirable consequence of the excessive time gap required for the left turn vehicles. In order to avoid this condition, this model can be applied to allow the specification of a second left turn lane as the volume in the turn lane and the opposing traffic increase. This can be accomplished by specifying a practical limit of the turn lane length for the worst traffic condition in the area during the peak hour. If the analysis determines that within a specified reliability and time gap, the lane length requirement is excessive, a specification for a second lane and or widening of the roadway to accommodate more volume can be recommended.

5.6.1: Safety of Existing Turn Lane

In order to provide a safe design, FDOT standard index 301 requires a minimum of 2 cars for storage or queue length of 50 feet. The index also provide a note that reads:" Total deceleration distances must not be reduced except where lesser values are imposed by “unrelocatable”

Control points". However, there is no procedure to ensure that the total deceleration distances are computed with respect to the demand on the turn lane. This tool can be used to evaluate existing left turn lane with respect to the constraint of the standard index 301. First the traffic count is obtained for both the left turn and the opposing traffic. At a desired reliability level, the required lane length is determined and compared with existing. If the desired lane length is less than existing, the left turn lane meets current standards. If the existing turn lane is less than the demand by the traffic, then existing turn lane does not meet current standards and require correction to meet current standard. The deceleration rate of the reaction-breaking distance, which is the safety component of this research, is computed by subtracting the queue length from the total lane length and solving equation 5.19 for the deceleration (a). An increase in the deceleration is an indication of a safety problem that needs to be addressed. One of the possible outcomes of not addressing this issue is traffic incidents such as rear end collision due to rapid stop and side swipe due to rapid lane change.

Example 2: From Table 5.6, the number of cars in the queue for the opposing traffic volume of 1200 vph and a flow rate of 200 vph in the left turn lane is 4. If the existing lane is 205 feet long per FDOT standard index with a minimum of 2 cars in the queue. Determine the acceleration required to stop a passenger car with an entry speed of 30 mph?

Solution:

Length of turn lane demanded = 25*25 = 625 feet

Length of turn Lane provided = 205 feet

The extent of encroachment into the reaction-breaking distances = 4-2 = 2 cars.

Length of encroachment = 2cars*25feet/car = 50 feet.

Distance remaining for reaction-breaking maneuver = 205-50 = 155 feet

From equation 5.19,

$$L_d = 1.47vt + \frac{1.075v^2}{a} = 1.47*30*2.5 + \frac{1.075*30^2}{a} = 155$$

$$155 - 1.47vt = \frac{1.075v^2}{a}$$

$$a = \frac{1.075v^2}{155 - 1.47vt}$$

$$a = \frac{1.075 * 30^2}{155 - 1.47 * 30 * 2.5} = \underline{21.62 \text{ ft/sec}^2}$$

This value when compared to AASHTO and FDOT standard required deceleration rate of 11.2 ft/sec^2 is more than 2 times the breaking rate. This represents a serious compromise of safety for the existing condition. The relative safety effect is a possible rear end collision or side swipe as vehicles in the inner lane rapidly change lanes to avoid rear end collisions.

5.7: Summary and Conclusion

The advantage of this design procedure is that it takes into account the left turn volume expected and the opposing flow expected without the actual traffic count. This can allow planning office to set budget and plan for adequate turn lane length prior to actual engineering design. The above procedure was used in producing the results shown in tables 5.3-6 as well as figure 5.3-6. The design process is simple and can be readily used without any need for sophisticated software such as SYNCHRO, FTSUM, TSIM, NETSIM, or higher knowledge of mathematics. A technician with intermediate computation skill can produce results that are reliable for design. The safety of the existing intersection left turn lane can be readily evaluated using this model for use in expert witnessing. This approach also ensures that the designer is aware of the reliability or the likelihood of failure of the design prior to construction; such knowledge makes the design defensible in a litigious system such as the USA. The departure of the deceleration rate form AASHTO criteria can be readily seen numerically by performing the computations shown in example 2. Wu's method provided in the HCM is recommended for the computation of the queue length for the Analysis. Wu's approach is more stable and allows a wider use both for, single and multiple lanes. The simulation results from SYNCHRO validated the research as the queue exceeds AASHTO current design criteria. The current AASHTO's design criterion is based on average value of the expected queue length at the un-signalized intersection and not reliable when the degree of saturation exceeds 50% of capacity. This model provides a new tool for evaluating, the performance of an un-signalized intersection for safety, the design of the turn lane based on the demand and the reliability of the turn lane to service the expected turning movements. It provides additional tool that can be employed along with standard practice of determining and LOS as the design input for the un-signalized intersection. This scope of this model has been limited to un-signalized intersection; there are sufficient and simple procedures for determining length of queue and delays at signalized intersection in current use. However, the actual reliability of a signalized intersection can be evaluated by the extension of this method. Such evaluation will require empirical data. The data will include the actual measurements of the arrival and discharge rates as well as the queue length of the vehicles waiting in the turn bay per each Cycle; the red phase being the service time in the turn bay. This is a subject for further research.

Chapter 6: Effect of Variability of Peak Hour Volumes on Intersection Signal Delay Performance

6.0 Background:

Current practice uses mean traffic volumes as input for traffic signal control at roadway intersections. Variations in traffic flows affect the performance of intersection performance measured by the delay experience per vehicle traversing the intersection in seconds. In order to account for surge in the traffic stream, Peak hour factor, (PHF) which is the ratio of the hourly volume divided by the peak 15-min flow rate within the peak hour is adopted by the Highway Capacity Manual (HCM) (Lan, Abia and Chimba 2009). The use of PHF allows queue discharge at an intersection which may have built up during a short period surge. HCM suggests a design value for PHF of 0.92 for congested urban areas and 0.88 for rural areas if there is no field measurement available. Variation in traffic volumes does not lend itself to fixed PHF values as the PHF also vary with respect to time within the peak periods. Using these fixed values may not allow optimal signal operation and may allow a level of delay not proportionate to the prevailing traffic conditions. In view of this concern, a study to explore the effect of variability of the peak hour volumes on the design hourly volume and intersection delays performance was conducted. This study is divided into three sections. First, a model of PHF as a function of the degree of saturation (x- volume-to-capacity ratio) on surface streets is developed. A total of 1669 data points were obtained from the West Palm Beach County and Broward County area. The results show that, among several functional forms, the simple power function established with functional classification of roadways could be used to explain 47% (R^2) of data variation, which is considered a well acceptable given the significant variability presented by the data (standard deviation of the prediction error is about 7.7% of the observed values). The 95th percentile confidence intervals on the mean estimates are also provided. The average standard deviation of the mean estimate error is around 0.26% (30 times smaller compared to the data variability), suggesting the proposed mean estimates are fairly reliable. The model is found to be transferable with view to universal application. In section two, a new model is developed that relates the standard deviation of the flow rate to the mean flow with high coefficient of determination (R^2) of 76%. It is also established that modeling the variation of the design hourly volumes with respect to the coefficient of variation (*CV*) is not reliable as it returns very low coefficient of determination *(R^2 = 0.15)- Hellinga and Abdy (2008)*. The two models are combined in section three to examine the effect of the variation of the design hourly volumes on intersection signal delay using simulation. The results show that the assumption of Poisson distribution for quantification of design hourly volume is not reliable as actual data analysis did not fit the Poisson model. It is also established that traffic signal delays varies with respect to variation of the design hourly volume and thus adaptive signal system would be advantageous.

6.1 Developing Model for Peak Hour Factor (PHF)

6.1.1 Data Description

The intersection traffic counts data were provided by the Traffic Division of the Palm Beach County Engineering Office and the Broward County. The intersection data were compiled from the following major arterials located across the Palm Beach and Broward

Counties were selected:

Northern Palm Beach County:

- Indiantown Rd
- Donald Ross Rd
- and PGA Blvd (544 data points)

Central Palm Beach County:

- 45th Street, Belvedere Rd
- Forest Hill Rd
- Lantana Rd; (554 data points)

Southern Palm Beach County/Broward County:

- West Atlantic Ave
- Linton Blvd
- Glades Rd
- Atlantic Blvd (571 data points).

6.1.2 Field verification of Data Verification

To ensure the validity of the data, field data verification were conducted for each of the intersection used in the study for the following purposes:

1. To verify the existence of a reported count station
2. To ensure that the approach number of lanes used in the study match the assumed approach capacity.
3. To ensure that recent modification of the roadway did not skew the expected out come.
4. To determine current construction activities in and around the study intersections.

5. To determine functional classification of the roadway whether it was arterial or collector road.

6.1.3 Data Contents and Screening

The data consisted of traffic volumes for both the morning (AM) and afternoon (PM) peak hour and peak hour factors (PHF) from eight different approaches per intersection. The degree of saturation (X) for each approach volumes were computed using the volume information and the capacity of the approach. The data was screened for size and compatibility with existing roadway as well as availability for the specified study period. It was also screened for balance, for instance, intersection where there was no recording of data for the morning peak period and a recording for afternoon peak period were discarded as unbalanced data. After screening the dataset, an average of 550 data points from each part of Counties were obtained. A total of 1669 data points were used for modeling purpose. The corresponding capacity information taken from FDOT QLOS table was also recorded into the database to calculate the degree of saturation (or v/c ratio). For example, 850, 1800 and 2710 vehicles per hour which correspond to LOS E directional service volumes were used as the approach capacities for a two-lane, four-lane and six-lane road, respectively, given the traffic signal density is between 2 and 4.5 per mile. Finally, an indicator of 1 was recorded for the intersection approach if it is on an arterial and 0 if it is on a collector/local road. The data set are as depicted in table A-1 in Appendix A. The dataset in the column format ready for regression analysis is also available upon request from the authors.

6.1.4 Comparison and Transferability of Tarko's Model

The purpose of the following sections is twofold. First, examine the prediction function proposed by Tarko et al. (2005) using the dataset established in this study to determine whether their prediction function is transferrable and applicable in other geographical areas. Statistical significance of variables is also examined through nonlinear regression in the same functional form. Second, propose an alternate functional form to provide more accurate predictions and to establish the predictive limits.

Analysis of the predictability of the original Tarko's prediction function with the dataset used in this study was conducted. Note that the population indicator variable, *POP*, is set to 1.0 for all observations since all cities in the study area have a size of population greater than 20,000. The coefficient of determination calculated for the model was *negative*, suggesting the predictions are not in a good agreement with the actual peak hour factors. It is therefore suggested that the model transferability to other geographical areas is lacking from the Tarko's model. The similar conclusion was also found in Hellinga and Abdy (2008), where the authors postulated modeling the variation of the PHF with respect to the *CV*. The prediction model using *CV* as the response variable to the mean volume returned low coefficient of determination and could not explain the variation in the PHF adequately. In the followings, based on the same functional form, the authors also investigated the statistical significance of variables to see if any other explanatory variables can be used to improve the model performance.

The population variable originally included in Tarko's model is not considered here due in part to the geographical characteristics in which the data is collected from. It is not straightforward to establish a well-defined relationship between the population and the peak effects of roadways that serves which population. For example, a long-stretched arterial that primarily serves commuters may cross various city boundaries/jurisdictions from a major generator to the destinations. Instead, the functional classification of roadways was taken into consideration, which is believed to bear a more direct relationship with the peaking effects.

Through series of nonlinear least square (NLS) regression analyses, similar to the stepwise analysis the State Road (*SR*) variable is removed due to its statistical insignificance. The *AM* binary variable also tested insignificant in the analysis. Removing both insignificant variables and adding the functional classification (denoted as *FC*) indicator variable, the resulted regression model can be written as:

$$\hat{p} = 1 - \exp(-\underset{(78.6)}{1.501} - \underset{(14.4)}{0.632}\, v - \underset{(3.9)}{0.164}\, FC) \tag{1}$$

(The numbers shown in parenthesis represent the *t*-statistics which are all significant).

Where: $\hat{p} = PHF(predicted)$

FC = 1 for arterials and = 0 for collectors/local roads. The coefficient of determination (R^2) is 0.355 and the standard deviation of the prediction error is 0.0719. When the hourly volume approaches capacity, traffic distributed into each 15-min time interval tends to be uniform and results in higher peak hour factors. Therefore, another idea is to replace hourly volume with the volume-to-capacity ratio (denoted as *X*) as the explanatory variable in the prediction model. Performing the nonlinear regression analysis again yields:

$$\hat{p} = 1 - \exp(-\underset{(61.9)}{1.329} - \underset{(16.8)}{1.567}\, X - \underset{(6.9)}{0.269}\, FC) \tag{2}$$

where:

$X = v/c$ and c = intersection approach capacity.

$\hat{p} = PHF(predicted)$.

The intersection approach capacity can be set based on the LOS E directional service volumes proposed by Florida Department of Transportation Quality Level of Service Handbook (FDOT QLOS); namely, 850, 1800 and 2710 vehicles per hour as the approach capacities for a two-lane, four-lane and six-lane road, respectively. The model coefficient of determination is 0.4, suggesting that replacing volume with volume-to-capacity ratio improves the model performance. The standard deviation (σ) of the prediction error is 0.0694. All parameters are significant based on the t-statistics shown in the parentheses. Compared to the original Tarko's model, the modified predictor enhances the model performance significantly based on the coefficient of determination (improved from *negative* value to 0.4). This exercise also strongly supports the inclusion of the volume-to-capacity ratio and the functional classification of roadways will have significant contribution to the model predictability. Figure 6.1 shows fitted peak hour factors as a function of volume-to-capacity ratio for arterials versus collectors/ local roads (from Equation (2)).

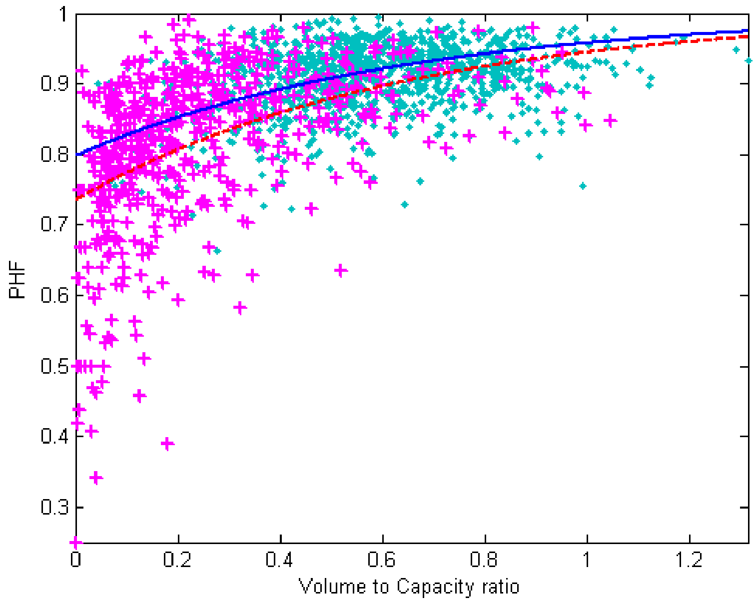

Figure 6.1: Fitted peak hour factors as a function of volume-to-capacity ratio from Equation (2) (dot = actual PHF from arterials, "+" = actual PHF from collectors/local roads, solid line = estimated PHF for arterials, and dash line = estimated PHF for collectors/local roads)

6.1.5 Regression Analysis for the Proposed Model

Several runs of regression analysis using other functional forms with the same set of explanatory variables, namely, volume-to-capacity ratio and functional classes of roadways, to determine if alternative functions yield better results. Since being defined as $v/(4 \cdot v_{15\max})$, where v denotes the peak-hour volume here and $v_{15\max}$ is the peak 15-min volume within peak hour, the peak hour factor (*PHF*) is ranged from 0.25 (when all traffic arrives in 15 min during an hour) to 1.0 (when all traffic arrives uniformly among 15-min time intervals). This task was accomplished using NLINFIT-Nonlinear least-squares data fitting by the Gauss-Newton method in MathLab6p5.

NLINFIT(X, Y, FUN, BETA0) estimates the coefficients of a nonlinear function using least squares. Y is a vector of response (dependent variable) values. Typically, X is a design matrix of predictor (independent variable) values, with one row for each value in Y. However, X may be any array that FUN is prepared to accept. FUN is a function that accepts two arguments, a coefficient vector and the array X, and returns a vector of fitted Y values. BETA0 (β_o) is a vector containing initial values for the coefficients. The prediction model obtained using this process is the following simple power function:

$$\begin{aligned}\hat{p} &= 0.25 + a_1 X^{b_1}\text{, for arterials} \\ &= 0.25 + a_2 X^{b_2}\text{, for collectors/local streets}\end{aligned} \tag{3}$$

It is noted that, since arrival flow pattern should become uniform among 15-min intervals when the hourly volume approaches capacity, the corresponding peak hour factor should be similar; hence, the functional classification of the roadways should be ignored. To accomplish that, the estimated values of a_1 and a_2 are constrained to be equal at capacity in the regression analysis. In addition, to demonstrate the statistical significance of the contribution from functional classification, Equation (3) is tested against the overall prediction model shown below and the results are summarized in Table 6.1.

$$\hat{p} = 0.25 + aX^{b} \tag{4}$$

Table 6.1: Summary of NLS regression analysis on functional classification

Model type \ Statistics			Parameter value	t statistics	Log-likelihood	R^2
Equ. (3)	Arterials	a_1	0.6836	181.5	2193.8	0.474
		b_1	0.0551	7.2		
	Collectors/ Local Roads	a_2	0.6975	105.7		
		b_2	0.1224	23.5		
	Prediction error (standard deviation)	σ	0.0650	57.6		
Equ. (4)	Overall	a	0.7035	239.5	2151.1	0.447
		b	0.1163	30.7		
	Prediction error (standard deviation)	σ	0.0666	56.8		

As shown, all parameters are statistically significant. The coefficient of determination for Equation (3) is slightly higher than Equation (4), indicating that categorizing roadway functional class seems to marginally improve estimation accuracy. However, based on the likelihood ratio test, the test statistics calculated as:

$$2\times ln[L(\text{Equ. 3})/L(\text{Equ. 4})]\ (\approx 85.4) >> \chi^2_{.05,2}\ (\approx 6.0),$$

where $ln[\ ]$ is the natural logarithm operator,

and $L(\ )$ is the value of the likelihood function.

Therefore, there is statistical evidence to support that Equation (3) is significantly improved over Equation (4). Equation (4) can be used to estimate peak hour factor if no information is available regarding the functional classes of roadways. Otherwise, utilizing Equation (3) will be expected to give more accurate estimates.

Compared to Tarko's model, i.e., Equation (2), the estimation accuracy is improved by 19% in term of R^2. This can be shown as:

$$[(R^2_{new} - R^2_T)/R^2_T]*100\% = [0.474-0.4)/0.4]*100\% \approx 19\%$$

Where: R^2_{new} = the new prediction model

R^2_T = prediction model based on Tarko's postulates.

The fitted peak hour factors from Equations (3) and (4) are also depicted in Figures 2 and 3.

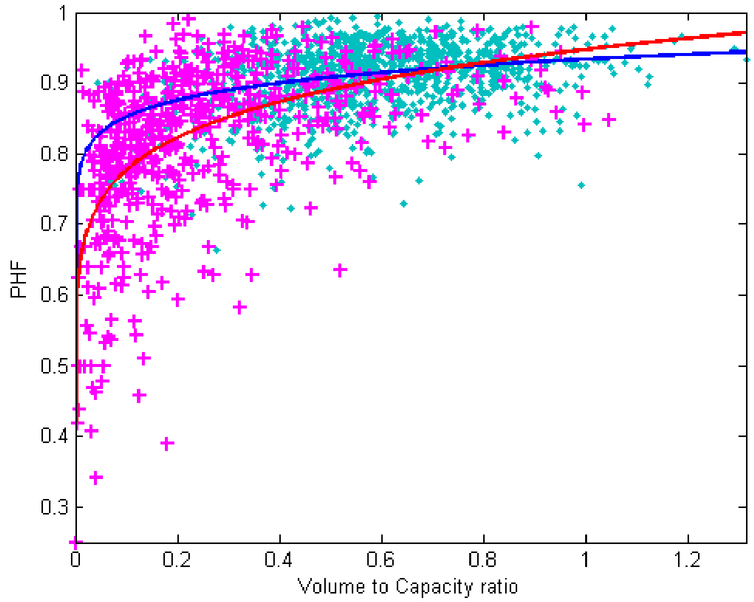

Figure 6.2: The proposed PHF design values (from Equation (3)) (dot = actual PHF from arterials, "+" = actual PHF from collectors/local roads, solid line = estimated PHF for arterials, and dash line = estimated PHF for collectors/local roads)

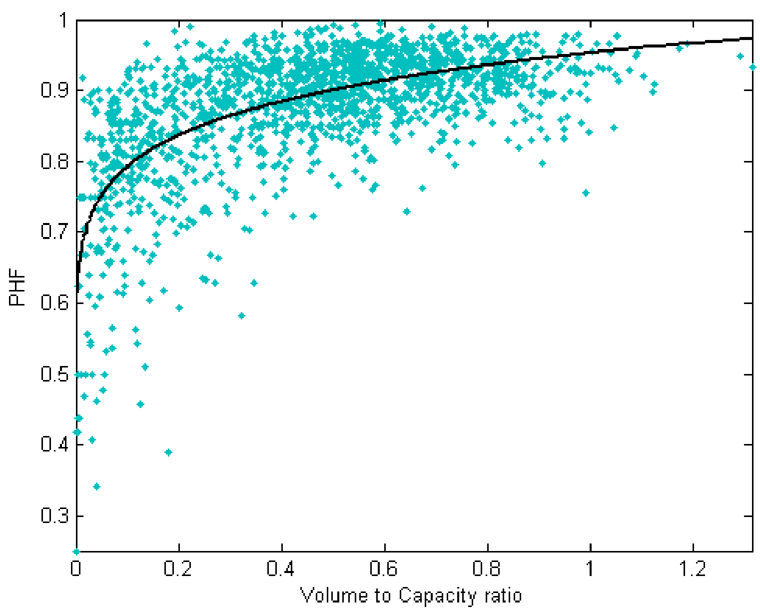

Figure 6.3: The proposed PHF design values (from Equation (4))

6.1.6 Confidence Intervals

The 95% confidence intervals of the mean estimates, constructed from the mean estimation error, are also plotted to give readers an idea on the reliability of the mean estimates. The variance of the mean estimation error can be calculated using the following Delta method (Casella and Berger, 2002).

$$Var(\hat{p}) = \sigma_{\hat{p}}^2 = \left(\frac{\partial \hat{p}}{\partial \mathbf{b}}\right)^T \operatorname{cov}(\mathbf{b}) \left(\frac{\partial \hat{p}}{\partial \mathbf{b}}\right) \tag{5}$$

where:

b is the parameter set in column vector ($=[a \quad b]^T$), and cov(**b**) is the covariance matrix of the parameter set. It is assumed that the arrival is normally distributed and the PHF is also normally distributed; based on this normality assumption, the confidence intervals are then constructed as [$\hat{p}$ -$z_{\alpha/2}\sigma_{\hat{p}}$ $\hat{p}$ +$z_{\alpha/2}\sigma_{\hat{p}}$] at the (1-α) confidence level ($z_{\alpha/2}$ = 1.96 when α = 0.05). One could see the confidence intervals are tighter (meaning the mean estimate is more reliable) at the location where more data is available and concentrated. At the locations where less data is available, one can find the intervals are wider. The standard deviation of the mean estimation error ranges from 0.16% to 2.63%, with an average equal to around 0.26%. Compared to the standard deviation of the prediction error (=7.71%), the average standard deviation of the mean estimation error is about thirty times smaller. This gives readers an idea (1) how significant is the variability of the data, which is the primary cause for the moderately low R^2, relatively compared to the variability of the mean estimates; and (2) the mean estimates are considered reliable due to sufficient sizes of observations distributed over the entire range of degree of saturations. Figures 4 and 5 show the confidence intervals information from the proposed designed PHF for arterials and collectors/local roads, respectively.

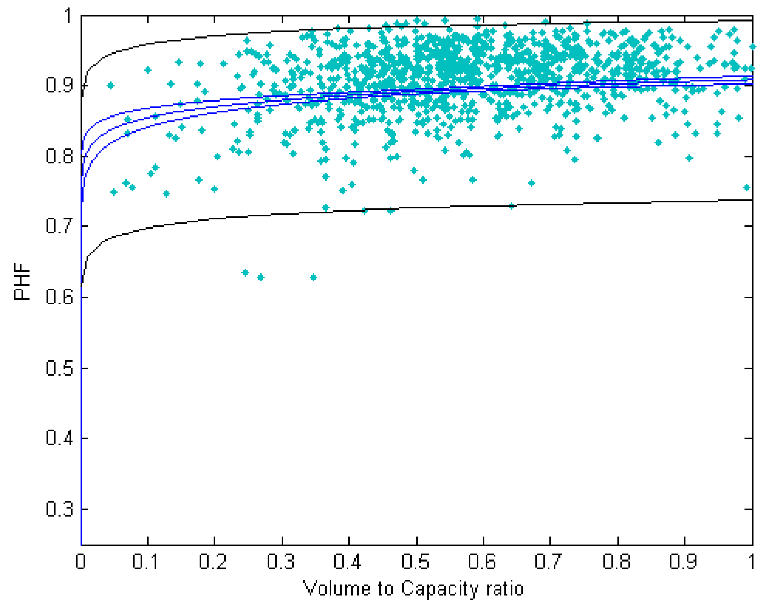

Figure 6.4: PHF mean estimates, confidence intervals (inner bands) and predictive limits (outer bands) for arterials

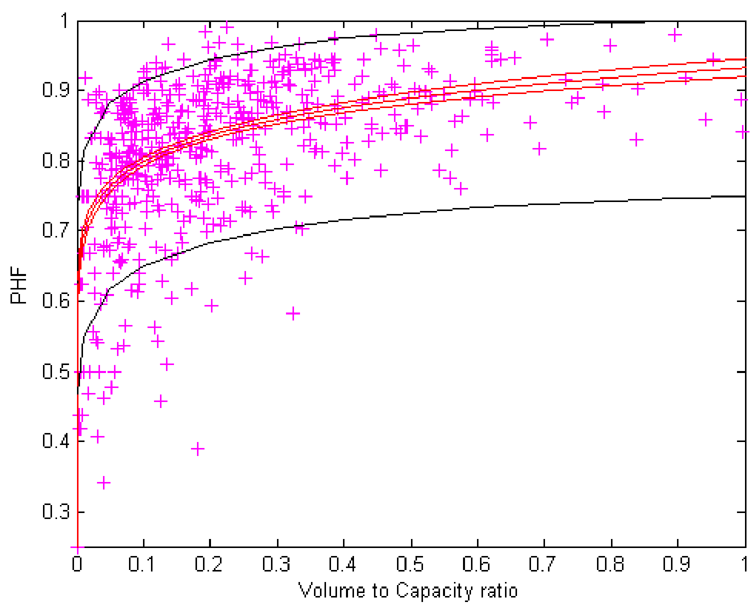

Figure 6.5: PHF mean estimates, confidence intervals (inner bands) and predictive limits (outer bands) for collectors and local roads

6.1.7 Predictive Limits

The predictive limits here are also referred to the confidence limits on the predictions, which can be used to quantify the variability of the design hourly volumes (defined as peak-hour volume divided by peak hour factor) for the intersection approaches and the effects of the variability of the design hourly volumes on the intersection delay estimates. This Investigation of the effect of variability of the peak hour volume on the design hourly volume is provided in section 6.3. Due to the significant data variability presented here, the predictive limits can be fairly large as well. To show this, one needs to first identify an appropriate probability density function (PDF) that fits the observations. Since the peak hour factor ranges between two fixed points (0.25 to 1.0), a natural choice of PDF will be the Beta distribution which can be expressed as:

$$f(p;\alpha,\beta,A,B) = \frac{1}{B-A}\frac{\Gamma(\alpha+\beta)}{\Gamma(\alpha)\Gamma(\beta)}\left(\frac{p-A}{B-A}\right)^{\alpha-1}\left(\frac{B-p}{B-A}\right)^{\beta-1}, A \le p \le B,\ \alpha > 0,\ \beta > 0$$

(6)

where: $\Gamma(\alpha)$ is called the Gamma function and is given as:

$\Gamma(\alpha) = \int_0^\infty \hat{p}^{\alpha-1} e^{-\hat{p}} d\hat{p}$; with respect to *p*.

Since the predictive limits [A, B] is different from [0, 1], p-hat is replaced with [($\hat{p}$ - *A*)/(*B*-*A*)] and the variance (σ^2) also is replaced with the quantity $(\sigma^2)/(B-A)^2$. And the parameters α and β are given as shown below:

$$\alpha = \frac{\hat{p}-A}{B-A}\left[\frac{(\hat{p}-A)(B-\hat{p})}{\sigma^2}-1\right],\ \beta = \frac{B-\hat{p}}{B-A}\left[\frac{(\hat{p}-A)(B-\hat{p})}{\sigma^2}-1\right],$$

and $\hat{p}$ is the mean estimation function as shown in Equation (3).

Setting A = 0 and B = 1 will result in the standard beta distribution. For data fitting using maximum likelihood estimation (MLE) method, the author allows A to vary between 0 and the lower limit of the data and B to vary between the upper limit of the data and 1. The estimation results show a standard beta distribution, i.e, A = 0 and B = 1, is resulted as the likelihood function is maximized. The resulted parameter values and statistics are summarized in Table 2. Similar to the nonlinear least square (NLS) method, all parameters are statistically significant but slightly different from the NLS estimator. The value of R^2 is slightly lower as expected since the NLS estimator provides more accurate predictions. The contribution of the functional classification is also shown to be significant in the Beta regression based on the following likelihood ratio test statistics: $2\times ln[L(\text{Equ. 3})/L(\text{Equ. 4})]$ (≈72.2) >> $\chi^2_{.05,2}$ (≈6.0).

Table 6.2. Summary of Beta regression analysis on functional classification

<table>
<tr><th colspan="2">Statistics / Model type</th><th colspan="2">Parameter value</th><th>t statistics</th><th>Log-likelihood</th><th>R^2</th></tr>
<tr><td rowspan="5">Equ. (3)</td><td rowspan="2">Arterials</td><td>a_1</td><td>0.6578</td><td>217.7</td><td rowspan="5">2356.1</td><td rowspan="5">0.435</td></tr>
<tr><td>b_1</td><td>0.0361</td><td>5.7</td></tr>
<tr><td rowspan="2">Collectors/ Local Roads</td><td>a_2</td><td>0.6796</td><td>113.0</td></tr>
<tr><td>b_2</td><td>0.0973</td><td>19.3</td></tr>
<tr><td>Prediction error (standard deviation)</td><td>σ</td><td>0.0678</td><td>50.2</td></tr>
<tr><td rowspan="3">Equ. (4)</td><td rowspan="2">Overall</td><td>a</td><td>0.6711</td><td>290.3</td><td rowspan="3">2320.0</td><td rowspan="3">0.398</td></tr>
<tr><td>b</td><td>0.0814</td><td>25.7</td></tr>
<tr><td>Prediction error (standard deviation)</td><td>σ</td><td>0.0696</td><td>50.2</td></tr>
</table>

Once the probability density function is calibrated, given the degree of saturation and estimated parameters one can calculate the upper $(1-\alpha/2)^{th}$ and lower $(\alpha/2)^{th}$ percentile predictive limits. The predictive limits at the 95^{th} confidence level (α = 0.05) are depicted in Figures 4 and 5. As shown in Figure 5, the low tail of the observations from collectors/local roads does not fit as well as expected, primarily due to heavier low tail distribution at *v/c* ratios between 0.4 and 0.6. (see Figure 6) A mixture of distributions could be used to fix the problem but the author decided not to pursue that for simplicity. However, the histogram has apparent approximation to the Beta Distribution of the form described above.

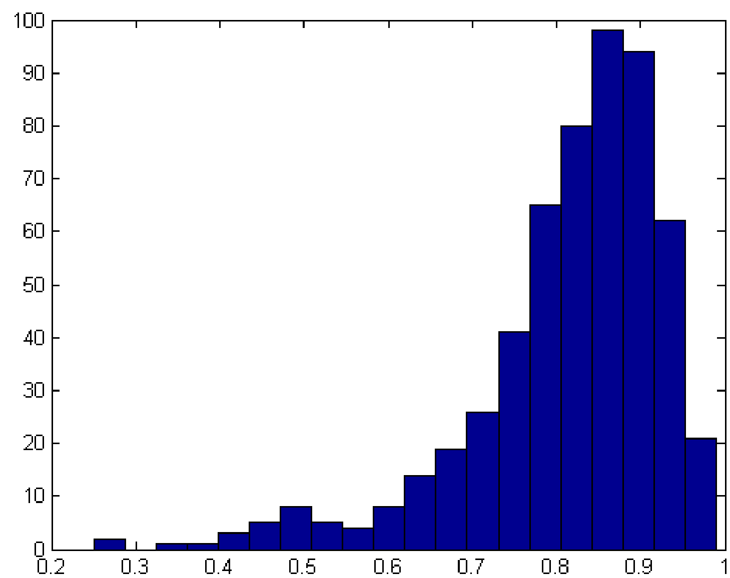

Figure 6.6: Histogram of the peak hour factors for collectors/local roads

6.1.8 Model Validation and Recommended Design Values

In order to test the transferability of the proposed model, given the data availability the authors perform model validation using the peak hour factors collected from signalized intersections from two other geographical areas, including Palm City and City of Stuart in Martin County, Florida and City of Grand Junction, Colorado. A total of 336 additional peak hour factor observations (around 20% of the estimation dataset) from 19 signalized intersections were obtained, along with the attributes such as volume-to-capacity ratio, functional classification of roadways, time of day and populations. Although close to the highly populated and urbanized Palm Beach County (1.35 million in 2007) and Broward County (1.76 million), the suburban Martin County has only around one-tenth of population (139,000). The population in the suburban City of Grand Junction in Colorado was 54,000. Because of the differences in population size and urbanization characteristics, these two areas are deemed good candidates for testing the model transferability.

The NLS estimator listed in Table 1 was used to generate predictions and compared with the observed peak hour factors. The resulted R^2 is calculated as 0.393. For a variable with large data variability, a model explaining almost 40% of data variation is fairly adequate. Compared to the predictions made with Tarko's original model, which yields *negative* R^2 again, the proposed model is considered much more transferable.

Based on all abovementioned statistics and findings, the authors recommend the use of simple power function for modeling peak hour factors. The mean estimates of peak hour factors from Equations (3) and (4) are deployed for practical applications. As shown in Table 3, the recommended design values for Equation (4) are given in the 2nd column, and the designed values for Equation (3) are given in the 3rd and 4th columns. When the functional class of roadways can be classified, it is recommended that peak hour factors be selected from Table 3 depending on the functional classification of the roadway. Otherwise, a good estimate can be obtained using the overall prediction equation given in equation 4.

Table 6.3: Recommended PHF Design Values

v/c ratio	Overall	Arterials	Collectors/ Local roads
≤0.15	0.78*	0.85*	0.79*
>0.15 - 0.25	0.80	0.87	0.81
>0.25 - 0.35	0.84	0.88	0.85
>0.35 - 0.45	0.86	0.89	0.87
>0.45 - 0.55	0.88	0.90	0.89
>0.55 - 0.65	0.90	0.91	0.91
>0.65 - 0.75	0.91	0.92	0.92
>0.75 - 0.85	0.92	0.92	0.93
>0.85 - 0.95	0.93	0.93	0.94
>0.95	0.94	0.93	0.95

Note: * value taken at $v/c = 0.1$.

6.1.9 Conclusions

The major challenge of modeling peak hour factors can be attributable to significant data variability, although a general pattern over the range of degree of saturation on surface streets can be identified. To evaluate existing traffic conditions, it might be more appropriate to use locally available flow measurements to calculate peak hour factors. Due to its significant day-to-day variations, it might be beneficial to collect data from sufficient number of days in order to obtain a reliable mean estimate. To evaluate future traffic condition, however, a reliable model for predicting peak hour factors is required since existing flow measurements might not be representative enough for the future condition.

This study first revisited the model proposed by Tarko et al. (2005) using a larger dataset and concluded that:

(1) Time of day (AM versus PM peak period) and state road indicator variables are not significant;

(2) Using volume-to-capacity instead of volume improves the accuracy of model

estimation;

(3) Functional classification of roadways is a significant variable to explain peaking effects; and

(4) The model is not transferable to either the estimation dataset collected from West Palm Beach and Broward Counties in Florida, or the validation dataset collected from two other geographical locations. The coefficients of determination in both cases were all negative.

In addition to the inclusion of *v/c* ratio and functional classification explanatory variables, the simple power function proposed here is also found to enhance the quality of data fitting. The proposed model explains 47% of the data variation, which is considered fairly satisfactory given the large data variability. Confidence intervals about the mean estimation function are tight (30 times smaller than the data variability), indicating that the mean estimates are considered reliable due to sufficient sizes of observations distributed over the entire range of degree of saturations. The predictive limits, which can be used to quantify the variability of the design hourly volume (peak-hour volume divided by peak hour factor) and the effects of the variability of the design hourly volumes on the intersection delay estimates, are also provided here based on the Beta probability density function assumed for the peak hour factor.

Finally, the authors performed model validation using data collected from other geographical areas, including Martin County in Florida and City of Grand Junction in Colorado. The proposed model is able to explain almost 40% of the data variation, which is considered fairly adequate given the large data variability and the low coefficient of determination from the Tarko's model. An important application that can be derived from this study is to investigate the effects of variability in peak hour factors on the design hourly volume and delay performance of the signalized intersections, which is the subject of the next section.

6.2 Developing Model of the Variability of Peak Hour Volumes on the Design Hourly Volume (V_d)

6.2.1 Data Description

An investigation of the effect of arrival flow uncertainties or variation with respect to the design hourly volume was conducted using traffic counts obtained from 14 counties in the state of Florida and a total of 37 counting stations. The breakdown of the counties and their various counting stations is given in table (4) below.

Table 6.4: Counting Stations

COUNTY CODE	COUNTY NAME	NUMBER OF STATIONS	COUNTY CODE	COUNTY NAME	NUMBER OF STATIONS
17	Saratosa	1	88	Indian River	1
86	Broward	10	89	Martin	2
04	DeSoto	1	93	Palm Beach	4
87	Miami-Dade	6	97	Turn Pike	1
72	Duval	2	01	Charlotte	3
75	Orange	1	02	Citrus	3
77	Seminole	1	03	Collier	1

The 24-hour counts for 2007 were randomly selected with emphasis on the urban areas and used in the analyses, 37 sites in all. The maximum and minimum AM and PM peak periods were also sorted out and used in the analyses. In sorting out the maximum and minimum AM and PM peak periods, care was exercised to ensure that unbalanced data were screened out. Unbalanced data represented those counting stations where no counts data were available or counts data were available in one period only. For instance, there was an available data for the AM peak period at a counting station but no data available for the PM peak period and vice versa. A particular attention was paid to excessive counts or extreme fluctuation within a count station; where excessive count was present, the count station was investigated for construction activities and traffic incidents. Where no conclusive evidence existed, the data were included in the analysis or removed if tainted by traffic diversion and incident. Also, a t-statistic was conducted to ensure that suspected counts (Low or high) belong to the mean volume obtained. Weekends and holidays were removed by masking the data from the computation and the variation of the week end data treated separately; after screening the dataset this resulted to a total of 27174 observations. A total of 27174 data points were used for modeling purpose of the design hourly volume variation (V_{std}). The data was first analyzed for basic statistics and general characteristics. The data behavior was inconclusive with respect to its distribution type. Therefore, a common base was necessary to reduce the data to that base to allow for a meaningful analysis. The common base adopted was to find the mean, standard deviation and coefficient of determination of each of the count sites and use the mean and standard deviation for the prediction model development. Coefficients of variation (CV) were computed for each of the counting stations separated into the AM and PM peak. The data included those published by Sullivan (2006) and Hellinga (2008) and a total of 246 sample sizes were used in the modeling of the CV. The analysis conducted with various sample sizes showed that sample sizes of between 200 to 250 produce a stable mean volumes range for a reliable analysis and result. The dataset used for the *CV* modeling is presented in table A-2 in Appendix A. The data set in the column format ready for regression analysis is also available upon request from the author. The table include data sources with the Florida's count station designated by county codes and site numbers; the mean, standard deviation, coefficient of variation, number of observations and t-test.

6.2.2 Data Characteristics

The data were separated into morning peak hour volumes (AM) and afternoon peak hour volumes (PM). The overall mean, standard deviation and coefficient of variation for the Am peak hour were: 2675.59, 2372.26 and 0.89. The maximum volume was recorded as 9314 vehicles per hour (vph) and the minimum volume was recorded as 86 vph. Also, the overall mean, standard deviation and coefficient of variation for the PM peak volumes were: 2801.42, 2304.73 and 0.82. The maximum volume recorded for the PM peak volume was 9226 vph and the minimum volume recorded for the same peak hour from all count stations was 86 vph. The general data characteristics with it statistics are as depicted in tables 5 and 6 below.

6.2.3 Variation between AM and PM Peak-Hour Volumes

The data was separated into Am and PM peak-hour volume to evaluate the variability between the two peak-hour volumes. The comparison is carried out by using t-statistics as follows:

T-test:

Given : AM Mean ($\overline{X}_1$) = 2675.585, the AM Standard deviation (s_1) = 2372.73, and the AM observations (N_1) = 13587;

PM Mean ($\overline{X}_2$) = 2801.421, PM Standard Deviation (s_2) = 2304.73 and the PM observations (N2) = 13587;

The value of using a two-tailed test (Dixon & Massey 1983) is computed as follows:

$$t = \frac{\overline{x}_1 - \overline{x}_2}{S_p{}^2 \sqrt{\frac{1}{N_1} + \frac{1}{N_2}}} \qquad 7$$

and

$$S_p{}^2 = \frac{(N_1 - 1)s_1{}^2 + (N_2 - 1)s_2{}^2}{N_1 + N_2 - 2}$$

Where:

t is the calculated t-statistics and

S^2_p is the pooled variance of the AM and the PM peak volumes as given above.

By substituting the values of the means, variances and the number observations given above into the above equations, the calculated t value is found to be +/-0.4302.

The variation between the AM peak hour volumes and the PM peak hour volumes is not significant at the 5% level of significance based on the two-tailed t-test **($t_{\alpha/2,\infty}$p(-0.1.96)<t(+/-0.4302)< $t_{(1-\alpha/2),\infty}$(+1.96)** performed on the data with respect to the means and variances of the two periods. The small value of the t-statistics suggests a high probability that the two samples are of the same population. As a result, the AM mean and the PM mean volumes were combined in the prediction model. The basic statistics of the AM and PM distributions are presented in tables 5 and 6, and figures 7-10.

6.2.4 Data Distribution and Poisson Assumption

Traffic characteristics and vehicle arrival at an intersection approaches are often assumed to be a Poisson distribution (HCM 2000). One of the characteristics of a Poisson distribution is that the mean and the variance are equal. Analysis of the peak hour volumes rendered this assumption invalid as the variance (5627617.5 for AM Peak and 5311780.37 for PM peak) and the mean (2675.585 for the AM Peak and 2801.42 for the PM Peak) were significantly different and the variances were in the order of 2100 times the means as depicted in tables 5 and 6. In order to examine the distribution of the data, the data were classed and graphed as depicted in figure 7, 8, 9, and 10. It can be seen that from the histogram, the data are compartmentalized into three groups which appear to be normally distributed. The compartments range from low to medium to high. The low volumes ranges from 86 vph to less than 3500 vph for the AM peak volumes, this accounts for about 71 percent of the data, the medium range is from 3500 vph to 6000 vph which accounts for about 15 percent of the data; the high range is from 6000 vph to 9314 vph which accounts for about 14 percent of the data.

Table 6.5: AM- PEAK HOUR VOLUME DISTRIBUTION AND STATISTICS.

Class	Frequency	Probability	Percentile	%Cumulative Frequency	Mid Range
<500	1719	0.126518	12.6518	12.65179951	250
500-1000	2289	0.1684699	16.84699	29.4987856	750
1000-1500	1973	0.1452123	14.52123	44.02001914	1250
1500-2000	1530	0.1126076	11.26076	55.2807831	1750
2000-2500	941	0.0692574	6.925738	62.20652094	2250
2500-3000	670	0.0493118	4.931184	67.13770516	2750
3000-3500	607	0.0446751	4.467506	71.60521086	3250
3500-4000	380	0.0279679	2.796791	74.40200191	3750
4000-4500	449	0.0330463	3.304629	77.70663134	4250
4500-5000	551	0.0405535	4.055347	81.76197836	4750
5000-5500	356	0.0262015	2.620152	84.38212998	5250
5500-6000	254	0.0186943	1.869434	86.25156399	5750
6000-6500	232	0.0170751	1.707515	87.95907853	6250
6500-7000	442	0.0325311	3.25311	91.21218812	6750
7000-7500	468	0.0344447	3.444469	94.6566571	7250
7500-8000	187	0.0137632	1.376316	96.03297269	7750
8000-8500	277	0.0203871	2.038713	98.07168617	8250
8500-9000	221	0.0162655	1.626555	99.69824097	8750
9000-9500	41	0.0030176	0.301759	100	9250
Total	***13587***	***1***	***100***		
Mean Volume = 2675.59					
Std Deviation = 2372.26					
Coefficient of Variation (CV) = 0.89					
Minimum Volume = 86 vph					
Maximum Volume =9314 vph					

Similarly, The low volumes ranges from 104 vph to less than 3000 vph for the PM peak volumes, this accounts for about 69 percent of the data, the medium range is from 3000 vph to 6500 vph which accounts for about 19 percent of the data; the high range is from 6500 vph to 9226 vph which accounts for about 12 percent of the data. Based on this break down, it is established that there is no significant difference between the AM peak volumes and the PM peak volumes. However, its exact distribution cannot be determined but the compartments appear to be normally distributed.

Table 6.6: PM- PEAK HOUR VOLUME DISTRIBUTION AND STATISTICS.

Class	Frequency	Probability	Percentile	Cum. Freq.	Mid Range
<500	1520	0.1117894	11.178937	11.17893653	250
500-1000	1468	0.107965	10.796499	21.97543576	750
1000-1500	2059	0.1514305	15.143046	37.11848202	1250
1500-2000	1761	0.1295139	12.951386	50.06986835	1750
2000-2500	1509	0.1109804	11.098036	61.16790468	2250
2500-3000	812	0.0597191	5.9719056	67.13981025	2750
3000-3500	182	0.0133853	1.3385306	68.47834081	3250
3500-4000	535	0.0393469	3.9346915	72.41303229	3750
4000-4500	695	0.0511142	5.1114216	77.52445392	4250
4500-5000	705	0.0518497	5.1849673	82.7094212	4750
5000-5500	408	0.0300066	3.0006619	85.71008311	5250
5500-6000	255	0.0187541	1.8754137	87.5854968	5750
6000-6500	146	0.0107377	1.0737663	88.65926307	6250
6500-7000	206	0.0151504	1.5150401	90.17430316	6750
7000-7500	452	0.0332426	3.3242627	93.49856586	7250
7500-8000	304	0.0223579	2.2357873	95.73435317	7750
8000-8500	355	0.0261087	2.61087	98.34522321	8250
8500-9000	219	0.0161065	1.6106494	99.95587262	8750
9000-9500	6	0.0004413	0.0441274	100	9250
Total	***13597***	***1***	***100***		

MEAN = 2802.14

Standard Deviation = 2305.03

CV = 0.82

Minimum Volume = 104 vph

Maximum Volume =9226 vph

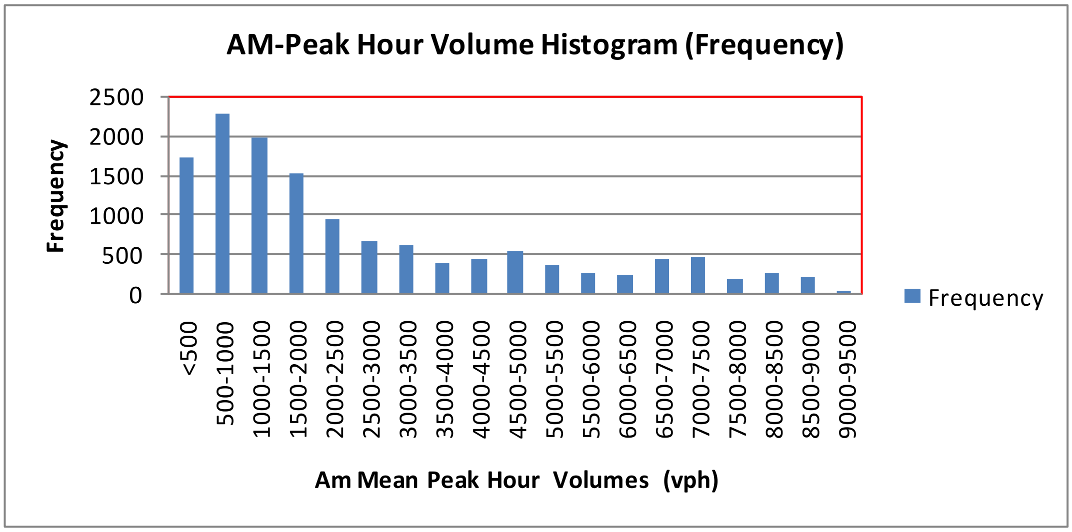

Figure 7: Frequency Diagram fot the AM Peak Volumes

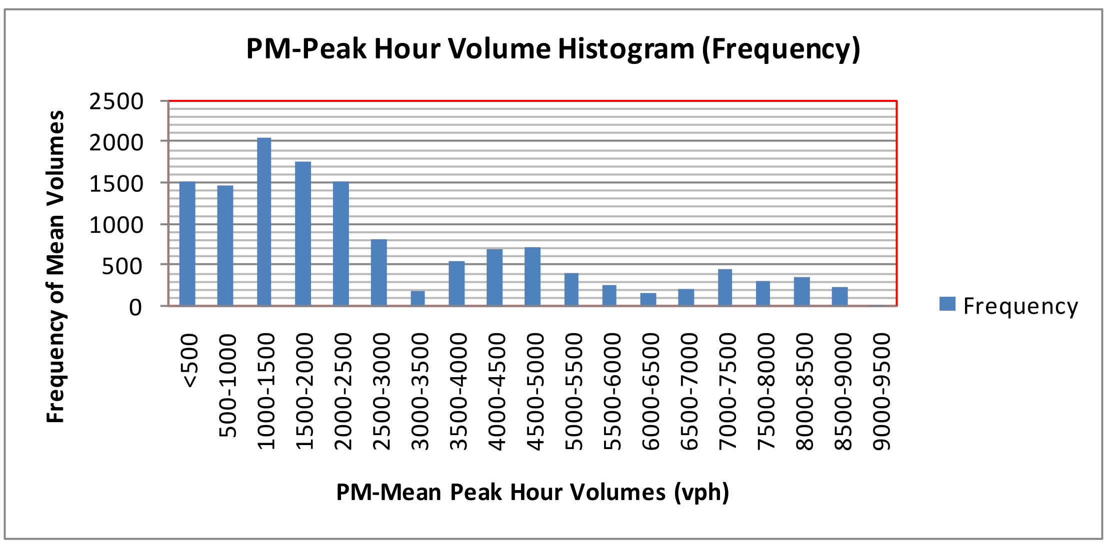

Figure 6.8: Frequency Diagram for the PM Peak Volumes

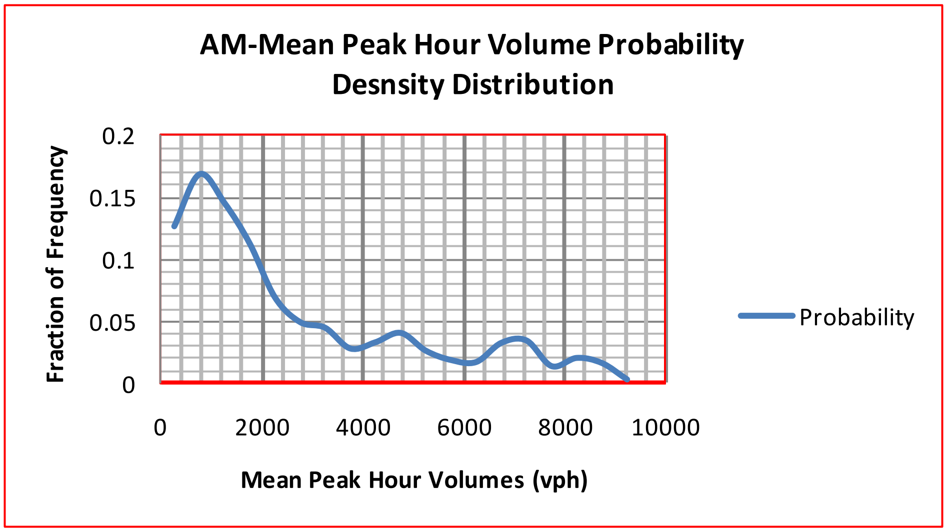

Figure 6. 9: Probability Distribution of the AM-Mean Peak Hour Volumes.

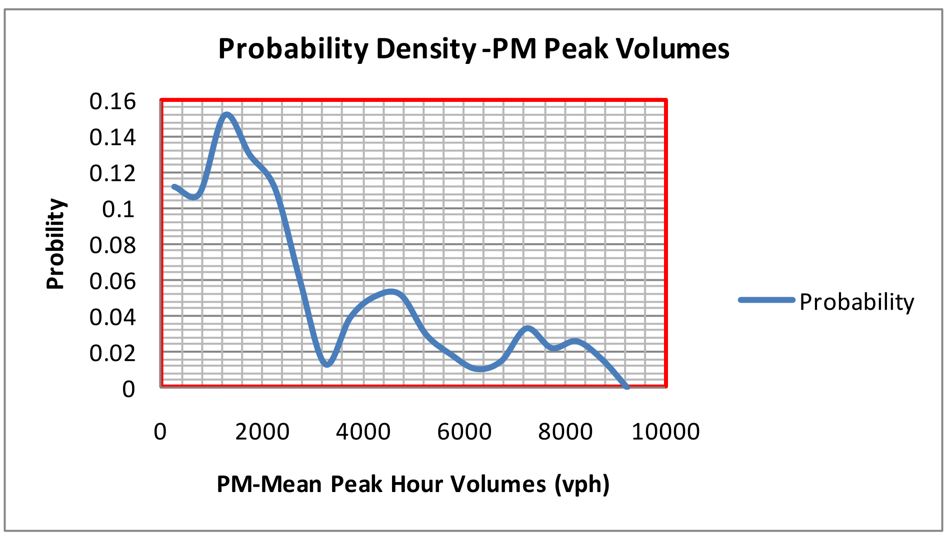

Figure 6. 10: Probability Distribution of the PM-Mean Peak Hour Volumes

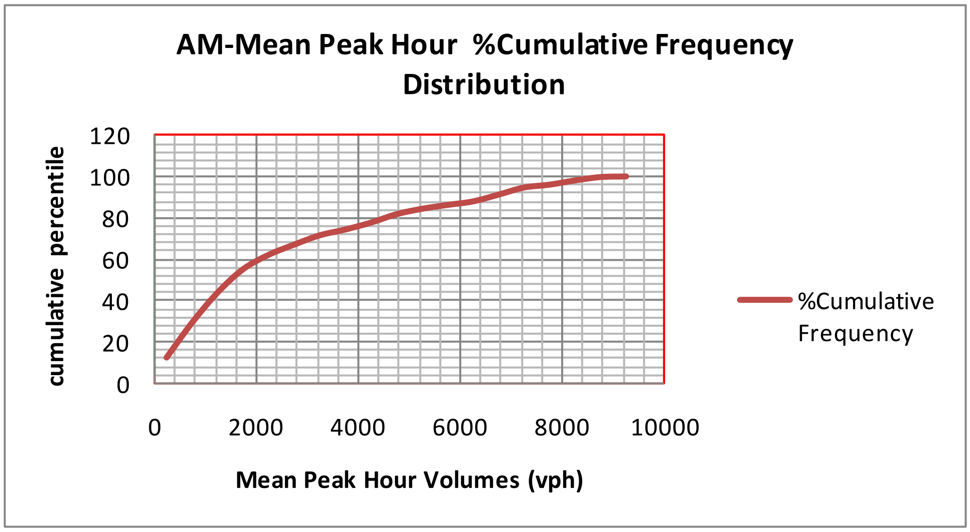

Figure 6. 11: Cumulative Frequency Distribution of the PM-Mean Peak Hour Volumes

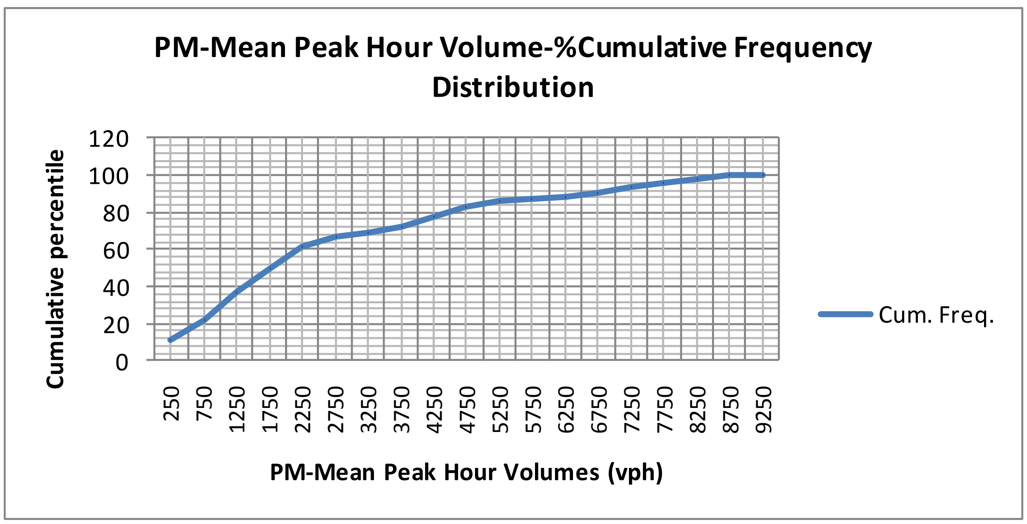

Figure 6.12: Cumulative (Density) Frequency Diagram fot the PM Peak Volumes.

As can be seen from figures 5 through 12, the distribution of the overall volumes cannot be easily determined. Due to the characteristics of the peak hour volume data, which exhibits compartments of normal distribution from low to high volumes categorization, the data was normalized by modeling the means of the count stations against the standard deviations for the prediction model that follows.

6.2.5 Regression Analysis for the Proposed Model

A prediction model was developed using Non-Linear regression analysis for the arrival flows with respect to the design hourly volumes for the AM and PM peak periods. Two models were developed for design hourly volumes. First, A nonlinear least squares (NLS) method with the mean arrival volumes (V_{mean}) as independent variable and the standard deviation of the design hourly volume (V_{std}) as the dependent variable; and the second model employed a linear regression analysis method with the mean arrival volumes (V_{mean}) as independent variable and the standard deviation of the design hourly volume (V_{std}) as the dependent variable. The first model was accomplished through the use of MATLAB6p5 analysis software. These Peak-Hour volumes data were read into MATLAB6p5 editor and a regression program coded into the editor to generate the reported parameters for the proposed NLS model. The second model was modeled by the use of Engineering and Statistical Tool Pack in the Microsoft Excel Spread Sheet (2007). Based on the available literatures, the modeling of *CV* as a function of the mean is much more difficult and return low coefficient of determination (R^2= 0.15) Hellinga and Abdy (2008) therefore, a new model for *CV* was also developed using the mean (V_{mean}) arrival volumes as independent variable and the standard deviation as the dependent variable. The prediction models using non-linear regression (NLS) analysis developed is a simple power function shown below.

$$V_{std} = \underset{(16.9)}{79.022}(V/1000)^{\overset{0.7914}{(22.1)}} \quad \text{for NLS method} \tag{8}$$

$R^2 = 0.731$ and adjusted $R^2 = 0.729$

The values in parenthesis are *t*-statistics; all parameters are significant at *95*% confidence interval.

The above equations are fitted into the data as depicted in figure (6.13).

Figure 6.13: Graph of V_{mean} Vs V_{std}

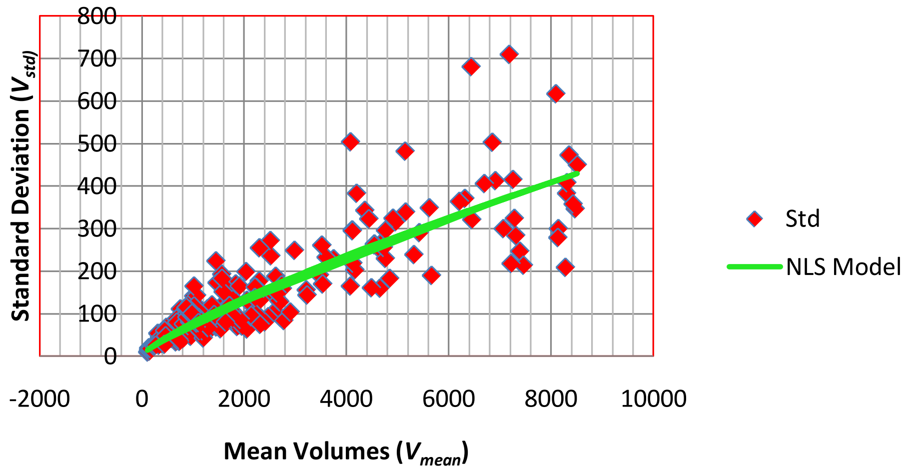

In Figure 6.13, the diamonds represent the scatter plot of the actual data while the curve represents the power function developed for the data from equation 8. The coefficient of determination (R^2) is *0.731* and adjusted R^2 is *0.729*, this shows that the model can explain *73%* of the variation in the data and that there is a good correlation between the mean and the standard deviation.

Similarly, a NLS regression function was developed for the CV and the functions are given as follows:

$$CV = 0.0553 + 0.0753(0.3505^{V/1000}),\ \text{(t = 19.4, 10.0, and 5.6) - NLS Estimator.} \tag{9}$$

$$R^2 = 0.359 \text{ and adjusted } R^2 = 0.351$$

The above equations are fitted into the data as depicted in figure (6.14).

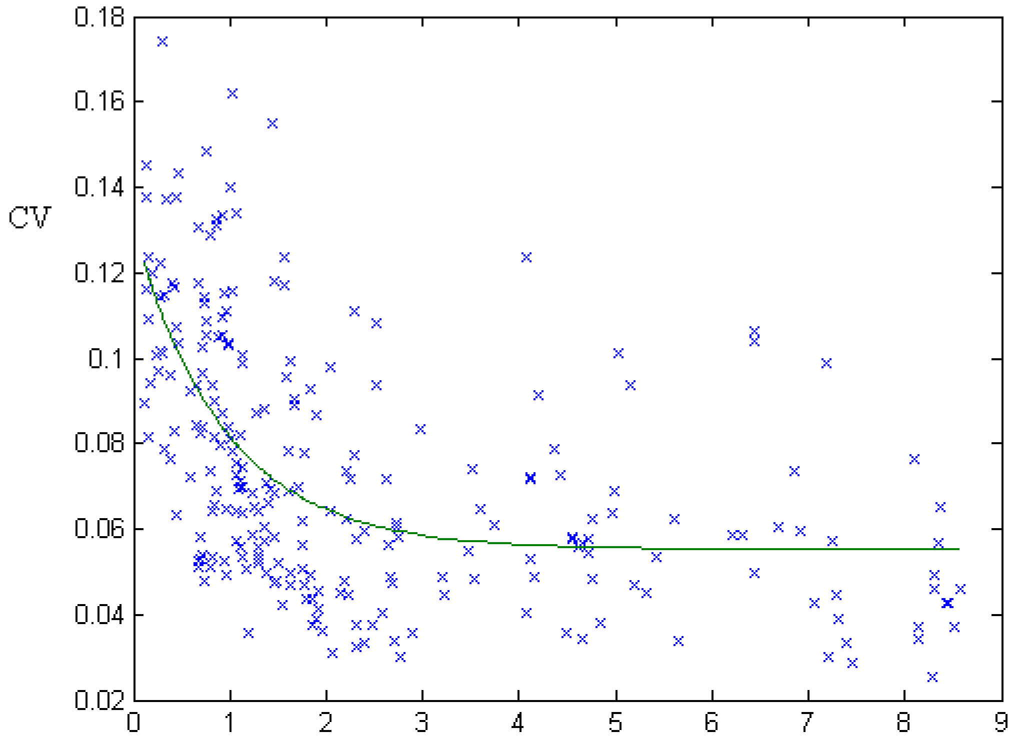

Figure 6.14: Coefficient of Variation as a Function of Mean Peak Hr Vol.

As stated earlier a second model relating the mean and the standadrd deviation using Linear Regression Analisis was also developed and the simple linear equation for the prediction of the mean volumes is as follows:

$V_{std} = 0.0482V_{mean} + 31.08$ 6.10

$R^2 = 0.7369$

It can be seen that the linear prediction model has a coefficient of determination ($R^2 = 0.7369$) very close to the NLS ($R^2 = 0.731, 0.729$ adjusted) model which is easier to use. It is slightly better than the NLS model with fewer parameters to which may increase the errors due to the model. The high R^2 value suggests a high correlation between the mean and the standard deviation. The model can be used to explain 74% of the variations in the Peak-Hour Volumes.

Figure 6.15 below is the scatter plot of the Peak-Hour Volumes fitted with the Linear Model.

Figure 6.15: Graph of V_{mean} Vs V_{std}

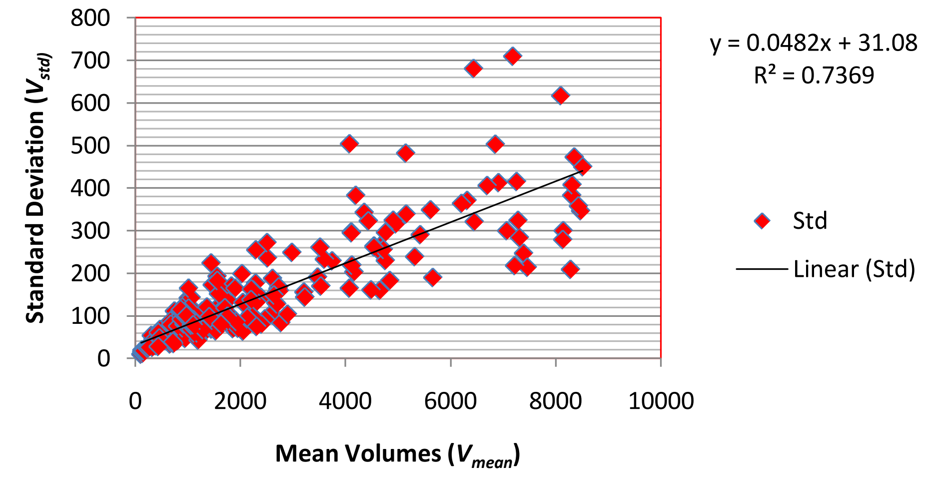

Table 6.7 below provides the model parameters and statistics for the above described linear model for further understanding.

Table 6.7: STATISTICS (LINEAR Model)	
Parameter	Values
Slope	0.0486
Standard Error (Se_n)	0.0019
R^{2*}	0.74
F- Statistic	690.21
SS_{reg}	2694992.14
Intercept	30.67
Standard Error (Se_b)	5.92
Standard Error (Se_y)	62.49
D_f	242.00
$SS_{resdual}$	944910.51
* R2 = SSreg/(SSreg+SSresidual)	
Model: $E[V_{std}/V = v_{mean} = 31 + 0.0482V_{mean}$	

6.2.5 Model Comparisons

The two models developed were compared with the means and the standard deviation of the actual data. The deviation for the means and standard deviation are 1.2% and 11.7%, for the NLS respectively. And, the deviation recorded for the mean and standard deviations for the linear model were 0.05% and 14.11%, respectively. Based on the closeness of the two models, to the actual data, there appear to be no discernible advantage using either of the models. The parameters of comparisons are summarized in table (6.8) below. Also, a graphical presentation showing the similarity in the two models is given in figure (6.16) below.

Table 6.8: Model Comparison

Models of Standard Deviations as functions of the Means			
Parameter	**Actual Data**	**Non-Linear (NLS)**	**Linear Model**
V_{std} (Mean)	145.96	147.74	146.03
Std Dev.	122.07	107.82	104.85
R^2		0.73	0.74
t (calculated)		0.0012	0.003
$t_{0.025,\ 246}<t<t_{0.975,246}$		+/- 1.96	+/-1.96
Deviation from actual Mean		1.20%	0.05%
Deviation from actual Std Dev		11.70%	14.10%

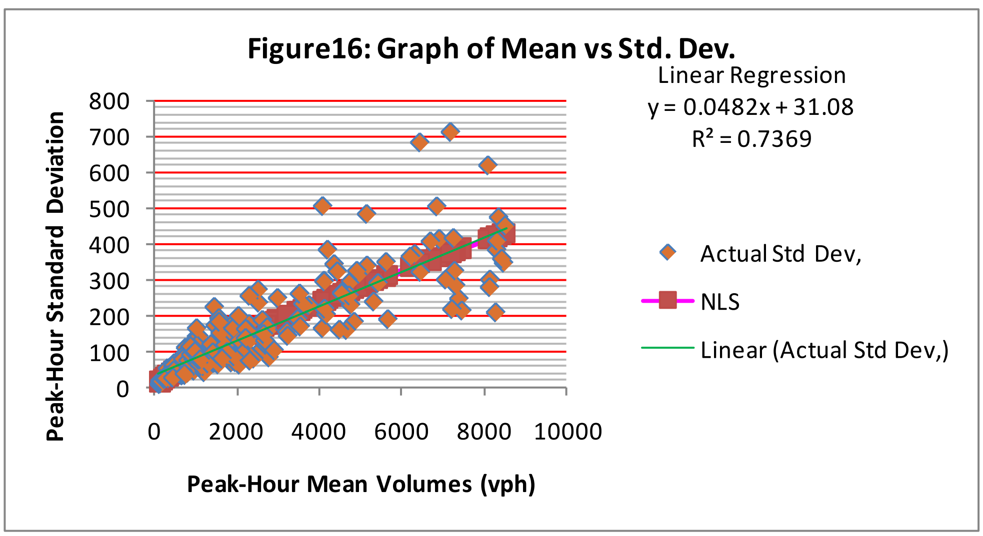

6.2.6 Summary of Results

From table (6.9) and the proposed models for V_{std} and CV, the following can be deduced:

-The standard deviation of the peak hour volumes increases with the mean volumes.

-The variability of the standard deviation increases as well with the mean volumes.

-Modeling *CV* as a function of mean volumes as being done in the literature is more difficult and returns very low R^2 (0.15from previous study and 0.35 from this study) hence, the result is inconclusive.

-There is no uniform pattern or trend of the *CV* decreasing with high volumes and increasing with low volumes as stated in the previous research by Sullivan, et al (2006).

-Modeling *CV* as a function of the arrival flow rates produces a better correlation coefficient ($R^2 = 0.35$, adjusted $R^2 = 0.351$) with significant t-statistics for all parameters.

-The variation of arrival flows has a high correlation coefficient with respect to the design hourly volumes as shown in the model prediction for V_{std} derived from this study with significant *t*-statistics for all parameters.

-Traffic arrival at roadway intersection approaches do not always follows a Poisson distribution where the mean is equal to the variance.

-Traffic data for the peak volumes presented above can be modeled as a linear function with high accuracy ($R^2 = 0.74$).

- It is better to analyze traffic volumes distribution to determine the degree of variability in the data set rather than assume a specific function for analysis. This approach will minimize errors in the analysis and minimize risk of failures which can be very costly.

The practical application of this exercise will be demonstrated in the section that follows.

6.3: Derivation of the Mean and Variance of the Design Hourly Volume (V_d)

In the previous section we developed a model for predicting the PHF as a function of the degree of saturation (X). This model will be used in this section to derive the mean and variance of the design hourly volume with respect to the arrival flow rates within the peak period.

In section 6.3.5, the PHF predictor denoted by $\hat{p}$ is given as:

$$\begin{aligned}\hat{p} &= 0.25 + a_1 X^{b_1}, \text{for arterials} \\ &= 0.25 + a_2 X^{b_2}, \text{for collectors/local streets}\end{aligned} \qquad 6.4$$

It is to be noted that X is given as the ratio of the arrival flow rate (volume) divided by the capacity of the given lane in the direction and movement under the analysis. Thus, we can write: $X = v_i/c_i$. 6.5

and

$v_i = c_i X$ 6.6

where:

c_i = the capacity of lane i in vehicles per hour and

v_i = arrival flow rate for lane i. in vehicles per hour

The design hourly volume (V_d) is given as the ratio of the flow rate in lane i divided by PHF in lane i. Hence, the V_d can be written as:

$V_d = v_i/p_i = c_i X/p_i$ 6.7

where: p_i is the PHF and has no unit and is a function of the arrival flow rate (v_i).

Using Taylor's linear series expansion, the expected value of V_d E(V_d), the variance of V_d var(V_d) with respect to the flow rate (v_i) and the peak hour factor (p_i) can be derived as follows:

$$V_d \approx \frac{v_i}{p_i} \qquad 6.8$$

$$Vd \approx \frac{\overline{V}}{\overline{p}} + V'(v - \overline{v}) + \frac{V''(v - \overline{v})^2}{2} \qquad 6.9$$

The partial derivatives of V_d with respect to v_i and p_i, are given as:

$$V' \approx \frac{p - p'v}{p^2} = \frac{1}{p} - \frac{vp'}{p^2} \qquad 6.10$$

$$V'' \approx -p'/p^2 - ((vp')'p^2 - 2pp'vp')/p^4 = p'/p^2 - (1/p^2)(p' + vp'') + (2v/p^3)(\mathrm{p}')^2$$

(6.11)

By applying the expectation operator to equation (8) and simplifying, the expected value of V_d can be approximated as:

$$E(Vd) \approx \frac{\overline{v}}{\overline{p}} + \frac{V''\,\mathrm{var}(v)}{2} \qquad 6.12$$

and the variance of V_d is given as:

$$\mathrm{var}(Vd) \approx (V')^2\ \mathrm{var}(v) \qquad 6.13$$

From equation (*4*) and replacing X with v_i/c_i from equation*5*, the first derivative of p(p') is given as:

$$p' \approx (ab(v/c)^{b-1})/c \qquad 6.14$$

And the second derivative of p (p'') is given as:

$$p'' \approx ((b-1)(ab)(v/c)^{b-2})/c^2 \qquad 6.15$$

Substituting the values of equations (*14*) and (*15*) into equations (*10*) and (*11*), equations (*14*) and (*15*) can be solved for the expected value and variance of V_d. However, these equations were written into MATLAB6p5 to obtain the means and variances of V_d. The expected value and variance of the design hourly volumes allow for the determination of the degree of variability of the design hourly volume within the design peak period. It was shown in section 6.2.4 that Poisson assumption that the means is always equal to the variance is not to be generalized in all traffic conditions. The effect of this variation is explored in the next section.

6.4: Effect of Variation of the Design Hourly Volumes on Intersection Signal Delay Performance

From these two models for Peak Hour Factor (PHF) and Standard Deviation of the mean peak hourly volume (V_{std},), the delay analysis was performed using the minimization subroutine called "Fmincon" in the MATLab6p5. FMINCON minimization subroutine in the MATLAB, finds a constrained minimum of a function of several variables and attempts to solve problems of the form:

```
min F(X)  subject to:  A*X  <= B, Aeq*X  = Beq (linear constraints)
 X                    C(X) <= 0, Ceq(X) = 0   (nonlinear constraints)
                       LB <= X <= UB        (Lower and Upper bounds).
```

In this case, the objective function is:

```
function f=Criteria_fn(p,Strategy,v,s,l,N,YAR,Leg,T,k,Scenario,power)
```

where;

Strategy = 'Minimize Average Delay'; all other parameters are defined in the program's structure.

To do this, the Design Hourly Volumes (V_d,) were generated randomly using the simulations NORMRND ($V_{mean,}$ V_{std});

Where: NORMND is the normal random numbers,

V (mean) is the single day mean count for a specific intersection count station and

V_{std} is the standard deviation of the mean count developed in section 6.5

The generated volume was divided by the PHF developed in section 6.1.5 to obtain V_d. A simple 8-movement, 4-phase signal phasing with a Bench Mark volumes designated as bm was used in the analysis. A minimization program was written into the MATLAB6p5 to minimize delay using both the deterministic control (Bench Mark volumes) and the stochastic control (randomly generated volume based on the V_{std} and PHF models) to compute intersection signal delays based on the equalized critical lane ratios strategy (HCM2000). In this strategy, the green time is allocated proportionately to each phase based on the flow ratio of the critical lane group for that phase. In order to simulate a real life condition, 365 runs of the simulations were performed and the average delays for the deterministic control and the stochastic delay compared along with other parameters of interests.

6.4.1 Results:

The analyses show that the coefficient of variation (table 6.9) for the design hourly volume is higher (17%) for low degree of saturation (X) and low mean critical lane ratio (Xc) and decreases to about 10% at full saturation and slightly lower (8.5%) as the degree of saturation exceeds 100% as depicted in figure 6.17. This is to be expected as the traffic level reaches capacity; the variation in the design hourly volume approaches a steady state condition. The ratio of the variance to mean ranged from 1.05 to 4.4 times that of the mean. The average deviation between the stochastic delay and the deterministic control was 4.4 seconds at Xc = 0.91 and reaches a maximum value of 6.2 seconds when the Xc reaches 1.16. The deterministic control delay remained consistently higher than the stochastic delay-figure 6.18. The effect of the critical movement ratios on the delay were examined; the increase in the critical lane movement ratio Xc caused an exponential increase in the delay for both deterministic and stochastic delays the increase ranged from 24.10 seconds for Xc = 0.19 to 109.1 seconds for stochastic delays, 115.3 seconds for deterministic control for Xc = 1.15 (see figure 6.19).

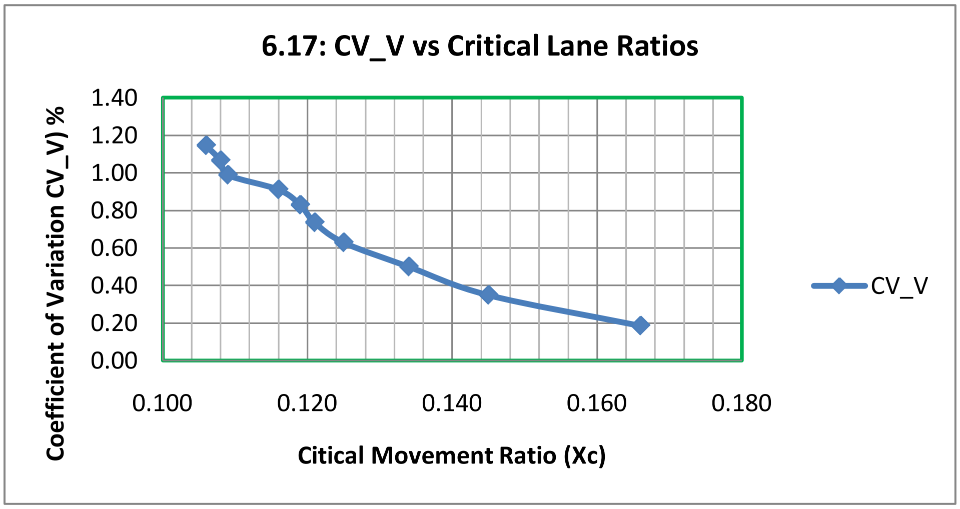

Table 6.9: EFFECT OF VARIATION OF PEAK HOUR VOLUMES ON INTERSECTION SIGNAL DELAYS

C-MAX = 240 COEFFICIENT OF VARIATIONS					STOCHASTIC DELAY (AD)	DETERMI-NISTIC CONTROL (Ad_bm)	Mean Cylcle Length	Mean Critical Lane Ratio-Xc	Design Hourly Volume var/mean
CV_V	CV_AD	CV_Adbm	CV_Cycle	CV_Split					
0.166	0.006	0.001	0.002	0.004	24.40	24.40	64.00	0.19	1.05
0.145	0.014	0.002	0.013	0.021	26.30	26.40	64.90	0.35	1.62
0.134	0.024	0.005	0.019	0.038	28.80	29.10	66.90	0.50	2.12
0.125	0.038	0.007	0.030	0.070	32.40	33.10	71.00	0.63	2.41
0.121	0.054	0.021	0.046	0.094	37.40	38.90	78.80	0.74	2.84
0.119	0.077	0.016	0.059	0.105	44.20	46.50	88.80	0.83	3.29
0.116	0.109	0.025	0.078	0.125	53.40	57.80	100.50	0.91	3.68
0.109	0.129	0.027	0.085	0.130	67.90	73.60	118.00	0.99	3.74
0.108	0.138	0.020	0.073	0.118	86.67	92.70	136.40	1.07	4.14
0.106	0.137	0.022	0.062	0.107	109.10	115.30	152.60	1.15	4.40

Figure 6.18: Deviation Between Stochastiic Delay and Deterministic Control

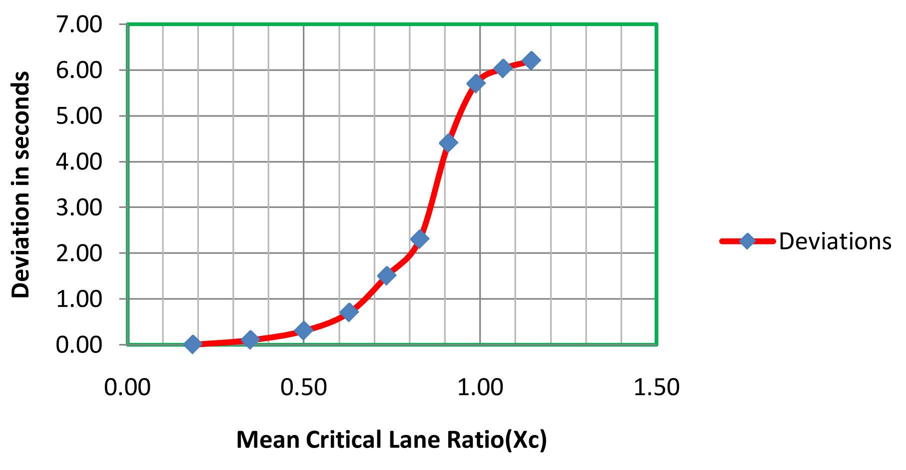

Figure 6.19: Effect of Critical Movement Ratios on Delay

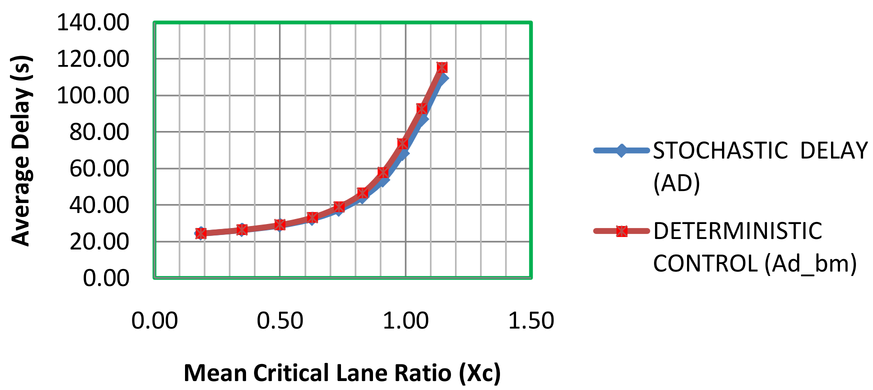

6.4.2 Cost Implication and Environmental Impacts:

To answer the question of the effect of the variability of the design hourly volume on the intersection signal delay, the 6.2 seconds difference in delay per vehicle needs to be examined for it impact as relating to cost and environmental effect. Many researchers have proposed several cost implications of intersection as well as travel time delays.

Estimation of fuel consumption and automotive exhaust pollutant emissions has been studied and a model developed by many; one such example is aaSIDRA and aaMOTION developed by Acelik and Associates (Acelik 2007). However, a simple cost of delay used in TRNSYT software gives the fuel consumption equation as follows:

$F = 0.1*L + 1.5D + 0.008S$ 6.16

Where:

F = amount of fuel consumed in Liters,

L = the total Distance Traveled in meters or feet,

D = Delays in seconds, and

S = numbers of stops made during the trip.

Example 6.1: For a given congestion level such Xc = 1.07, the computed change in total stops is given as 32 vehicles and the change in delays is given as 6.03 seconds. The fuel consumption due to designing the intersection with respect to the variations of the peak our volumes rather than fixed single mean value (the difference in fuel consumption) can be computed as:

F = 0.0*0+1.5*6.03+0.008*32 = 9.301 Liters = 2.46 gallons (see table 6.10), per peak hour. If we assume 4 hours per day for AM and PM peak period and 250 work days per year, the annual fuel cost per intersection for annual fuel price per gallon of $2.80 (AAA average fuel price for 2009) can be estimated as:

2.46 gallons*4hrs/day*250days*$2.80/gallon = $6,888.00 per intersection. According to the Miami-Dade County ATMS for 2008, there are more than 2690 signals locations in Miami-Dade County alone and this number represents 1% of all signals in the United States of America. The annual cost savings in adopting this model for Miami-Dade and the USA is estimated at $18,528,720.00 ($18.5 millions) and $1,852,872,000.00 (1.9 billions) respectively for fuel consumption only.

The cost of delay to users with respect to time lost can be computed using recent a study of the Chicago Metropolitan Planning Department. Based on this study, the cost per hour due to intersection delay is estimated at $14.75 per hour of delay of automotive users. Thus for the scenario used in this study, the cost per hour for eight different movements (sum of all volumes = 3790 vehicles) with average vehicle occupancy of 1.2 persons per car, can be estimated as 14.75*1.2*(3790)*6.03/3600 = $112.36 per hour per intersection. If we assume a 4-hr peak period per day for 250-workday, we can estimate the annual delay-time-cost as:

$112.36*4*250 = $112,364.03 per intersection. Again, this is projected to cost $302,259,227.25 (302.3 millions) and $30,225,922,725.00 ($30.2 billion) annually for Miami-Dade County and the USA respectively.

Environmental impact of the saving in delay was also analyzed with respect to automotive exhaust emission of known pollutants: Hydrocarbon (HC), Carbon monoxide (CO) and Nitric oxides (NOx) (see table 6.11).

Table 6.10: EFFECT OF VARIATION OF PEAK HOUR VOLUMES ON FUEL CONSUMPTION

STCHSTC DELAY (AD)	DTRMNSTC CONTROL (Ad_bm)	Mean Cylcle Length	Mean Critical Lane Ratio-Xc	ABS Delay Deviation	Average Stchstc Stops	Average Control Stops	Abs Stop Deviation	Change in Fuel Consmptn (Liters)
24.40	24.40	64.00	0.19	0.00	422.20	422.20	0.00	0.00
26.30	26.40	64.90	0.35	0.10	815.50	814.50	1.00	0.16
28.80	29.10	66.90	0.50	0.30	1211.10	1208.70	2.40	0.47
32.40	33.10	71.00	0.63	0.70	1594.00	1588.20	5.80	1.10
37.40	38.90	78.80	0.74	1.50	1972.90	1965.90	7.00	2.31
44.20	46.50	88.80	0.83	2.30	2360.70	2347.10	13.60	3.56
53.40	57.80	100.50	0.91	4.40	2744.90	2723.80	21.10	6.77
67.90	73.60	118.00	0.99	5.70	3143.20	3110.50	32.70	8.81
86.67	92.70	136.40	1.07	6.03	3532.80	3501.20	31.60	9.30
109.10	115.30	152.60	1.15	6.20	3902.30	3879.90	22.40	9.48

6.11: EFFECT OF VARIATION OF PEAK HOUR VOLUMES ON POLLUTANTS EMISSIONS

Type of Pollutant q_R	Rate of Emission* grams/HR	Change In Delay	POLLUTANTS EMISSIONS (E_R) Change In Stops	Total idle Time (HRS)	Emission Per HR	One Intsctn Annual Emssn-grm	Miami-Dade** Total Annual Emission(grm)
HC	0.004	6.030	32.000	0.054	0.00020	0.20	546.46
CO	0.037	6.030	32.000	0.054	0.00197	1.97	5304.53
Nox	0.002	6.030	32.000	0.054	0.00008	0.08	216.42

*Based on NCHRP535, 2005 CHEM Model
**Based on over 2690 signalized intersections in Miami-Dade

The methodology adopted for the analyses were that provided by the NCHRP535: Predicting Air Quality Effects of Traffic Flow Improvements: Final Report User Guide, TRB 2005. The model adopted was the CHEM model where the emission rates for automotives are provided. The emission equation is given as:

$$E_R = \Sigma_{(i,j)}(q_R(i,j)*V(i,j)) \qquad 6.17$$

Where:

E_R = emissions for pollutant R in grams,

$q_R(i,j)$ = CHEM emission rate for pollutant R in terms of grams per hour for movement at speed i and acceleration j. and, V(i,j) = vehicle hour travel at speed i and acceleration j.

In our scenario, the acceleration and speed = 0.00, the rate for HC, CO and NOx are as provided on table 6.11, column two. The total idle time is computed by multiplying the change in stops by the delay per stopped vehicle in the hour divided by 3600seconds per hour as in column five. Column six is computed by multiplying column two by column five; that is the rate of emission per hour times the delay time in hours. If we assume a 4-hr peak period per day for 250-workday, we can estimate the annual delay-emissions saving as:

HC: 0.0040*250*4 = 0.2 grams per intersection per year,

CO: 0.37*250*4 = 1.97 grams per intersection per year,

NOx: 0.0002*4*250 = 0.08 grams per intersection per year, and based on the over 2690 signal locations in Miami-Dade County, the total emission per pollutant is as shown in the last column of table 6.11. This may add up to billions of grams of reductions in the automotive exhaust emissions in the USA.

6.4.3 Summary and Conclusion:

This research has examined an extensive traffic data, established two new input models for signal timing design and analyzed the effect of the variation of design hourly volume to intersection delay performance. It has been shown that traffic flow do not always follow Poisson distribution and thus traffic signal analysis should take cognizant of the variations inherent in the arrival of the traffic flow within the peak period. To account for this variation a new model for the standard deviation (V_{std}) as a function of the mean volume was developed to predict the design hourly volume. It has also been demonstrated that Peak Hour Factor based on a single or few days count may not be a good representative value for design and a new model was developed to properly predict PHF for design in both arterials and local roads. Lastly, the combination of these predictors equations were employed to compute intersection delays. The mean delay generated through 365 simulations show that a significant difference exists between using average design values for intersection delay analysis in comparison with adaptive process where the signal adjust to the prevailing traffic condition. This difference is largely magnified when the cost due fuel consumption, cost due to time lost which adds up to billions of dollars if a nation-wide implementation were to be adopted. The environmental impact of the proposed model also showed significant reductions in automotive exhaust pollutants' emission due to time saving in delay reduction. The cost implication of not using adaptive signal system can go into billions of dollars annually. The conclusion here is that adaptive signal system should be the industry standard and the effect of variation of the design hourly volumes within the peak period needs to be adjusted for in signal timing design.

Chapter 7: Conclusions

In Chapter 4, application of reliability analysis to superelevation design was presented; it was demonstrated that reliability approach is straightforward to apply and produces superelevation rates that are reasonably comparable to Method 5 and NCHRP 439 distribution method. As stated earlier, the use of Method 5 represents a mathematical convenience without much consideration to the speed variation, as well as the inherent lengthy process required to obtain the superelevation *e* distribution. The NCHRP 439 approach in attempt to eliminate the inconsistency in using significantly different superelevation rate at the same design speed on curves of similar radius due to the use of multiple maximum superelevation rates on nearby facilities is commendable. In addition, simplification of computational procedure enables users to manually calculate superelevation rates without relying on look-up Tables and Figures. However, the proposed speed reduction for the equation does not represent a significant difference with the current 85^{th} percentile speed used in practice.

Compared to NCHRP 439 method, the reliability analysis proposed here results in an even simpler and more straightforward distribution method for calculating required superelevation at a specific level of confidence. It can be easily applied as an alternative means to evaluate existing curves as well as used in the design of new curves. It is believed that the use of method 1 to account for the distribution of side friction factor is logical but the inherent assumption of uniform speed might place drivers at risk when cornering on curves. The use of reliability approach accounts for the variation in speed and thus eliminates the expectation of constant speed that is the major drawback for method 1. The resulted reliability-based superelevation rates are fairly comparable to NCHRP 439 in general, but are more conservative at sharper curves given the same design speed. In addition, users must be cautioned that the required minimum turning radius from reliability constraints is also more conservative than the $R_{\min}$ defined in NCHRP 439 and Method 5. As curve radius increases, these differences diminish and the reliability-based superelevation becomes less than NCHRP 439, which is typically 1% less than NCHRP 439 at much flatter curves for a given design speeds. This implies that the results provided by the proposed method, if adopted for design, should produce cost savings to state agency when excess embankment required for elongated curves is eliminated.

In comparison with Method 5, almost all the reliability-based superelevations at 95% level of confidence are much (1%-2%) less at any design speed and curve radius. These differences are more pronounced at lower design speeds (60 mph and below). Similar comparisons were also found in between NCHRP 439 and Method 5, indicating that the superelevation rates as recommended by AASHTO are overly conservative. A new concept in highway design is highlighted through the incorporation of factor of safety or reliability index in the design. Finally, it is also demonstrated here that ignoring speed variation will lead to a significant underestimation of the required superelevation rates, which will in turn place greater portion of drivers in risk when cornering curves.

In Chapter 5, we developed a methodology for evaluating safety performance of Intersection Left Turn bay using reliability analysis. The advantage of this design procedure is that it takes into account the left turn volume expected and the opposing flow expected without the actual traffic count. This can allow planning office to set budget and plan for adequate turn lane length prior to actual engineering design. The above procedure was used in producing the results shown in tables 5.3-6 as well as figure 5.3-6. The design process is simple and can be readily used without any need for sophisticated software such as SYNCHRO, FTSUM, TSIM, NETSIM, or higher knowledge of mathematics. A technician with intermediate computation skill can produce results that are reliable for design. The safety of the existing intersection left turn lane can be readily evaluated using this model for use in expert witnessing. This approach also ensures that the designer is aware of the reliability or the likelihood of failure of the design prior to construction; such knowledge makes the design defensible in a litigious system such as the USA. The departure of the deceleration rate form AASHTO criteria can be readily seen numerically by performing the computations shown in example 2. Wu's method provided in the HCM is recommended for the computation of the queue length for the Analysis. Wu's approach is more stable and allows a wider use both for, single and multiple lanes. The simulation results from SYNCHRO validated the research as the queue exceeds AASHTO current design criteria. The current AASHTO's design criterion is based on average value of the expected queue length at the un-signalized intersection and not reliable when the degree of saturation exceeds $50^{\%}$ of capacity. This model provides a new tool for evaluating, the performance of an un-signalized intersection for safety, the design of the turn lane based on the demand and the reliability of the turn lane to service the expected turning movements. It provides additional tool that can be employed along with standard practice of determining and LOS as the design input for the un-signalized intersection. This scope of this model has been limited to un-signalized intersection; there are sufficient and simple procedures for determining length of queue and delays at signalized intersection in current use. However, the actual reliability of a signalized intersection can be evaluated by the extension of this method. Such evaluation will require empirical data. The data will include the actual measurements of the arrival and discharge rates as well as the queue length of the vehicles waiting in the turn bay per each Cycle; the red phase being the service time in the turn bay. This is a subject for further research.

In Chapter 6, we examined the effect of variation of peak hour volume on intersection signal delay performance. This research has examined an extensive traffic data, established two new input models for signal timing design and analyzed the effect of the variation of design hourly volume to intersection delay performance. It has been shown that traffic flow do not always follow Poisson distribution and thus traffic signal analysis should take cognizant of the variations inherent in the arrival of the traffic flow within the peak period. To account for this variation a new model for the standard deviation (V_{std}) as a function of the mean volume was developed to predict the design hourly volume. It has also been demonstrated that Peak Hour Factor based on a single or few days count may not be a good representative value for design and a new model was developed to properly predict PHF for design in both arterials and local roads. Lastly, the combination of these predictors equations were employed to compute intersection delays. The mean delay generated through 365 simulations show that a significant difference exists between using average design values for intersection delay analysis in comparison with adaptive process where the signal adjust to the prevailing traffic condition. This difference is largely magnified when the cost due fuel consumption, cost due to time lost which adds up to billions of dollars if a nation-wide implementation were to be adopted. The environmental impact of the proposed model also showed significant reductions in automotive exhaust pollutants' emission due to time saving in delay reduction. The cost implication of not using adaptive signal system can go into billions of dollars annually. The conclusion here is that adaptive signal system should be the industry standard and the effect of variation of the design hourly volumes within the peak period needs to be adjusted for in signal timing design.

7.2: Future Work

Intersection signal timing requires the allocation of minimum and maximum green time to each signal phase. This study has shown that traffic arrival is a stochastic process, a deterministic input for traffic signal design leads to unused green time in all phases. Unused green time on a phase due to low traffic volume on that phase is a high contributory cause of delay at signalized intersection. An intelligent signal system that can allocate green time to only the vehicle/s present at the intersection will eliminate the unused green time in any phase and minimize overall delay at signalized intersection. The tremendous benefits associated with this possibility require further investigation.

REFERENCES

AASHTO. *A Policy on Geometric Design of Highways and Streets*. American Association of State Highway and Transportation Officials, Washington D.C. 1984, 2001, 2004 and 2005.

AASHTO. AASHTO Guide for Design of Pavement Structures, 1993. American Association of State Highway and Transportation Officials, Washington D.C., 2001. pp I-53-I-56

Acelik, R. Traffic Signal Capacity and Timing Analysis. Research 123 Australian Road Research Board, Vermont South. 1981.

Acelik, R and Besly, M. Operating cost, fuel consumption, and Emission Models in aaSIDRA and aaMotion, 25th Conference of Australian Institute of Transport Research (CAITR 2003), University South Australia, Adelaide, Australia, 3-5 December 2003, 2nd Version: 23 December 03-Minor Correction 21 June 04. Note (4 December 2007): aaMotion has been renamed SIDRA TRIP, December 2007. pp1-15.

Aedeshir Faghri and Michael J. Demetsky – Reliability and Risk Assessment in the Prediction of Hazards at Rail-Highway Grade Crossings. Transportation Research Record 1160, TRB, National Research Council, Washington D.C., 1988. pp 45-51.

Allsop, R. E., Delay at a Fixed Time Traffic Signal: Theoretical Analysis. Transportation Science, Vol. 6, pp 260-285. 1972.

Al-Khafaji, A. W. and Tooley J. R., Numerical Methods in Engineering Practice, CBS College Publishing, 1986, pp 160-201.

Beckman, M. J., McGuire, C. B., and Winsten, C. B. Studies in the Economics in Transportation. New Haven, Yale University press, 1956.

Bonneson, J. A. Superelevation Distribution Methods and Transition Designs. NCHRP Report 439, 2000.

Brilon, W, Wu, Ning and Bonzio, L.-Unsignalized Intersection inGermany- Astate of the Art. Proceedings of the Third International Symposium on Intersections Without Traffic Signals, Portland, Oregon, U.S.A, July 1997. University of Idaho, Moscow, U.S.A., 1997.

Casella, G. and Berger, R. L. Statistical Inference, 2nd ed., 2002.

Chakroborty, P., Kikuchi, S. and Luszcz, M. – Lengths of Left-Turn Lanes at Unsignalized Intersections. In Transportation Research Record 1500, TRB, National Research Council, Washington D.C., 1995.

Cronje, W. B., Derivation of Equations for Queue Lengths, Stops and Delay for Fixed-Time Traffic Signals. Transportation Research Record 905, TRB, National Research Council, Washington D.C., 1983, PP. 93-95.

Darroch, J. N., On the Traffic-Light Queue. Ann. Math. Statistics, 35, pp. 380-388, 1964.

Dowling, R. G. Use of Default Parameters for Estimating Signalized Intersection Level of Service. Transportation Research Record 1457, TRB, National Research Council, Washington D.C, 1994. pp 82 – 95.

Easa, M. S., Reilability Approach to Intersection Sight Distance Design in Transportation Research Record 1701, TRB National Research Council, Washington D.C. 2000. PP. 42-52.

Easa, S. M., Distributing Superelevation to Maximize Highway Design Consistency: Journal of Transportation Engineering, Vol.129, No.2, March 1, 2003. ©ASCE. pp. 411-418.

FDOT, Site Impact Handbook, FDOT, April 1997.

Fisk, C. S. – Priority Intersection Capacity: A Generalization of Tanner's Formula. Transportation Research Part B, Volume 23B, No. 4, pp. 281 -286, 1989.

Fitzpatrick, K, P. Carlson, M. A. Brewer, M. D. Wooldridge, and S-P Miaou. Design Speed, Operating Speed, and Posted Speed Practices. NCHRP Report 504, 2003.

Fitzpatrick, K. and Mason, Jr., J. - Review of AASHTO Case III Procedure for Intersection Sight Distance. Transportation Research Record 1385, TRB, National Research Council, Washington D.C., 1990. pp 216-226.

Fitzpatrick, K., Mason, Jr., J. and Harwood, D. W. – Comparison of sight Distance Procedures for Turning Vehicles from a Stop-Controlled Approach. Transportation Research Record 1385, TRB, National Research Council, Washington D.C., 1993. pp 1-7.

Grimmett, G. and D. Stirzaker, Probability and Random Processes, 3rd ed. Oxford, 2001.

Haldar, A. and Mahadevan, S. Probability, Reliability and Statistical Methods in Engineering Design. John Wiley & Sons. Inc. 2000, pp 1-273.

Hellinga, B and Abdy, Z. Signalized Intersection Analysis and Design: Implications of Day-to-Day Variability in Peak-Hour Volumes on Delay, Journal of Transportation Engineering, Volume 134, Issue 7, 2008, pp. 307-318.

Hellinga, B., Abdy, Z. Impact of Day-to-Day Variability of Peak Hour Volumes on Signalized Intersection Performance. Transportation Research Board 86th annual meeting. 2008.

Highway Capacity Manual, Transportation Research Board, 2000, TRB, Washington D.C.

Krames, A. R. Design Speed and Operating Speed in Rural Highway Alignment Design. Transportation Research Record 1701, TRB National Research Council, Washington D.C. 2000. PP68-75.

Lan, C. J., Abia, S. D. and Chimba, D. Determining Peak Hour Factor for Capacity Analysis, ASCE Working Paper, December 2009.

MATLAB6p5, 2002.

McNeil, D. R. – A Solution to the Fixed-Cycle Traffic Light Problem for Compound Poisson Arrivals. 1968, pp 624-635.

Miller, A. J. (1968a) – Australian Road Capacity Guide – Provisional Introduction and Signalized Intersections. Australian Road Research Board Bulletin No. 4, (Supervised by ARRB report No. 123, 1981).

Milton, J. S. and Arnold, Jesse C., Probability and Statistic in the Engineering and Computing Sciences, McGraw-Hill, Inc. 1986, pp 97-100, 117, 336-435.

NCHRP 535: Predicting Air Quality Effects of Traffic Flow Movements: Final Report User Guide. TRB, Washinton Dc, 2005, pp 24-27.

Newel, G. F. Approximation Methods for Queues with Application to the Fixed Cycle Traffic Light. SIAM Review, Vol. 17, 1965.

Nicholson, A. Superelevation, Side Friction, Roadway Consistency: Journal of Transportation Engineering, Vol.124, No.5, September/October, 1998. ©ASCE. pp 411-418.

State Of The Art of Highway Geometric Design Consistency: Journal of Transportation Engineering, Vol.125, No.5, July/August, 1999. ©ASCE. pp 305-313.

Ottesen and Krames , Speed Profile Model for Design in the United States, Transportation Research Transportation Research Record 1701, TRB National Research Council, Washington, D.C. 2000, pp. 85.

Olson, P. L., Cleveland, D. E., Fancher, P. S., Kotyniuk, L. P. and L. W. Schneider, N.C.H.R.P. Report 270: Parameters affecting Stopping Sight Distance. TRB, National Research Council, Washington D.C., 1984.

Papoulis, A. Probability, Random Variables, and Stochastic Processes, 3rd ed. McGraw-Hill. (1991), pp. 113-114.

Little, J. D. C. A Proof of the Queuing Formula L = Lambda*W". Operation Research, 9, pp 383-387 (1961).

Troutbeck, R. J., and Brilon, W. Unsignalized Intersection Theory. In Capacity and Level of Service at Finish Unsignalized Intersections. 2004, pp 31.

Targo, A. P., Perez-Cartagena, R. I. Variability of Peak Hour Factor at Intersections, Transportation Research Record: Journal of the Transportation Research Board No. 1920. Washington D.C, 2005. pp. 125 – 130.

Sullivan, D., Levinson, H. S., Bryson, R. W. Effects of Urban Traffic Volumes on Services Levels. Paper # 06-2381 presented at the 85^{th} annual meeting of the Transportation Research Board, 2006.

http://www.FuelgaugeReport.com AAA Daily Fuel Report: Downloaded on June 1, 2010.
http://www.MD-ATMS.com, Downloaded on June 1, 2010.

Transportation Cost and Benefits Analysis II – Congestion Cost, Victoria Transport Institute, April 2010, PP5.5-17 (www.vtpi.org).

NYDOT. Recommendation for AASHTO Superelevation Design, Design Quality Assurance Bureau, 2000.

Wu, N. An Approximation for Distribution of Queue Lengths at Unsignalized Intersections. In Acelik R. (ed), Proceeding of the second International Symposium on Highway Capacity, Sydney, 1994, Volume 2, pp. 717-736.

Webster, F. V. and B. M. Cobbe, Traffic Signals, Road Research Technical Paper No. 39, Her Majesty Stationery Office, London, 1958.

APPENDIX A: PHF, DEGREE OF SATURATION AND PEAK PERIOD VOLUME DATA

Table A-1: Traffic Count Data-Peak Hour Volumes

Approach Volume	AM				PM			
	SB	NB	WB	EB	SB	NB	WB	EB
ITR/Pratt W(10/15/07)	312	99	325	100	102	421	178	65
ITR/Pratt W(10/18/07)	208	80	271	64	48	353	165	54
ITR/Marc D(3/21/07)	108	303	550	811	165	136	1089	534
ITR/Jupiter Farm(3/21/07)	99999	637	888	1293	99999	341	1780	801
ITR/Marsala(4/12/08)	26	46	780	1992	35	58	1742	913
ITR/Tpk(8/23/06)	818	44	1550	1760	823	33	2350	992
ITR/Tpk(9/15/08)	855	6	1553	1930	788	8	2343	966
ITR/Tpk(9/29/08)	907	7	1463	1826	810	4	2256	861
ITR/Tpk(2/5/09)	1012	1	1258	1972	930	5	2327	963
ITR/Island Way(8/15/06)	371	151	2082	2571	215	134	2630	2365
ITR/Island Way(10/15/07)	437	195	1901	2638	289	205	2312	2332
ITR/Island Way(10/22/07)	387	145	1871	2544	234	180	2394	2047
ITR/Island Way(2/5/09)	389	168	1878	2482	222	205	2469	2382
ITR/J West Plz(8/23/06)	160	177	2022	2257	224	118	2602	1873
ITR/J West Plz(9/15/08)	91	195	1996	2641	128	141	2346	1741
ITR/J West Plz(9/17/08)	91	121	1956	2402	204	76	2365	1951
ITR/Central(8/23/06)	845	1062	1470	2157	570	1464	2224	1835
ITR/Central(1/31;16/07)	888	832	1402	2468	790	1302	2444	2323
ITR/Central(2/2508)	846.1	986	1604	2589	824	1272	2705	2011
ITR/Central(4/1708)	760.0	966	1445	2568	702	1434	2402	2244
ITR/Central(5/8/\08)	714.56	1102	1490	2398	602	1302	2213	1870
ITR/Central(5/22/08)	800.632	828	1455	2398	667	1236	2242	1875
ITR/Central(2/4/09)	712.124	854	1362	2335	704	1228	2208	1998
ITR/Chasewood(8/23)	28	218	1503	2157	16	310	2264	1798
ITR/Chasewood(8/28;9/5/06)	47	186	1639	2400	59	332	2446	1712
ITR/Chasewood(5/5/08)	52	327	1467	2263	57	364	2242	1750
ITR/Chasewood(5/22/08)	55	137	1391	2348	51	296	2145	1753
ITR/Center(8/23/06)	699	246	1518	2155	602	293	2119	1805
ITR/Center(5/5/08)	834	237	1449	2536	620	289	2111	1844
ITR/Center(5/22/08)	843	69	1237	2450	657	248	2000	1861
ITR/Center(2/4/09)	755	73	988	2214	626	298	2375	1758
ITR/Maplewood(9/13/06)	61	509	1284	1841	157	726	1754	1510
ITR/Maplewood(3/27/07)	38	484	1376	2364	87	695	1890	1771
ITR/Maplewood(2/4/09)	5	416	880	2308	57	694	2041	1534
ITR/Delaware(9/7/06)	90	83	1298	1844	70	113	1774	1496
ITR/Delaware(9/15/08)	106	122	1165	1924	65	164	1703	1459
ITR/Delaware(9/17/08)	108	121	1065	1938	62	105	1283	1482
ITR/Pennock	435	291	1670	2152	288	252	2238	2004
ITR/Military	114	751	1107	1942	140	1072	1492	1564
ITR/Military(2/4/09)	68	679	975	1782	152	1084	2035	1522
ITR/Lox.	193	199	1051	1827	131	161	1479	1553
ITR/alt A1A	1326	987	882	1766	1123	1306	1371	1571
ITR/alt A1A(2/9/09)	1408	901	683	1367	1041	1278	1856	1477

Table A-1 Contd: Traffic Count Data-Peak Hour Volumes

	AM				PM			
Approach Volume	SB	NB	WB	EB	SB	NB	WB	EB
Donald Ross RD @I-95	716	840	1175	838	333	1311	1398	423
Donald Ross RD @Iheights BL	629	0	936	1672	214	0	1402	1310
Donald Ross RD @Parkside DR	282	0	791	1904	309	0	1283	1220
Donald Ross RD @ Central BL	509	1048	933	1869	701	849	1572	1107
Donald Ross RD @ Military Trail	1525	1013	1001	1608	1500	1038	1567	1108
Donald Ross RD @SR-818/Alt A1A	1263	1042	1000	1726	1060	1368	1511	1079
Donald Ross RD @Frenchman Creek Dr/Be	62	197	854	1334	75	190	1258	889
Donald Ross RD @ Ellison Wilson RD	0	240	1069	1459	0	527	1328	1047
Donald Ross RD @ US-1	1405	902	254	1033	1193	1536	266	1103
PGA BL @ Beeline HWY	489	554	194	0	642	382	232	0
PGA BL @ Ryder Cup BL/Jog RD	95	212	312	164	114	153	341	188
PGA BL @ AVE of the Champions	428	93	865	348	389	140	804	367
PGA BL @ Fl Turnpike	1552	468	1761	686	761	610	749	2225
PGA BL @ Balen Isles DR	45	111	1536	2082	62	116	1789	1463
PGA BL @Central BL	898	148	1355	2147	761	158	1968	1711
PGA BL @ Military Trail	1676	1871	1260	2003	1432	2034	2133	1878
PGA BL @ I-95 West Side	810	0	1215	2326	313	0	2076	1808
PGA BL @I-95 East Side	0	1480	2202	2202	0	1289	1546	1546
PGA BL @ Victoria Gardens Blvd	164	476	1583	2991	356	696	2172	2246
PGA BL @ FairChild Gardens Ave	651	470	1400	2210	958	614	1930	1986
PGA BL @ Gardens Mall Main Entrance	133	106	1185	1911	274	103	1886	1682
PGA BL @Prosperity Farms Rd	884	920	1345	1620	869	1181	1817	1405
PGA BL @ Ellison Wilson RD	386	214	947	1866	598	263	1088	1472
PGA BL @ US-1	1325	908	675	1215	1345	1213	744	1189
Grandiflora/Central	724	657	74	153	576	567	31	114
Grandiflora/Military	971	992	80	75	991	974	45	35
Jog/Hood	43	250	236	99999	48	124	143	99999
45th Street @ Haverhill Rd 11/10/06	617	1587	855	383	787	1176	1327	316
45th Street @ Military Trail 07/05/08	1357	1418	1068	1455	1466	968	1721	971
45th Street @ Village Bl 07/05/08	335	1170	1317	1907	609	711	2061	1273
45th Street @ North Point BL 13/11/08	409	178	2052	2258	466	387	2201	1644
45th Street @ I-95 27/08/08	1440	1176	1473	2202	976	933	2378	1932
45th Street @ Corporate Way 27/08/08	155	23	1513	2490	274	15	2285	1541
45th Street @ Congress Ave 16/05/08	1287	928	1834	2410	1476	1315	2353	1629
45th Street @ South Pl/Tiffany Dr 09/12/08	45	48	1511	2265	42	106	2234	1412
45th Street @ North Shore DR 02/09/08	126	330	1066	2057	169	281	1676	1394
45th Street @ Australian AV 05/11/07	842	1152	949	1815	1032	1417	1499	1303
45th Street @ Old Dixie HWY/GREENWOC	719	108	569	859	641	105	695	891
45th Street @ Pinewood AV 08/05/07	65	92	476	957	100	129	476	769
45th Street @ Broadway Road/US-1	1342	750	202	802	1099	1166	242	552
Belvedere RD @ SR-7	1594	1469	721	554	1582	1528	1491	320
Belvedere RD @ Walmart/Mayacoo Lakes I	68	177	645	1245	60	223	1245	671
Belvedere RD @ Sansbury Way	462	529	1160	1528	302	491	1880	847

Table A-1 Contd: Traffic Count Data-Peak Hour Volumes

	AM				PM			
Approach Volume	SB	NB	WB	EB	SB	NB	WB	EB
Belvedere RD @ Benoist Farms RD	187	184	1235	1791	222	266	1805	1126
Belvedere RD @ Skees RD	309	0	1150	1730	256	0	1764	1085
Belvedere RD @ Jog RD	977	1712	874	1782	1409	1440	1840	1304
Belvedere RD @ Drexel RD/Flat Rock DR	345	86	825	1475	393	55	1629	1090
Belvedere RD @ Caroline AV 24-Apr-07	0	269	869	2110	0	168	1840	1268
Belvedere RD @ Haverhill RD 15-09-08	705	985	721	1534	970	873	1572	962
Belvedere RD @ 5th Street 18-04-07	129	0	928	1730	160	0	1748	1053
Belvedere RD @ Military TR 17-09-08	1047	1648	715	1437	1685	1413	1448	934
Belvedere RD @ Congress AVE 16-09-08	589	122	1075	1404	1031	139	1691	830
Belvedere RD @ Australian Ave 15-09-08	719	2512	996	1381	1884	1192	1307	1457
Belvedere RD @ Mercer Ave	193	0	1246	1687	476	0	1317	1449
Belvedere RD @ Parker AVE 25-09-07	358	565	783	1500	726	341	985	985
Belvedere RD @ Georgia AVE 25-09-07	78	269	522	1170	89	248	736	746
Belvedere RD @ Dixeie HWY	521	796	126	1029	974	564	201	621
Forest Hill/South Shore/12th Fairway 10/14/(	129	1059	1436	1224	80	883	2413	1219
Forest Hill/@Polo Club Rd/Royal Fern 10/14	523	120	1345	2125	386	153	2212	1656
Forest Hill/Fairlane Farm Rd 09/23/07	0	210	1536	2943	0	475	2641	1889
Forest Hill/@Wellington Edge/Wellington Gr	286	309	1304	2087	142	486	2289	1574
Forest Hill/Wellington Green Commons(Mai	0	257	1306	2142	0	423	2162	1731
Forest Hill/SR-7 10/14/08	1747	1395	1167	2080	2230	1852	1507	1719
Forest Hill/Olympia/Buena Vida 10/09/08	60	123	1211	1459	51	91	1805	1551
Forest Hill Rd @Ranch Rd/Lyons Rd 10/06/(	484	654	1295	1420	534	261	1599	1410
Forest Hill Bl @ Pinhurst Dr 19/05/08	60	430	1504	1686	87	406	1775	1529
Forest Hill Bl @ River Bridge BL/Olive Tree I	326	158	1512	1767	215	242	1921	1535
Forest Hill @ Jog Rd 14/10/08	1518	1877	1290	1729	2231	1892	1479	1549
Forest Hill @ Sherwood Forest Bl 14/10/08	47	251	1697	1562	32	212	1409	1559
Forest Hill @ Haverhill Rd 06/10/08	903	1217	1000	1934	1297	970	1640	1416
Forest Hill @ Military Trail 22/04/08	1180	1767	1246	1657	1772	1639	1637	1338
Forest Hill @ Kirk Rd Rd 14/10/08	461	1119	1224	1781	603	784	1789	1343
Forest Hill @ Davis Rd/Tuker Rd 14/10/08	254	106	1169	1977	206	210	1712	1339
Forest Hill Bl @ Congress Ave 14/10/08	1184	1430	1236	1850	1610	1438	1596	1505
Forest Hill Bl @ Florida Mango Rd 15/10/08	375	577	1158	1614	390	405	1804	1374
Forest Hill Bl @ Pine Tree LN 06/10/08	0	173	1485	1977	0	113	1787	1310
Forest Hill Bl @ I-95 15/10/08	779	639	1005	2047	924	856	1097	1287
Forest Hill Bl @ Parkewr Ave 07/10/08	410	366	926	1250	370	273	1040	1019
Forest Hill Bl @ Lake Ave 07/10/08	84	24	745	957	72	34	899	818
Forest Hill Bl @ Gerogia Ave 06/10/08	138	164	687	1047	179	171	772	786
Forest Hill @ Dixie HWY 06/10/08	653	961	230	834	926	834	265	672
Lantana RD @ SR-7 10-Sep-08	2079	709	775	294	1266	1598	759	229
Lantana RD @ Target 10 Sep 08	58	0	775	596	96	0	759	920
Lantana RD @ Bellagio Lakes BL 10 Sep 08	7	107	767	596	5	123	780	920
Lantana RD @ Lyons RD 10 Sep 07	366	420	1118	693	442	498	1154	906
Lantana RD @ Aquarius BL/Grand Lacuna 1	166	159	1019	943	105	78	1299	1272
Lantana RD @ Bantbrook BL 01-May-07	311	0	1160	1179	168	0	1514	1143

Table A-1 Contd: Traffic Count Data-Peak Hour Volumes

West Atlantic AV @ Military Trail 15/04/08	2007	1447	1358	1491	1594	2004	1502	1548
West Atlantic AV @ Whatley Rd 15/09/08	211	112	119	1234	272	56	1304	1145
West Atlantic AV @ Barwick Rd 04/09/07	526	50	1233	1400	441	40	1597	1383
West Atlantic AV @ Hamlet DR 13/09/06	65	92	1309	1398	38	104	1605	1265
West Atlantic AV @ Homewood BL/High Po	95	250	1257	1391	71	304	1658	1391
West Atlantic AV @ CONGRESS AV 05/09	1585	935	1515	1427	1237	1570	1542	1435
West Atlantic AV @ I-95 (West) 08/09/08	1258	0	1333	1390	743	0	1388	1515
West Atlantic AV @ I-95 (East) 08/09/08	0	997	1201	1376	0	1076	1458	1314
West Atlantic AV @ SW/NW 12th AV 03/12	240	299	1054	1570	207	405	1418	1433
West Atlantic AV @ SW/NW 10th AV 10/10	109	69	1246	1729	147	107	1705	1365
West Atlantic AV @ SW/NW 8th AV 01/10/	121	103	861	1250	102	152	1211	1133
West Atlantic AV @ SW/NW 5th AV 01/10/	97	62	797	1214	127	81	1157	986
West Atlantic AV @ SW 2nd AV 18/04/07	0	118	835	1023	0	152	929	978
West Atlantic AV @ SWINTON AV18/04/07	599	295	468	925	522	384	484	883
EAST Atlantic AV @ SE/NE 2nd AV 02/09/(	139	11	404	478	166	1	431	440
East Atlantic AV @ US-1 NE 5th AV 03/09/(	1053	0	427	367	853	0	458	326
East Atlantic AV @ US-1 NE 6th AV 03/09/(	0	826	368	376	0	1071	465	347
Diego DR West/North(05/05/08)	187	172	639	918	117	130	1028	714
Glades Rd/Cains BL(04/30/07)	809	99999	687	1152	774	99999	1216	858
Glades_SR-7(28/04/08)	1879	2261	1437	1435	2037	2111	1921	1009
Glades_Shadowood SC((04/24/0)	267	400	1355	1626	330	468	1840	1363
Glades_95th Ave S(04/28/08)	221	470	1510	1769	237	582	1923	1678
	AM				PM			
Approach Volume	SB	NB	WB	EB	SB	NB	WB	EB
Glades_Lyons RD(04/28/08)	1224	1127	1503	1510	1386	1053	2044	1923
Glades_Boca Lake/Sommerset Mall	156	70	1470	2044	203	66	2016	1736
Glades_Golf Course/Concord Grn	130	39	2296	1950	116	30	2296	1810
Glades_Boca Rio Rd	346	694	1602	1784	347	678	2277	1695
Glades_Turnpike	273	90	1548	2332	1661	113	2632	2016
Glades_Boca West/Encina Ln	219	122	1595	2837	317	90	2860	1913
Glades_Jog/Powerline Rd(1/19/08)	1140	1484	1139	3557	1449	1200	2713	2296
Glades_Jog/Powerline Rd	1142	1212	1477	2818	1293	1061	2556	1902
Glades_Boca Corp Ctr	134	89	1637	3213	144	128	2845	1996
Linton BL @ Jog RD	2107	1260	971	272	1347	1595	1333	314
Linton BL @ Sims RD 17-Nov-08	233	52	950	1221	162	40	1216	997
Linton BL @ Las Verdes Way/Delray Hospi	66	280	849	1322	61	364	896	980
Linton BL @ Military Trail 19-Nov-08	2313	1157	1309	1181	1360	1895	1444	1137
Linton BL @ Old German Town RD 13-Nov	0	489	1152	1312	0	671	1089	1467
Linton BL @ Homewood BL 05-Nov-07	354	99	1106	1327	209	138	1232	1170
Linton BL @ Congress 13-Nov-07	1373	675	1501	1405	1109	1509	1466	1314
Linton BL @ I-95 18-Nov-08	1275	934	1560	1246	748	1043	2165	1593
Linton BL @ Wallace/waterfort PL 13-Nov-(	253	528	1508	1935	375	679	1945	1950
Linton BL @ SW 10th AVE 10-Sep-08	158	398	1114	1491	182	357	1379	1341
Linton BL @ SW 4th AVE 09-Sep-08	212	213	1353	1543	210	190	1282	1490
Linton BL @ OLD DIXIE HWY 09-Sep-08	247	350	1353	1046	205	569	1282	1323
Linton BL @ US-1/Federal HWY	1262	1063	540	1032	1142	1469	612	1177

Table A-1 Contd: Traffic Count Data-Peak Hour Volumes

	AM				PM			
Approach Volume	SB	NB	WB	EB	SB	NB	WB	EB
Glades_Lyons RD(04/28/08)	1224	1127	1503	1510	1386	1053	2044	1923
Glades_Boca Lake/Sommerset Mall	156	70	1470	2044	203	66	2016	1736
Glades_Golf Course/Concord Grn	130	39	2296	1950	116	30	2296	1810
Glades_Boca Rio Rd	346	694	1602	1784	347	678	2277	1695
Glades_Turnpike	273	90	1548	2332	1661	113	2632	2016
Glades_Boca West/Encina Ln	219	122	1595	2837	317	90	2860	1913
Glades_Jog/Powerline Rd(1/19/08)	1140	1484	1139	3557	1449	1200	2713	2296
Glades_Jog/Powerline Rd	1142	1212	1477	2818	1293	1061	2556	1902
Glades_Boca Corp Ctr	134	89	1637	3213	144	128	2845	1996
Linton BL @ Jog RD	2107	1260	971	272	1347	1595	1333	314
Linton BL @ Sims RD 17-Nov-08	233	52	950	1221	162	40	1216	997
Linton BL @ Las Verdes Way/Delray Hospita	66	280	849	1322	61	364	896	980
Linton BL @ Military Trail 19-Nov-08	2313	1157	1309	1181	1360	1895	1444	1137
Linton BL @ Old German Town RD 13-Nov-(	0	489	1152	1312	0	671	1089	1467
Linton BL @ Homewood BL 05-Nov-07	354	99	1106	1327	209	138	1232	1170
Linton BL @ Congress 13-Nov-07	1373	675	1501	1405	1109	1509	1466	1314
Linton BL @ I-95 18-Nov-08	1275	934	1560	1246	748	1043	2165	1593
Linton BL @ Wallace/waterfort PL 13-Nov-07	253	528	1508	1935	375	679	1945	1950
Linton BL @ SW 10th AVE 10-Sep-08	158	398	1114	1491	182	357	1379	1341
Linton BL @ SW 4th AVE 09-Sep-08	212	213	1353	1543	210	190	1282	1490
Linton BL @ OLD DIXIE HWY 09-Sep-08	247	350	1353	1046	205	569	1282	1323
Linton BL @ US-1/Federal HWY	1262	1063	540	1032	1142	1469	612	1177
Linton BL @ A1A	413	507	8	488	447	540	15	596
Atlantic Blvd@ Riverside West	104	246	787	671	70	168	623	1184
Atlantic Blvd@ Coral Ridge DR	1036	1607	1159	681	1053	889	1092	993
Atlantic Blvd@ Pine Island RD	1074	1287	1244	954	892	1164	1630	1230
Atlantic Blvd@ BW 98 AV	73	121	971	1351	275	245	1585	1482
Atlantic Blvd@ University DR	1023	2749	1366	1074	1958	1691	1506	1212
Atlantic Blvd@ Riverside DR	814	831	1137	933	917	1656	2118	1167
Atlantic Blvd@ Ramblewood DR	113	49	1043	1097	129	54	2043	1391
Atlantic Blvd@ NW 80th Ter	22	24	1587	1153	9	39	2019	1469
Atlantic Blvd@ NW 76th AV	128	64	876	2153	179	67	2407	1469
Atlantic Blvd@ Palm Lakes Plaza	4	144	1133	1056	0	163	2170	1578
Atlantic Blvd@ Rock Island RD	1555	918	819	1513	1304	1175	1734	1692
Atlantic Blvd@ NW 66th AV	136	73	762	1563	113	84	2109	1478
Atlantic Blvd@ SR-7(US-441)	1892	2170	1918	2398	2191	2315	3042	1661
Atlantic Blvd@ Lakewodd Circle	30	27	743	2050	265	29	1275	1132
Atlantic Blvd@ Banks RD	461	105	1107	2458	579	106	2575	1677
Atlantic Blvd@ Powerline RD	2357	1551	1581	2499	2286	2601	2202	2951
Atlantic Blvd@ West Circle Mall Entrance	104	246	787	671	70	168	623	1184
Atlantic Blvd@ E CRCL MALL ENT	129	53	864	714	193	70	1332	1036
Atlantic Blvd@ E CRCL MALL ENT	104	246	787	671	70	168	623	1184

Table A-1 Contd. V/C	AM				PM			
	SB	NB	WB	EB	SB	NB	WB	EB
ITR/Pratt W(10/15/07)	0.3671	0.1165	0.3824	0.1176	0.1200	0.4953	0.2094	0.0765
ITR/Pratt W(10/18/07)	0.2447	0.0941	0.3188	0.0753	0.0565	0.4153	0.1941	0.0635
ITR/Marc D(3/21/07)	0.1271	0.3565	0.3056	0.4506	0.1941	0.1600	0.6050	0.2967
ITR/Jupiter Farm(3/21/07)	0.0000	0.7494	0.4933	0.7183	0.0000	0.4012	0.9889	0.4450
ITR/Marsala(4/12/08)	0.0306	0.0541	0.2878	0.7351	0.0412	0.0682	0.6428	0.3369
ITR/Tpk(8/23/06)	0.4544	0.0518	0.5720	0.9778	0.4572	0.0388	0.8672	0.5511
ITR/Tpk(9/15/08)	0.4750	0.0071	0.5731	0.7122	0.4378	0.0094	0.8646	0.3565
ITR/Tpk(9/29/08)	0.5039	0.0082	0.5399	0.6738	0.4500	0.0047	0.8325	0.3177
ITR/Tpk(2/5/09)	0.5622	0.0012	0.4642	0.7277	0.5167	0.0059	0.8587	0.3554
ITR/Island Way(8/15/06)	0.4365	0.1776	0.7683	0.9487	0.2529	0.1576	0.9705	0.8727
ITR/Island Way(10/15/07)	0.5141	0.2294	0.7015	0.9734	0.3400	0.2412	0.8531	0.8605
ITR/Island Way(10/22/07)	0.4553	0.1706	0.6904	0.9387	0.2753	0.2118	0.8834	0.7554
ITR/Island Way(2/5/09)	0.4576	0.1976	0.6930	0.9159	0.2612	0.2412	0.9111	0.8790
ITR/J West Plz(8/23/06)	0.1882	0.2082	0.7461	0.8328	0.2635	0.1388	0.9601	0.6911
ITR/J West Plz(9/15/08)	0.1071	0.2294	0.7365	0.9745	0.1506	0.1659	0.8657	0.6424
ITR/J West Plz(9/17/08)	0.1071	0.1424	0.7218	0.8863	0.2400	0.0894	0.8727	0.7199
ITR/Central(8/23/06)	0.9941	0.5900	0.5424	0.7959	0.4302	0.8133	0.8207	0.6771
ITR/Central(1/31;16/07)	1.0447	0.4622	0.5173	0.9107	0.5962	0.7233	0.9018	0.8572
ITR/Central(2/2508)	0.9954	0.5478	0.5919	0.9554	0.6219	0.7067	0.9982	0.7421
ITR/Central(4/1708)	0.8942	0.5367	0.5332	0.9476	0.5298	0.7967	0.8863	0.8280
ITR/Central(5/8/\08)	0.8407	0.6122	0.5498	0.8849	0.4543	0.7233	0.8166	0.6900
ITR/Central(5/22/08)	0.9419	0.4600	0.5369	0.8849	0.5034	0.6867	0.8273	0.6919
ITR/Central(2/4/09)	0.8378	0.4744	0.5026	0.8616	0.5313	0.6822	0.8148	0.7373
ITR/Chasewood(8/23)	0.0329	0.2565	0.5546	0.7959	0.0188	0.3647	0.8354	0.6635
ITR/Chasewood(8/28;9/5/0	0.0553	0.2188	0.6048	0.8856	0.0694	0.3906	0.9026	0.6317
ITR/Chasewood(5/5/08)	0.0612	0.3847	0.5413	0.8351	0.0671	0.4282	0.8273	0.6458
ITR/Chasewood(5/22/08)	0.0647	0.1612	0.5133	0.8664	0.0600	0.3482	0.7915	0.6469
ITR/Center(8/23/06)	0.8224	0.2894	0.5601	0.7952	0.7082	0.3447	0.7819	0.6661
ITR/Center(5/5/08)	0.9812	0.2788	0.5347	0.9358	0.7294	0.3400	0.7790	0.6804
ITR/Center(5/22/08)	0.9918	0.0812	0.4565	0.9041	0.7729	0.2918	0.7380	0.6867
ITR/Center(2/4/09)	0.8882	0.0859	0.3646	0.8170	0.7365	0.3506	0.8764	0.6487
ITR/Maplewood(9/13/06)	0.0718	0.2828	0.4738	0.6793	0.1847	0.4033	0.6472	0.5572
ITR/Maplewood(3/27/07)	0.0447	0.2689	0.5077	0.8723	0.1024	0.3861	0.6974	0.6535
ITR/Maplewood(2/4/09)	0.0059	0.2311	0.3247	0.8517	0.0671	0.3856	0.7531	0.5661
ITR/Delaware(9/7/06)	0.1059	0.0976	0.4790	0.6804	0.0824	0.1329	0.6546	0.5520
ITR/Delaware(9/15/08)	0.1247	0.1435	0.4299	0.7100	0.0765	0.1929	0.6284	0.5384
ITR/Delaware(9/17/08)	0.1271	0.1424	0.3930	0.7151	0.0729	0.1235	0.4734	0.5469
ITR/Pennock	0.5118	0.3424	0.6162	0.7941	0.3388	0.2965	0.8258	0.7395
ITR/Military	0.1341	0.2771	0.4085	0.7166	0.1647	0.3956	0.5506	0.5771
ITR/Military(2/4/09)	0.0800	0.2506	0.3598	0.6576	0.1788	0.4000	0.7509	0.5616
ITR/Lox.	0.2271	0.2341	0.3878	0.6742	0.1541	0.1894	0.5458	0.5731
ITR/alt A1A	0.7367	0.5483	0.3255	0.6517	0.6239	0.7256	0.5059	0.5797
ITR/alt A1A(2/9/09)	0.7822	0.5006	0.2520	0.5044	0.5783	0.7100	0.6849	0.5450

Table A-1 Contd.	AM				PM			
V/C	SB	NB	WB	EB	SB	NB	WB	EB
Donald Ross RD @I-95	0.8424	0.4667	0.6528	0.4656	0.3918	0.7283	0.7767	0.2350
Donald Ross RD @Iheights E	0.7400	0.0000	0.3454	0.6170	0.2518	0.0000	0.5173	0.4834
Donald Ross RD @Parkside	0.1567	0.0000	0.2919	0.7026	0.1717	0.0000	0.4734	0.4502
Donald Ross RD @ Central E	0.2828	0.5822	0.3443	0.6897	0.3894	0.4717	0.5801	0.4085
Donald Ross RD @ Military T	0.5627	0.3738	0.3694	0.5934	0.5535	0.3830	0.5782	0.4089
Donald Ross RD @SR-818/A	0.4661	0.3845	0.3690	0.6369	0.3911	0.5048	0.5576	0.3982
Donald Ross RD @Frenchma	0.0729	0.1094	0.3151	0.4923	0.0882	0.1056	0.4642	0.3280
Donald Ross RD @ Ellison W	0.0000	0.2824	0.5939	0.8106	0.0000	0.6200	0.7378	0.5817
Donald Ross RD @ US-1	0.7806	0.5011	0.1411	0.5739	0.6628	0.8533	0.1478	0.6128
PGA BL @ Beeline HWY	0.2717	0.3078	0.2282	0.0000	0.3567	0.2122	0.2729	0.0000
PGA BL @ Ryder Cup BL/Jo	0.1118	0.1178	0.1733	0.0911	0.1341	0.0850	0.1894	0.1044
PGA BL @ AVE of the Chan	0.2378	0.0517	0.3192	0.1284	0.2161	0.0778	0.2967	0.1354
PGA BL @ Fl Turnpike	0.5727	0.2600	0.9783	0.2531	0.2808	0.3389	0.4161	0.8210
PGA BL @ Balen Isles DR	0.0529	0.0617	0.5668	0.7683	0.0729	0.0644	0.6601	0.5399
PGA BL @Central BL	0.4989	0.0822	0.5000	0.7923	0.4228	0.0878	0.7262	0.6314
PGA BL @ Military Trail	0.6185	0.6904	0.4649	0.7391	0.5284	0.7506	0.7871	0.6930
PGA BL @ I-95 West Side	0.4500	0.0000	0.4483	0.8583	0.1739	0.0000	0.7661	0.6672
PGA BL @I-95 East Side	0.0000	0.8222	0.8125	0.8125	0.0000	0.7161	0.5705	0.5705
PGA BL @ Victoria Gardens	0.0911	0.2644	0.5841	1.1037	0.1978	0.3867	0.8015	0.8288
PGA BL @ FairChild Garden	0.3617	0.2611	0.5166	0.8155	0.5322	0.3411	0.7122	0.7328
PGA BL @ Gardens Mall Ma	0.0491	0.1247	0.4373	0.7052	0.1011	0.1212	0.6959	0.6207
PGA BL @Prosperity Farms	0.4911	0.5111	0.4963	0.5978	0.4828	0.6561	0.6705	0.5185
PGA BL @ Ellison Wilson R	0.2144	0.2518	0.3494	0.6886	0.3322	0.3094	0.4015	0.5432
PGA BL @ US-1	0.7361	0.5044	0.3750	0.6750	0.7472	0.6739	0.4133	0.6606
Grandiflora/Central	0.4022	0.3650	0.0871	0.1800	0.3200	0.3150	0.0365	0.1341
Grandiflora/Military	0.3583	0.3661	0.0941	0.0882	0.3657	0.3594	0.0529	0.0412
Jog/Hood	0.0506	0.2941	0.2776	0.0000	0.0565	0.1459	0.1682	0.0000
45th Street @ Haverhill Rd 1	0.3428	0.8817	0.4750	0.2128	0.4372	0.6533	0.7372	0.1756
45th Street @ Military Trail 07	0.5007	0.5232	0.3941	0.5369	0.5410	0.3572	0.6351	0.3583
45th Street @ Village Bl 07/0	0.1861	0.6500	0.4860	0.7037	0.3383	0.3950	0.7605	0.4697
45th Street @ North Point BL	0.2272	0.0989	0.7572	0.8332	0.2589	0.2150	0.8122	0.6066
45th Street @ I-95 27/08/08	0.8000	0.6533	0.5435	0.8125	0.5422	0.5183	0.8775	0.7129
45th Street @ Corporate Wa	0.1824	0.0271	0.5583	0.9188	0.1522	0.0083	0.8432	0.5686
45th Street @ Congress Ave	0.4749	0.3424	0.6768	0.8893	0.5446	0.4852	0.8683	0.6011
45th Street @ South Pl/Tiffa	0.0529	0.0565	0.5576	0.8358	0.0494	0.1247	0.8244	0.5210
45th Street @ North Shore D	0.0700	0.1833	0.3934	0.7590	0.0939	0.1561	0.6185	0.5144
45th Street @ Australian AV	0.4678	0.6400	0.3502	0.6697	0.5733	0.7872	0.5531	0.4808
45th Street @ Old Dixie HWY	0.3994	0.1271	0.3161	0.4772	0.3561	0.1235	0.3861	0.4950
45th Street @ Pinewood AV	0.0765	0.1082	0.2644	0.5317	0.1176	0.1518	0.2644	0.4272
45th Street @ Broadway Roa	0.7456	0.4167	0.1122	0.4456	0.6106	0.6478	0.1344	0.3067
Belvedere RD @ SR-7	0.5882	0.5421	0.2661	0.3078	0.5838	0.5638	0.5502	0.1778
Belvedere RD @ Walmart/Ma	0.0800	0.2082	0.2380	0.4594	0.0706	0.2624	0.4594	0.2476
Belvedere RD @ Sansbury W	0.5435	0.6224	0.4280	0.5638	0.3553	0.5776	0.6937	0.3125
Belvedere RD @ Benoist Far	0.2200	0.2165	0.4557	0.6609	0.2612	0.3129	0.6661	0.4155
Belvedere RD @ Skees RD	0.3635	0.0000	0.4244	0.6384	0.3012	0.0000	0.6509	0.4004

Table A-1 Contd.	AM				PM			
V/C	SB	NB	WB	EB	SB	NB	WB	EB
Belvedere RD @ Jog RD	0.3605	0.6317	0.3225	0.9900	0.5199	0.5314	0.6790	0.7244
Belvedere RD @ Drexel RD/I	0.4059	0.1012	0.4583	0.8194	0.4624	0.0647	0.9050	0.6056
Belvedere RD @ Caroline AV	0.0000	0.3165	0.4828	1.1722	0.0000	0.1976	1.0222	0.7044
Belvedere RD @ Haverhill RI	0.3917	0.5472	0.4006	0.8522	0.5389	0.4850	0.8733	0.5344
Belvedere RD @ 5th Street 1	0.1518	0.0000	0.3424	0.6384	0.1882	0.0000	0.6450	0.3886
Belvedere RD @ Military TR	0.3863	0.6081	0.3972	0.7983	0.6218	0.5214	0.8044	0.5189
Belvedere RD @ Congress A	0.3272	0.0678	0.3967	0.5181	0.5728	0.0772	0.6240	0.3063
Belvedere RD @ Australian A	0.2653	0.9269	0.3675	0.5096	0.6952	0.4399	0.4823	0.5376
Belvedere RD @ Mercer Ave	0.2271	0.0000	0.4598	0.6225	0.5600	0.0000	0.4860	0.5347
Belvedere RD @ Parker AVE	0.1989	0.3139	0.4350	0.8333	0.4033	0.1894	0.5472	0.5472
Belvedere RD @ Georgia AV	0.0918	0.3165	0.2900	0.6500	0.1047	0.2918	0.4089	0.4144
Belvedere RD @ Dixeie HWY	0.2894	0.4422	0.0700	0.5717	0.5411	0.3133	0.1117	0.3450
Forest Hill/South Shore/12th	0.1518	0.5883	0.5299	0.4517	0.0941	0.4906	0.8904	0.4498
Forest Hill/@Polo Club Rd/R	0.2906	0.0667	0.4963	0.7841	0.2144	0.0850	0.8162	0.6111
Forest Hill/Fairlane Farm Rd	0.0000	0.2471	0.5668	1.0860	0.0000	0.5588	0.9745	0.6970
Forest Hill/@Wellington Edge	0.1589	0.1717	0.4812	0.7701	0.0789	0.2700	0.8446	0.5808
Forest Hill/Wellington Green	0.0000	0.3024	0.4819	0.7904	0.0000	0.4976	0.7978	0.6387
Forest Hill/SR-7 10/14/08	0.6446	0.5148	0.4306	0.7675	0.8229	0.6834	0.5561	0.6343
Forest Hill/Olympia/Buena Vi	0.0333	0.0683	0.4469	0.5384	0.0283	0.0506	0.6661	0.5723
Forest Hill Rd @Ranch Rd/Ly	0.5694	0.7694	0.4779	0.5240	0.6282	0.3071	0.5900	0.5203
Forest Hill Bl @ Pinhurst Dr 1	0.0706	0.5059	0.5550	0.6221	0.1024	0.4776	0.6550	0.5642
Forest Hill Bl @ River Bridge	0.1811	0.1859	0.5579	0.6520	0.1194	0.2847	0.7089	0.5664
Forest Hill @ Jog Rd 14/10/0	0.5601	0.6926	0.4760	0.6380	0.8232	0.6982	0.5458	0.5716
Forest Hill @ Sherwood Fore	0.0261	0.1394	0.6262	0.5764	0.0178	0.1178	0.5199	0.5753
Forest Hill @ Haverhill Rd 06	0.5017	0.6761	0.3690	0.7137	0.7206	0.5389	0.6052	0.5225
Forest Hill @ Military Trail 22	0.4354	0.6520	0.4598	0.6114	0.6539	0.6048	0.6041	0.4937
Forest Hill @ Kirk Rd Rd 14/1	0.2561	0.6217	0.4517	0.6572	0.3350	0.4356	0.6601	0.4956
Forest Hill @ Davis Rd/Tuker	0.2988	0.1247	0.4314	0.7295	0.2424	0.2471	0.6317	0.4941
Forest Hill Bl @ Congress Av	0.4369	0.5277	0.4561	0.6827	0.5941	0.5306	0.5889	0.5554
Forest Hill Bl @ Florida Mang	0.4412	0.6788	0.4273	0.5956	0.4588	0.4765	0.6657	0.5070
Forest Hill Bl @ Pine Tree LN	0.0000	0.2035	0.5480	0.7295	0.0000	0.1329	0.6594	0.4834
Forest Hill Bl @ I-95 15/10/08	0.2875	0.2358	0.3708	0.7554	0.3410	0.3159	0.4048	0.4749
Forest Hill Bl @ Parkewr Ave	0.2278	0.2033	0.3417	0.4613	0.2056	0.1517	0.3838	0.3760
Forest Hill Bl @ Lake Ave 07	0.0988	0.0282	0.4139	0.5317	0.0847	0.0400	0.4994	0.4544
Forest Hill Bl @ Gerogia Ave	0.1624	0.1929	0.3817	0.5817	0.2106	0.2012	0.4289	0.4367
Forest Hill @ Dixie HWY 06/1	0.3628	0.5339	0.1278	0.4633	0.5144	0.4633	0.1472	0.3733
Lantana RD @ SR-7 10-Sep-	0.7672	0.2616	0.4306	0.3459	0.4672	0.5897	0.4217	0.2694
Lantana RD @ Target 10 Se	0.0682	0.0000	0.4306	0.3311	0.1129	0.0000	0.4217	0.5111
Lantana RD @ Bellagio Lake	0.0039	0.0594	0.4261	0.3311	0.0028	0.0683	0.4333	0.5111
Lantana RD @ Lyons RD 10	0.2033	0.2333	0.6211	0.3850	0.2456	0.2767	0.6411	0.5033
Lantana RD @ Aquarius BL/(	0.1953	0.0883	0.5661	0.5239	0.1235	0.0433	0.7217	0.7067
Lantana RD @ Bantbrook BL	0.3659	0.0000	0.6444	0.6550	0.1976	0.0000	0.8411	0.6350
Lantana RD @ Hagen Ranch	0.0235	0.6918	0.3985	0.9006	0.0188	0.7871	0.5587	0.7933
Lantana RD @ Jog RD 10-Se	0.4509	0.4491	0.4775	0.6129	0.5185	0.5672	0.6214	0.5133

Table A-1 Contd.	AM				PM			
V/C	SB	NB	WB	EB	SB	NB	WB	EB
Lantana RD @ EDGECLIFF	0.7318	0.0000	0.4985	0.5690	0.3906	0.0000	0.6900	0.5424
Lantana RD @ Haverhill RD	0.8341	0.5871	0.4760	0.7937	0.7882	0.5659	0.7705	0.5941
Lantana RD @ Military Trail 1	0.5480	0.5413	0.4328	0.8380	0.5565	0.5413	0.7421	0.5900
Lantana RD @ Lawrence RD	0.0000	0.5588	0.5347	0.8214	0.0000	0.5647	1.0373	0.5347
Lantana RD @ Congress 03-	0.6689	0.4783	0.4524	0.8565	0.9783	0.6483	0.8240	0.5498
Lantana RD @ High Ridge 23	0.3094	0.1282	0.5906	1.0122	0.4471	0.1671	1.0350	0.7300
Lantana RD @ I-95 24-Mar-0	0.3378	0.3817	0.6344	1.0744	0.4989	0.6711	0.8161	0.8244
Lantana RD @ 13th ST/Andr	0.2412	0.3365	0.4450	0.6394	0.3153	0.3106	0.5811	0.7050
Lantana RD @ Broadway/6th	0.0518	0.3282	0.3056	0.3883	0.0506	0.3965	0.3683	0.4417
Lantana RD @ US-1 24-Oct-	0.9776	0.7788	0.0494	0.3544	1.2894	1.1200	0.0706	0.3722
West Atlantic AV @ SR-7 24/	0.9444	0.4189	0.4694	0.1847	0.3678	0.7367	0.4694	0.1812
West Atlantic AV @ Hagen R	0.5294	0.0000	0.5017	0.9656	0.4356	0.0000	0.7250	0.8083
West Atlantic AV @ Legends	0.1567	0.0511	0.3362	0.6033	0.1661	0.0583	0.7411	0.5606
West Atlantic AV @ Cumberl	0.1117	0.0000	0.5017	0.5244	0.1056	0.0000	0.7017	0.6850
West Atlantic AV @ Kings Po	0.0000	0.1189	0.5839	0.8933	0.0000	0.1061	0.6756	0.6656
West Atlantic AV @ Jog Rd (	0.7922	0.4498	0.3594	0.5900	0.5072	0.6015	0.4144	0.4775
West Atlantic AV @ EL Clair	0.2929	0.1506	0.4712	0.4708	0.2882	0.1529	0.5354	0.4494
West Atlantic AV @ Lakes of	0.0800	0.0811	0.4487	0.5616	0.1153	0.0856	0.5638	0.5362
West Atlantic AV @ Via Flora	0.2071	0.0929	0.4827	0.5461	0.1894	0.1176	0.5568	0.5162
West Atlantic AV @ Market F	0.1918	0.0365	0.4782	0.6948	0.1953	0.0765	0.5365	0.5989
West Atlantic AV @ Military T	0.7406	0.5339	0.5011	0.5502	0.5882	0.7395	0.5542	0.5712
West Atlantic AV @ Whatley	0.2482	0.1318	0.0439	0.4554	0.3200	0.0659	0.4812	0.4225
West Atlantic AV @ Barwick	0.2922	0.0278	0.4550	0.5166	0.2450	0.0222	0.5893	0.5103
West Atlantic AV @ Hamlet D	0.0765	0.1082	0.4830	0.5159	0.0447	0.1224	0.5923	0.4668
West Atlantic AV @ Homewo	0.1118	0.2941	0.4638	0.5133	0.0835	0.3576	0.6118	0.5133
West Atlantic AV @ CONGR	0.5849	0.3450	0.5590	0.5266	0.4565	0.5793	0.5690	0.5295
West Atlantic AV @ I-95 (We	0.6989	0.0000	0.4919	0.5129	0.4128	0.0000	0.5122	0.5590
West Atlantic AV @ I-95 (Eas	0.0000	0.5539	0.6672	0.7644	0.0000	0.5978	0.8100	0.7300
West Atlantic AV @ SW/NW	0.2824	0.3518	0.5856	0.8722	0.2435	0.4765	0.7878	0.7961
West Atlantic AV @ SW/NW	0.1282	0.0812	0.6922	0.9606	0.1729	0.1259	0.9472	0.7583
West Atlantic AV @ SW/NW	0.1424	0.1212	0.4783	0.6944	0.1200	0.1788	0.6728	0.6294
West Atlantic AV @ SW/NW	0.1141	0.0729	0.4428	0.6744	0.1494	0.0953	0.6428	0.5478
West Atlantic AV @ SW 2nd	0.0000	0.1388	0.4639	0.5683	0.0000	0.1788	0.5161	0.5433
West Atlantic AV @ SWINTC	0.7047	0.3471	0.2600	0.5139	0.6141	0.4518	0.2689	0.4906
EAST Atlantic AV @ SE/NE 2	0.1635	0.0129	0.4753	0.5624	0.1953	0.0012	0.5071	0.5176
East Atlantic AV @ US-1 NE	0.5850	0.0000	0.5024	0.4318	0.4739	0.0000	0.5388	0.3835
East Atlantic AV @ US-1 NE	0.0000	0.4589	0.4329	0.4424	0.0000	0.5950	0.5471	0.4082
Diego DR West/North(05/05/	0.2200	0.2024	0.2358	0.3387	0.1376	0.1529	0.3793	0.2635
Glades Rd/Cains BL(04/30/0	0.9518	0.0000	0.2535	0.4251	0.9106	0.0000	0.4487	0.3166
Glades_SR-7(28/04/08)	0.6934	0.8343	0.5303	0.5295	0.7517	0.7790	0.7089	0.3723
Glades_Shadowood SC((04/2	0.3141	0.4706	0.5000	0.6000	0.3882	0.5506	0.6790	0.5030
Glades_95th Ave S(04/28/08	0.2600	0.2611	0.5572	0.6528	0.2788	0.3233	0.7096	0.6192
Glades_Lyons RD(04/28/08)	0.6800	0.6261	0.5546	0.5572	0.7700	0.5850	0.7542	0.7096

Table A-1 Contd.	AM				PM			
V/C	SB	NB	WB	EB	SB	NB	WB	EB
Glades_Boca Lake/Sommers	0.1835	0.0824	0.5424	0.7542	0.2388	0.0776	0.7439	0.6406
Glades_Golf Course/Concord	0.1529	0.0459	0.8472	0.7196	0.1365	0.0353	0.8472	0.6679
Glades_Boca Rio Rd	0.1922	0.3856	0.5911	0.6583	0.1928	0.3767	0.8402	0.6255
Glades_Turnpike	0.1007	0.1059	0.5712	0.8605	0.6129	0.1329	0.9712	0.7439
Glades_Boca West/Encina L	0.2576	0.1435	0.5886	1.0469	0.3729	0.1059	1.0554	0.7059
Glades_Jog/Powerline Rd(1/	0.6333	0.8244	0.4203	1.3125	0.8050	0.6667	1.0011	0.8472
Glades_Jog/Powerline Rd	0.6344	0.6733	0.5450	1.0399	0.7183	0.5894	0.9432	0.7018
Glades_Boca Corp Ctr	0.0744	0.0494	0.6041	1.1856	0.0800	0.0711	1.0498	0.7365
Linton BL @ Jog RD	0.7775	0.4649	0.5394	0.1511	0.4970	0.5886	0.7406	0.1744
Linton BL @ Sims RD 17-No	0.2741	0.0612	0.5278	0.6783	0.1906	0.0471	0.6756	0.5539
Linton BL @ Las Verdes Wa	0.0367	0.3294	0.3133	0.4878	0.0339	0.4282	0.3306	0.3616
Linton BL @ Military Trail 19-	0.8535	0.4269	0.4830	0.4358	0.5018	0.6993	0.5328	0.4196
Linton BL @ Old German To	0.0000	0.5753	0.4251	0.4841	0.0000	0.7894	0.4018	0.5413
Linton BL @ Homewood BL (	0.1967	0.1165	0.4081	0.4897	0.1161	0.1624	0.4546	0.4317
Linton BL @ Congress 13-No	0.5066	0.2491	0.5539	0.5185	0.4092	0.5568	0.5410	0.4849
Linton BL @ I-95 18-Nov-08	0.7083	0.5189	0.5756	0.4598	0.4156	0.5794	0.7989	0.5878
Linton BL @ Wallace/waterfo	0.2976	0.6212	0.5565	0.7140	0.4412	0.7988	0.7177	0.7196
Linton BL @ SW 10th AVE 1	0.1859	0.2211	0.4111	0.5502	0.2141	0.1983	0.5089	0.4948
Linton BL @ SW 4th AVE 09	0.2494	0.2506	0.4993	0.5694	0.2471	0.2235	0.4731	0.5498
Linton BL @ OLD DIXIE HW	0.2906	0.4118	0.4993	0.3860	0.2412	0.6694	0.4731	0.4882
Linton BL @ US-1/Federal H	0.7011	0.5906	0.1993	0.3808	0.6344	0.8161	0.2258	0.4343
Linton BL @ A1A	0.4859	0.5965	0.0094	0.2711	0.5259	0.6353	0.0176	0.3311
Atlantic Blvd@ Riverside We	0.0578	0.1367	0.2904	0.2476	0.0389	0.0933	0.2299	0.4369
Atlantic Blvd@ Coral Ridge D	0.5756	0.8928	0.4277	0.2513	0.5850	0.4939	0.4030	0.3664
Atlantic Blvd@ Pine Island R	0.5967	0.7150	0.4590	0.3520	0.4956	0.6467	0.6015	0.4539
Atlantic Blvd@ BW 98 AV	0.0406	0.0672	0.3583	0.4985	0.1528	0.1361	0.5849	0.5469
Atlantic Blvd@ University DR	0.3775	1.0144	0.5041	0.3963	0.7225	0.6240	0.5557	0.4472
Atlantic Blvd@ Riverside DR	0.4522	0.4617	0.4196	0.3443	0.5094	0.9200	0.7815	0.4306
Atlantic Blvd@ Ramblewood	0.0628	0.0272	0.3849	0.4048	0.0717	0.0300	0.7539	0.5133
Atlantic Blvd@ NW 80th Ter	0.0259	0.0282	0.5856	0.4255	0.0106	0.0459	0.7450	0.5421
Atlantic Blvd@ NW 76th AV	0.1506	0.0753	0.3232	0.7945	0.2106	0.0788	0.8882	0.5421
Atlantic Blvd@ Palm Lakes P	0.0047	0.1694	0.4181	0.3897	0.0000	0.1918	0.8007	0.5823
Atlantic Blvd@ Rock Island R	0.8639	0.5100	0.3022	0.5583	0.7244	0.6528	0.6399	0.6244
Atlantic Blvd@ NW 66th AV	0.0756	0.0406	0.2812	0.5768	0.0628	0.0467	0.7782	0.5454
Atlantic Blvd@ SR-7(US-441	0.6982	0.8007	0.7077	0.8849	0.8085	0.8542	1.1225	0.6129
Atlantic Blvd@ Lakewodd Cir	0.0167	0.0150	0.2742	0.7565	0.1472	0.0161	0.4705	0.4177
Atlantic Blvd@ Banks RD	0.2561	0.0583	0.4085	0.9070	0.3217	0.0589	0.9502	0.6188
Atlantic Blvd@ Powerline RD	0.8697	0.5723	0.5834	0.9221	0.8435	0.9598	0.8125	1.0889
Atlantic Blvd@ West Circle M	0.0578	0.1367	0.2904	0.2476	0.0389	0.0933	0.2299	0.4369
Atlantic Blvd@ E CRCL MAL	0.0717	0.0294	0.3188	0.2635	0.1072	0.0389	0.4915	0.3823
Atlantic Blvd@ E CRCL MAL	0.0578	0.1367	0.2904	0.2476	0.0389	0.0933	0.2299	0.4369
Average	0.3488	0.2988	0.4612	0.6683	0.3295	0.3327	0.6488	0.5360
Std	0.2825	0.2326	0.1478	0.2303	0.2469	0.2489	0.2169	0.1765

Table A-1 Contd.	AM				PM			
PHF	SB	NB	WB	EB	SB	NB	WB	EB
ITR/Pratt W(10/15/07)	0.8130	0.5630	0.9450	0.8060	0.7730	0.8490	0.9080	0.8130
ITR/Pratt W(10/18/07)	0.8670	0.6250	0.8690	0.8890	0.7060	0.8020	0.8590	0.9000
ITR/Marc D(3/21/07)	0.6280	0.9130	0.8330	0.8550	0.6990	0.9440	0.9550	0.8900
ITR/Jupiter Farm(3/21/07)	0.0000	0.8900	0.8990	0.9780	0.0000	0.8610	0.9240	0.9020
ITR/Marsala(4/12/08)	0.4060	0.6390	0.9240	0.8650	0.4610	0.6590	0.9110	0.9710
ITR/Tpk(8/23/06)	0.8120	0.4780	0.9270	0.9630	0.8360	0.7500	0.9690	0.8410
ITR/Tpk(9/15/08)	0.9170	0.7500	0.9290	0.9240	0.9000	0.6670	0.9780	0.9510
ITR/Tpk(9/29/08)	0.8590	0.4380	0.9280	0.9060	0.9290	0.5000	0.9110	0.9080
ITR/Tpk(2/5/09)	0.8180	0.2500	0.8810	0.9000	0.8330	0.4170	0.9340	0.9440
ITR/Island Way(8/15/06)	0.8280	0.8030	0.8930	0.8450	0.6320	0.6840	0.9340	0.9550
ITR/Island Way(10/15/07)	0.8340	0.9200	0.9510	0.9240	0.8210	0.9670	0.8960	0.9460
ITR/Island Way(10/22/07)	0.7870	0.8240	0.9570	0.9560	0.8860	0.8820	0.8660	0.9150
ITR/Island Way(2/5/09)	0.8380	0.7370	0.9260	0.8330	0.8670	0.9150	0.8970	0.9040
ITR/J West Plz(8/23/06)	0.8160	0.9410	0.9400	0.9220	0.8360	0.7760	0.8980	0.9370
ITR/J West Plz(9/15/08)	0.7580	0.8550	0.9490	0.9800	0.6670	0.8390	0.9510	0.9300
ITR/J West Plz(9/17/08)	0.8430	0.7380	0.8920	0.9070	0.9440	0.7920	0.9400	0.9580
ITR/Central(8/23/06)	0.8880	0.9830	0.9160	0.9410	0.9440	0.9430	0.9030	0.9600
ITR/Central(1/31;16/07)	0.8470	0.7970	0.8510	0.8910	0.9100	0.8940	0.8820	0.9200
ITR/Central(2/2508)	0.8400	0.9270	0.9410	0.8620	0.9410	0.8280	0.9250	0.9190
ITR/Central(4/1708)	0.9790	0.9220	0.8940	0.8330	0.8910	0.8870	0.9210	0.9240
ITR/Central(5/8/\08)	0.9020	0.9530	0.9600	0.9040	0.9590	0.8590	0.9640	0.9460
ITR/Central(5/22/08)	0.8590	0.8480	0.8700	0.8310	0.9640	0.9750	0.9040	0.9910
ITR/Central(2/4/09)	0.8300	0.9320	0.9200	0.8180	0.9260	0.8980	0.9290	0.9530
ITR/Chasewood(8/23)	0.5000	0.9080	0.9210	0.8850	0.5000	0.9340	0.8940	0.9650
ITR/Chasewood(8/28;9/5/06)	0.7340	0.9120	0.9290	0.8930	0.7760	0.8740	0.8990	0.9430
ITR/Chasewood(5/5/08)	0.7650	0.9400	0.8840	0.9520	0.7920	0.9190	0.9470	0.9530
ITR/Chasewood(5/22/08)	0.6550	0.7140	0.9080	0.9070	0.5310	0.8310	0.8650	0.9360
ITR/Center(8/23/06)	0.9650	0.8910	0.9230	0.9010	0.8910	0.8830	0.9100	0.9460
ITR/Center(5/5/08)	0.8550	0.8840	0.8800	0.9310	0.9060	0.9380	0.9750	0.9150
ITR/Center(5/22/08)	0.7550	0.8210	0.8840	0.8460	0.9330	0.9120	0.8730	0.9070
ITR/Center(2/4/09)	0.9210	0.8300	0.7940	0.9100	0.7940	0.9310	0.9800	0.9550
ITR/Maplewood(9/13/06)	0.5650	0.7850	0.9120	0.9170	0.8180	0.8250	0.9370	0.9300
ITR/Maplewood(3/27/07)	0.7310	0.8180	0.8730	0.8720	0.7770	0.9290	0.9300	0.9130
ITR/Maplewood(2/4/09)	0.6250	0.7700	0.9240	0.8540	0.7500	0.7920	0.9280	0.8920
ITR/Delaware(9/7/06)	0.9000	0.8300	0.8990	0.9310	0.7950	0.8070	0.9420	0.9400
ITR/Delaware(9/15/08)	0.7790	0.8030	0.9810	0.8890	0.8550	0.7740	0.9380	0.9430
ITR/Delaware(9/17/08)	0.9000	0.6050	0.8760	0.8760	0.7050	0.7290	0.8760	0.9450
ITR/Pennock	0.8990	0.7500	0.9280	0.8940	0.8470	0.7590	0.8950	0.9710
ITR/Military	0.8640	0.8810	0.9190	0.8860	0.8330	0.7980	0.8560	0.9380
ITR/Military(2/4/09)	0.6800	0.8660	0.8180	0.8870	0.8840	0.9090	0.8850	0.9710
ITR/Lox.	0.9100	0.8290	0.8590	0.9230	0.9100	0.7190	0.9040	0.8880
ITR/alt A1A	0.8750	0.9170	0.8680	0.9030	0.8670	0.8610	0.8900	0.9110
ITR/alt A1A(2/9/09)	0.8610	0.9010	0.8290	0.8740	0.8530	0.9370	0.9220	0.8730
Donald Ross RD @I-95	0.9090	0.9290	0.9420	0.8220	0.9570	0.9810	0.8890	0.8220

Table A-1 Contd.	AM				PM			
PHF	SB	NB	WB	EB	SB	NB	WB	EB
Donald Ross RD @Iheights B	0.8830	0.0000	0.9560	0.8910	0.7750	0.0000	0.9370	0.9200
Donald Ross RD @Parkside [	0.8200	0.0000	0.8870	0.8960	0.6180	0.0000	0.8490	0.8640
Donald Ross RD @ Central B	0.9570	0.8400	0.8770	0.9290	0.7520	0.9190	0.8020	0.9070
Donald Ross RD @ Military Tr	0.8930	0.9240	0.8750	0.9660	0.9190	0.9110	0.9170	0.9080
Donald Ross RD @SR-818/Al	0.9180	0.9820	0.8680	0.9240	0.9640	0.9240	0.9470	0.9330
Donald Ross RD @Frenchma	0.8610	0.8070	0.8970	0.8710	0.8520	0.9310	0.8300	0.9110
Donald Ross RD @ Ellison W	0.0000	0.7690	0.9180	0.9570	0.0000	0.9620	0.8490	0.9090
Donald Ross RD @ US-1	0.8800	0.8480	0.8250	0.8050	0.9210	0.9280	0.8750	0.8780
PGA BL @ Beeline HWY	0.8670	0.9230	0.7130	0.0000	0.9440	0.9100	0.7950	0.0000
PGA BL @ Ryder Cup BL/Jog	0.7660	0.8330	0.8860	0.7590	0.7920	0.8140	0.8970	0.7700
PGA BL @ AVE of the Cham	0.8290	0.8300	0.9280	0.7910	0.9170	0.8540	0.9140	0.8820
PGA BL @ Fl Turnpike	0.9330	0.9290	0.8950	0.9070	0.9330	0.8710	0.9090	0.9320
PGA BL @ Balen Isles DR	0.8040	0.8670	0.9190	0.9200	0.7750	0.6900	0.9380	0.9500
PGA BL @Central BL	0.8350	0.8400	0.8990	0.9210	0.7230	0.8400	0.9670	0.8890
PGA BL @ Military Trail	0.9370	0.9280	0.9000	0.8280	0.9570	0.9430	0.9360	0.9100
PGA BL @ I-95 West Side	0.9690	0.0000	0.8680	0.9140	0.8790	0.0000	0.9370	0.9210
PGA BL @I-95 East Side	0.0000	0.9140	0.9160	0.9160	0.0000	0.9370	0.9640	0.9640
PGA BL @ Victoria Gardens	0.6120	0.8500	0.9160	0.9210	0.8400	0.8790	0.9460	0.9610
PGA BL @ FairChild Gardens	0.8800	0.9550	0.8840	0.9270	0.8810	0.9300	0.8740	0.9480
PGA BL @ Gardens Mall Mai	0.8110	0.9140	0.8690	0.9350	0.9260	0.8580	0.9210	0.9340
PGA BL @Prosperity Farms	0.8500	0.8750	0.7800	0.8860	0.9570	0.9460	0.9070	0.9270
PGA BL @ Ellison Wilson RD	0.7850	0.7330	0.8520	0.8820	0.9650	0.7560	0.8830	0.8090
PGA BL @ US-1	0.9660	0.9270	0.9590	0.9400	0.9240	0.9750	0.8900	0.8690
Grandiflora/Central	0.8830	0.7710	0.7400	0.3900	0.8370	0.9200	0.5960	0.5090
Grandiflora/Military	0.8340	0.7270	0.6250	0.7810	0.8100	0.7930	0.7030	0.6730
Jog/Hood	0.7680	0.7270	0.6630	0.0000	0.5000	0.8380	0.8130	0.0000
45th Street @ Haverhill Rd 11	0.9290	0.9680	0.8520	0.9300	0.8900	0.9640	0.9240	0.7670
45th Street @ Military Trail 07	0.9270	0.8910	0.9240	0.9600	0.9420	0.9030	0.8760	0.8800
45th Street @ Village Bl 07/05	0.7550	0.9440	0.9250	0.9520	0.7020	0.9660	0.9220	0.9310
45th Street @ North Point BL	0.8810	0.8560	0.9640	0.9520	0.8960	0.7930	0.9370	0.9260
45th Street @ I-95 27/08/08	0.9250	0.9160	0.9280	0.9250	0.8650	0.9180	0.9540	0.9110
45th Street @ Corporate Way	0.7750	0.6390	0.9290	0.9400	0.7700	0.6250	0.9700	0.9220
45th Street @ Congress Ave	0.9350	0.8470	0.9410	0.9310	0.9340	0.9390	0.9220	0.9450
45th Street @ South Pl/Tiffan	0.8040	0.7500	0.9470	0.9300	0.8080	0.8550	0.9580	0.8960
45th Street @ North Shore DR	0.8290	0.7430	0.9450	0.8670	0.6400	0.6960	0.9210	0.9520
45th Street @ Australian AV 0	0.9230	0.8890	0.9640	0.8860	0.9080	0.9630	0.9050	0.9640
45th Street @ Old Dixie HWY	0.8810	0.9310	0.9000	0.9060	0.9110	0.7950	0.8910	0.8800
45th Street @ Pinewood AV 0	0.7740	0.7930	0.8750	0.8540	0.8330	0.7870	0.8590	0.9200
45th Street @ Broadway Road	0.9500	0.8930	0.8560	0.8720	0.8810	0.9500	0.9030	0.8790
Belvedere RD @ SR-7	0.9220	0.9300	0.8880	0.9360	0.8770	0.9650	0.9610	0.9300
Belvedere RD @ Walmart/Ma	0.8100	0.8680	0.8960	0.9260	0.5360	0.9290	0.9380	0.9480
Belvedere RD @ Sansbury W	0.7860	0.8820	0.9150	0.9320	0.8120	0.8640	0.9530	0.9450
Belvedere RD @ Benoist Farr	0.7190	0.7080	0.9620	0.9080	0.7820	0.9500	0.9360	0.8960
Belvedere RD @ Skees RD	0.9420	0.0000	0.9210	0.9720	0.8650	0.0000	0.9340	0.8790

Table A-1 Contd. PHF	AM SB	NB	WB	EB	PM SB	NB	WB	EB
Belvedere RD @ Jog RD	0.8980	0.8660	0.9380	0.9090	0.9700	0.9500	0.9310	0.9560
Belvedere RD @ Drexel RD/F	0.7910	0.8960	0.9010	0.9220	0.9010	0.8590	0.9560	0.9530
Belvedere RD @ Caroline AV	0.0000	0.9090	0.9320	0.9590	0.0000	0.8750	0.9310	0.9160
Belvedere RD @ Haverhill RD	0.9380	0.9150	0.9390	0.9290	0.9470	0.9610	0.9200	0.9250
Belvedere RD @ 5th Street 18	0.7870	0.0000	0.9170	0.9650	0.8160	0.0000	0.8570	0.9300
Belvedere RD @ Military TR 1	0.9450	0.8880	0.8980	0.9190	0.9510	0.8970	0.8870	0.8950
Belvedere RD @ Congress AV	0.8920	0.7630	0.8810	0.9390	0.8710	0.7550	0.9250	0.9060
Belvedere RD @ Australian A	0.9410	0.8950	0.9730	0.9410	0.8660	0.9000	0.8780	0.9340
Belvedere RD @ Mercer Ave	0.8770	0.0000	0.9530	0.9370	0.8150	0.0000	0.9330	0.9630
Belvedere RD @ Parker AVE	0.8440	0.8610	0.9280	0.9350	0.7760	0.8790	0.9660	0.9260
Belvedere RD @ Georgia AVE	0.7800	0.9340	0.9000	0.9060	0.7420	0.9690	0.8520	0.9420
Belvedere RD @ Dixeie HWY	0.9240	0.8920	0.8510	0.9060	0.8450	0.8980	0.7850	0.9760
Forest Hill/South Shore/12th F	0.7870	0.8880	0.9420	0.8840	0.9090	0.9350	0.9310	0.9640
Forest Hill/@Polo Club Rd/Ro	0.7350	0.8820	0.8780	0.9300	0.8620	0.8500	0.8980	0.9140
Forest Hill/Fairlane Farm Rd (	0.0000	0.8330	0.9370	0.9490	0.0000	0.7760	0.9460	0.9580
Forest Hill/@Wellington Edge/	0.8720	0.7500	0.9160	0.9450	0.8880	0.8870	0.9240	0.9030
Forest Hill/Wellington Green (	0.0000	0.9450	0.9090	0.9450	0.0000	0.8890	0.9450	0.9390
Forest Hill/SR-7 10/14/08	0.8910	0.8630	0.9600	0.9590	0.9390	0.9590	0.9710	0.9700
Forest Hill/Olympia/Buena Vid	0.7890	0.8790	0.9150	0.9010	0.7970	0.7580	0.9030	0.9250
Forest Hill Rd @Ranch Rd/Ly	0.8010	0.8260	0.9380	0.8680	0.8610	0.8160	0.9700	0.9400
Forest Hill Bl @ Pinhurst Dr 1	0.8820	0.9030	0.9310	0.8730	0.7020	0.8460	0.9580	0.9510
Forest Hill Bl @ River Bridge E	0.9060	0.7750	0.9400	0.8610	0.8670	0.8770	0.9470	0.9090
Forest Hill @ Jog Rd 14/10/08	0.9210	0.9270	0.8670	0.9610	0.9450	0.9520	0.9310	0.8900
Forest Hill @ Sherwood Fores	0.8390	0.8370	0.8880	0.9620	0.8870	0.9300	0.8960	0.9650
Forest Hill @ Haverhill Rd 06/	0.9370	0.8740	0.9290	0.8290	0.9430	0.9440	0.9760	0.9490
Forest Hill @ Military Trail 22/	0.9310	0.8870	0.9080	0.9630	0.9190	0.9530	0.9700	0.9110
Forest Hill @ Kirk Rd Rd 14/1	0.9150	0.8500	0.9050	0.9580	0.9190	0.8790	0.9360	0.8980
Forest Hill @ Davis Rd/Tuker	0.8820	0.4570	0.9370	0.8760	0.8440	0.7290	0.9510	0.8670
Forest Hill Bl @ Congress Ave	0.8810	0.8720	0.9220	0.9140	0.9430	0.9460	0.9500	0.8870
Forest Hill Bl @ Florida Mang	0.8520	0.8540	0.9590	0.9340	0.8940	0.9040	0.9490	0.9680
Forest Hill Bl @ Pine Tree LN	0.0000	0.7090	0.9140	0.9140	0.0000	0.6730	0.9350	0.8880
Forest Hill Bl @ I-95 15/10/08	0.8930	0.9450	0.8880	0.8840	0.8820	0.9150	0.8410	0.9170
Forest Hill Bl @ Parkewr Ave	0.7880	0.7630	0.8940	0.8200	0.9440	0.7260	0.8520	0.9000
Forest Hill Bl @ Lake Ave 07/	0.8080	0.5450	0.8470	0.8280	0.9000	0.3400	0.9170	0.9510
Forest Hill Bl @ Gerogia Ave (	0.8410	0.7740	0.9280	0.9180	0.8950	0.5940	0.8980	0.9540
Forest Hill @ Dixie HWY 06/1	0.8870	0.8260	0.7470	0.9070	0.8900	0.9070	0.9330	0.9330
Lantana RD @ SR-7 10-Sep-(	0.9170	0.9430	0.9540	0.6290	0.8970	0.8630	0.9210	0.6290
Lantana RD @ Target 10 Sep	0.7250	0.0000	0.9360	0.9680	0.7500	0.0000	0.9210	0.8460
Lantana RD @ Bellagio Lakes	0.4380	0.8110	0.9090	0.9680	0.4170	0.8790	0.9330	0.8460
Lantana RD @ Lyons RD 10 S	0.8000	0.9130	0.8270	0.8660	0.6350	0.9430	0.8960	0.9560
Lantana RD @ Aquarius BL/G	0.7690	0.8110	0.9070	0.9070	0.8200	0.7500	0.9550	0.9060
Lantana RD @ Bantbrook BL	0.8540	0.0000	0.9630	0.9150	0.9130	0.0000	0.9210	0.8570
Lantana RD @ Hagen Ranch	0.5560	0.8170	0.9150	0.8640	0.6670	0.9090	0.9490	0.9730

Table A-1 Contd.	AM				PM			
PHF	SB	NB	WB	EB	SB	NB	WB	EB
Lantana RD @ Jog RD 10-Se	0.9230	0.8520	0.9830	0.9010	0.9200	0.9680	0.9290	0.9580
Lantana RD @ EDGECLIFF A	0.9150	0.0000	0.9230	0.9240	0.8920	0.0000	0.9410	0.9450
Lantana RD @ Haverhill RD 0	0.9380	0.9520	0.9430	0.9160	0.9740	0.8530	0.9320	0.9700
Lantana RD @ Military Trail 1	0.9450	0.9110	0.9400	0.9380	0.9540	0.9630	0.9280	0.9020
Lantana RD @ Lawrence RD	0.0000	0.9130	0.9150	0.9170	0.0000	0.8570	0.9300	0.9340
Lantana RD @ Congress 03-M	0.9380	0.9200	0.9260	0.9580	0.9630	0.9200	0.9590	0.9800
Lantana RD @ High Ridge 23	0.9260	0.8010	0.9630	0.9670	0.9790	0.8450	0.9660	0.9410
Lantana RD @ I-95 24-Mar-08	0.9330	0.9090	0.9330	0.9280	0.9760	0.9120	0.9020	0.9160
Lantana RD @ 13th ST/Andre	0.8840	0.8940	0.9360	0.8690	0.8700	0.7500	0.9240	0.9120
Lantana RD @ Broadway/6th	0.7860	0.7050	0.8870	0.8400	0.6720	0.8100	0.9260	0.9380
Lantana RD @ US-1 24-Oct-0	0.9270	0.9090	0.7500	0.8480	0.9480	0.8980	0.8330	0.9100
West Atlantic AV @ SR-7 24/1	0.9680	0.8730	0.8910	0.8920	0.9620	0.9210	0.8920	0.8370
West Atlantic AV @ Hagen Ra	0.9450	0.0000	0.8960	0.9720	0.9200	0.0000	0.9620	0.9750
West Atlantic AV @ Legends	0.8700	0.7190	0.8730	0.9600	0.8690	0.7290	0.8940	0.9480
West Atlantic AV @ Cumberla	0.8520	0.0000	0.9410	0.9630	0.9180	0.0000	0.9400	0.9040
West Atlantic AV @ Kings Poi	0.0000	0.9390	0.9520	0.9640	0.0000	0.9010	0.8910	0.9480
West Atlantic AV @ Jog Rd 0	0.9090	0.9150	0.9260	0.9940	0.9430	0.8860	0.8800	0.9570
West Atlantic AV @ EL Clair F	0.8770	0.8550	0.9880	0.9660	0.9420	0.8550	0.9300	0.9310
West Atlantic AV @ Lakes of	0.7390	0.8690	0.9740	0.8910	0.8750	0.8560	0.9550	0.9010
West Atlantic AV @ Via Flora	0.9360	0.6580	0.9210	0.9540	0.8390	0.6760	0.8960	0.9010
West Atlantic AV @ Market Pl	0.8860	0.7750	0.9390	0.9210	0.9020	0.6770	0.9370	0.9520
West Atlantic AV @ Military T	0.9540	0.9280	0.9480	0.9390	0.9530	0.9400	0.8920	0.9680
West Atlantic AV @ Whatley F	0.7330	0.9330	0.9000	0.9860	0.9070	0.7780	0.9340	0.9450
West Atlantic AV @ Barwick F	0.8830	0.8930	0.9400	0.9620	0.8680	0.8330	0.9510	0.9550
West Atlantic AV @ Hamlet D	0.7740	0.8520	0.9650	0.8720	0.6790	0.8670	0.9350	0.8690
West Atlantic AV @ Homewoo	0.8190	0.9330	0.9350	0.8920	0.7720	0.8170	0.9400	0.9880
West Atlantic AV @ CONGRE	0.9620	0.9700	0.9710	0.9470	0.9430	0.8650	0.9310	0.9470
West Atlantic AV @ I-95 (Wes	0.8710	0.0000	0.9260	0.9520	0.9020	0.0000	0.8900	0.9260
West Atlantic AV @ I-95 (Eas	0.0000	0.9130	0.8960	0.9120	0.0000	0.9470	0.8540	0.9520
West Atlantic AV @ SW/NW 1	0.8450	0.9010	0.9310	0.8590	0.8770	0.8650	0.8710	0.9710
West Atlantic AV @ SW/NW 1	0.8260	0.6160	0.9160	0.9300	0.9190	0.8110	0.8900	0.9590
West Atlantic AV @ SW/NW 8	0.6580	0.7360	0.9080	0.9080	0.5430	0.8090	0.7630	0.8880
West Atlantic AV @ SW/NW 5	0.8660	0.7750	0.9140	0.9670	0.9070	0.8100	0.7290	0.9480
West Atlantic AV @ SW 2nd	0.0000	0.8940	0.9400	0.8640	0.0000	0.7450	0.8930	0.9610
West Atlantic AV @ SWINTO	0.9720	0.8580	0.9210	0.8940	0.8370	0.8970	0.9030	0.8940
EAST Atlantic AV @ SE/NE 2	0.7720	0.9170	0.9100	0.8920	0.8140	0.2500	0.9210	0.9090
East Atlantic AV @ US-1 NE 5	0.9270	0.0000	0.9360	0.9180	0.9310	0.0000	0.8950	0.9260
East Atlantic AV @ US-1 NE 6	0.0000	0.9790	0.9200	0.8700	0.0000	0.9630	0.8300	0.8760
Diego DR West/North(05/05/0	0.9170	0.8130	0.8070	0.8380	0.8130	0.9030	0.9350	0.8500
Glades Rd/Cains BL(04/30/07	0.9450	0.0000	0.9490	0.9440	0.9170	0.0000	0.9470	0.8030
Glades_SR-7(28/04/08)	0.9630	0.9530	0.8370	0.8770	0.9410	0.9260	0.9780	0.8950
Glades_Shadowood SC((04/2	0.7950	0.9090	0.9930	0.8860	0.8510	0.8930	0.9260	0.9140
Glades_95th Ave S(04/28/08)	0.7270	0.6680	0.9120	0.8390	0.9120	0.5820	0.9710	0.9000
Glades_Lyons RD(04/28/08)	0.9190	0.8560	0.9230	0.9120	0.8250	0.9500	0.9880	0.9710
Glades_Boca Lake/Sommerse	0.8860	0.8750	0.9470	0.9770	0.8600	0.8680	0.9470	0.9640

Table A-1 Contd.	AM				PM			
PHF	SB	NB	WB	EB	SB	NB	WB	EB
Glades_Golf Course/Concord	0.8330	0.8860	0.9300	0.9380	0.9670	0.8330	0.9750	0.9490
Glades_Boca Rio Rd	0.9830	0.9750	0.9020	0.9450	0.9230	0.9210	0.9650	0.9420
Glades_Turnpike	0.9230	0.7760	0.8820	0.9500	0.9770	0.8310	0.9320	0.9320
Glades_Boca West/Encina Ln	0.9130	0.8470	0.9430	0.9220	0.8520	0.7260	0.9140	0.9380
Glades_Jog/Powerline Rd(1/1	0.9860	0.9370	0.8470	0.9330	0.9560	0.8600	0.9540	0.9320
Glades_Jog/Powerline Rd	0.9580	0.9320	0.8850	0.9530	0.9420	0.9680	0.9360	0.9320
Glades_Boca Corp Ctr	0.7980	0.8240	0.9720	0.9670	0.8000	0.8650	0.9770	0.9730
Linton BL @ Jog RD	0.9020	0.8330	0.8830	0.8400	0.9030	0.9540	0.8680	0.9020
Linton BL @ Sims RD 17-Nov	0.8090	0.6840	0.9690	0.8930	0.8620	0.8330	0.9330	0.9200
Linton BL @ Las Verdes Way	0.8680	0.9460	0.8290	0.8930	0.8970	0.8830	0.9180	0.8480
Linton BL @ Military Trail 19-N	0.9570	0.9480	0.8940	0.9280	0.9660	0.8810	0.9430	0.9020
Linton BL @ Old German Tow	0.0000	0.7590	0.8700	0.9370	0.0000	0.8690	0.9760	0.9330
Linton BL @ Homewood BL 0	0.9620	0.8530	0.8160	0.8970	0.8860	0.7670	0.9450	0.9140
Linton BL @ Congress 13-Nov	0.9400	0.8070	0.9000	0.9240	0.8430	0.8690	0.8790	0.9890
Linton BL @ I-95 18-Nov-08	0.9030	0.8810	0.9330	0.9270	0.8820	0.9250	0.9400	0.9240
Linton BL @ Wallace/waterfor	0.9040	0.9570	0.9670	0.9680	0.8450	0.9640	0.9440	0.9620
Linton BL @ SW 10th AVE 10	0.8060	0.9050	0.9570	0.9340	0.9680	0.9300	0.8910	0.9240
Linton BL @ SW 4th AVE 09-	0.8690	0.8590	0.9580	0.9300	0.8610	0.9900	0.9570	0.9170
Linton BL @ OLD DIXIE HWY	0.9220	0.9020	0.9580	0.9370	0.8990	0.9300	0.9570	0.9340
Linton BL @ US-1/Federal HW	0.9390	0.9360	0.7540	0.9560	0.8730	0.9370	0.8100	0.8860
Linton BL @ A1A	0.8390	0.8990	0.5000	0.8970	0.9310	0.9440	0.7500	0.9370
Atlantic Blvd@ Riverside Wes	0.7880	0.8790	0.8860	0.9640	0.8750	0.8080	0.8460	0.8530
Atlantic Blvd@ Coral Ridge D	0.9120	0.9340	0.8700	0.8350	0.8520	0.8850	0.8890	0.9260
Atlantic Blvd@ Pine Island RD	0.9070	0.8380	0.9790	0.8740	0.8990	0.8930	0.9730	0.8940
Atlantic Blvd@ BW 98 AV	0.8690	0.8380	0.8520	0.8960	0.8930	0.7950	0.9240	0.8680
Atlantic Blvd@ University DR	0.9100	0.9340	0.9510	0.8980	0.9430	0.8900	0.9230	0.8990
Atlantic Blvd@ Riverside DR	0.8800	0.7220	0.9220	0.8720	0.7670	0.8940	0.9100	0.8530
Atlantic Blvd@ Ramblewood D	0.6570	0.6810	0.9550	0.7600	0.8720	0.5400	0.9060	0.8760
Atlantic Blvd@ NW 80th Ter	0.6110	0.7500	0.9100	0.9240	0.7500	0.6090	0.9490	0.9250
Atlantic Blvd@ NW 76th AV	0.8210	0.8000	0.8690	0.8870	0.7460	0.8820	0.9090	0.9930
Atlantic Blvd@ Palm Lakes Pl	0.5000	0.7200	0.9260	0.9400	0.0000	0.8490	0.9180	0.8710
Atlantic Blvd@ Rock Island R	0.8780	0.8500	0.8190	0.8500	0.8090	0.9090	0.9590	0.8290
Atlantic Blvd@ NW 66th AV	0.7910	0.6760	0.8660	0.8630	0.8070	0.7500	0.9730	0.9060
Atlantic Blvd@ SR-7(US-441)	0.9420	0.9420	0.8400	0.9070	0.8850	0.9170	0.9100	0.8970
Atlantic Blvd@ Lakewodd Circ	0.4690	0.7500	0.9330	0.8690	0.8390	0.7050	0.7990	0.8630
Atlantic Blvd@ Banks RD	0.8600	0.7380	0.8360	0.7980	0.8460	0.8030	0.9770	0.8540
Atlantic Blvd@ Powerline RD	0.9160	0.9080	0.7670	0.9240	0.8960	0.9280	0.9760	0.9520
Atlantic Blvd@ West Circle Ma	0.7880	0.8790	0.8860	0.9640	0.8750	0.8080	0.8460	0.8530
Atlantic Blvd@ E CRCL MALL	0.8720	0.8830	0.9390	0.8540	0.8320	0.7950	0.9000	0.8840
Atlantic Blvd@ E CRCL MALL	0.7880	0.8790	0.8860	0.9640	0.8750	0.8080	0.8460	0.8530
Average	0.8114	0.8481	0.9020	0.8935	0.8296	0.8588	0.9134	0.9351
Std	0.1081	0.0819	0.0419	0.0387	0.1135	0.0753	0.0315	0.0258

Table A-2: Data Source, Mean V, Std Deviation, Coef. of Variation, # of Observations and t-test.

Data Source	Mean	Stdev	CV	Obs	t-tst	Data Source	Mean	Stdev	CV	Obs	t-test
Sullivan	1508	78	0.052			860255 High AM (W	1487	71	0.048	82	3.5
	1670	151	0.090			860255 PM (W)	1909	79	0.041	244	
	1012	142	0.140			860255 Low AM (W	1454	69	0.047	162	
	790	102	0.129			860298 High AM (E)	2520	236	0.094	68	7.2
	1446	224	0.155			860298 High PM (E)	2053	64	0.031	68	10.0
	1466	100	0.068			860298 Low AM (E)	2292	177	0.077	162	
	1137	72	0.064			860298 Low PM (E)	1957	71	0.036	162	
	838	55	0.065			860298 High AM (W	1752	108	0.062	67	8.1
	860	59	0.069			860298 High PM (W	2471	93	0.038	67	12.8
	838	75	0.090			860298 Low AM (W	1635	77	0.047	162	
	1616	126	0.078			860298 Low PM (W	2302	86	0.037	162	
	2197	105	0.048			930010 High AM (E)	824	44	0.053	80	7.2
	1366	78	0.057			930010 High PM (E)	1465	85	0.058	80	13.7
	1252	82	0.065			930010 Low AM (E)	765	83	0.108	159	
	1234	84	0.068			930010 Low PM (E)	1306	84	0.064	159	
	1120	111	0.099			930010 High AM (W	1120	113	0.101	80	3.0
	750	111	0.148			930010 High PM (W	1106	77	0.070	80	6.8
	985	102	0.104			930010 Low AM (W	1069	143	0.134	159	
	929	124	0.133			930010 Low PM (W	1019	118	0.116	159	
	923	97	0.105			930099 High AM (E)	652	55	0.084	70	9.5
	1356	82	0.061			930099 High PM (E)	1614	111	0.069	70	2.7
	1400	93	0.066			930099 Low AM (E)	582	42	0.072	156	
Hellinga	1287	70	0.054	209		930099 Low PM (E)	1560	193	0.124	156	
	1375	98	0.071	213		930099 High AM (W	1833	170	0.093	63	2.8
	658	62	0.093	213		930099 High PM (W	789	58	0.074	63	11.2
	594	55	0.092	213		930099 Low AM (W	1766	137	0.078	150	
	1282	112	0.087	213		930099 Low PM (W	674	88	0.131	150	
	971	63	0.064	214		930101 AM (E)	2050	132	0.064	129	
	822	53	0.064	214		930101 PM (E)	1536	64.6	0.042	129	
	855	112	0.131	214		930101 AM (W)	1224	71.6	0.058	128	
	720	69	0.096	204		930101 PM (W)	2405	80.6	0.034	128	
FDOT	961	107	0.111	171		860150 High AM (E)	2394	143	0.060	82	4.3
860214 High AM (E	2705	92	0.034	76	8.3	860150 PM (E)	2235	99.4	0.044	244	
860214 High PM (E)	1857	81	0.044	76	2.5	860150 Low AM (E)	2313	133	0.058	162	
860214 Low AM (E	2592	105	0.041	146		860150 AM (W)	1368	121	0.088	241	
860214 Low PM (E)	1827	90	0.049	146		860150 High PM (W	1761	89	0.051	79	6.5
860214 High AM (W	1373	68	0.050	79	6.8	860150 Low PM (W	1662	148	0.089	162	
860214 High PM (W	2774	84	0.030	79	5.5	860256 High AM (E)	1632	162	0.099	74	7.0
860214 Low AM (W	1306	73	0.056	141		860256 PM (E)	983	82.6	0.084	233	
860214 Low PM (W	2695	128	0.047	141		860256 Low AM (E)	1468	173	0.118	159	
860255 High AM (E	1904	74	0.039	82	10.7	860256 High AM (W	744	85	0.114	79	2.0
860255 High PM (E)	1861	70	0.038	82	8.5	860256 High PM (W	1709	119	0.070	79	6.7
860255 Low AM (E	1795	78	0.043	162		860256 Low AM (W	722	74	0.102	153	
860255 Low PM (E)	1775	83	0.047	162		860256 Low PM (W	1587	152	0.096	153	

Table A-2: Contd

Data Source	Mean	Std	CV	Obs	t-tst	Data Source	Mean	Stdev	CV	Obs	t-tst
870258 High AM (E	704	41	0.058	81	6.5	979933 AM (E)	3747	229	0.061	228	
870258 High PM (E)	1110	62	0.056	81	4.7	979933 High PM (E)	4842	183	0.038	81	6.2
870258 Low AM (E)	668	35	0.052	123		979933 Low PM (E)	4658	264	0.057	147	
870258 Low PM (E)	1069	61	0.057	123		979933 High AM (W	4758	230	0.048	82	4.7
870258 High AM (W	832	68	0.082	82	3.8	979933 High PM (W	4074	165	0.041	82	18.3
870258 High PM (W	955	47	0.049	82	3.1	979933 Low AM (W	4605	257	0.056	158	
870258 Low AM (W	801	41	0.051	162		979933 Low PM (W	3599	233	0.065	158	
870258 Low PM (W	935	49	0.052	162		0228 High AM (E)	1140	85	0.075	68	10.6
872560 High AM (E	1132	79	0.070	83	2.1	0228 High PM (E)	1411	98	0.069	68	25.0
872560 High PM (E)	1200	43	0.036	83	2.8	0228 Low AM (E)	1011	82	0.081	157	
872560 Low AM (E)	1108	91	0.082	162		0228 Low PM (E)	1079	75	0.070	157	
872560 Low PM (E)	1181	60	0.051	162		0228 High AM (W)	1121	60	0.054	68	23.2
872560 AM (W)	1037	81	0.078	245		0228 High PM (W)	1289	68	0.053	68	20.3
872560 PM (W)	1291	67	0.052	245		0228 Low AM (W)	906	72	0.079	157	
890289 High AM (E	138	20	0.145	82	11.0	0228 Low PM (W)	1076	81	0.075	157	
890289 High PM (E)	170	16	0.094	82	13.5	0191 High AM (N)	2136	96	0.045	70	15.0
890289 Low AM (E)	112	10	0.089	143		0191 High PM (N)	2746	159	0.058	70	3.1
890289 Low PM (E)	138	19	0.138	143		0191 Low AM (N)	1922	87	0.045	105	
890289 High AM (W	147	12	0.082	82	9.9	0191 Low PM (N)	2675	131	0.049	105	
890289 High PM (W	162	20	0.123	82	11.4	0191 AM (S)	2717	164	0.060	176	
890289 Low AM (W	129	15	0.116	143		0191 High PM (S)	2614	188	0.072	70	13.6
890289 Low PM (W	131	19	0.145	143		0191 Low PM (S)	2242	161	0.072	106	
860306 High AM (E	343	47	0.137	79	2.0	0044 High AM (N)	735	35	0.048	80	6.0
860306 High PM (E)	448	48	0.107	79	5.9	0044 High PM (N)	745	84	0.113	80	4.5
860306 Low AM (E)	331	38	0.115	155		0044 High AM (S)	697	37	0.053	56	
860306 Low PM (E)	409	48	0.117	155		0044 High PM (S)	681	80	0.117	56	
860306 High AM (W	310	54	0.174	78	2.1	0044 Low AM (N)	463	48	0.104	80	3.4
860306 High PM (W	475	68	0.143	78	5.4	0044 Low PM (N)	810	76	0.094	80	9.0
860306 Low AM (W	296	30	0.101	154		0044 Low AM (S)	441	28	0.063	59	
860306 Low PM (W	428	50	0.117	154		0044 Low PM (S)	721	39	0.054	59	
880326 High AM (E	767	81	0.106	70	4.9	0324 High AM (E)	932	81	0.087	75	4.5
880326 High PM (E)	422	35	0.083	70	5.8	0324 High PM (E)	1062	68	0.064	75	9.8
880326 Low AM (E)	714	60	0.084	160		0324 Low AM (E)	878	92	0.105	149	
880326 Low PM (E)	394	30	0.076	160		0324 Low PM (E)	946	109	0.115	149	
880326 High AM (W	289	33	0.114	70	2.9	0324 High AM (W)	929	102	0.110	75	4.0
880326 High PM (W	690	57	0.083	70	3.6	0324 High PM (W)	1071	78	0.073	75	7.5
880326 Low AM (W	276	28	0.101	160		0324 Low AM (W)	868	115	0.132	149	
880326 Low PM (W	664	34	0.051	160		0324 Low PM (W)	979	101	0.103	149	
890259 High AM (E	200	24	0.120	69	10.9	0225 High AM (E)	4435	323	0.073	62	6.2
890259 High PM (E)	443	61	0.138	69	20.0	0225 High PM (E)	4110	297	0.072	62	13.8
890259 Low AM (E)	165	18	0.109	159		0225 Low AM (E)	4161	203	0.049	156	
890259 Low PM (E)	286	35	0.122	159		0225 Low PM (E)	3517	261	0.074	156	
890259 High AM (W	331	26	0.079	64	24.7	0225 High AM (W)	3532	170	0.048	62	12.5
890259 High PM (W	386	37	0.096	64	23.3	0225 High PM (W)	4543	264	0.058	62	11.2
890259 Low AM (W	238	24	0.101	158		0225 Low AM (W)	3227	144	0.045	159	
890259 Low PM (W	268	26	0.097	158		0225 Low PM (W)	4121	219	0.053	159	

Table A-2: Contd.

Data Source	Mean	Std	CV	Obs	t-tst		Mean	Std	CV	Obs	t-tst
0106 High AM (E)	3471	191	0.055	79	10.5	720171 AM (W)	5154	339	0.066	216	
0106 High PM (E)	4760	296	0.062	79	9.4	720171 PM (W)	5421	291	0.054	216	
0106 Low AM (E)	3211	156	0.049	156		750196 AM (E)	5617	349	0.062	214	
0106 Low PM (E)	4356	343	0.079	156		750196 PM (E)	4908	325	0.066	214	
0106 AM (W)	5144	482	0.094	240		750196 AM (W)	6692	406	0.061	215	
0106 High PM (W)	4195	383	0.091	82	2.0	750196 PM (W)	6448	321	0.050	215	
0106 Low PM (W)	4077	504	0.124	158		170225 High AM (E)	4435	323	0.073	63	6.3
0224 High AM (E)	2982	249	0.084	79	2.9	170225 High PM (E)	4114	295	0.072	63	14.0
0224 High PM (E)	2510	272	0.108	79	5.8	170225 Low AM (E)	4161	203	0.049	156	
0224 Low AM (E)	2898	104	0.036	156		170225 Low PM (E)	3517	261	0.074	156	
0224 Low PM (E)	2296	255	0.111	156		170225 High AM (W	3532	170	0.048	62	12.5
0224 High AM (W)	1902	165	0.087	78	7.1	170225 High PM (W	4542	262	0.058	62	11.2
0224 High PM (W)	2733	168	0.061	78	4.1	170225 Low AM (W	3227	144	0.045	160	
0224 Low AM (W)	1758	99	0.056	153		170225 Low PM (W	4121	219	0.053	160	
0224 Low PM (W)	2640	149	0.056	153		930198 High AM (E)	4653	160	0.034	82	7.7
860163 Hi AM (E)	7385	247	0.033	80	5.2	930198 High PM (E)	8428	358	0.042	82	2.4
860163 Hi PM (E)	7457	214	0.029	80	4.6	930198 Low AM (E)	4485	161	0.036	160	
860163 L AM (E)	7215	218	0.030	157		930198 Low PM (E)	8307	408	0.049	160	
860163 L PM (E)	7306	284	0.039	157		930198 AM (W)	8510	450	0.053	241	
860163 AM (W)	6908	413	0.060	231		930198 High PM (W	5660	190	0.034	82	12.2
860163 PM (W)	7279	324	0.045	235		930198 Low PM (W	5316	239	0.045	159	
860331 Hi AM (E)	8348	473	0.057	65	3.3						
860331 Hi PM (E)	8277	209	0.025	65	4.3						
860331 L AM (E)	8139	300	0.037	157							
860331 L PM (E)	8130	279	0.034	157							
860331 AM (W)	7252	415	0.057	216							
860331 PM (W)	8469	347	0.041	216							
860186 Hig AM (E	8300	383	0.046	55	2.9						
860186 Hi PM (E)	7064	300	0.042	55	3.7						
860186 L AM (E)	8091	617	0.076	141							
860186 L PM (E)	6848	503	0.073	141							
860186 AM (W)	6435	681	0.106	183							
860186 PM (W)	7179	710	0.099	183							
879930 Hi AM (E)	1107	79	0.071	78	5.0						
879930 Hi PM (E)	1633	81	0.050	78	3.6						
879930 L AM (E)	1018	165	0.162	116							
879930 L PM (E)	1564	183	0.117	116							
879930 Hi AM (W)	2211	163	0.074	83	7.3						
879930 Hi PM (W)	2311	75	0.032	83	7.5						
879930 L AM (W)	2034	199	0.098	148							
879930 L PM (W)	2206	138	0.063	148							
720171 Hi AM (E)	6312	371	0.059	76	2.1						
720171 Hi PM (E)	4957	316	0.064	76	5.7						
720171 L AM (E)	6205	364	0.059	154							
720171 L PM (E)	4721	256	0.054	154							